MONDRAGON
UNIBERTSITATEA

GOI ESKOLA
POLITEKNIKOA

ESCUELA
POLITÉCNICA
SUPERIOR

THESIS

Submitted for the degree of EUROPEAN DOCTOR
in MONDRAGON UNIBERTSITATEA

INFLUENCE OF ALTERNATIVE MOULD MATERIALS AND INHIBITORS ON MOULD-METAL REACTIONS IN MAGNESIUM INVESTMENT CASTING

NURIA HERRERO-DORCA

Supervisors:

Dr. Gurutze Arruebarrena

Dr. Iñaki Hurtado

July 2012

PREFACE

Declaration

I hereby declare that this thesis is the result of my own work and that, to the best of my knowledge and belief, no part of this dissertation has previously been submitted for any similar qualification or degree.

Nuria Herrero-Dorca

(July 2012)

Copyright and reproduction

This thesis is copyright Nuria Herrero-Dorca, 2012.

I authorize Mondragon Unibertsitatea to reproduce this thesis, in part or in whole, at the request of other institutions or individuals for the purpose of academic research.

A mis padres, Luis y Rosa, y a mi hermano Iñaki

ABSTRACT

Investment casting of magnesium is a process well suited for the production of aeronautic and automotive components, as light density components in medium and small series are obtained. But, still nowadays, this process has not been properly developed. Due to its large negative Gibbs free energy value, MgO is one of the most stable compounds. In investment casting, the refractory oxides of the shell tend to decompose and form the more stable MgO. As a result, molten magnesium reacts with commercial shell materials, based in aluminosilicates, producing a non-desired oxide layer on the part surface.

Mould-metal reactions can be inhibited by the use of alternative mould materials and/or with fluorine-based inhibitors, which create a protective surface layer on the casting. With the aim of developing a reaction-free process for the magnesium investment casting industry, in this thesis different mould materials and inhibitors were tested. Employment of an Al_2O_3-based shell with protective KBF_4 inhibitor has proved to be the most effective one. The obtained surfaces were characterised by means of XRF, SEM/EDS, XRD, XPS and FactSage® chemical equilibrium software. Combining the information obtained through FactSage® with the chemical surface analysis data, reaction mechanisms that lead to both reacted and protected surfaces were proposed. In the last stage of this work, aircraft housing was cast in a Al_2O_3 mould, protected with KBF_4.

RESUMEN

El moldeo a la cera perdida es un proceso de fundición orientado a sectores como la aeronáutica o la automoción, al ser un método con mucha versatilidad que permite obtener piezas de diverso tamaño y geometría a un costo reducido para series pequeñas. No obstante, no existe en la actualidad un desarrollo apreciable de la tecnología de microfusión aplicada a la obtención de componentes ligeros en aleaciones de magnesio. Esto se debe a la alta reactividad del magnesio con las cáscaras cerámicas convencionales, el cual ha limitado su industrialización. Dada la gran estabilidad de la magnesia, los materiales refractarios de la cáscara se descomponen para formar MgO. Como resultado, el magnesio fundido reacciona prácticamente con todos los refractarios comúnmente utilizados en la producción de moldes de microfusión, provocando la aparición de óxidos superficiales no deseados en las piezas.

El empleo de materiales de molde alternativos y/o de inhibidores evita las reacciones molde-metal a través de la formación de una capa protectora sobre la pieza. Con el propósito de desarrollar el proceso de microfusión de magnesio, en este trabajo se han realizado diversos ensayos con materiales de molde alternativos e inhibidores diferentes. Como resultado, el empleo de moldes basados en alúmina, e inhibidos con KBF_4, ha sido elegido como la combinación más efectiva a la hora de evitar las reacciones molde-metal. Las superficies obtenidas han sido analizadas por XRF, SEM/EDS, XRD, XPS y el software de equilibrio termodinámico FactSage®. Gracias a los resultados obtenidos, se han propuesto los mecanismos que dan lugar tanto a superficies protegidas como a superficies cubiertas de reacciones molde-metal. Por último, se ha colado una carcasa de motor empleada en el sector de la aeronáutica, en un molde de alúmina protegido con KBF_4.

LABURPENA

Argizari galduzko galdaketa aeronautika eta automozio sektoreetara ondo egokitutako prozesua da, tamaina eta geometria konplexuko piezak serie txikitan eta kostu baxuan lortzen baitira. Hala ere, magnesioaren erreaktibotasuna dela eta, gaur egun argizari galduzko galdaketa prozesua ez dago oraindik garatuta magnesiozko piezak lortzeko. Magnesioak moldeen ohizko material zeramikoekin erreakzionatzen du, egonkorragoa den MgO konposatua osatzeko. Honen ondorioz, piezaren gainazalean desiragarriak ez diren erreakzioak azaltzen dira.

Molde eta metalaren arteko erreakzioak piezaren gainazalean geruza babesle bat sortzen duten material alternatiboen eta/edo inhibitzaileen erabileraren bitartez saihes daitezke. Argizari galduzko magnesioaren galdaketa prozesua garatzeko asmoz, lan honetan molde material alternatibo eta inhibitzaile ezberdinak esperimentatu dira. Al_2O_3 molde materiala KBF_4 inhibitzailearekin erabilita lortu dira emaitza eraginkorrenak. Lortutako emaitzak XRF, SEM/EDS, XRD, XPS eta oreka termodinamikoa kalkulatzen duen FactSage® software-aren bitartez aztertu dira. Azterketa kimiko eta FactSage®-ren bidez lortutako emaitzak partekatuta, gainazal babestu edota erreakzionatu batera daramaten erreakzio mekanismoak proposatu dira. Azkenik, aeronautika sektorean erabiltzen den motor karkasa bat KBF_4 inhibitzailearekin babestutako Al_2O_3 molde batean galdatu da.

CONTENTS

LIST OF FIGURES

LIST OF TABLES

CHAPTER I

INTRODUCTION

In this chapter, an overall view of the current thesis is presented. First of all, the framework of the thesis and the motivation to carry out this research are presented.

Then, the research objectives of the thesis are presented. Working methodology followed to accomplish the objectives is depicted; the main stages of the thesis are briefly presented and discussed at this section.

1.1 Motivation and background

Weight reduction was and still is an important issue for a wide variety of applications, from transportation vehicles to sport materials. The main reason behind the lightening of products, regardless the application, is the reduction of the work needed when moving a lighter mass. Consequently, the benefits of the energy reduction are also achieved, such as reduction of greenhouse gas emissions generated by fossil energy sources, the possibility of reaching longer distances for the same amount of stored energy and mainly the reduction in economic costs that it implies. In addition, in some applications, reducing weight may also report benefits in the inertial performance of moving masses. Therefore, new lighter materials are being searched for and used by engineers when designing their products to optimize the structure for strength and weight. However, the cost of these new light materials also plays an essential role in their use level, which, in turn, relates to several parameters such as availability, quality, manufacturability and environmental compatibility during life cycle. Moreover, the industry in which they are used is also crucial, for instance, the estimated value of a pound saved in weight is US\$ 300, 3000, 30000 and 3 respectively in commercial/transport, fighter, space and automobile industries [Fri06]. Magnesium being the lightest metallic structural material with a density of 1.74 g/cm3, approximately 75% lighter than steel and 33% lighter than aluminium, is an interesting material for weight reduction purposes. Moreover, due to its excellent

damping capacity, which provides vibration absorption ability, corrosion resistance and excellent machining characteristics, use of magnesium in industry is consistently increasing.

Magnesium alloys shows limited formability at room temperature and therefore, casting and forging technologies have traditionally been used to manufacture magnesium parts [Kim00]. Investment casting of magnesium is a process well suited for the production of aeronautic and automotive components, as light density components in medium and small series are obtained. The degree of freedom in design is larger in contrast to pressurized casting processes, such as die casting and semisolid forming [Kim00]. Moreover, near net shape castings are produced, eliminating expensive finishing costs. Although castings of 20 kg or more are routinely produced, it is the tiny castings (10-20 grams) that are literally unique in this process [Sha04]. Investment casting process is also capable of producing castings of tighter tolerances, and also thin wall sections if severe casting temperatures are employed to enhance mould filling. On this regard, additional weight reduction in vehicles can be achieved by converting assembled parts to complex components by investment casting.

Unfortunately, still nowadays, this process has not been properly developed and one reason for that are mould-metal reactions. Due to its large negative Gibbs free energy value, MgO is one of the most stable compounds. This means that, in investment casting, the refractory oxides of the mould tend to decompose thermally and form the more stable MgO compound. As a result, molten magnesium reacts with commercial shell materials (aluminosilicates) producing a non-desired oxide layer on the part surface. Severe surface reactions may even cause the destruction of the mould [Cin06]. Due to this, little research has been published on magnesium investment casting. Suppression of the reactions has already been achieved, through the use of alternative mould-materials and inhibitors that produce a protective surface layer of metallic appearance on the casting [Yan07, Cin06, Zha04, Kim01, Kim00, Idr96]. Nevertheless, the mechanisms that lead to mould-metal and to protective reactions are still not fully understood.

Therefore, in order to overcome this limitation, magnesium investment casting industry requires the development of specific mould materials and inhibitors that can avoid the formation of the non-desired surface reactions. A compromise between filling ability, to produce thin-walled complex components, and mould-metal reactivity, which governs the quality of the cast surface, needs also to be found. A better understanding of the reaction mechanisms that lead to both reacted or effectively protected surfaces is though to be essential to accomplish the above mentioned features.

1.2   Scope of the present dissertation

The main objective of this dissertation is to obtain mould-metal reaction-free surfaces in magnesium investment casting. For such a purpose, this thesis is divided into three specific objectives:

o Select the most effective mould material-inhibitor combination for Mg investment casting.

o Determine the elements and compounds present in the surface layers.

o Propose the reaction mechanisms that lead to both protected and reacted surfaces.

1.3   Outline of the present dissertation

This thesis covers both theoretical and experimental work, divided into three main subsections.

The first section (Chapter 2) deals with the literature review, where the main features of mould-metal reactions in magnesium investment casting are depicted. The review is divided into four main subsections: oxidation of magnesium and its alloys, magnesium melt protection, review of Mg investment casting reactions, and methods employed to avoid mould-metal reactions (alternative mould materials and inhibitors).

The second section, corresponding to Chapters 3, 4, 5, and 8, consist in a serial of investment casting experiments performed to obtain mould-metal reaction-free surfaces. It comprises, in turn, two big subsections: selection of an inhibitor (Chapter 4) and mould material (Chapter 5). Tested materials and chemicals are chosen among commercial options existent in the market, to ensure that a future implementation of the improvements found through this thesis are possible (Chapter 3). The surfaces obtained in the experiments are analysed in each chapter by means of X-ray fluorescence (XRF), Energy dispersive spectroscopy (EDS) and X-ray diffraction (XRD) to determine which are the elements and compounds that participate in the reactions. As a result, the most effective mould material-inhibitor combination for magnesium investment casting has been selected, and employed in the casting of a real prototype (Chapter 8).

In the third section the mechanisms that lead to protected and reacted surfaces are presented. As a result of the information obtained after the X-ray Photoelectron Spectroscopy (XPS) analysis and the thermodynamic modelling of the reactions, a proposal of the mould-metal and protective mechanism has been presented. Last, the different surfaces encountered during this work are analysed on basis to the presented mechanisms (Chapters 6 and 7).

LITERATURE REVIEW

2.1   Introduction

In this chapter main features necessary to understand the basis of mould-metal reactions in magnesium investment casting are depicted. Mould-metal reactions can be defined as the reactions happening between the atmosphere, the magnesium melt and the mould material, which start in the pouring moment and happen while the metal solidifies inside the shell. Considering this, the literature review has been divided into four main aspects.

The first of those aspects is the oxidation of magnesium and its alloy. After introducing magnesium's general properties, behaviour of magnesium and its alloys in air atmospheres, at a temperature range that covers from ambient temperature to melting temperatures has been analysed (Sections 2.2 and 2.3).

Second one is referred to melt protectors. Inhibitors employed to protect liquid magnesium are presented and described, emphasising in the mechanisms that lead to a protected surface in the melt (Sections 2.4 and 2.5).

After that, a review of the different reactions that happen in magnesium investment casting involving the metal, the mould and the atmosphere are presented (Section 2.7). Practical features of the process and composition of conventional slurries are also presented (Section 2.6).

Next, the two methods employed to avoid the formation of the mould-metal reactions (alternative mould materials and inhibitors) are presented. Results obtained by different authors after the implementation of silica-free shells and the use of melt protectors as inhibitors in magnesium investment casting are presented (Section 2.8).

Last, a resume of the main conclusions extracted from each aspect is presented.

2.2   Magnesium and magnesium-aluminium alloys: a brief introduction

Magnesium is the eighth most common element on earth. It is produced through either the metallothermic reduction of magnesium oxide with silicon or the electrolysis of magnesium chloride melts from seawater: Each cubic metre of the sea water contains approximately 1.3 kg (0.3 wt.%) magnesium. Magnesium is the lightest of all the engineering metals, having a density of 1.74 g/cm^3. It is 35% lighter than aluminium (2.7 g/cm^3) and over four times lighter than steel (7.86 g/cm^3). Alloying magnesium with other elements increases the strength to weight ratio, making them important materials for applications where weight reduction is important, and where it is imperative to reduce inertial forces. Because of this property, denser material (not only steels, cast iron and copper base alloys, but even aluminium alloys) are replaced by Mg-based alloys. More than 90% of Mg alloy structural components are produced by casting processes. Magnesium has good die-filling properties and large, thin-walled and complex components can be produced by casting rather than by joining smaller parts together [Yan07].

Alloys with aluminium as the major alloying element are specially employed in casting due to its excellent castability. Main commercial Mg-Al alloys include the AZ series (Mg-Al-Zn), AM series (Mg-Al-Mn) and AE series (Mg-Al-RE). The range of aluminium contents for the commercial alloys is 2-9 wt% Al, from AM20 to AZ91. Although magnesium alloys containing aluminium generally possess good mechanical properties, ternary alloys with zinc, manganese, silicon and rare-earth elements in addition to aluminium are used to obtain improved mechanical properties. Zinc is added to improve the room temperature strength and fluidity while silicon is added to improve the creep strength of the alloys by forming Mg_2Si particles on the grain boundaries. Addition of manganese is required to control the corrosion behaviour, and magnesium alloys with aluminium and manganese (AM60, AM50) are commonly used for components where good ductility and impact strength are required [Dah01]. In last decades the AZ series cast Mg alloys, (especially AZ91) have been extensively studied and used because of high specific strength, good castability and relative low price [Yan07]. Actually, by using AZ91 alloy, thin walled castings with thicknesses minor than 1mm can be easily obtained in pressure assisted casting processes, like high pressure die casting [Bla04].

Figure 2.1.a shows the magnesium-aluminium equilibrium phase diagram. Maximum solid solubility of Al in Mg at the eutectic temperature is about 13 wt.%, and a eutectic between α-Mg and the intermetallic γ-$Mg_{17}Al_{12}$ appears at about 33 wt.% Al. All the aluminium contents used in commercial alloys are below the maximum solid solubility limit [Dah01]. However, the cooling rates that the alloys experience during the casting processes are so high that the Mg alloys solidify under non-equilibrium conditions. Solidification starts with the formation of α-Mg crystals, but during the cooling the remaining liquid phase becomes so enriched in Al content that the eutectic structure

appears [Arr08]. The non-equilibrium, metastable eutectic can be present in the as-cast microstructure in Mg-Al alloys down to about 2 wt% Al [Dah01].
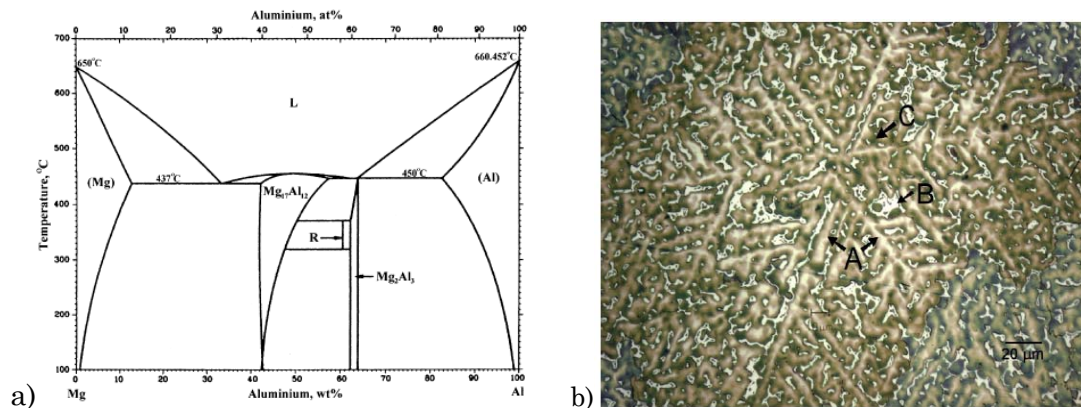
Figure 2.1: a) Mg-Al equilibrium diagram [Dah01] b) Micrograph of fully developed dendrites in a die-cast Mg-15wt% Al alloy [Stj03]

Figure 2.1.b shows a typical microstructure of Mg-Al alloys. Because magnesium has a hexagonal close-packed structure, the dendrite arms branch has a six-fold symmetry [Stj03]. On Figure 2.1.b, point A shows magnesium dendrites with secondary arms, B is the γ-$Al_{12}Mg_{17}$ phase and C shows the α-Mg solid solution rich in aluminium, which are located in the interdendritic regions.

2.3 Magnesium and magnesium-aluminium alloy oxidation: an overview

2.3.1 Introduction

Due to its high reactivity, Mg offers limited corrosion properties in many environments. The reason is that MgO is not stable in aqueous solutions. It reacts with water and, as a result, a $Mg(OH)_2$ film is formed on the surface (Equation 2.1).

$$Mg + 2H_2O \rightarrow Mg(OH)_2 + H_2 \qquad\qquad 2.1$$

This $Mg(OH)_2$ film provides protection against further corrosion only at pH values higher than 11, when a stable $Mg(OH)_2$ layer is formed. Carbon dioxide dissolved in water also reacts with Mg and forms hydrated magnesium-carbonate. The protecting hydroxide and carbonate products are broken down in agitated water if the solution contains chlorides or heavy metal salts. Therefore, almost all Mg products exposed to outdoor environments have to be surface treated in order to limit the corrosion attack of the material [Fou02].

While this aqueous corrosion is recognized to be a major problem of Mg alloys, oxidation at elevated temperature is often ignored as a shortcoming for alloy application and is not very widely studied. Magnesium has a high affinity to oxygen so in its presence it rapidly reacts according to Equation 2.2:

$$Mg + \tfrac{1}{2} O_2 \rightarrow MgO \qquad\qquad\qquad\qquad 2.2$$

The free energy change that accompanies the formation of the oxide at 25^oC is $\Delta G_f = -1138$ kJ/mol O_2; which is more negative than for most metals with only few exceptions (Be and some rare earths). Therefore, the resistance of Mg and its alloys to oxidation directly depends on the protective properties of the oxide film that forms first [Eli02].

The Pilling-Bedworth ratio (*PBR*), which is the volume ratio between a metal's oxide and the metal itself, was widely employed as a guideline to determine whether an oxide film will act as a protective film or not. The *PBR* is expressed as:

$$PBR = \frac{V_{oxide}}{V_{metal}} \qquad\qquad\qquad\qquad 2.3$$

Where V_{oxide} corresponds to the molar volume of the oxide, and V_{metal} to the volume of metal consumed for the formation of 1 mol of oxide. If *PBR* is less than one, the oxide is not able to cover the entire metal surface. The oxide film is discontinuous, porous and non protective. Accordingly, if *PBR* is higher than one, the film will cover the surface effectively and protect it. However, *PBR* is of limited validity. It has to be taken into account that the surface properties are different from the bulk, and that there may be some re-alignment of the atoms at the surface. Therefore, the Pilling Bedworth ratio seems to be valid for metals with a simple atomic structure such as the alkali and alkali earth metals, but not for metals with a complex structure such as Ti, Nb and Ta [Aar04]. The *PBR* concept does not work either for those metals having a *PBR* greatly exceeding unity. These oxides, owing to its high volume ratio, develop severe biaxial stresses that eventually lead to rupturing of the oxide film. It can be said, then, that for oxides with 1<*PBR* <2, the oxide layer is generally dense, giving good coverage [Syv07].

It has also been assumed that it is relevant to employ an average Pilling Bedworth ratio when two separate phases form, for instance MgO and MgS. However, this procedure fails for mixtures, e.g. Mg-Ca-O or Mg-Be-O. Table 1.2 presents Pilling-Bedworth ratios for interesting compounds, regarding magnesium protection. *PBR* for MgO is equal to 0.81, so the oxide offers a poor coverage of the surface.

Table 2.1: Pilling-Bedworth ratios found on protective and non-protective Mg melt film compounds [Aar04]

Compound	MgO	MgF_2	$MgSO_4$	MgS	$MgCO_3$	Mg_3N_2	CaO	BeO	Al_2O_3
PBR	0.81	1.45	3.2	1.4	1.6	0.89	0.64	1.68	1.28

2.3.2 Magnesium oxidation

- *Magnesium oxidation at ambient temperature*

Magnesium exhibits good oxidation resistance in dry air at ambient temperature due to the formation of an amorphous, highly stable and protective film. This film is an unstable structural modification of MgO crystals which grow oriented with the metal substrate, building a very thin compact layer. Above a critical oxide thickness, however, the normal cubic lattice forms and the arising stresses lead to film cracking [Eli02, Nor97]. Generally, it is recognized that the initial oxidation of Mg proceeds by the following steps [Shi07, Vin06, Cze02, Eli02]:

1. Oxygen chemisorption

2. Formation of the oxide layer (nucleation and lateral growth)

3. Oxide thickening.

Initially, oxygen is adsorbed on the clean metal surface and forms a chemisorbed monolayer. A rearrangement of valence electrons of the metal and the gas is then necessary for the formation of chemical bonds. In the second stage, additional layers of oxide build up forming oxide islands; place exchange and surface diffusion are the important factors. This island growth is fast and linearly dependent on the oxygen exposure. The oxide thickening stage following coalescence of the oxide islands is slow and diffusion controlled [Eli02]. This last stage requires transport of (charged) species (possibly cations, anions, electrons, holes and vacancies) through the developing oxide film towards the oxide-gas interface and/or the metal-oxide interface.

Presence of water in the environment (humid air or aqueous environments) modifies the film composition, by the formation of a hydrated oxide (Equation 2.1). This film is a mixture of amorphous MgO and 50–60 wt.% $Mg(OH)_2$ [Fot06, Cze02, Eli02, Nor97]. The MgO-$Mg(OH)_2$ film was successfully reported by Nordlien *et al.* in 1997, who analysed the films formed naturally on pure magnesium (Figure 2.2) [Nor97].

Figure 2.2: Cross view of a film obtained after Mg exposure to humid environment. The film exhibits a duplex structure with a dense amorphous outer layer (black arrows) and a hydroxide inner layer [Nor97]

Authors found that first the dense and amorphous MgO film reported for dry atmospheres is formed. Afterwards, an increase in the film thickness with an increase in the humidity level of the air was noticed. XPS and TEM analysis revealed a two layered structure, composed of the original air-formed oxide film and an additional hydrated inner layer. This new hydroxide layer results from metal-water interaction at the metal-oxide interface. The water necessary for this process is obtained from the humid environment by diffusion through the initial air-formed film [Nor97]. Although stable and dense, the outer amorphous layer is permeable to water.

The two-layered film possesses a protective effect on the magnesium surface. However, the corrosion rate of the environment increases considerably at relative humidity >90%. In such conditions heavier films, composed mainly of crystalline $Mg(OH)_2$, develop on the Mg surface. Due to the internal stresses of this thicker film, and to the amount of H_2 gas liberated (Equation 2.1), cracking and curling of the film may occur [, Fot06]. In extended atmospheric exposures of Mg and Mg alloys, the presence of acid gases as SO_2 also alters the composition of the oxide film. Hydroxides, sulphites, or sulphates will form preferentially, thus reducing the film stability . Carbon dioxide present in the atmosphere or dissolved in water also reacts with Mg and forms hydrated magnesium-carbonate [Kim07, Eli02].

- *Magnesium thermal oxidation at solid state*

At temperatures below 450°C in dry oxygen, or below 380°C in moist oxygen, the amorphous MgO oxide film formed at ambient temperature is protective for considerable lengths of time. However, this behaviour changes at higher temperatures as the structure of the film changes, leading to porous and non-protective surface films [Eli02].

Magnesium hydroxide is not stable at high temperatures, and begins to decompose above 350°C forming crystalline MgO, which has a *PBR* of only 0.81. This transformation is also associated with a large decrease in volume that makes the oxide film crack, exposing fresh surface to the atmosphere. Pure Mg reacts again with atmospheric O_2, but in this case crystalline and loose MgO is formed on the metal surface instead of amorphous MgO.

The film that forms above 450°C in dry atmospheres is not protective either. At those temperatures, the oxidation rate of Mg increases considerably due to the high vapour pressure of Mg which causes the cracking of the oxide, exposing the metal surface. It evaporates and forms porous, loose crystalline MgO nodules on the surface by reaction with oxygen [Wan08, Shi07, Eli02, Fou02]. For a vacuum environment, the evaporation rate of magnesium is described by the Arrhenius relation (Equation 2.4):

$$K_{evap} = 0.6^{-25000/RT} \qquad [\text{g/cm}^2 \cdot \text{s}] \qquad\qquad 2.4$$

The higher the reaction temperature, the more evaporation beats oxidation kinetically. Above 450º C, the Mg evaporation rate is so high that the vapour not only saturates all the pores within the nodule but also reaches the nodule/oxygen interface where it forms a continuous film. It is suspected that for such a high evaporation rate, the reaction can even occur at a considerable distance from the surface and the resultant product would be released as incandescent MgO gas. The open nodules continue to grow by the transfer of Mg vapour through voids and simultaneous reaction with oxygen, forming a product with cauliflower-like morphology [Cze04, Cze02].

- *Magnesium thermal oxidation at liquid state: melting temperatures*

Besides higher evaporation rates, liquid metals do not follow the same oxidation mechanisms that solid metals do. At temperatures near their melting point, metals dissolve gases such as oxygen. Liquid metals contain higher amounts of oxygen dissolved than its corresponding solid phase. When oxygen saturation is attained, the oxide phase is nucleated and forms a separate phase. Due to the high solubility of gases in liquid metal and favourable kinetic factors, chemical reactions can take place in and on the liquid metal, forming gaseous, liquid or solid oxides [Kor04].

 As commented before, magnesium also possesses a significant vapour pressure at normal melt temperatures, unlike aluminium and zinc. At its melting point (650°C) magnesium has a vapour pressure of almost 3mmHg (Table 2.2), which results in active oxidation on melt surfaces exposed to air. Initially, only oxide blooms may appear on the surface of an unprotected melt [Aar04]. Generally, the structure of these oxides is porous and non-protective so MgO forms continuously during melting. In addition, the formation heat of MgO is so large that local zones are heated to a considerably high temperature. This speeds up the oxidation reaction and results in active combustion or even burns, with an intense white light [Zen01].

Table 2.2: Equilibrium vapour pressure (EVP, mmHg) of liquid metals as a function of temperature [Iid88]

	EVP at melting point	EVP at 680ºC	EVP at 720ºC	Melting Point (ªC)
Magnesium	2.69	4.65	9.14	650
Aluminium	$6 \cdot 10^{-9}$	$1.4 \cdot 10^{-8}$	$6.7 \cdot 10^{-8}$	660
Tin	$3.44 \cdot 10^{-23}$	$9 \cdot 10^{-9}$	$4.1 \cdot 10^{-8}$	232
Gold	$6.178 \cdot 10^{-6}$	-	-	1063
Lead	$3.6 \cdot 10^{-9}$	$3.98 \cdot 10^{-3}$	$2.8 \cdot 10^{-2}$	328

2.3.3 Magnesium-aluminium alloy oxidation

- *Magnesium Aluminium alloy oxidation at ambient temperature*
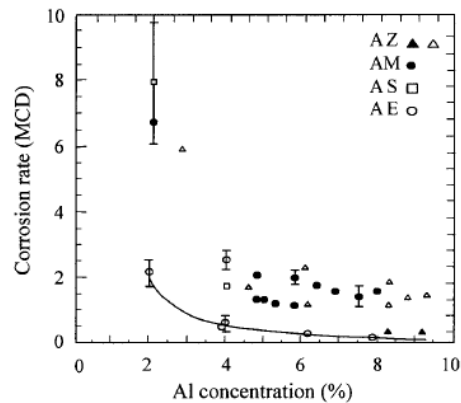
Figure 2.3: Influence of Al concentration on the corrosion rate
of die-cast Mg alloys during immersion in 5% NaCl [Eli02]

Alloying with Al improves the properties of the surface film. With increasing Al content, all layers of the film formed on Mg–Al alloys become continuously enriched in Al_2O_3 and dehydrated. In water containing atmospheres, such stabilization of the film is especially advantageous for the inner layer, which is responsible for the passivity of the surface in the presence of water. The beneficial changes are significant for Al contents higher than 4% wt Al in the alloy, and cause the sudden decrease in the corrosion rate observed in Figure 2.3:

However, alloying with at least 4% Al is necessary to obtain an oxide with optimum corrosion properties. Only at this threshold the Al_2O_3 component forms a continuous passivating network, which could be a skeletal structure in the amorphous mixture of aluminium and magnesium (hydr-)oxides. At around 4% of alloyed Al a threshold of 35% Al in the oxide film is achieved and further alloying does not enhance corrosion resistance significantly because the amount of Al in the oxide remains unchanged [Eli02].
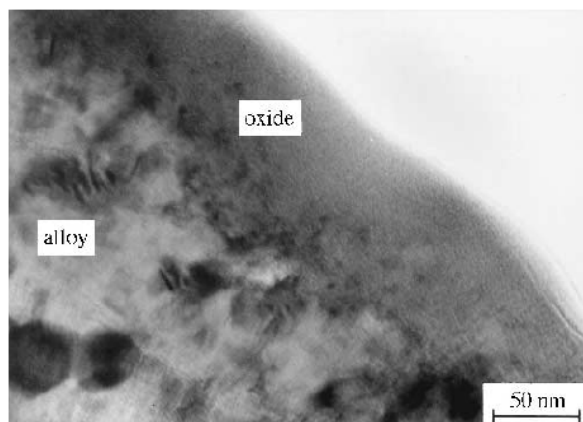
Figure 2.4: TEM cross section of an oxide film formed
naturally on AZ91 alloys exposed to the atmosphere [Eli02]

- *Magnesium aluminium alloys. Solid and liquid thermal oxidation*

As for the thermal oxidation of pure metals, oxidation of a bare alloy surface proceeds via a series of steps, such as chemisorption of oxygen molecules, oxide nucleation and growth. After the formation of a closed oxide film which covers the substrate surface, further oxide-film growth requires transport of species through the developing film towards the oxide gas interface and/or the metal-oxide interface.

Up to date, investigations on the thermal oxidation of binary and ternary alloys were mainly performed in solid alloys at high temperatures (i.e. T > 500ºC), presumably because these conditions are relevant for the application of alloys in high temperature-resistant coatings. At these high temperatures, local thermodynamic equilibrium generally prevails at the reacting metal/oxide, oxide/oxide and oxide/gas interfaces, and the thermal energy is sufficient to allow existing ions or electrons to surmount their energy barriers for movement into and through the developing oxide layer. Consequently, relatively thick (in the micrometer range) oxide scales, composed of multiple, crystalline oxide phases, develop on the alloy surface by sequential, preferential oxidation of the alloy constituents. Then, oxide-layer growth continues by solid-state diffusion of charged reactants through the developing oxide layer, under influence of (electro)chemical potential gradients [Vin06].

As with pure magnesium, the thin and protective oxide layer formed under ambient temperature is stable during heating at low temperatures (Figure 2.5.a).
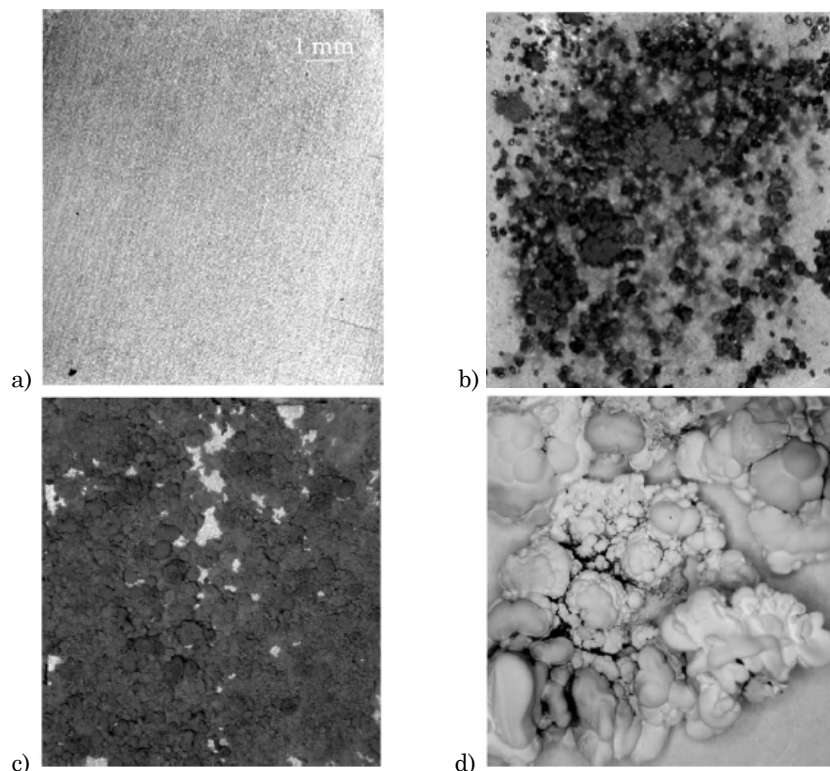
Figure 2.5: Macroscopic images of AZ91D alloy surfaces after air exposures: a) at 387ºC for 10 h b) 472ºC for 1 h c) 497ºC for 1 h d) 547ºC for 10 min [Cze02]

This film is protective up to 450ºC in case of pure Mg and Mg alloys that do not form a eutectic phase. However, most commercial Mg-Al alloys exhibit a different behaviour. Those alloys contain the $Mg_{17}Al_{12}$ eutectic phase in their microstructure and are protected by the oxide layer up to the first incipient fusion of the eutectic at 437ºC. At this temperature the first liquid phase appears, with high magnesium pressure, and the nodular growth is activated due to Mg evaporation. The protective film is destroyed and the so-called spongy growth of MgO oxide starts. The open nodules continue to grow by the transfer of Mg vapour through voids and simultaneous reaction with oxygen, forming a product with cauliflower-like morphology (Figure 2.5.b). Subsequent coalescence of the nodules leads to continuous ultra-fine grained and non-protective scales with a loose structure. Oxidation is intensified with time and temperature (Figure 2.5).

Above 437ºC, the degree of Mg volatility is so high that vapour does not only fill up all the pores in nodules but also fills the surface where the oxide films are formed. The selective oxidation of Mg results in the formation of an alloy depleted of Mg (i.e. rich in Al) as the oxide moves inwards to fill the space of the consumed metal [Med09, Cze02]. As proven by X-ray measurements performed by Czerwinsky, the oxidation of Mg to MgO is the predominant process and the direct reaction between Al and oxygen occurs only during combustion (Fig. 5b). During gradual oxidation, Al reacts to form $MgAl_2O_4$ spinel and this latter phase increases with the depth of the oxide film, in conjunction with the Al content [Jaf11, Shi07, Cze02]. Further growth of the oxide film depends on the selection of oxidizing components of the alloy that stimulate the reaction on the surface between the oxide and metal. Oxidation of this kind is destructive and usually leads to complete degradation of the material [Med09].
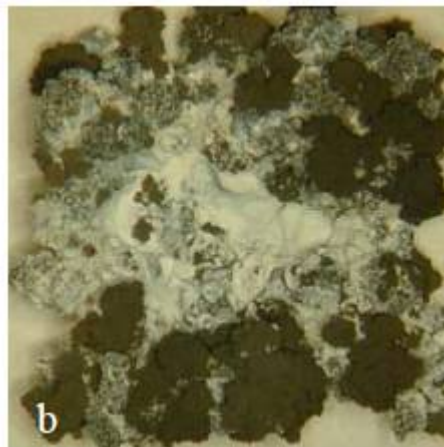
Figure 2.6: Product of alloy combustion [Cze02]

2.4 Magnesium melt protection: conventional methods

2.4.1 Introduction

During casting processes, excessive oxidation of the melt leads to increased costs due to metal losses. It also degrades the quality and performance of components produced [Hil02]. To process molten Mg safely and efficiently, the melt has to be protected either by exclusion of oxygen (e.g. covering with salt flux, CO_2 snow or inert gas) or by changing the nature of the surface oxide, to slow the oxidation rate down to an acceptable level (e.g. with a cover gas or addition of allowing elements). This surface film may have protective properties, and its efficacy varies mostly with the alloy, temperature and exposure time [Aar04].

2.4.2 Fluxes

The spread over the melt surface of fluxes (solid chemical powders) was the first protective medium employed to inhibit the oxidation of Mg melts. The protective effect of fluxes is achieved when they melt and form an impermeable layer of molten salts over liquid magnesium. A physical barrier between the metal and the atmospheric oxygen is formed, preventing the formation of MgO [Mil03].

Fluxes started being studied around 1940, when sulphur powders were employed to prevent oxide formation. But its employment was limited due to the toxic and corrosive nature of sulphur. Consequently, different flux compositions were developed, even achieving specific flux compositions for the different Mg alloys. Anyway, a general flux composition for Mg alloys would include 49% $MgCl_2$, 27% KCl, 20% BaCl2 and 4% CaF_2. The magnesium and potassium chloride salts provide a low-melting eutectic temperature, which guarantees that the salts will be melted far before the alloy, protecting the metal from the very beginning of the melting process. CaF_2 assures surface wettability and chemical reactivity with MgO on the melt surface, and barium chloride is used as the density component to ensure the mixing and sludging of the salts [Cas99, Eml66].

However, the disadvantages associated with the use of fluxes moved industry towards a flux free protection of molten magnesium. Flux itself oxidizes, and forms a thick and hard layer that cracks and re-exposes the melt to the atmosphere. It also leads to flux dust and fumes that release HCl and cause corrosion problems in foundries. Moreover, fluxes have a tendency to be mixed into the melt, forming later chlorine inclusions that accelerate corrosion mechanisms and reduce the quality of the casting part. In many cases, there is also unacceptable metal loss in the dross and flux sludge [Mil03, Fru69].

2.4.3 Sulphur dioxide

Due to the effectiveness of the initial sulphur fluxes, SO_2 cover gas atmospheres were tried next to as Mg melt protectors. The employment of SO_2 was a common practice in industry for several decades, as it is cheap and it can be easily extracted from gas mixtures due to its high solubility in water [Ha06a]. However, its use requires care, since SO_2 is toxic, corrosive and environmentally unacceptable: it contributes to acid rain.

One of the first works in SO_2, dated 1940, was performed by Schneider and Esch who protected effectively Mg melt under pure SO_2 atmospheres at 700°C [Sch40 in Cas99]. Nevertheless, due to its harmful character, following studies have employed gas mixtures of SO_2 and a carrier gas to reduce the SO_2 content. Concentrations and flow of SO_2 required to protect Mg melts effectively still vary considerably in literature. The reactions that undergo between SO_2 and Mg and form a protective film are also still not fully understood.

The early doctoral thesis of Fruehling compared the effectivity of SO_2 and SF_6, both diluted in air [Fru69 in Cas99]. Although this work is nowadays seen as mostly qualitative, Fruehling made some interesting conclusions. The author stated that a continuous supply of both inhibitors was needed to protect the melt of AZ91B alloy. Analysis by XRD of the surface film formed under SO_2 revealed that it was mostly composed of MgO, although traces of MgS could be found depending on the SO_2 concentration and the exposure time. The most important contribution of Fruehling, however, came after the comparison between SO_2 and SF_6. The author concluded that SF_6 was more effective than SO_2. Lower concentrations were needed to protect Mg when SF_6 was used, with the advantages of being non toxic and non corrosive. Due to this, next decades the focus of subsequent research was directed towards the use of SF_6.

After that, little research on melt protection under SO_2 mixtures can be found. Some years later, Aleksandrova and Roshchina also probed that SO_2 could effectively protect magnesium melt at 750°C. The theoretical reactions taking place at 600°C between Mg and SO_2 were expressed as follows by the authors [Ale77]:

$$\begin{cases} 2Mg + SO_2 \rightarrow 2MgO + MgS & \text{(a)} \\ MgS + 2SO_2 \rightarrow MgSO_4 + S_2 & \text{(b)} \end{cases} \qquad 2.5$$

However, at 750°C the author only found MgO and MgS on the melt surface. The authors point that this protective effect is due to the formation of magnesium sulphides, which blocks the defects in the film creating a coherent layer that prevents Mg evaporation.

Gjestland *et al.* proposed a three-step reaction mechanism for air/SO_2 mixtures, produced at 700°C (Figure 2.7). In the first step, a layer of $MgSO_4$ is formed according to Equation 2.6.a. Next, reaction

2.6.b occurs between the surface layer and liquid magnesium, producing MgS and MgO. Meanwhile, due to the high *PBR* of MgSO$_4$ (*PBR*=3.4), the surface oxide cracks and reaction 2.6.c provides the last step of the mechanism [Gje96].

$$\begin{cases} \text{Mg(l)} + \text{O}_2 + \text{SO}_2 \rightarrow \text{MgSO}_4(\text{s}) & \text{(a)} \\ \text{MgSO}_4 + \text{Mg(l)} \rightarrow \text{MgS(s)} + \text{MgO(s)} & \text{(b)} \\ \text{MgS(s)} + \text{MgO(s)} + \text{SO}_2 + \text{O}_2 \rightarrow \text{MgSO}_4(\text{s}) & \text{(c)} \end{cases} \qquad 2.6$$
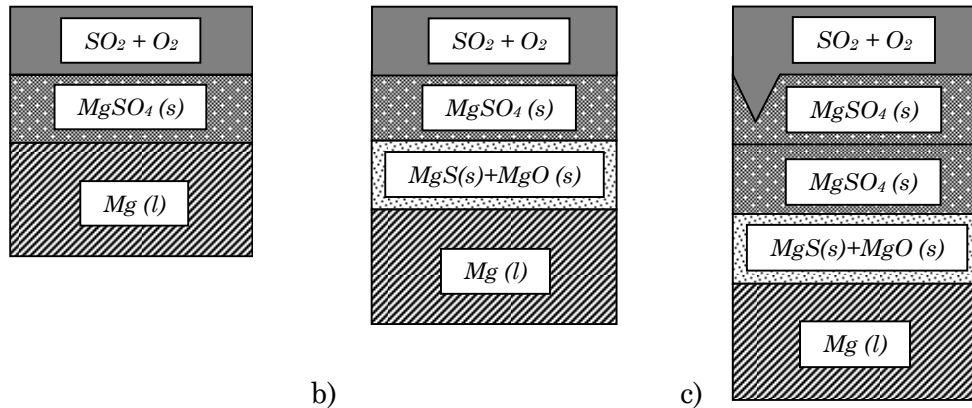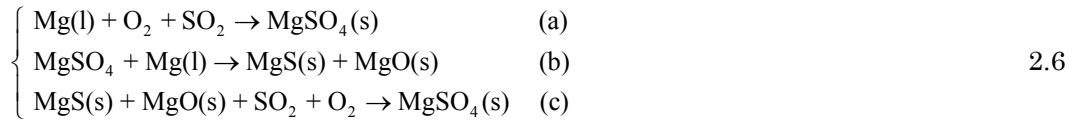
Figure 2.7: Schematic diagram of the three-step mechanism proposed by Gjestland *et al* [Gje96]

Proposal of Gjestland *et al.* for the layered surface film correlates with the experimental data of the XPS and Auger analysis performed by Cashion, who performed melt protection experiments at 700ºC under Argon/30%SO$_2$ and 100%SO$_2$ atmospheres [Cas99]. However, Cashion proposes a different configuration, where the initial MgSO$_4$ layer would be covered by an oxide film in the case of the Ar/30%SO$_2$ atmosphere (Figure 2.8). The Auger profile of the sample formed under 100%SO$_2$ suggests that also a MgS layer is formed between solid MgSO$_4$ and liquid magnesium (Figure 2.8.b).
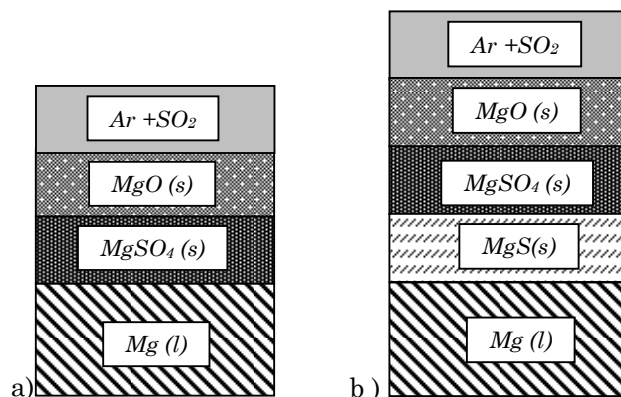
Figure 2.8: Diagram of the two-step mechanism proposed by Cashion [Cas99]

A more recent study conducted by Pettersen *el al.* studied the protection of pure magnesium in 1%SO$_2$/air atmosphere, at 700ºC. The authors state that the protective behaviour of the thin, dense

and continuous surface film is due to the formation of small grains of MgO, with sulphur dissolved on it. No independent sulphur compounds were found on melt surfaces [Pet02].
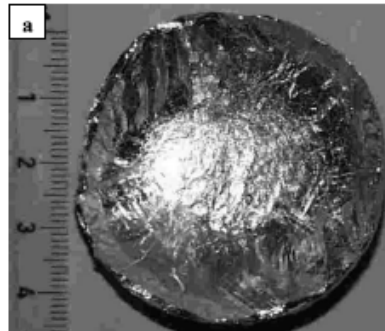
Figure 2.9: Surface film formed on molten magnesium at 700 °C after 2 min of exposure to 1% SO_2. The melt surface is shiny and metallic [Pet02]

In a more recent study, Wang *et al*. analyzed the surface films produced on AZ91D alloy under N_2/SO_2 and N_2/SO_2/air cover gases [Wan11]. Experiments performed in an open melting furnace, at temperatures lower than 700ºC. N_2/SO_2 atmospheres did not protect efficiently the melt surface and cauliflower-like MgO formed on the surface (Figure 2.10)
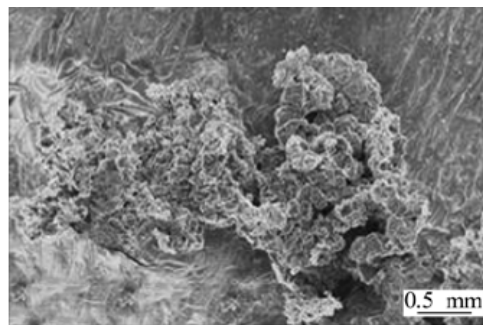
Figure 2.10: SEM micrograph of surface film (AZ91D, 680 °C, 4.0% SO_2+96.0% N_2, 60 min) [Wan11]

The cover gas containing SO_2 and air protected molten magnesium alloy efficiently. A coherent, protective film with a network structure composed of MgO was formed. With holding time, MgS particles also formed below the oxide film. The authors stated that, to build the protective film, a cover gas containing O_2 is needed to form the prior MgO compound. Later, SO_2 molecules diffuse through the porous MgO film and react with magnesium ions of the melt surface. The *PBR* combination of both compounds increases the value of the initial oxide film.

2.4.4 Sulphur hexafluoride

As early as 1934, Reimers suggested a number of fluorine compounds that could be used for magnesium melt protection [Rei34 in Cas99]. However, they were not extensively tested until the '70s, when the use of SF_6 in melt protection of magnesium spread after the work of Fruehling *et al*. [Fru69 in Cas99]. As commented before, SF_6 became the dominate cover gas agent in operations

using molten magnesium because of its several advantages when compared to SO_2: SF_6 is non-toxic, efficient, easily used in holding furnaces and in nearly all casting operations with pure magnesium and most of its alloys. However, although SF_6 was used for more than 3 decades, it was only recently that the mechanisms of protections were thoroughly investigated.

Fruehling *et al*. were the first to analyse the protective action of SF_6. The authors attributed the SF_6 protection mechanism to the formation of a thin and continuous reaction film that reduced further oxidation and vaporisation of the melt. The samples, analysed with XRD, revealed a film comprised mainly of MgO with traces of fluorine, so it was suggested that the protection mechanism of SF_6 was via gas adsorption onto the melt surface. According to the authors, the adsorbed gas boundary film would form a barrier to diffusion of oxygen and vaporisation of magnesium [Fru69 in Cas99].

Few years later, Couling studied the protection afforded by SF_6-containing atmospheres to melts of pure magnesium and AZ91B alloy [Cou79 in Cas99]. The author found that CO_2 additions improved the protective action of SF_6. In the experiments, Couling observed that all SF_6 was consumed and suggested two possible mechanisms: adsorption of SF_6 species into the MgO surface film and/or direct reaction of the gas with the melt to form MgF_2. The same year, Aleksandrova *et al* reported after a XRD analysis that the surface films formed on Mg under SF_6 were composed of MgO and MgF_2 [Ale77].

Since then, most of the authors have also reported that the protective layer is formed by a combination of solid MgO and MgF_2 crystals, without traces of other sulphur species [Xio10, Xio07, Ha06b, Aar04, Pet02, Cas02]. These authors assume that all the fluorine in the samples is bound as MgF_2, and all the oxygen as MgO. This assumption is supported by works that have analysed the ternary Mg/O/F system [Put88, Sha88 in Aar04]. According to them, this system is most likely to separate into the binary compounds MgO and MgF_2, rather than forming the Mg_2OF_2 ternary compound. However, it is still unknown to what extent magnesium fluoride may contain oxygen or magnesium oxide can contain fluorine. After decades of research, the mechanism that makes SF_6 protect Mg melts is not fully understood, although it is clear that fluorine plays the key role in melt protection.

- *The Protection mechanism*

Aarstad, Ha *et al* and Xiong *et al*. explain the protective behaviour by means of Pilling-Bedworth ratios [Aar04, Ha06b, Ha06a, Xio10]]. The authors consider that the protective behaviour of the surface is due to the formation of a dense film which combines MgO (*PBR* = 0.81) and MgF_2 (*PBR* = 1.45). This surface film is supposed to cover the melt and act as a barrier to further Mg oxidation, as MgF_2 increases the *PBR* closer to unity. Xiong *et al*. also noticed that, in the early stage of oxidation the surface films initially consist of small crystallites of MgO, due to the fast kinetics of the Mg-O_2

reaction [Xio10]. The authors believe that afterwards magnesium reacts to form MgF_2, increasing the value of the *PBR*. Accordingly, MgF_2 particles were found between the oxide film and the bulk Mg (Figure 2.11). The fluorine atoms are thought to diffuse through the porous surface film to the interface, and react there with the magnesium ions. This diffusion mechanism continues until the protective film is formed. At that moment, the diffusing inward-fluorine and outward-magnesium ions are blocked by the new MgF_2 particles [Xio10, Xio07].
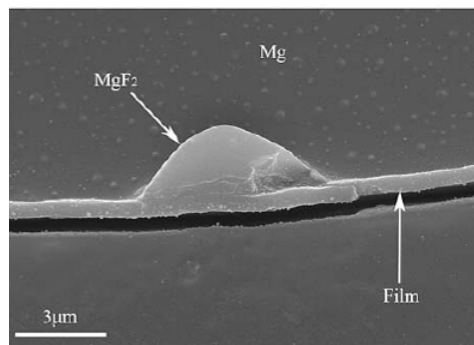
Figure 2.11: SEM image of a MgF_2 particle between bulk magnesium and uniform film. Cross section of the sample with 0.3%SF_6 produced at 650ºC for 10 min [Xio07]

This initial MgO layer had also been previously reported by Petttersen *et al* [Pet02]. Although both works suggest the inward diffusion of fluorine, in this work the authors believe that fluorine diffuse from the oxide film itself. Pettersen *et al.* proposed that while MgO is being formed, due to faster kinetics, SF_6 dissociates providing atomic fluorine. This fluorine could be present in the film as amorphous, at the oxide surface, or as a dissolved element in the MgO structure. The fluorine concentration would increase until a dense film of fluorine-containing MgO is formed, reducing the oxidation rate. Finally, MgF_2-phase grains would nucleate from the surface film and grow into the bulk magnesium, forming the innermost layer of large MgF_2 grains. The fluorine would diffuse inwards, and the oxygen is confined to a narrow band of small crystals as shown in Figure 2.12.
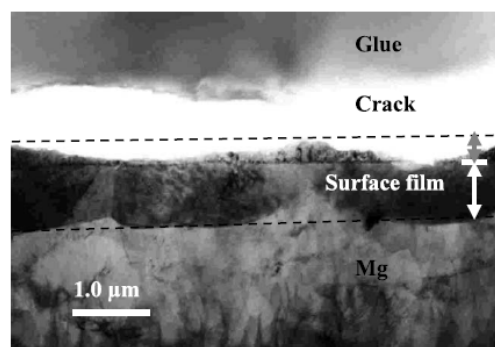
Figure 2.12: TEM micrograph from a sample exposed to 1% SF_6 in air for 20 min. The surface film has a innermost layer of large MgF_2 crystals (white arrow) covered by a very thin and straight fine-grained layer (white line) [Pet02]

Experiments performed by Aarstad resume four different situations that could lead to a protective film (Figure 2.13) [Aar04]. The explanations given by the author to describe these four situations could be considered as a join of the previous theories.
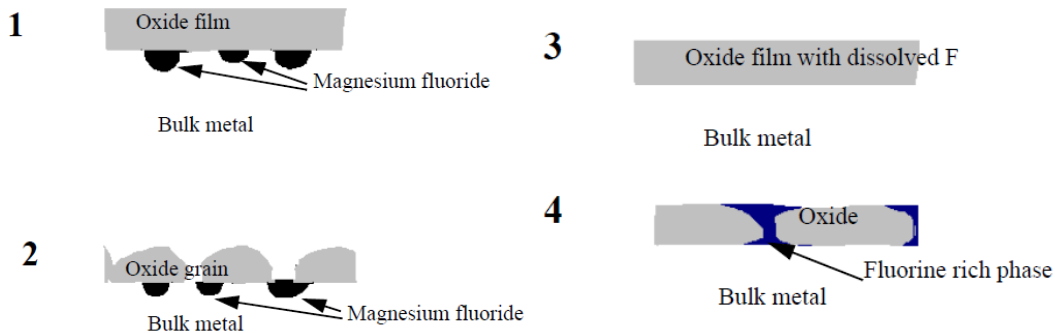
Figure 2.13: Illustration of the four different situations seen when Mg is exposed to SF_6 [Aar04]

The theory of Pettersen *et al.* of a first MgO film saturated in fluorine is also supported by Aarstad. The author opines that sometimes the MgF_2 particles nucleate underneath the oxides after the fluorine diffusion. The oxides on the melt surface may be present as a continuous film, as situation 1, or like larger oxide grains like in situation 2.

Situation 3 is when the film is composed of magnesium oxide grains with dissolved fluorine. The protective behaviour of this MgO film, unknown by Pettersen *et al.*, is explained by Aarstad due to an expansion of the magnesium oxide lattice, while it is built, in presence of fluorine. This modified oxide could have more volume than pure MgO, covering effectively the molten metal surface. Finally, in situation 4, a fluorine richer matrix would form in between the oxide grains to fill cracks in the initial oxide film. A continuous film with an average *PBR* of at least one is then formed, as stated by Ha *et al.* [Ha06b, Ha06a].

Cashion, unlike the previous authors, did not explain the protective action of the films by means of *PBR* [Cas99]. The author also found that liquid and evaporating Mg reacts primarily with oxygen to form a layer of MgO crystals. The protective action of this film, supposed to be loose and non-protective, is explained by the improved wetting between MgO particles and magnesium observed in SF_6 atmospheres in immersion experiments. Wetting causes the MgO particles to be attracted by capillary forces and form a dense, flexible surface film (Figure 2.14). After SF_6 decomposition, MgF_2 might also occupy sites within the product layer.
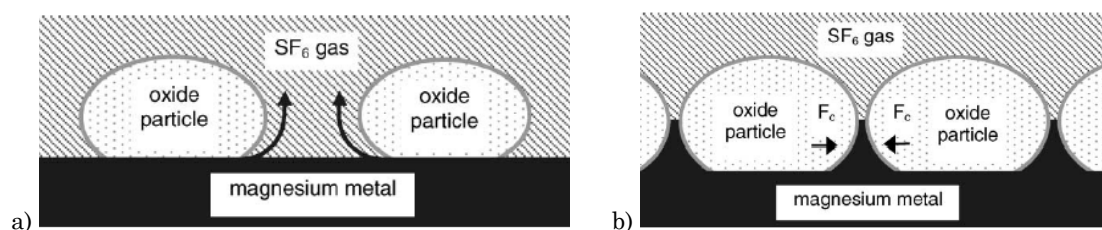
Figure 2.14: a) Wetting of oxide particles in the presence of SF_6 b) Oxide particles on molten magnesium, being drawn together due to capillary forces [Cas99]

It was previously commented that most of the authors have not found any sulphur species in the surface layer. However, in the work presented by Zhang *et al.*, the XPS results after only 3 minutes of exposure time revealed that MgO, MgF_2 and $MgSO_4$ chemical compounds were present in the protective film [Zha09a]. The authors opined that solid $MgSO_4$ later reacted with water vapour, and decomposed into H_2 and SO_4^{2-}. In fact, both gases were measured by gas chromatography (GC) and ion chromatography (IC). The authors also consider that the decomposition of $MgSO_4$ may cause the destruction of the protective film. Mirak *et al.* [Mir10] also analyzed the early stages of surface oxidation of liquid Mg, under various atmospheres. Under 3.5%SF_6-air, the EDS spectrum revealed the presence of the S peak. However, there is not any indication of the form that it takes. Cashion also detected sulphur in the samples. The XPS spectrums suggested the presence of sulphates in the samples produced under air/5%SF_6. No sulphur was found in the films formed under 0.1%SF_6, 0.3%SF_6 or 1%SF_6 so Cashion concluded that high SF_6 levels, and thus S levels, were needed for MgS to appear [Cas99]. On the contrary, the films produced by Zhang *et al.* were formed under 0.1%SF_6 air atmospheres [Zha09a].
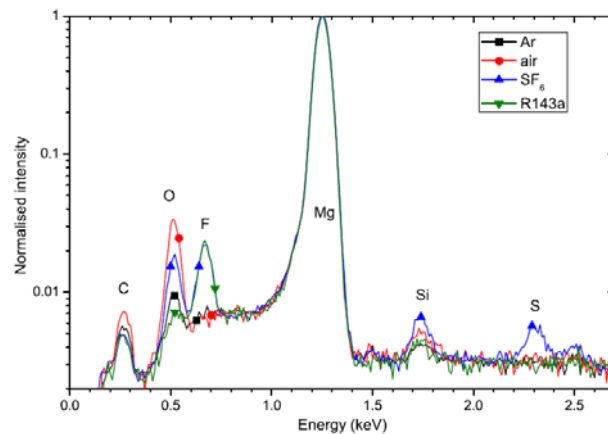
Figure 2.15: Representative EDS spectra (normalised to the Mg Ka peak) of Mg melt surface films obtained under different atmospheres. Results show the presence of S under the SF_6 atmosphere [Mir10]

- *Carrier gases*

SF_6+Air or SF_6+Air/CO_2 atmospheres were used in high-pressure casting for more than 20 years. The employment of only pure CO_2 as a carrier gas implies the formation of a dark and poor quality film over the melt, probably due to soot formation [Aar04, Arg03]. The works by Tranell *et al*, Argo *et al.* and Hillis declare that a better protection is achieved when using CO_2/Air carrier gas, instead of 100% dry air [Tra04, Arg03, Hil02]. When 100% air is used, the MgO oxidation is not limited by the oxygen supply, as too much O_2 is present. To overcome this situation, higher SF_6 % is needed to form the protective film [Tra04]. Zhang *et al.* also found that, aside from the SF_6 increase due to the melt temperature, the dew point of the carrier air also affects the efficiency of the gas mixture to protect molten AZ91 magnesium alloy [Zha09a]. As expected, more SF_6 is needed to prevent burning of molten Mg alloys at higher humidity levels.

Tranell *et al.* also observed that, with 100% air atmospheres, a raise of the melting temperature provokes a considerable increase of Mg oxidation kinetics. Due to this, they concluded that air is not a suitable carrier gas at temperatures higher than $700^{\circ}C$, as too much SF_6 is needed to protect the melt. This last conclusion is also held by Hillis [Hil02] and confirmed by Argo and Lefebvre [Arg03]. Argo *et al.* also employed dry air-SF_6 mixtures to melt AJ52 alloy at $720^{\circ}C$ with bad results.

Pettersen *et al.* probed that, in N_2 atmospheres, SO_2 and SF_6-additions did not protect magnesium [Pet02]. According to the protection mechanism presented by the authors, a rapid initial formation of MgO is necessary to obtain protective films. The unsatisfactory experiments performed by Aarstad, where SF_6 was tested under nitrogen and argon atmospheres, support this theory [Aar04]. Pettersen *et al* also stated that, for fluorine to enter the MgO film, the larger molecules of SF_6 must first dissociate to form smaller and more reactive fluorine species like F or F_2, as in Equation 2.7. The speed of the dissociation reactions is the upper limit to the formation rate of MgF_2, and favours the formation of MgO in the early stages.

$$SF_6 \rightarrow SF_4 + nF + \left(1 - \frac{n}{2}\right)F_2 \qquad\qquad 2.7$$

This observation is in agreement with the formation mechanism presented by Cashion in his PhD thesis [Cas99]. He suggested that, while SF_6 decomposes to SF_4, F and SO_2F_2, the liquid and evaporating magnesium reacts primarily with oxygen to form MgO, and later with the fluorine to form MgF_2. According to this author, this vapour phase crystal growth would explain the irregular topography of the produced surface film, with fibrous formations in random orientations. SF_4 can also react with oxygen, forming SO_2F_2 and liberating further fluorine to form MgF_2. Figure 2.16 illustrates this mechanism, proposed for the production of protective surface films in air/SF_6 mixtures.
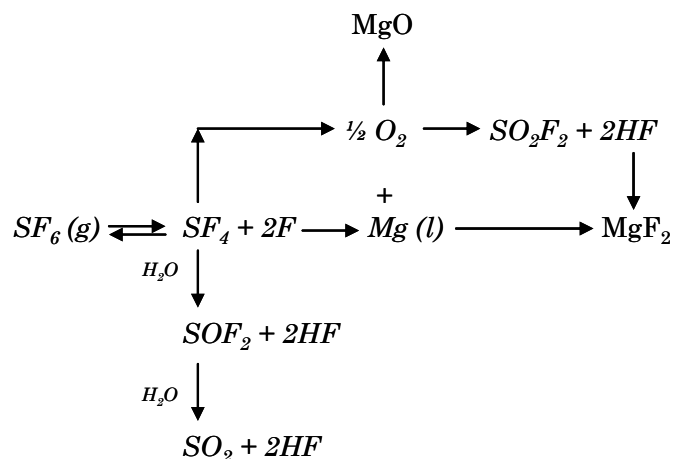
Figure 2.16: SF_6 decomposition mechanism. Formation of protective MgO and MgF_2 surface film [Cas99]

- *Influence of Experimental Factors on the film composition*

Xiong *et al.* [Xio07] found that the compositions of the cover gas, melting temperature and holding time were the three most important factors which could visibly affect the surface films. By keeping two of the three parameters constant and changing the other one, the authors obtained the trend of the reaction (Figure 2.17).
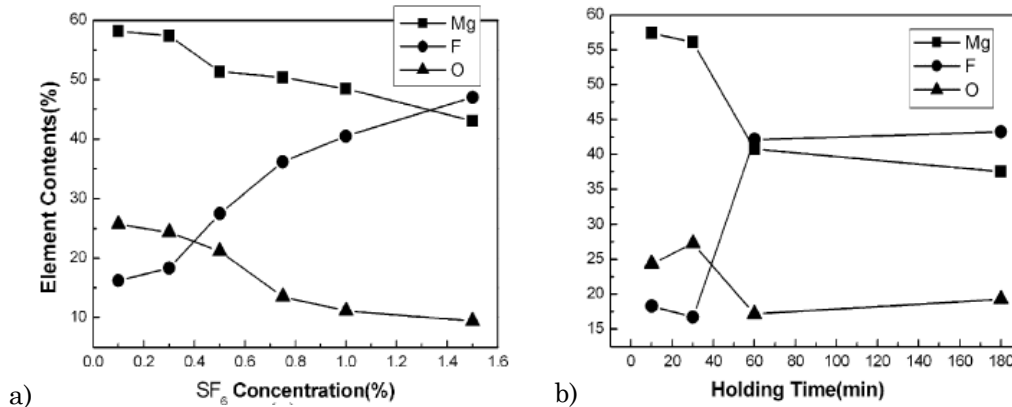
Figure 2.17: Composition of films produced under different experiment conditions, analysed by AES (Auger electron spectroscopy) a) holding time: 10 min, temperature: 650ºC b) 0.3% SF_6, 650ºC

Figure 2.17.a shows the changes in the element concentration of the film when the SF_6 % is increased. Results show that concentrations of Mg and O elements decrease, while the concentration of F (and thus of MgF_2) increases with the SF_6 concentration. Therefore, so does also the inhibitor effectiveness. This effect has also been reported by several authors [Ha06b, Cas99]. Ha *et al.* also found that, despite of the changes in element concentration, the *PBR* of the surface continued maintaining a value close to one, as shown in Figure 2.18 [Ha06b].
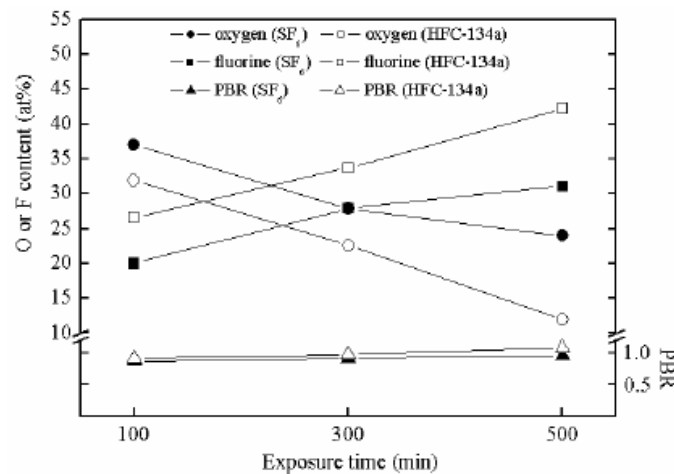
Figure 2.18: *PBR* as a function to SF_6 and HFC-134a gas exposure time [Ha06b]

Figure 2.17.b shows the element % vs. holding time. Results show that, while the amount of Mg and O decreases, the amount of fluorine in the surface film also increases with the holding time [Xio07].

In another work, Xiong *et al.* also reported the time-depending increase of fluorine and related it to variations in the surface morphology of the films (Figure 2.19) [Xio10].
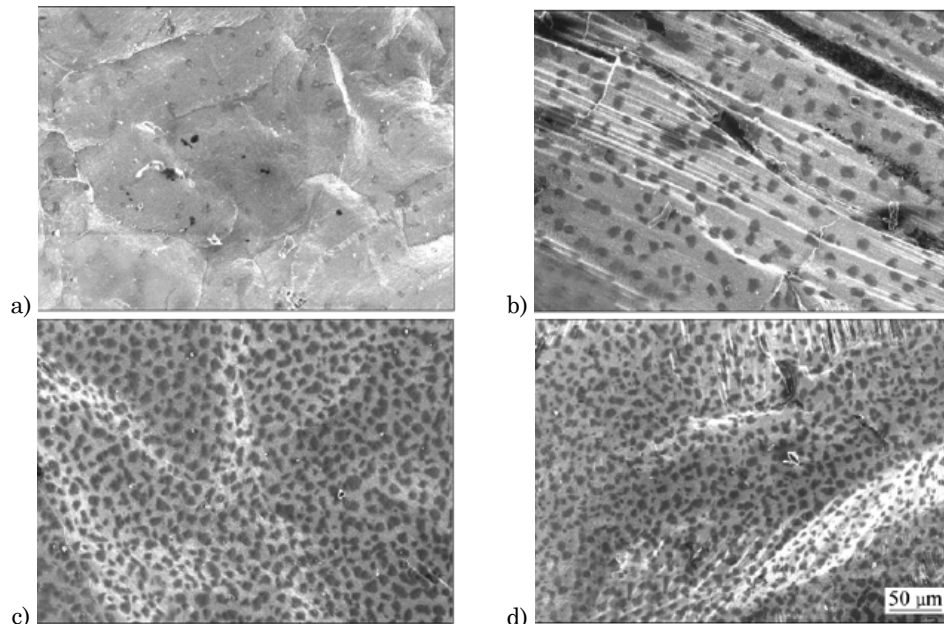
Figure 2.19: SEM images of surface morphology in samples protected under 0.1% SF_6 at 680ºC for different exposure times: a) 3 min b) 10 min c) 30 min d) 60 min [Xio10]

2.5   Magnesium melt protection: alternatives to SF_6 and SO_2

2.5.1 Introduction

The last decade growth in Mg die cast alloy volume has mainly been motivated by automotive industry. The employment of low density materials was encouraged by the requirements to reduce the impact of vehicles' CO_2 emissions on Global Warming. Before that, during the 80-90's, while the greenhouse gas emission reduction was focused on CO_2, NO_x, and methane a continued growth in Mg automotive applications happened. In 1994, environmental scientists of the International Panel on Climate Change added fully fluorinated chemicals to the list of greenhouse gases of concern [Hou94]. A number of very stable fluorocarbon compounds were included, but the SF_6 molecule had the distinction of possessing the highest global warming potential (GWP) of any compound identified to-date: On a 100 year time frame, its GWP was reported to be 23,900 times that of CO_2.

In a lifecycle analysis of vehicles this large GWP, associated with the emissions from Mg melt protection, negates much of the advantage of the magnesium weight saving. Due to this, the Magnesium Industry recognized the need to eliminate SF_6 from the production and processing of the alloys, and started searching for alternatives [Hil02]. The requirements for a gaseous cover gas for magnesium melt protection are [Ric01]:

o Protection for pure magnesium and a wide range of alloys

o Low global warning potential

o Zero ozone depletion potential

o Safety and non-toxicity at room temperature

o Non-flammability

o Minimal (or manageable) toxic thermal decomposition products

o Non-corrosive behaviour at room and molten metal temperatures

o Reasonable price

o Available worldwide from more than one supplier

Unfortunately, the SF_6 replacements that existed at that moment were only those that had been generally abandoned with good reason in the early 70's: salt fluxes or SO_2 blends with air. Consequently the following years the efforts were conducted to identify new melt protection alternatives with low toxicity and limited environmental impact [Hil02]. Table 2.3 resumes the Global Warning potential of those new gases.

Table 2.3: Lifetimes and global warming potentials of SF_6 replacements [Xio10, Mil03, Hil02]

Formula	Lifetime (years)	GWP	Name
CO_2	100-150	1	
SF_6	3200	23900	
C_3F_8	2600	8600	PFCs
C_4F_{10}	2600	8600	
C_6F_{14}	3200	9000	
CF_3CH_2F	13,6	1600	HFC-134a
$C_4F_9OCH_3$	-	-	HFE7100
CF_3CHF_2	32,6	3800	
CHF_3	243	14800	
SO_2F_2	-	1	
$C_3F_7C(O)C_2F_5$	0,014	1	KFs

While the other fluorinated materials previously suggested in the 70's are highly toxic, others such as perfluorocarbons (PFCs) are safe and nearly as stable as SF_6. Unfortunately, this stability is associated with a high GWP, which eliminates them as replacements. Hydrofluorocarbons (HFCs) and HFE7100, introduced as replacements for CFCs to eliminate ozone destruction, are safe and they were shown to be useful in protecting magnesium, but they also have significant GWP [Mil03]. Due to this, they were used only like transitional substitutes for SF_6. Sulfuryl Fluoride, SO_2F_2, possesses a low GWP and has also been found effective in melt protection but this compound is toxic. Its principal

commercial use is as termite fumigant [Hil02]. Recently, another class of fluorinated materials, fluoroketones ($C_3F_7C(O)C_2F_5$), were introduced with a global warming impact similar to that of CO_2 [Mil03]. Further details about HFCs and FK are given below. Table 2.4 shows the characteristics of the new inhibitor gases.

Table 2.4: Characteristics of new inhibitor gases [Ha06a]

Gas	Formula	Boiling point (°C)	Toxicity	Thermal decomposition products	Corrosion Property
SF_6	SF_6	-64	Non-toxic	SF_x, SO_x	Non-corrosive
HFC-134a	CF_3CH_2F	-26.5	Slightly irritating	HF, PFC	Non-corrosive
HFE7100	$C_4F_9OCH_3$	61	Non-toxic	HF, PFIB	Non-corrosive
Novec™ 612	$C_3F_7C(O)C_2F_5$	49	Non-toxic	HF	Non-corrosive
Sulphuryl Fluoride	SO_2F_2	-55.4	Toxic (inhalation)	SO_x	Non-corrosive
Sulphur dioxide	SO_2F_2	-10	Toxic	SO_x	Corrosive

General physical state of HFE7100 and Novec™ 612 at room temperature is liquid. SO_2 is extremely toxic, HFC-134a and sulphuryl fluoride are slightly toxic, and the other gases are non toxic. All gases are non corrosive except SO_2. However, at molten magnesium temperature, highly corrosive hydrogen fluoride can be formed from HFC-134a, HFE7100 and Novec™ 612 by thermal decomposition. HF also can be produced from SF_6 and sulphuryl fluoride by water reaction. However, it can be reduced by controlling the moisture of the inhibitor or the carrier gas [Ha06a].

2.5.2 HFC-134a

HFC-134a is a hydrofluorocarbon commonly used as a refrigerant in vehicle air conditioners. The compound has several manufacturers but its use as a magnesium protectant is patented by the Australian Magnesium Corporation (AMC) [Tra04]. HFC-134a cannot be mixed with air, as HF is formed causing severe problems for magnesium melting devices. Suitable diluents, such as N_2 or CO_2 should be used for the use of HFC-134a as an inhibitor gas [Ha06b].

The studies on the films formed under SF_6 and HFC-134a agree in the key role of MgF_2 to protect the melt. Unlike with SF_6, it is widely accepted that the protective mechanism is due to an increase in the *PBR* of the surface, which creates a dense and protective layer [Ha06b, Che06, Ha06a, Tra04]. In fact, HFC-134a gives better protection than SF_6 for Mg and Mg alloys melt protection under identical essay conditions. Lower flow rates and inhibitor concentrations are needed to protect melt surfaces [Mir10, Ha06b, Tra04, Hil02].
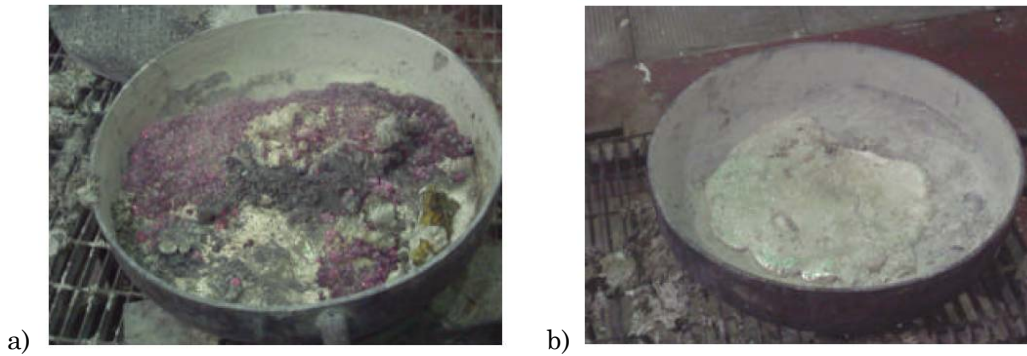
Figure 2.20: Difference in dross formation under SF$_6$ and HFC-134a cover gas mixtures, where the improved efficiency of HFC-134a is seen [Ric03]

Differences between SF$_6$ and HFC-134a arise from the fact that HFC-134a provides fluorine easier than SF$_6$. Thermal decomposition of SF$_6$ starts from 800 ºC but that of HFC-134a starts at 250 ºC, although the decomposition tendency also depends on the moisture content of the atmosphere and the presence of catalytic materials [Ha06b]. Due to this, the films formed under HFC-134a contain a higher proportion of magnesium fluoride [Ha06b].

These statements are in agreement with the results presented by Mirak *et al*., who examined the early stages of surface oxidation of liquid Mg through the introduction of cover gases via bubble stream into the melt. After the surface analysis of the films formed under HFC-134a, the authors observed that the film was predominantly MgF$_2$, with a small amount of MgO. Thus, it was suggested that the reaction under this cover gas with fluorine must be quite rapid, suppressing oxide formation at a very early stage [Mir10].

This low MgO concentration on the protective films has also been reported by Liu *et al*, Zhang *et al* and Chen *et al*. [Liu09, Zha09b, Che10, Che06]. The XRD measurements of the protective films performed in these four works did not reveal the presence of MgO for samples protected in atmospheres with >%1 HFC-134a. However, XPS measurements performed by Liu *et al* of these samples revealed the presence of MgO, indicating that MgO is present but in such a low content that the XRD technique cannot reveal it [Liu09].
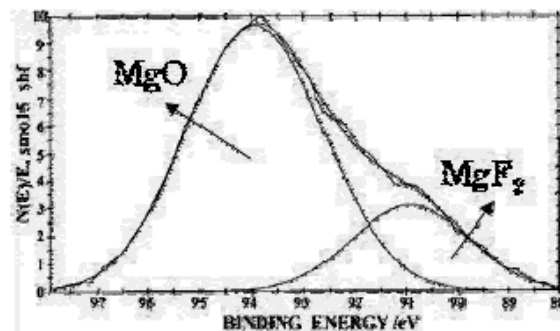
Figure 2.21: XPS Mg 2s spectrum. The lower binding energy peak is assigned to MgO and the higher binding energy peak to MgF$_2$ [Liu09]

Morphology of the film varies depending on the author. Ha *et al.* [Ha06b] stated that it consists of MgO and MgF_2 in a fine-grained and dense layer. Chen *et al.* [Che06] stated that it mainly consisted of MgF_2, MgO and C, but that MgF_2 was predominant at the top layer and decreased gradually with depth while MgO and C held constant in small amounts. According to Chen *et al.*, the reactions that take place under HFC-134a can be summarized as follows:

$$\begin{cases} C_2H_2F_4(g) \rightarrow 2C(s) + 2HF(g) + F_2(g) & \text{(a)} \\ Mg(l) + F_2(g) \rightarrow MgF_2(s) & \Delta G_2^0 = -1120000 + 171.2T & \text{(b)} \\ Mg(l) + \frac{1}{2}O_2 \rightarrow MgO(s) & \Delta G_3^0 = -612955 + 128.08T & \text{(c)} \end{cases} \qquad 2.8$$
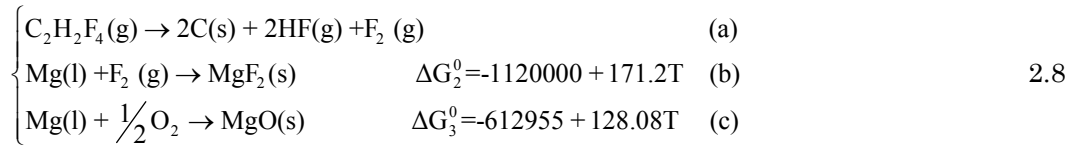
Since MgF_2 is more stable than MgO, (Equations 2.8.b and 2.8.c), as soon as the Mg surface is covered by HFC-134a thermal decomposition gaseous products, MgF_2 forms prior to MgO in the outer layer, making the film dense and compact. However, the formation of MgO seems to be faster so when molten Mg is exposed to a HFC-134a+O_2 gas mixture, Mg rapidly reacts with oxygen to form a thin film of MgO. Mg vapour diffuses outwards through the loose MgO film and reacts with F_2 to form MgF_2 within the film. This theory is also held by Liu *et al.* and Zhang *et al.* [Liu09, Zha09b]. Both authors analyzed the compounds that are formed on the surface of pure magnesium and AZ91E alloy. Table 2.5 resumes the compounds formed on both melts, depending on the HFC-134a % in air:

Table 2.5: Films under various HFC-134a % at 760ºC. Phases are listed in relevancy order [Zha09b]

% HFC-134a	Films on pure Mg		Films on AZ91E	
	XRD	XPS	XRD	XPS
5	MgF_2		MgF_2,C	
3	MgF_2		MgF_2,C	
1	MgF_2	MgF_2,MgO, C,CO,CO_2	MgF_2,C	MgF_2,Mg(OH)$_2$,MgO C,CO,CO_2
0.1	MgF_2,MgO		MgO,Mg_3N_2,AlN,MgF_2	
0.01	MgO, MgF_2,C		MgO,Mg_3N_2,AlN,$MgAl_2O_4$	
0.001	MgO,Mg_3N_2		MgO,Mg_3N_2,AlN,$MgAl_2O_4$	

Table 2.5 shows that oxidation products are different depending on the HFC-134a concentration. As HFC-134a % increases, the amount of MgF_2 in the film also increases and the Mg oxidation rate decreases. The carbon in the film also plays an important role. The decomposition of HFC-134a gas might produce C, according to reaction 2.8.a. This carbon, mainly in the film as a simple substance, fills up the holes of MgO making the film more compact. Surface films on molten AZ91D alloy in the air containing high concentration of HFC-134a were mainly composed of MgF_2 and C with small amount of MgO and AlF_3. The presence of AlF_3 and C makes the film denser and more compact compared with the molten magnesium film. So the oxidation rate of AZ91D alloy in air atmospheres with high concentrations of HFC-134a is lower than that of magnesium in the same atmospheres. According to Liu *et al* and Zhao *et al*, at low inhibitor concentrations the surface film is also composed

of Mg_3N_2 and AlN. As the atmospheric O_2 content decreases near the film due to the metal oxidation, the N_2 concentration increases. However, the authors considered that the effects of the nitrides on the oxidation behaviour of molten AZ91D alloy could be negligible [Liu09, Zha09b].

2.5.3 Fluoroketones

This compound is mainly targeted at fire fighting applications but manufactured as licensed for use as magnesium protectant by 3M®. Fluoroketones (FK) are liquid at room temperatures but they can be evaporated into a carrier gas stream. When compared to SF_6, FK are much less stable: FK undergo significant thermal degradation at Mg melting temperature, whereas SF_6 is thermally very stable up to 800°C. In fact, only a small portion of the SF_6 in the cover gas mixture actually reacts with Mg, and a significant amount is emitted to the atmosphere unchanged. Fluorinated ketones degrade at surface temperatures above 550°C, so they react faster than SF_6 with Mg to form MgF_2. In addition, they also contain more F atoms per molecule than SF_6, so more fluorine is available per molecule to form protective MgF_2. Due to this, FK have probed to be more efficient (lower use rates for equivalent protection) in the experiments performed on magnesium and some selected alloys by Milbrath *et al.* [Mil03] and Tranell *et al.* [Tra04]. Tests performed in both works have given very good results. To understand the chemical reactions that occur, Milbrath *et al.* analysed the gaseous products formed after thermal degradation of fluoroketones, as it can be seen in Figure 2.22.
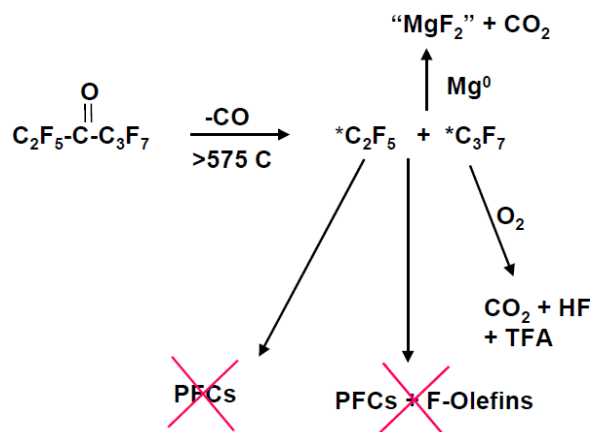
Figure 2.22: Reactions of FK over molten magnesium [Mil03]

According to Figure 2.22, FK begin to thermally degrade at 550-575°C. The fluorochemical fragments remaining (fluoroalkyl radicals) are very reactive and will be totally consumed by unprotected magnesium surfaces and magnesium vapours, producing MgF_2 and CO_2. Once the protective film is formed, less Mg is available and the fluorochemical radicals may undergo additional reactions producing perfluorocarbons (PFCs, high GWP) and fluoro-olefins (F-olefins, some are toxic). However, the authors mention the possibility of adding small additions of dry air (1-5%) to the CO_2 carrier. If there is sufficient O_2 present in the cover gas mixture, the radicals appear to oxidize forming HF, CO_2, and possibly some trifluoroacetic acid (TFA) that consumes the radicals.

2.5.4 Inert gas atmospheres

Magnesium melt protection by inert atmospheres, such as N_2, He or Ar, is not possible. As these atmospheres do not contain oxygen, burning of magnesium melt is prevented but no protective surface layer is created on the melt. This means that magnesium evaporation is not avoided, taking place an undesirable loss of material. The early attempts of Aleksandrova *et al.* already proved that a pure nitrogen atmosphere does not protect magnesium melts, due to the formation of Mg_3N_2 phase which does not prevent Mg evaporation [Ale77]. Latter works, as the ones performed by Cashion *et al.* and Tranell *et al.* have confirmed these results [Tra04, Cas02]. Surface layers formed under an Ar/N_2 mixture were a conglomeration of spherical particles that formed a weak and non-adhesive film.

- *CO_2 atmospheres*

Fruehling *et al.* were the first who concluded that an atmosphere of pure CO_2 could protect molten magnesium [Fru69 in Cas99]. Aleksandrova *et al.* were also able to build a protective film in CO_2 (or CO_2/inert gas) atmospheres. A protective mechanism is achieved when a dense layer of soot is formed on the melt surface. The authors described the interaction between Mg and CO_2 as follows [Ale77]:

$$2Mg + CO_2 \rightarrow 2MgO + C \text{ (soot)} \qquad\qquad 2.9$$

However, Aarstad in his thesis concluded that too little work on CO_2 as protective atmosphere was performed to affirm that this inhibitor is an adequate melt protector. The author points that soot formation should be solved before the industrialization of CO_2, as it may form an undesirable black surface on the casting [Aar04].

A work by Bach *et al.* suggests the use of CO_2 snow instead of gaseous CO_2, to prevent the formation of CO and soot. Authors state that, when enough CO_2-snow is deposited on the melt surface, the temperature and the oxidation kinetics of the surface are reduced. Additionally, sublimation of the CO_2 snow displaces the atmospheric O_2, protecting the melt surface [Bac04].

2.5.5 Boron trifluoride

BF_3 gas is well known as an efficient Mg melt protector since the 70's. However, the storage of compressed gas and its expensive price discarded its industrialization since the very beginning. A recent method called the Magshield system, presented by Revankar *et al.* produces BF_3 in situ by KBF_4 thermal decomposition [Rev00]. As BF_3 is also considered as a highly toxic compound, this system is sealed to prevent BF_3 leakages. The authors protected the AM60B alloy with varying amounts of BF_3 (0.3-1.0 % volume) in dry air with results qualified as excellent. Melt protection lasted for 45 minutes after the gas was shut of, whereas with SF_6 it lasted for 30 minutes. However, BF_3 concentrations smaller than 0.5% gave a discoloration of the melt surface.

2.5.6 Addition of elements to the melt

- *Beryllium*

Zeng *et al.* [Zen01] performed a thorough study of the oxide film formed on a molten Mg-9Al-0.5Zn-0.3Be alloy, AZB910 alloy. They stated that the oxide film is protective and can increase the oxidation resistance of magnesium alloys so greatly it that can be melted in the atmosphere without further protection. The analysis of the surface film of AZB910 alloy exhibited a duplex structure, where the outer layer consisted of MgO and the inner layer, of a mixture of MgO and BeO. The authors proposed the following oxidation sequence for the molten AZB910 alloy, described by Equation 2.10:

$$\begin{cases} Mg + \frac{1}{2}O_2 \rightarrow MgO & (a) \\ Be + MgO \rightarrow Mg + BeO & (b) \end{cases} \qquad 2.10$$

Firstly, fast reaction between magnesium and the absorbed oxygen takes place at the air/alloy interface, forming a MgO thin film. This period is regarded as the interface reaction period, described by Equation 2.10.a. Secondly, the rapid growth period comes. During this period the outer layer grows mainly by the reaction between diffused Mg^{2+} and oxygen at the air/oxide interface. With the growth of the outer layer, magnesium is depleted and thus beryllium enriched in the melt surface. When beryllium reaches a certain concentration, BeO is produced according to Equation 2.10.b. Therefore, a uniform and dense inner layer that contains MgO and BeO is formed, which acts as a barrier to the magnesium diffusion and protects the melt. This oxidation period is regarded as the slow growth period (Figure 2.23).
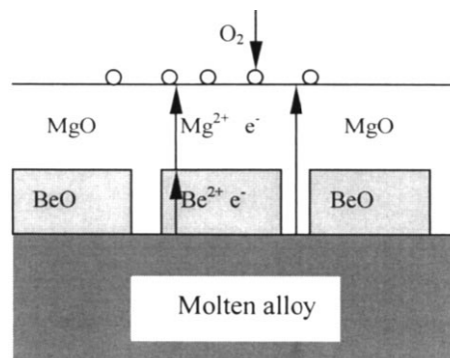
Figure 2.23: Oxidation model for molten surface of Mg–9%Al–0.5%Zn–0.3%Be alloy [Zen01]

However, there is a disadvantage to this method. To protect the melt, beryllium oxide must be formed, and the dust of the BeO is poisonous if inhaled, although concentrations of BeO under 0.002 mg/m^3 in working atmospheres are considered secure [Aar04]. High Be concentrations on the alloys also decrease their mechanical properties [Lee08].

- *Calcium*

Ca additions to magnesium alloys are also effective to suppress melt oxidation. Choi *et al.* [1273], for example, studied the effect of Ca additions on oxidation resistance at elevated temperatures. The authors probed that Ca additions increase the ignition temperature of AZ91E magnesium alloy. In addition, they found that the oxidation rate of the melt also decreases considerably, due to the formation of a compact and protective surface film. This film possesses a two layered structure where the outer mainly consists of CaO, but the inner is a mixture of CaO, MgO and Al_2O_3.

Kim *et al.*, in fact, compared the oxidation resistance of Mg-Ca and Mg-Ca-Al alloy. They concluded that the addition of aluminium increases even more the oxidation resistance due to the presence of Al_2O_3. They also studied the effect of protecting those two alloys under various inert gases, and found that N_2 was more effective than CO_2. The film formed on Mg-Ca alloy under N_2 was composed by a mixture of CaO, MgO, Ca_3N_2 and Mg_3N_2. This dense film was so thin that no layered structures were detectable by XRD. On the other hand, the film formed under CO_2 was thicker and here the two layered structure was visible. The upper layer was composed of CaC_2 and Mg_2C_3, whereas the inner one of CaO and MgO [Kim03].

However, Ca addition for melt protection also has its disadvantages: Ca is expensive and difficult to handle, due to its high reactivity under ambient atmosphere. Moreover, Ca decreases fluidity and increases hot tearing susceptibility during casting processes [Lee08].

- *Calcium and beryllium*

The behaviour of the oxidation of molten AZ91 alloys containing both Ca and Be was studied by Choi *et al.* [Cho06]. Oxidation test were performed on AZ91, AZ91-2Ca and AZ91-2Ca-0.06Be alloys at 670ºC for 10 min. Results show that the combined addition of Ca and Be is more effective than only Ca for the suppression of the ignition of the molten alloys (Figure 2.24). In addition, the surface film formed on the AZ91-2Ca alloy was loose and thicker, whereas the Ca+Be alloys had very small oxide particles, and the oxide layer was compact and dense (Figure 2.25).

Figure 2.24: Surface s after the oxidation treatment of: a) AZ91 b) AZ91-2Ca c) AZ91-2Ca-0.06Be [Cho06]

Analysis of the surface film formed on the AZ91-2Ca-0.06Be alloy indicated that the oxide layer exhibits a complex three-layered structure. The uppermost surface layer consists of CaO, the middle layer is a mixture of CaO, MgO, and BeO, and the inner layer is composed of Al_2O_3 [Cho06].
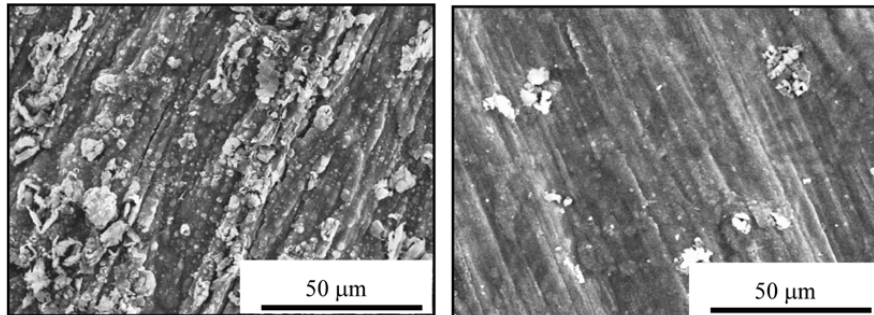
Figure 2.25: Surface morphologies of AZ91 alloys containing Ca and Be after oxidation treatment of: a) AZ91-2Ca b) AZ91-2Ca-0.06Be [Cho06]

- *Fluorine Saturation of the melt*

The method of protecting magnesium melt by fluorine saturation was firstly tested by Cashion in his doctoral thesis [Cas99]. Cashion bubbled 100% SF_6 through a AM60B melt for 10 min and exposed the melt to ambient air atmosphere. Surface burning was prevented for 60 minutes and large quantities of fluorine where detected in the samples. However, the author admits that this protective effect may be more due to the use of an alloy that contains 11ppm of beryllium. In another experiment, Cashion introduced a molten eutectic mixture of KF and AlF_3 salts in the melt. It was protected for 10 minutes but the analysis of the surface revealed also the presence of K and Al. According to Cashion, this may indicate that the salts, rather than dissolving fluorine, behaved as molten flux on the melt surface.

With the same aim, Aarstad studied the fluorine solubility in pure magnesium by melting Mg in a MgF_2 crucible. Although MgF_2 particles were found in samples extracted from the melt, Aarstad concluded that the solubility of fluorine at 700ºC is so low that the melt surface cannot be supplied with the necessary fluorine amount [Aar04]. Tranell *et al.*, on the other hand, also measured the fluorine solubility by the same method but they concluded that the dissolved fluorine should be enough to supply the metal surface [Tra04]. Two different experiments were performed, introducing MgF_2 and AlF_3 powder pressed briquettes in the melt but no protection was achieved by any of the procedures. Due to this, the authors stated that the mechanisms through which fluorine-containing gases form the protective films seem to happen in the gas phase. These fast, chemical vapour deposition to form MgO and MgF_2 seem to be instrumental for the melt protection.

2.6   Investment casting: a brief introduction

2.6.1 Introduction

Investment casting of magnesium is a process well suited for the production of aeronautic and automotive components, as light density components in medium and small series are obtained. Components of any shape or complexity can be made, such as turbine blades, with very high precision. Moreover, near net shape castings are produced, eliminating expensive finishing costs. Although castings of 20 kg or more are routinely produced, it is the tiny castings (10-20 grams) that are literally unique in this process [Sha04].

In investment casting, ceramic slurries are applied around a disposable wax pattern, and allowed to harden to form a disposable casting mould. The term disposable means that the pattern is destroyed during its removal from the mould and that the mould is destroyed to recover the casting. The principles can be traced back to 5000 BC, when Early Man employed the method to produce rudimentary tools. This was followed by centuries of use in jewellery and artistic products, before the advent of the 2nd World War saw the development of aerospace and subsequently engineering components. There are two distinct processes for making investment casting moulds: the solid investment process (Shaw mould) and the ceramic shell process. The ceramic shell process has become the predominant technique for engineering applications, displacing the solid investment process [Jon03, ASM88]. Basic steps in this process are illustrated in Figure 2.26:
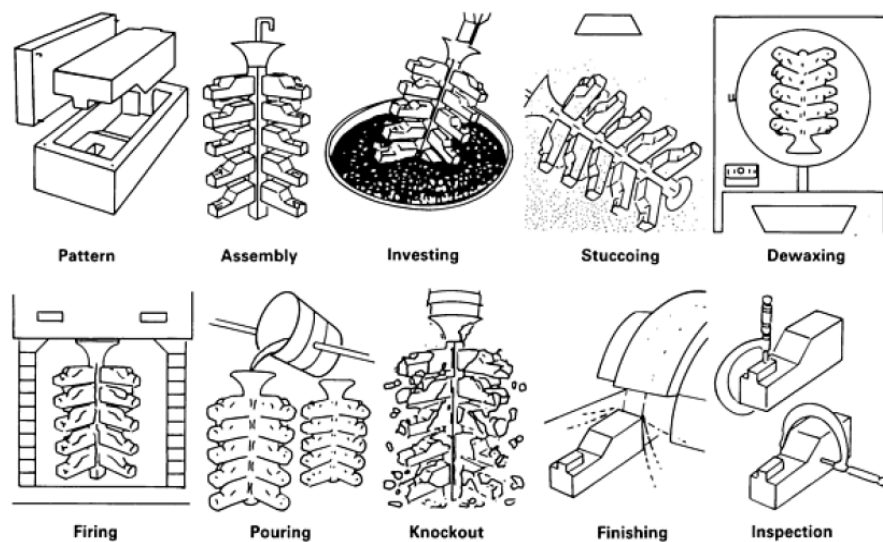
Figure 2.26: Steps in the investment casting process [ASM88]

Investment shell moulds are made by applying ceramic coatings to wax pattern assemblies. Each coating consists of a fine ceramic layer with coarse ceramic particles embedded in its outer surface. To obtain this coating, a wax assembly is first dipped into a ceramic slurry bath, composed of a fine refractory system and a colloidal binder system. The wax pattern is then withdrawn from the slurry

and manipulated to drain off excess slurry and produce a uniform layer. The wet layer is immediately stuccoed with relatively coarse ceramic particles, either by immersing it into a fluidized bed of the particles or by sprinkling the particles on it from above. The fine ceramic layer obtained from the slurry forms the inner face of the mould and reproduces every detail of the pattern, including its smooth surface. It also contains the bonding agent (binder), which provides strength to the structure.

The purpose of the stucco is to minimise drying stresses in the coatings by presenting a number of stress concentration centres which distribute and hence reduce the magnitude of the local drying stress. The second main purpose of the stucco is to present a rough surface, thus facilitating a mechanical bond between the primary coating and the back-up or secondary investment.
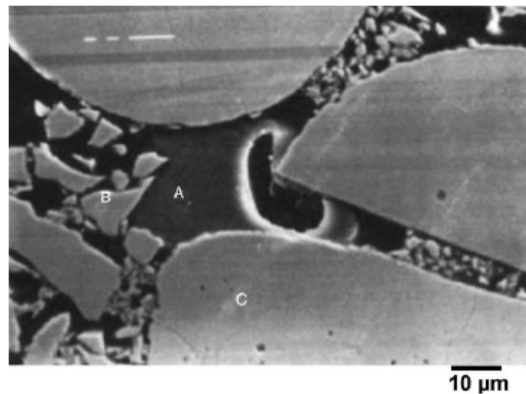
Figure 2.27: Secondary electron SEM image of colloidal binder network (A), surrounding refractory filler (B) and stucco (C) particles in an investment mould [Jon95]

When the primary coat has set (air-dried until the binder gels), the assembly is systematically dipped again into slurry, and stuccoed until the required thickness of shell is built up. The particle size of the stucco is increased as more coats are added to maintain maximum mould permeability. Each coating is allowed to harden before the next one is applied. The slurry does not have to be thoroughly dried between coats, but it must be dry enough so that the next coat can be applied without washing off the previous one. Final coat is usually left unstuccoed in order to avoid the occurrence of loose particles on the mould surface. This final layer is sometimes referred as the seal coat [Jon03, ASM88].

Key requirements of an investment casting mould are [Jon03]:

o Sufficient green (unfired) strength to withstand wax removal without failure.

o Sufficient fired strength to withstand the weight of cast metal.

o Sufficiently weak to prevent hot-tearing in susceptible alloys.

o High thermal shock resistance to prevent cracking during metal pouring.

o High chemical stability.

o Low reactivity with the metals being cast to improve the surface finish.

o Sufficient mould permeability and thermal conductivity to maintain an adequate thermal transfer through the mould wall, and hence allow the metal to cool.

o Low thermal expansion to limit dimensional changes within the mould wall and ultimately the casting.

The quality of ceramic shells is dependent on the slurry and shell materials as well as the process by which the shells are built. Even a good slurry formula will not produce castings if the slurry is prepared in a substandard way. For example, poorly wet-in slurry will not develop its maximum strength potential and may result in serious shell problems such as shell cracking [Sid08]. The slurry formulation is a significant factor in investment casting. Control procedures for slurries vary considerably among foundries but the most prevalent controls are the measurement of the initial ingredients and viscosity of the slurry. The goal of any slurry makeup is to produce stable slurries, well mixed to a point where the viscosity of the slurry is stable. Slurry mixing has a remarkable effect on the surface quality and strength of the shell.

2.6.2 Conventional investment ceramic moulds

- *Mould material: refractories*

The most common refractories for ceramic shell moulds are siliceous (silica itself, zircon, and various aluminium silicates composed of mullite and (usually) free silica). These three types in various combinations are used for most applications. Alumina has also had some use for super-alloy casting, and this use has increased with the growth of directional solidification processes. However, Al_2O_3 is generally considered too expensive and unnecessary for commercial hardware casting [ASM88].

Silica, zircon, aluminium silicates and alumina are used for both slurry refractories and stuccos; although stucco particles are commonly alumino-silicate based, for economy. Filler materials for slurries tend to be 200 mesh (75µm size), or a combination of 200 and 325 mesh (75 and 45µm, respectively) to achieve required primary surface finish and sufficient shell strength [Jon03, ASM88].
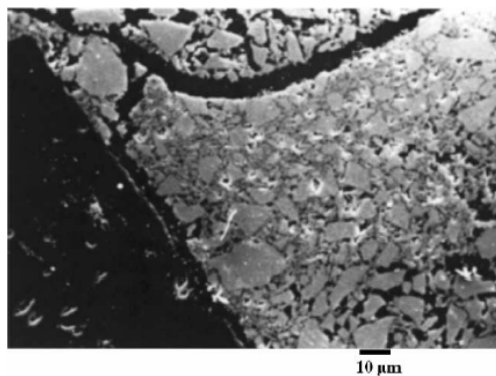
Figure 2.28: SEM image of filler particles, surrounding larger stucco refractory particles [Jon95]

Silica (SiO$_2$) is generally used in the form of silica glass (fused silica), which is made by melting natural quartz sand and then solidifying it to form a glass. It is crushed and screened to produce stucco particles, and it is ground to powder for slurries. Its extremely low coefficient of thermal expansion imparts thermal shock resistance to moulds [ASM88]. However, fused silica is susceptible to bow or twist if differential expansion forces are imposed. This problem is improved by using a modified composition, such as 90% silica glass and 10% crystalline cristobalite. Cristobalite experiments a phase and volume change at 220°C which makes difficult the use of pure cristobalite as raw material, but is ideal for assisting easy removal of moulds after casting [Bae08]. A typical chemical analysis of fused silica could be as follows:

Table 2.6: Example of a typical fused SiO$_2$ commercial composition [Cri91]

Silica (SiO$_2$)	99.63%
Alumina (Al$_2$O$_3$)	0.25%
Iron Oxide (Fe$_2$O$_3$)	0.05%
Lime (CaO)	0.03%
Magnesia (MgO)	0.02%
Alkalies (Na$_2$O+K$_2$O+Li$_2$O)	0.02%

Zircon (ZrSiO$_4$) occurs naturally as a sand, and it is used in this form as stucco. It is generally limited to use with prime coats because it does not occur in sizes coarse enough for stuccoing backup coats. It is also ground to powder or calcined for use in slurries, often in conjunction with fused silica and/or aluminium silicates. Its principal advantages are high refractoriness, resistance to wetting, round particle shape and availability [ASM88]. Contaminants within the zircon raw material batches can have a significant effect on investment shell integrity. Zircon is a host for a significant proportion of uranium, thorium, hafnium and other rare earth elements. For this reason, zircon is generally not available more than 98% pure. Typical chemical compositions of zircon could be as follows [Wil11]:

Table 2.7: Three different zircon compositions [Wil11]

	1	2	3
Zircon (ZrSiO$_4$)	98.72%	99.72%	99.48%
Titanium Oxide (TiO$_2$)	0.11%	0.12%	0.18%
Alumina (Al$_2$O$_3$)	0.75%	0.11%	0.12%
Iron Oxide (Fe$_2$O$_3$)	0.06%	0.05%	0.09%
Sodium Oxide (Na$_2$O)	0.024%	-	-
Yttria (Y$_2$O$_3$)	0.12%	-	0.13%

Aluminium silicates for investment casting are made by calcining fireclays or other suitable materials. As a result, a series of products ranging in alumina content from about 42 to 72%, with the remainder being silica plus impurities, are produced. The only stable compound between alumina and silica at elevated temperatures is mullite (3Al$_2$O$_3$·2SiO$_2$), which contains 72% alumina. Mixtures

containing less than 72% alumina produce mullite plus free silica. The latter is usually in the form of silica glass, although some crystalline silica in the cristobalite form may be present. Fired pellets of these materials are crushed or grounded to produce a range of powder sizes for use in slurries, and granular materials for use as stuccos [ASM88].

- *Mould material: binders*

The most commonly used binders are water based colloidal silica binders. It basically consists of a colloidal dispersion of spherical silica particles in water. The dispersion is stabilized by an ionic charge of sodium ions, which causes the particles to repel one another, thus preventing agglomeration. Gellation of the colloid to produce a binding phase for the refractory particles within the shell mould is achieved by removal of moisture. The amorphous network crystallises during the firing of the mould, to form a strong ceramic bond. The use of sodium also promotes crystallisation to cristobalite, producing a ceramic shell with sufficient strength to withstand the rigours of metal casting without failure or loss of integrity. However, unmodified colloid binders are exceptionally strong, leading to problems during casting of alloys susceptible to hot tearing. This is overcome by the use of polymer-modified binders which reduce the fired strength of the mould due to a burn out of the organic phase during the firing step. This in turn increases permeability of the ceramic, reducing the incidence of misruns or non-fills of the casting [Jon03, ASM88]. Silica-free binders were recently under study. Successful moulds binded with, for example, colloidal alumina can be found in literature [Ros04, Yua02]. However, these binders are still not completely developed for industrial purposes.

- *Slurry formulation*

Composition of shell slurries depends on the refractory powder, type and concentration of binder, liquid vehicle and desired viscosity. Composition generally falls in the following range by weight:

Table 2.8: Typical slurry composition [Ave99]

Ingredient Composition	%
Binder solids	5-10
Liquid (from binder or added)	15-30
Refractory powder	60-802

Slurries are prepared by adding the refractory powder to the liquid binder, using agitation to break up agglomerates and wet and disperse the powder. Continued stirring is required in production to keep the powder from settling out of suspension. Control procedures for slurries vary considerably among foundries. The most prevalent controls are the measurement of the initial ingredients and the viscosity of the slurry. Other parameters controlled are slurry temperature, density and pH [ASM88].

- *Aging of slurries*

During the shell making process different components in the slurry may interact with each other and cause aging. Aging is defined as any change in a slurry property or properties versus time. As slurries age, they lose their useful properties, and become useless or jeopardize the quality of the shell moulds [Yas98]. Commercial dip-coating processes require using large volumes of slurries. It may take weeks or months before an entire slurry preparation is consumed. Unfortunately, slurry aging typically requires that the slurry is discarded well before the entire quantity of the slurry initially formulated can be used to form casting moulds. This is both costly and wasteful [Yas02].

The degree of interaction among the different components differs between the different slurries. For example, aqueous MgO slurry with colloidal silica binder at pH 10.5 ages very rapidly and gels in less than an hour. Y_2O_3 slurry under similar conditions gels in a few hours. On the other hand, Al_2O_3 slurry under identical conditions remains stable for many months. This aging mechanism is shown to be the dissolution of polyvalent cationic ions from oxide flours, and then preferential adsorption of these ions on the surface of negatively charged colloidal silica particles. The different aging behaviours among slurries can be predicted from the speciation diagram of the flour in aqueous environment. Figure 2.29 compares the dissolution of yttria, magnesia and alumina. At pH=10.5, dissolution of alumina is about five orders of magnitude lower than that of yttria. Consequently, stable alumina slurries can be made at pH 10.5. On the other hand, magnesia dissolves over three orders of magnitude higher than yttria at pH 10.5. Consequently, long lasting stable magnesia investment casting aqueous slurry cannot be produced at the above pH. One method to increase the lifetime of slurries is to prepare the slurries at higher pH values. As the pH goes up, the concentration of dissolving ions decreases (Figure 2.29) and slurries do not age as rapidly [Yas98].
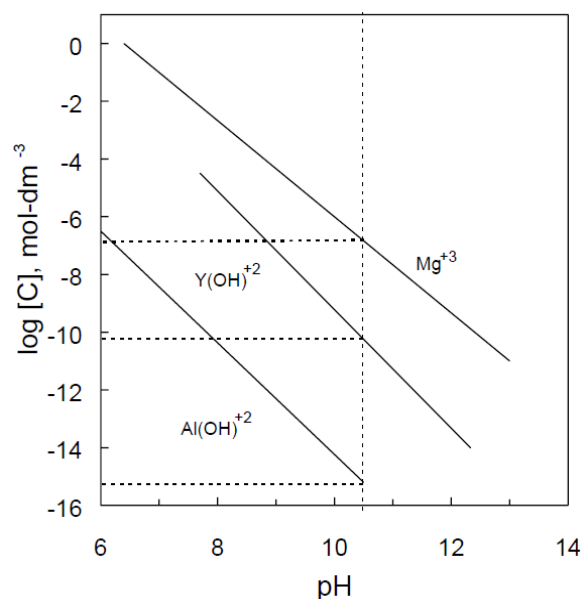
Figure 2.29: Ion concentration diagram as a function of pH. For simplicity, only the most dissolving ion specie from each flour is compared [Yas98]

- *Mould firing*

The usual firing temperature for investment moulds is of 900-1500ºC. Within the temperature range of 900-950ºC, the amorphous silica present in the mould crystallizes and it is transformed to cristobalite, although some trydimite may also be formed [Meu00, Jon95]. The presence of Na_2O in the binder decreases the crystallization temperature by nucleation of cristobalite at lower temperatures [Jon95]. During the cooling of the mould, the principal phases of SiO_2 change from the high temperature form to the low one. The degree of crystallization depends on the binder composition, the firing temperature and firing time. For example, depending on the temperature and the impurities in the binder different principal forms of SiO_2 can be expected. Jones *et al* found that binders with impurities lead to 100% crystobalite binder after the firing, whether trydimite could also be found in pure silica binders [Meu00, Jon95].

Table 2.9: Effect of the impurities on water based colloidal silica binders after firing [Jon95]

Binder	Composition	Firing T, ºC	Phase composition
Colloidal silica sol.	100% SiO_2	1000	Cristobalite+ small amount of trydimite
Colloidal silica sol.	32-37% Si	1000	100% Cristobalite
	64-74% O		
	2-49% Ca		
	0-54% Na		

More changes in the mould composition can also be expected after the firing. Venkar *et al.*, for instance, found that the refractoriness of the shell could be improved by adding fine particles of alumina to moulds initially formed with zircon flour and silica binders. After the firing at 1200ºC, silica and alumina were transformed *in situ* into mullite [Ven10].

2.7 Mould-Metal reactions in magnesium investment casting

2.7.1 Introduction

Investment casting of magnesium is a process well suited for the production of aeronautic and automotive components, as light density components in medium and small series are obtained. But, still nowadays, this process has not been properly developed and one reason for that are mould-metal reactions. Due to its large negative Gibbs free energy value, MgO is one of the most stable compounds. This means that, in investment casting, the refractory oxides of the mould tend to decompose thermally and form the more stable MgO compound. As a result, molten magnesium reacts with commercial shell materials (aluminosilicates) producing a non-desired oxide layer on the part surface. Severe surface reactions may even cause the destruction of the mould [Cin06].

Mould-metal reactions occur when the metal is in liquid state. This fact was proved by Cingi in his doctoral thesis. The author obtained reaction-free and reacted samples by casting AZ91E alloy in MgO and SiO_2 moulds, respectively. Cingi analysed the differences in the cooling curves of those samples by placing thermocouples near the mould/metal interface. The SiO_2 moulds recorded higher temperatures in both liquidus and liquidus + solidus regions, until the solidus temperature was achieved. This difference in temperatures was explained by Cingi by a heat release due to mould-metal reactions, which happened until the magnesium alloy reaches the solidus state [Cin06].

Figure 2.30: Investment casting mould burning due to severe mould-metal reactions [Arr07]

2.7.2 Types of mould-metal reactions in investment casting

The good surface quality obtained in investment casting is one of the big advantages of this process. However, a wide variety of surface reactions that involve the alloy, the mould and the atmosphere can take place during casting and solidification of the component. Those reactions, when visible, reduce the quality of the casting. Piwonka in 1994 resumed the 7 types of reactions that can lead to surface defects in investment casting [Piw94]:

1. Molten metal dissolves the mould. Most molten alloys dissolve moulds to some extent but for the most part this effect is negligible. The most known case is found in titanium castings. When molten titanium dissolves the mould, oxygen from the refractories goes into solution in titanium. When the oxygen content of titanium exceeds 250 ppm, the hardness of the metal surface increases. This hard outer "case" (the "alpha case") can cause premature failure of the cast component.

2. Molten metal reacts with the mould. According to Piwonka, the direct reaction of molten metal with the mould material is rare to occur: what is usually considered to be a mould/metal reaction is actually often a reaction with the atmosphere in the mould cavity.

3. Molten metal first dissolves and then reacts with the mould. This type of reaction is what normally happens in titanium casting.

4. Molten metal reacts with the atmosphere in the mould. Most of the mould/metal reactions which are encountered depend on the reactions of the metal with the atmosphere, usually air. Oxides are

formed in the surface of the casting and are carried by fluid flow into the casting in the form of inclusions, or thin oxide films. Although these inclusions lower the mechanical properties of the castings, they cannot be considered as surface defects.

5. Molten metal penetrates the mould, causing a rough surface. The pressure of the molten metal can force the liquid to physically enter in the interstices of the mould. This is more prevalent in sand casting rather than in investment casting. As the investment casting moulds are made with the fine grain refractories, the penetration into the first coat is impossible. Chemical penetration may also occur in investment casting, when a chemical reaction occurs between the metal and the mould.

6. Molten metal reacts with gas in the mould and the product reacts again with the mould materials. Iron oxide, for example, reacts with silica to form fayalite.

7. Solid metal reacts with the atmosphere. When the solid casting is cooling in the mould it may react with oxygen in the air, for example. In the case of steels this is known as decarburization.

The mechanisms why mould-metal reactions occur in magnesium casting are still under study. Although the number of works that can be found in literature is very scarce, according to the different authors four of these seven reactions take place in Mg investment casting:

- *Molten metal reacts with the mould*

Most of the authors that study the reactions in magnesium investment casting consider that the molten metal reacts directly with the mould, as in type 2 [Jaf11, Arr07, Sin06, Idr96]. Molten magnesium is considered to react with the silica present in conventional mould materials, according to the following reactions:

$$2Mg(l) + SiO_2(s) \rightarrow 2MgO(s) + Si(dissolved) \qquad\qquad 2.11$$

$$4Mg(l) + SiO_2(s) \rightarrow 2MgO(s) + Mg_2Si(s) \qquad\qquad 2.12$$
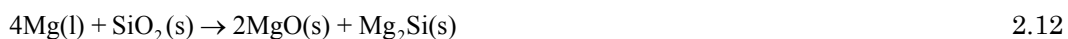
Due to this, mould-metal reactions were generally explored only on the basis of the free energy of formation of magnesia. The comparison between the free energy of formation of MgO (ΔG^0_{MgO}), and the one of mould refractories can thus be understood as the tendency of the melt to react with the mould, decompose it and produce MgO. A small difference of ΔG^0 will then indicate a weak driving force for MgO formation, and a high resistance of the mould refractory to oppose the thermal decomposition (reverse reaction) [Cin06]. This difference is therefore associated with a high reaction rate: Magnesia is supposed to need more time to decompose an oxide with a high stability; whereas a less stable mould material would be decomposed faster.

Gibbs free energy change can be written as:

$$\Delta G_T^{\circ} = \Delta H - T \Delta S \qquad\qquad 2.13$$

Where ΔH is the enthalpy change, ΔS is the entropy change and T the temperature of the reaction. ΔH and ΔS values for different reactions can be found in JANAF tables and consequently the ΔG_T^0 vs. temperature can be drawn [Cha75]. Figure 2.31.a and b illustrate the graphic representation of the free energies of formation of some binary and ternary oxides:
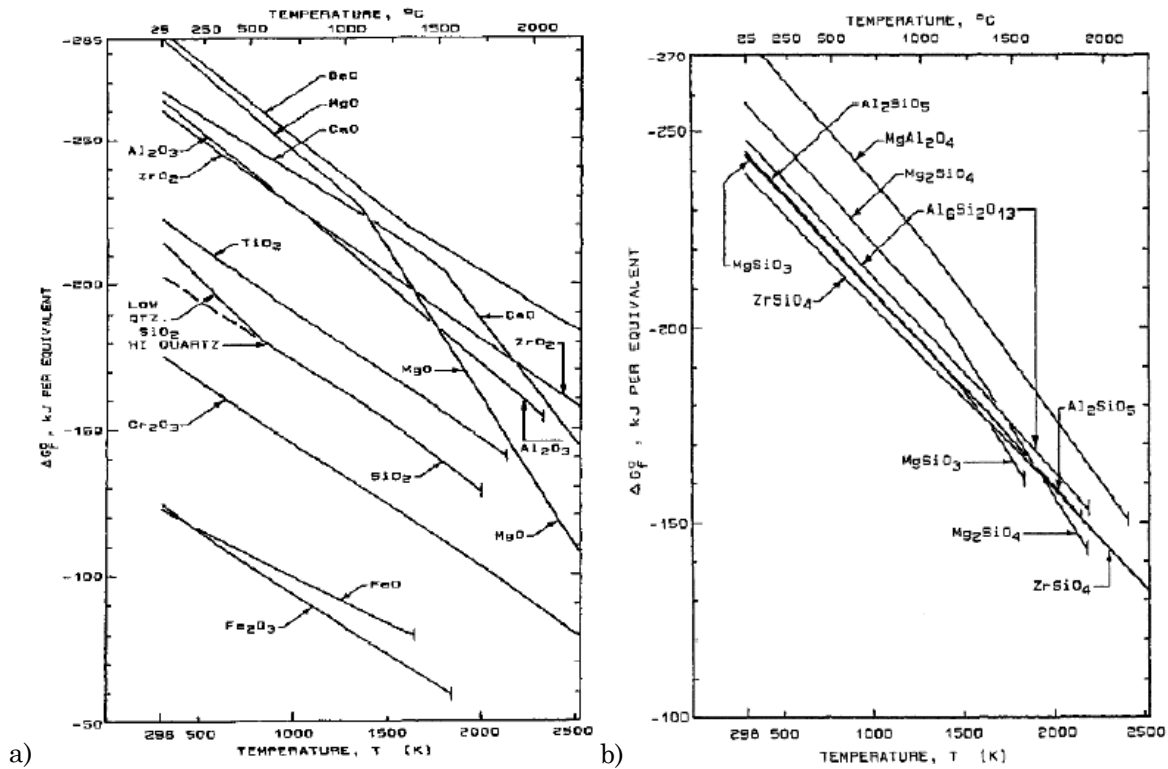
Figure 2.31: Free energy of formation (ΔG_T^0) of binary and ternary oxides vs. temperature (T) [Cin06]

Investigations on the thermal oxidation of solid alloys at high temperatures (i.e. T > 800 K) also consider Gibb's free energy of formation as the unique criterion to determine the creation of oxides. It is considered that, at these high temperatures, local thermodynamic equilibrium generally prevails at the reacting metal/oxide, oxide/oxide and oxide/gas interfaces, and the thermal energy is sufficient to allow existing ions or electrons to surmount their energy barriers for movement into and through the developing oxide layer [Vin06]. However, this has not to be necessarily so. Korpiola, for example, in his PhD thesis analysed the high temperature oxidation of metal powders in the HVOF spraying process, where the oxidation of spray particles is often in a molten state. The author recognized that thermodynamics is an important tool for use in predicting which species tend to oxidize, and defining the conditions for a metal to oxidise. However, as thermal spraying is a very rapid process (<2 ms), the author points that reactions cannot be determined by thermodynamics alone. Korpiola states that reaction kinetics need to be employed to explain the degree of oxidation reaction, which is dependent on time, area, mass transfer, temperature, etc [Kor04].

- *Molten metal reacts with the atmosphere in the mould.*

During pouring and filling, Mg melt reacts with the atmospheric O_2 present in the mould cavity, and MgO is formed. This oxide skin sticks to the cast surface, resembling a mould-metal reaction [Cin06].

- *Molten metal reacts with the atmosphere in the mould cavity and the reaction product reacts with the mould*

Cingi [Cin06] analysed the influence of atmospheric oxygen to determine if magnesium investment casting reactions could be classified as type 2 or type 6. The author performed dipping experiments, where the refractories where dipped in Mg melts during a period of time. These experiments showed that Mg melt does not react immediately with any of the refractories in the O_2 absence. The author stated that, rather than the direct reaction of Equation 2.14, magnesium melt reacts according to reaction type 6 (Equation 2.15), which in fact is more favourable due to a higher ΔG value.

$$2Mg(l) + 2SiO_2(s) \rightarrow 2MgSiO_4(s) + Si(diss) \qquad \Delta G_T^{\circ} = -298.534 \text{ kJ} \qquad\qquad 2.14$$

$$2Mg(l) + O_2 + 2SiO_2(s) \rightarrow 2MgSiO_4(s) \qquad \Delta G_T^{\circ} = -1054.681 \text{ kJ} \qquad\qquad 2.15$$

Cingi decomposed reaction 2.15 in two stages, and stated that reaction 2.16 is a precursor for reaction 2.17 to occur. This means that, avoiding the contact between Mg melt and O_2, mould-metal reactions would be completely suppressed as Equation 2.17 would never happen [Cin06]:

$$2Mg(l) + O_2 \rightarrow 2MgO(s) \qquad \Delta G_T^{\circ} = -991.865 \text{ kJ} \qquad\qquad 2.16$$

$$2Mg(l) + 2SiO_2(s) \rightarrow 2MgSiO_4(s) \qquad \Delta G_T^{\circ} = -62,817 \text{ kJ} \qquad\qquad 2.17$$
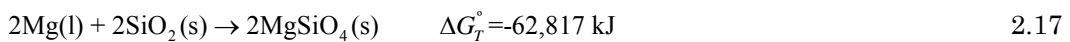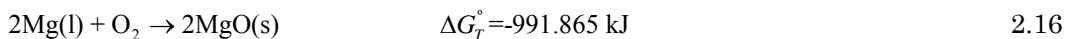
- *Molten metal penetrates the mould*

Jafari studied the oxidation of AZ91D alloy in molten state by heating magnesium alloy granules in an investment ZrO_2 open mould. The author found that increasing the heating temperature from 650ºC to 700ºC and 750ºC increased the mould-metal reaction, resulting in adhesion of patches of ceramic mould on the surface of AZ91D granules. The author states that, as the evaporation rate of magnesium increases considerably at higher temperatures, magnesium vapour easily reaches and enters into the mould. It reacts with the refractory oxides and finally, mould materials enter into the oxide layer [Jaf11]. So Jafari proposes a penetration mechanism, where liquid magnesium burns and evaporates penetrating in the mould, and reacting there with the oxides.

This mechanism is also proposed by Sin *et al.* [Sin06], who analysed the reactions between AZ91D alloy and plaster mould materials. As commented before, those authors consider that the interfacial reactions are due to a direct and very exothermic reaction of the Mg alloy with the SiO_2 in the mould.

The amount of heat liberated during the reaction, combined with the high Mg vapour pressure at casting temperature, leads to the vaporisation of the metal which diffuses through the mould and continues reacting with it. This theory was supported with the XPS analysis of the plaster mould that revealed the presence of magnesium inside it.

Zhang *et al*. also state that firstly a layer of MgO is formed on the casting, due to the reaction of the metal with air. Since the oxide film is porous and non-protective, magnesium will go through the oxide layer to react further with shell materials, as in Figure 2.32 [Zha04]:
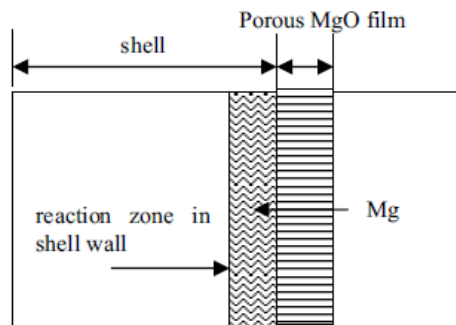
Figure 2.32: Model of mould-magnesium reaction proposed by Zhang *et al* [Zha04]

2.8   Methods to avoid mould-metal reactions in magnesium investment casting

2.8.1 Introduction

Magnesium melt reacts with air in the mould cavity and porous shell wall, as well as with shell materials as it enters and takes the form of the mould cavities. Thus, to prevent the Mg-O_2 reaction it is first necessary to prevent the contact with atmospheric oxygen, and secondly to prevent reaction between the metal and the mould materials [Yan07]. Both shortcomings can be accomplished by the use of inhibitors/barriers. The mould-metal reaction can also be prevented by the use of non-conventional refractory mould materials.

2.8.2 Use of non-conventional mould materials in Mg investment casting moulds

As commented before, MgO is one of the most stable compounds. In investment casting molten magnesium decomposes the shell materials (aluminosilicates) to form the more stable MgO compound. This reaction can be avoided if the first layer of the mould is composed of a refractory oxide+binder system that is at least as stable as MgO. Diagram of Figure 2.33 shows the stability of common oxides at room temperature.
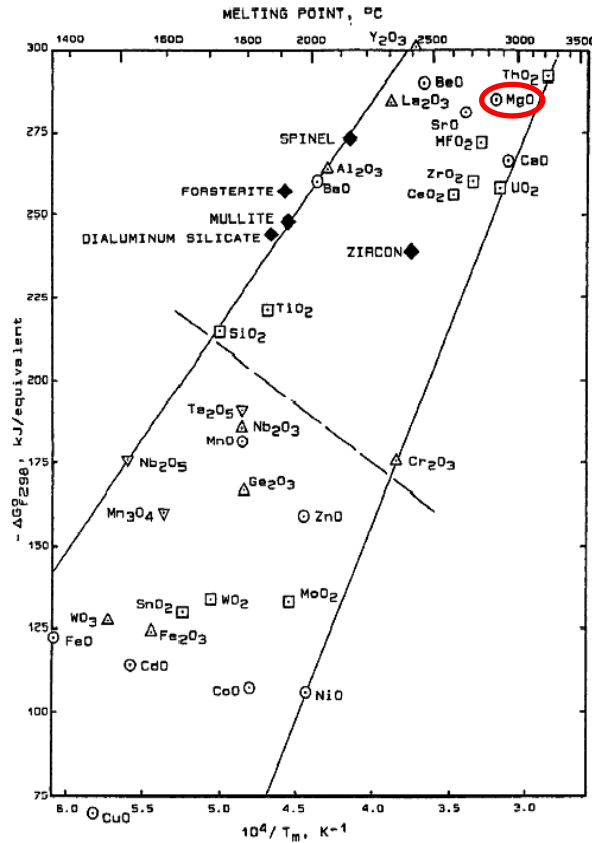
Figure 2.33: Free energy of formation at room temperature of common
binary and tertiary oxides (ΔG_{298}^0) versus its melting point (T_m) [Cin06]

The dashed line in the middle of the diagram, which is chosen arbitrarily, separates acceptable refractory compounds (above the dashed line) from unacceptable ones (below the dashed line). Unacceptable compounds are disqualified by the combined criteria of both melting point and chemical stability. For magnesium casting, high melting point is not very critical due to relatively low casting temperatures, but chemical stability is of importance.

Figure 2.33 shows that MgO, marked in red, is one of the most stable compounds. According to that diagram, only four oxides possess a ΔG_f equal or higher than magnesia: BeO, ThO_2, La_2O_3 and MgO itself. Unfortunately, BeO is human carcinogen and ThO_2 is radioactive. La_2O_3 is too expensive and the slurries made with MgO have a too short life, so the increase in cost of the castings would be too high for the foundries [Cin06]. Due to this, in Cingi's work the refractory oxides for the first were chosen among the ones with a stability value between the one of SiO_2 and the one of MgO: the higher the stability of the mould, the higher the time that magnesium needs to decompose it.

Kim *et al*. have tested investment moulds made with Al_2O_3, $ZrSiO_4$, $CaZrO_3$ and CaO refractory fillers [Kim01, Kim00]. After visual comparison of the obtained castings, the authors ranked the oxides in the order of higher to lower surface reaction degree as follows: CaO→$ZrSiO_4$→Al_2O_3→$CaZrO_3$. This grading corresponds to the free energy data for the formation of these oxides calculated by the

authors, except for the CaO mould that exhibited an unexpected poor performance. In fact, AZ91D alloy reacted with the CaO mould even when the mould was at room temperature, without preheating. To understand the behaviour of the CaO mould, Kim *et al.* repeated the CaO mould casting but in vacuum plasma arc furnace, filled with argon. Good results were achieved in this experiment. The authors concluded that the surface layer obtained in the first CaO mould could be due to the reaction between MgO and CaO. MgO would be formed after the reaction between the Mg melt and the air present inside the mould cavity.
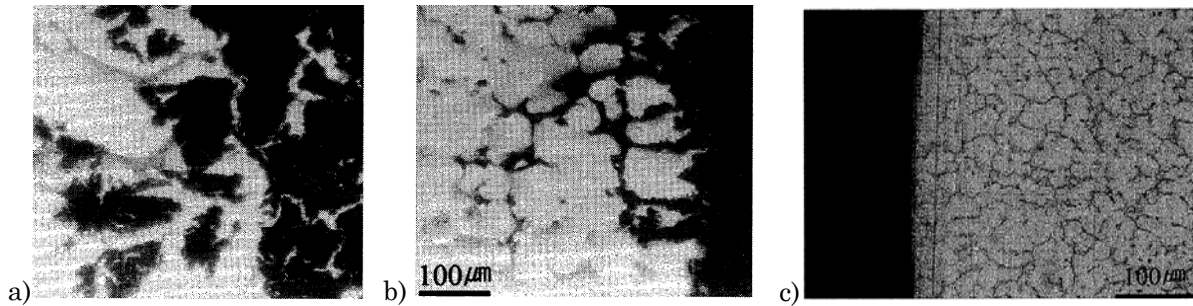
Figure 2.18: PBR as a function to SF6 and HFC-134a gas exposure time. Microstructures obtained for castings produced with a CaO mould: a) conventional casting with mould at room temperature b) conventional casting at a mould preheating temperature of 400ºC c) casting in a O_2 free atmosphere [Kim01]

Kim *et al.* did not perform further vacuum castings with the rest of the mould materials. The effect of the employment of silica-free binders has also been contrasted by these authors. The non-conventional moulds binded with SiO_2 showed no reaction at preheating temperatures of 400ºC but resulted in mould-metal reactions when the temperature was 600ºC. None of both temperatures produced interfacial reactions with non-conventional fillers and binders.

Zhang *et al* studied reactions between Mg and colloidal silica-bonded zircon shells and zirconia sol-bonded zirconia shells, preheated to 650ºC [Zha04]. Both shells showed mould-metal reactions. The mapping of elements Mg, O, Si and Zr by electron probe microanalysis (EPMA) showed the presence of a Mg oxide layer, which was thicker than 100µm.

Cingi employed different refractories as face-coats to study mould-metal reactions in AZ91E alloy castings [Cin06]. Excellent reaction resistance was noticed in the case of fused magnesia and yttria face-coated shells. Fused alumina and zircon face-coats also showed good resistance. Molochite and zirconia provided moderate to poor reaction resistance, and strong reactions were observed in the case of fused silica. The free energies of the formation of those refractories were also calculated by the author. The predicted order of stability agrees fairly with the experimental observations of reaction resistance to the mould-metal reactions. The SEM analysis of reaction layers indicated the presence of a mixture of oxides on the Mg casting surface mainly composed of MgO. The presence of Al and Si in the film was suggested to be due to the reaction of Mg with the mould oxides, or to the presence of unreacted oxides of the shell.

The silicon concentration of the SiO_2-coated sample was found to be too low. Due to that, Cingi suggested that silicon should be present as a ternary compound and performed a XRD analysis of the sample, concluding that Mg_2SiO_4 was the most likely compound [Cin06].

2.8.3 Use of inhibitors in Mg investment casting

Inhibitors have long been added to magnesium sand casting moulds. Their success was attributed to three different mechanisms [Idr96]:

o Formation of a protective film on the surface of molten Mg as it enters in the mould cavity

o Formation of a protective atmosphere in the mould cavity

o Formation of a protective atmosphere around the grains that compose the mould

During last years different fluorine containing melt protectors have been tested to protect Mg casting surfaces. At Mg casting temperatures, inhibitors decompose thermally and fill the cavity of the mould with a protective gas. As a result, as Mg melt enters in the cavity a protective surface layer that prevents reactions between magnesium, atmosphere and mould material is formed. The protective layer formed on the surface maintains the metallic appearance of the casting. The tested inhibitors can be classified in function of their initial state: solid, liquid and gaseous.

KBF_4 solid inhibitor was tested in Mg investment casting by Cingi and Idris *et al* (Shaw mould) due to the reported success of this compound in sand casting [Cin06, Idr96]. When the authors added KBF_4 grains to the shells during its preparation, moulds disintegrated. Unfortunately, as moulds are sintered at 800-950ºC, all the inhibitor was thermally decomposed in this stage. To overcome this problem, Cingi immersed the preheated mould in inhibitor grains before the pouring. It was expected that the mould, as it was preheated, would decompose KBF_4, and release the BF_3 protective gas. Small reduction in reactions was achieved with this technique.

$NaBF_4$ liquid inhibitor was also tested by Cingi, achieving very good results (Figure 2.34) [Cin06]. $NaBF_4$ possesses a 973g/l solubility at room temperature, so the author dissolved 42g $NaBF_4$ dry powder in 115g warm water to create a liquid inhibitor. Next, the author introduced a conventional molochite mould into this solution, and the mould absorbed the inhibitor. According to this author, the reductions due to the use of $NaBF_4$ can be attributed to one or both of the following factors:

o Liberation of BF_3 gas upon mould preheating and/or casting (Equation 2.18). $NaBF_4$ was dissociated during mould preheating and BF_3 protective gas was released, filling the entire cavity effectively.

$$NaBF_4 \, (s) \rightarrow BF_3 \, (g) + NaF \, (s) \qquad\qquad\qquad 2.18$$

o Modified surface energy of the mould walls. Presence of the inhibitor salt may increase the surface energy of the refractory, so that the mould is not wetted by the Mg alloy. This would explain the reduced reactions and the no-sticking of the face coat onto the cast surface.
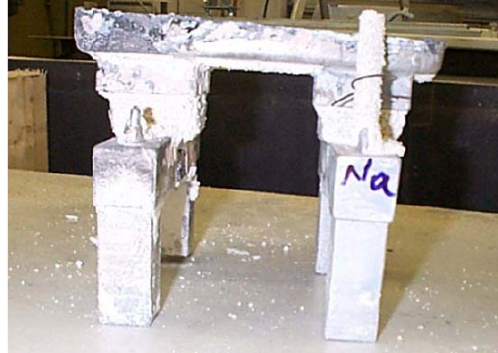
Figure 2.34: Employment of $NaBF_4$ leads to well-protected surfaces (right-hand-side marked Na). Left-hand-side pieces show ceramic material stuck on the surface due to mould-metal reactions [Cin06]

With regard to the gaseous inhibitors, several authors have probed the effectiveness of inhibiting Mg investment moulds with a mixture of SF_6. Idris and Clegg were the first ones to use SF_6 in investment casting [Idr96]. Nevertheless, the authors initially found that, after flushing the shells with a CO_2/SF_6, they were not obtaining significant mould-metal reductions. The authors stated that, although SF_6 is heavier than air, it might be pushed out of the mould due to turbulences during the pouring of the metal. To avoid the inhibitor loss, the authors placed the ceramic mould inside an enclosure or chamber, and flushed the whole system with the inhibitor (Figure 2.35). All the inhibitor flows employed gave clean surfaces, dull or metallic, achieving better results as long as the SF_6 content was increased. Following in the footsteps of Idris *et al.*, Arruebarrena *et al* inhibited Mg conventional shell moulds with different SF_6/CO_2 concentrations. Before the flushing, the shells were placed in steel chambers filled either with Ar of CO_2. Best results were obtained with CO_2 atmosphere and the higher SF_6 concentration [Arr07].
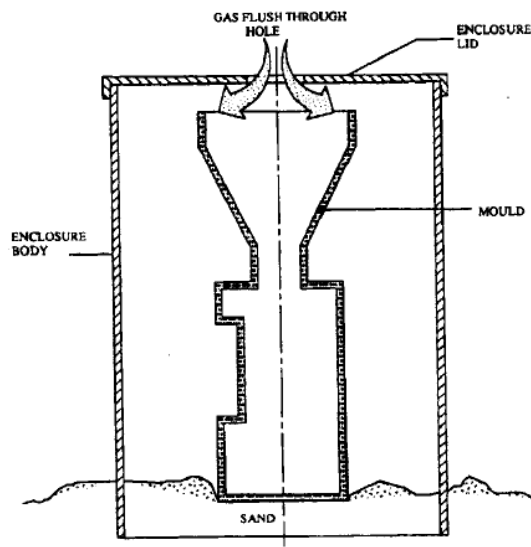
Figure 2.35: Schematic representation of the mould enclosure employed by Idris *et al.* [Idr96]

The new melt inhibitors (Section 2.5) developed during the last years to replace SF_6 have also been tested in Mg investment casting: HFC-134a has given good results when casting rare-earth containing Mg alloys in Zircon+SiO_2 binder moulds [Yan07]. Clean metallic surfaces were obtained in these experiments, performed with a Mg pouring temperature of 740°C. However, it has to be considered that mould preheating temperature was only 250°C.

Zhang *et al.*, in another set of experiments, placed the colloidal silica-bonded zircon shells and zirconia sol-bonded zirconia shells inside a chamber. The moulds, preheated at 650°C, were flushed with a 1%SF_6/CO_2 mixture before the pouring of the AZ91D alloy at 700°C. The effect of the conventional binder is shown again in these experiments: only the SiO_2 binder showed mould-metal reactions. An increase of the SF_6 concentration over 1% (unknown percentage) avoided the reactions even with the SiO_2 binder. A surface analysis revealed the presence of Mg, O, F, S, Si, and Al in the surface layer of the casting. The concentrations of Mg and Al increased with depth in the sample. Fluorine was found to be located in the outer part of the film, and sulphur in the inner one. This effect was related to the decomposition of the SF_6 gas. The surface obtained with the SiO_2 binder mould revealed also the presence of silicon near the surface, due to a reaction between the metal and the refractories of the binder [Zha04].

2.8.4 Factors affecting mould-metal reactions in magnesium investment casting

Suppression of the oxidation reaction in the mould is influenced by Mg casting temperature and mould preheating temperature (interface temperature) and casting section thickness (time). This was asserted by different authors. The detrimental effect of increasing casting thickness is mentioned by Idris and Clegg, and proved experimentally by Yang *et al* and Sin *et al* [Yan07, Sin06, Idr96]. These last authors analysed the reactions between AZ91D alloy and plaster mould materials. They found that the increase of mould temperature or section thickness proved to adversely affect more to the mould metal reactions than the increase in casting temperature. Within the range of casting temperatures studied (650°C-760°C) the authors found no significant influence of the melt temperature on reactivity and surface finish [Sin06]. Anyway, in investment casting Idris and Clegg found that a reduction of the pouring temperature of Mg-based alloys from 780°C to 700°C decreases the severity of the reactions [Idr96]. Jafari *et al.* also found that increasing the heating temperature of AZ91D alloy from 650°C to 700 and 750°C increased mould–metal reactions between the Mg alloy and the ceramic mould, resulting in the adhesion of ceramic on the metal's surface [Jaf11].

However, it has to be taken into account that melt filling is enhanced with increases in melt temperature, mould temperature and section thickness. Thus, a compromise between filling ability, to produce complex thin-walled components, and mould-metal reactivity, which governs the quality of

the cast surface must be found. Moreover, the efficiency of the inhibitors employed to improve the surface quality is also reduced with a temperature increase [Sin06].

Sin *et al.* [Sin06], during the AZ91E casting in conventional plaster moulds, observed the influence of the mould preheating temperature in mould-metal reactions. At low mould temperature, no reaction product was visible on the casting surface. At high mould temperature, the investment was adhered to the Mg alloy. A reaction layer, identified as MgO and Mg_2Si by EPMA and XRD, was formed at the interface due to reaction with SiO_2. The authors explain that, at high mould temperature, SF_6 is not efficient to prevent the formation of the reaction layer. Or, what is the same, to form a protective layer. This results in a lower concentration of fluorine at the surface of cast sheets when severe casting conditions are used.

2.9   Conclusions

This literature review has been divided into four main sections, necessary to understand the basis of mould-metal reactions in magnesium investment casting. Next, main conclusions extracted from each feature are briefly mentioned.

2.9.1 Oxidation of magnesium and its alloys

Magnesium oxidation, at ambient temperature in dry air atmospheres, produces a thin and protective amorphous MgO layer [Eli02, Nor97]. In humid air, a protective layer is also formed but in this case it exhibits a duplex structure: the previously mentioned amorphous MgO and an inner $Mg(OH)_2$ layer [Fot06, Cze02, Eli02, Nor97]. These protective layers are stable for considerable lengths of time. Concerning solid magnesium thermal oxidation, the protective behaviour of the film formed under humid air ends at 380ºC. Above this temperature, inner $Mg(OH)_2$ decomposes forming crystalline MgO and cracking the outer amorphous film. When fresh magnesium is exposed to air at those temperatures, crystalline and loose MgO is formed instead of amorphous MgO and the protective character of the film is lost. On the other hand, the protective behaviour of the film formed at dry air atmospheres ends at 450ºC. Above this temperature, the high vapour pressure causes the cracking of the amorphous MgO film [Wan08, Shi07, Eli02, Fou02].

Alloying magnesium with aluminium contents higher than 4wt.% improves the protective properties of the film. The layers formed on Mg-Al alloys become enriched in Al_2O_3 and dehydrated. As for pure magnesium, the thin and protective layer formed under ambient temperature is stable for considerable lengths of time and upon heating at low temperature [Eli02]. This film is protective up to 450ºC, when the high vapour pressure of magnesium fissures it. If the Mg alloy forms a eutectic

phase below this temperature (e.g. $Mg_{12}Al_{17}$ at 437ºC), at the eutectic temperature the first liquid phase will appear. The high vapour pressure associated to the liquid alloy activates the nodular growth, due to magnesium evaporation. During the oxidation, aluminium reacts to form $MgAl_2O_4$ [Shi07, Cze02].

At temperatures near their melting point, metals dissolve gases such as oxygen. Liquid metals contain higher amounts of oxygen dissolved than its corresponding solid phase. When oxygen saturation is attained, the oxide phase is nucleated and forms a separate phase. Due to the high solubility of gases in liquid metal and favourable kinetic factors, chemical reactions can take place in and on the liquid metal, forming gaseous, liquid or solid oxides [Kor04]. At its melting point (650 °C) magnesium has such a high vapour pressure that melt surfaces exposed to air are actively oxidised. In addition, the formation heat of MgO is so large that some local zones are heated to a considerably high temperature. This speeds up the oxidation reaction and results in active combustion or even burns, with an intense white light [Zen01]. Due to this, melting of magnesium is performed under the protective action of a melt protector.

2.9.2 Melt protection

To process molten Mg safely and efficiently, the melt has to be protected either by exclusion of oxygen (e.g. covering with salt flux, CO_2 snow or inert gas) or by changing the nature of the surface oxide, to slow the oxidation rate down to an acceptable level (e.g. with a cover gas or addition of allowing elements). Employment of SO_2 and SF_6 was the common practice in industry for several decades. Use of SO_2 requires care, since SO_2 is toxic, corrosive and environmentally unacceptable: it contributes to acid rain. SF_6 molecule has the distinction of possessing the highest global warming potential (GWP) of any compound identified to-date. Consequently in the last years efforts were conducted to identify new melt protection alternatives with low toxicity and limited environmental impact. Several alternative melt protection methods were analysed in Section 2.5 of this chapter but only a brief resume of the most relevant ones is presented in this section.

- *Sulphur dioxide*

The exact composition and reactions that take place to form protective films under the SO_2 atmospheres is still not fully understood. It seems that the protective films are initiated with a MgO layer, where sulphur dissolves [Wan11, Pet02]. Accordingly, carrier gases with O_2 have proven to provide effective results, whereas the N_2/SO_2 atmospheres are not able to protect the Mg melt effectively [Wan11, Ale77]. The surface layer could first form a dense film of sulphur-containing MgO which reduces the rate of oxidation. Longer exposures could increase the sulphur concentration sufficiently for sulphur compounds to nucleate.

The nature of the sulphur compounds that are formed under SO_2 atmospheres is still unknown. Some authors state that the protective films are composed of MgO and MgS [Wan11, Ale77], but other authors have reported that the film can also contain $MgSO_4$ [Cas99, Gje96]. According to Aleksandrova *et al.*, Mg reacts first to form MgS, and this MgS continues reacting with SO_2, to form $MgSO_4$ (Equation 2.5). So the presence of diverse sulphur compounds could be due to differences in the exposure time of the experiments, and further exposures could lead to the appearance of $MgSO_4$. $MgSO_4$ containing films, reported by Gjestland and Cashion, exhibit a complex and layered structure which certainly contains MgO, MgS and $MgSO_4$ compounds. However, the mechanisms suggested by these two authors differ from the one presented above. Gjestland opts for an initial $MgSO_4$ film which later decomposes into MgS and MgO. On the contrary, Cashion proposes an initial two layered structure which contains not only $MgSO_4$, but also MgO, which later develops also an inner MgS layer. Nevertheless, it has to be considered that the manifestation of different sulphur compounds can also be due to differences in the experimental temperature at which the reactions take place, and not only due to exposure time.

- *Sulphur hexafluoride*

The protective behaviour of SF_6 seems to be initiated with the fast formation of a MgO layer. Accordingly, inert gases such as N_2 or Ar are not adequate carrier gases for SF_6 [Aar04, Pet02]. For fluorine to enter the MgO film, the larger molecules of SF_6 must first dissociate to form smaller and more reactive fluorine species like F or F_2. The speed of the dissociation reactions is the upper limit to the rate of formation of MgF_2.

$$SF_6 \rightarrow SF_4 + nF + \left(1 - \frac{n}{2}\right)F_2 \qquad 2.19$$

While SF_6 decomposes to form more reactive fluorine compounds, magnesium reacts primarily with oxygen to form MgO, and later with fluorine to form MgF_2. The four different films presented in the doctoral thesis performed by Aarstad are likely to summarize the different situations that lead to a protective film under SF_6 atmospheres [Aar04].
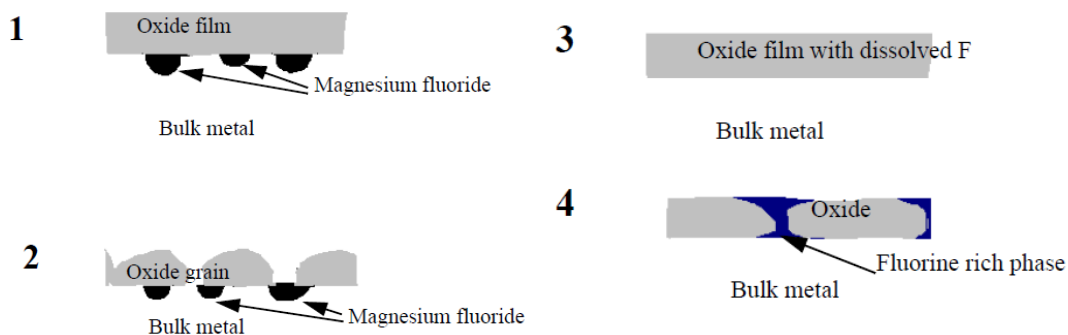
Figure 2.36: Schematic representation of the four different protective films observed when magnesium is exposed to SF_6 [Aar04]

The situations of Figure 2.36 can actually be divided into two different groups: In situation 1 and 3 a uniform and compact MgO layer is formed, whereas the MgO film of situation 2 and 4 is unconnected. The reaction temperature may be the factor affecting the formation of this prior MgO film, as the MgO formation is speed up with temperature.

Above a certain temperature, a uniform MgO film may be formed before the dissociation of SF_6, leading to the MgO films of situations 1 and 3. This film is already protective due to the improved wetting between MgO and Mg in SF_6 presence, and/or to the expansion of the MgO lattice due to the fluorine dissolved in the melt (situation 3). With the increase of the holding time, fluorine may diffuse inwards and react with magnesium, forming fluorine particles underneath the first MgO film (situation 1).

In situation 2, fluorine dissolved in the MgO film may increase its concentration sufficiently to nucleate before the MgO film forms a uniform layer, so fluorine diffuses inwards and MgF_2 particles are formed again underneath the oxide film. In situation 4, the fluorine particles would not diffuse through the film but they would directly react with the unprotected melt surface, creating a film which combines MgO and MgF_2 crystals. The reason why sometimes fluorine would diffuse through the MgO film, and sometimes directly react with the melt is still not fully understood. The answer may be in the rate at which the MgO film is saturated in fluorine. A slow saturation could lead to a direct reaction of the Mg with the fluorine present in the atmosphere.

- *HFC-134a*

Studies performed on the films formed under SF_6 and HFC-134a agree in the key role of MgF_2 to protect the melt [Mir10, Ha06b, Che06, Ha06a, Tra04]. HFC-134a gives better protection than SF_6 for Mg and Mg alloys melt protection, under identical essay conditions. Lower flow rates and inhibitor concentrations are needed to protect melt surfaces. Difference between SF_6 and HFC-134a arises from the fact that HFC-134a provides fluorine easier than SF_6. Thermal decomposition of SF_6 starts from 800 ºC but that of HFC-134a starts from 250 ºC. Due to this, the films formed under HFC-134a contain a higher proportion of magnesium fluoride.

When molten magnesium is exposed to a cover gas mixture containing HFC-134a and oxygen, Mg rapidly reacts with oxygen to form a thin film of MgO. Mg vapour diffuses outwards through the loose MgO film and reacts with F_2 to form MgF_2 within the film.

- *Fluoroketones*

Fluorinated ketones degrade at temperatures above 550°C, so they react faster that SF_6 with Mg to form MgF_2. In addition, they also contain more F atoms per molecule than SF_6, so more fluorine is

available per molecule to form protective MgF_2. Due to this, FK have probed to be more efficient to use (lower use rates for equivalent protection) in the experiments performed on pure magnesium and some selected alloys by Milbrath *et al*. and Tranell *et al*. [Tra04, Mil03].

- *Fluorine Saturation of the melt*

The method of protecting magnesium melt by fluorine saturation was tested by different authors, but none of the employed methods protected the surface melt effectively: Cashion bubbled 100% SF_6 through an AM60B melt and introduced a molten eutectic mixture of FK and AlF_3 salts in the melt [Cas99]. Aarstad studied the fluorine solubility in pure magnesium by melting Mg in a MgF_2 crucible [Aar04]. Tranell *et al* introduced MgF_2 and AlF_3 powder pressed briquettes in the melt, after measuring the fluorine that was necessary to cover the melt surface with MgF_2. Consequently, the authors stated that the mechanisms through which fluorine-containing gases form the protective films seem to happen in the gas phase [Tra04]. These fast, chemical vapour deposition to form MgO and MgF_2 seem to be instrumental for melt protection.

2.9.3 Mould-Metal reactions in investment casting

According to the heat-release measurement performed by Cingi, mould-metal reactions occur when the metal is in liquid state [Cin06]. This fact seems reasonable from the point of view of Mg thermal oxidation. As commented previously, the high vapour pressure associated to the liquid Mg alloy activates the nodular growth and speeds up the alloy oxidation rates, due to magnesium evaporation [Cze04, Cze02].

According to different authors, four different reactions may take place in Mg investment casting. It should be taken into account that maybe not only one but more than one may be happening at the same time, as all seem likely to occur.

Magnesium melt first reacts with oxygen in the mould cavity, during the filling of the mould. Once the solidification starts, magnesium reacts also with the O_2 present in the porous shell wall and with the shell materials. It is a well-known fact that molten magnesium oxidizes very rapidly when it is exposed to air. Even with infinitesimal amounts of oxygen in the atmosphere, molten magnesium will oxidize and form MgO. The calculations performed with FactSage by Aarstad, indeed, show that at 700°C, only an O_2 partial pressure of $5 \cdot 10^{-54}$ bar or higher is needed for magnesium oxidation to occur [Aar04]. Thus, thermodynamically, it is almost impossible to prevent magnesium oxidation.

However, once the O_2 content is consumed (or reduced), it is difficult to asses that the mould-metal reactions would be suppressed, as stated by Cingi [Cin06]. Direct reactions between mould materials and magnesium may also be initiated, as they are also thermodynamically favourable. Most of the

authors that study the reactions in magnesium investment casting consider that the molten metal reacts directly with the mould [Jaf11, Arr07, Sin06, Idr96]. Direct mould-metal reactions were generally explored only on the basis of the free energy of formation of magnesia. The comparison between the free energy of formation of MgO (ΔG^0_{MgO}), and the one of mould refractories is understood as the tendency of the melt to react with the mould, decompose it and produce MgO. A small difference of ΔG^0 will then indicate a weak driving force for MgO formation, and a high resistance of the mould refractory to oppose the thermal decomposition (reverse reaction) [Cin06]. Investigations on the thermal oxidation of solid alloys at high temperatures (i.e. T > 800 K) also consider Gibb's free energy of formation as the unique criterion to determine the creation of oxides. It is considered that, at these high temperatures, local thermodynamic equilibrium generally prevails at the reacting metal/oxide, oxide/oxide and oxide/gas interfaces, and the thermal energy is sufficient to allow existing ions or electrons to surmount their energy barriers for movement into and through the developing oxide layer [Vin06]. The consideration of Gibb's free energy of formation as the unique criterion to determine the creation of compounds seems feasible in investment casting, due not only to the high temperatures achieved but especially to the slow cooling rate of the mould-metal interface in this process. For those cases in which the interface cools down rapidly, reactions cannot be determined by thermodynamics alone. In rapid processes such as thermal spraying (<2 ms), for example, reaction kinetics need to be employed to explain the degree of oxidation reaction, which is dependent on time, area, mass transfer, temperature, etc [Kor04].

Additionally, Mg vapours may also penetrate in the mould and react with shell materials, producing mould-metal reactions far away from the interface. As commented in Section 2.3.2: Magnesium oxidation, above 450 ºC, the Mg evaporation rate is so high the reaction can even occur at a considerable distance from the surface [Cze04, Cze02].

2.9.4 Methods to avoid mould-metal reactions in investment casting

It was seen that mould materials with a ΔG_f higher (or equal) than the one of magnesia are not likely to be employed in Mg investment casting . This means that the mould refractories employed are always less stable than MgO. If a direct reaction between the Mg melt and the mould is considered, formation of the oxide will always be thermodynamically favourable. Due to that, the success of the employed materials depends on the severity of the conditions employed in the castings. Thus, suppression of the oxidation reaction in the mould is influenced by the stability of the refractory, Mg casting temperature and mould preheating temperature (interface temperature) and casting section thickness (solidification time of the interface). However, high melt and temperatures are often employed in investment casting to enhance the filling of thin-walled elements. Complex components, which may have thick parts, are also very common in this casting process. Because of this, when

severe experimental conditions are employed inhibitors are used in conjunction with the non-conventional moulds.

Inhibitors can be even used to protect effectively castings in conventional silica moulds. This silica can be present either as the refractory filler, or as the binder of the first layer of the mould. However, the effectiveness of the inhibitor is also related to the temperature conditions. Under high Mg melt and mould preheating temperatures, the inhibitor may be unable to form a coherent and thus protective layer. This effect is more pronounced in the case of the refractory filler than for the colloidal binder, as the amount of refractory oxides present in the mould is bigger. Unstable inhibitors that release fluorine fast and easily should be considered, as the effectiveness of the investment inhibitor, depends on its ability to form a coherent fluorine containing layer. This can be achieved again by using high SF_6 %, choosing and adequate carrier gas or by decreasing the temperature of the interface as the MgO formation is speed up with temperature.

CHAPTER III
GENERAL METHODOLOGY

3.1 Introduction

With the aim of developing a mould-metal reaction free process for the investment casting industry, two serials of investment casting experiments will be performed in next chapters. The objective of the first serial is to select a suitable inhibitor for Mg investment casting. This inhibitor will be used in the second serial of experiments, in which alternative mould materials will be tested. As a result, after the two serials the best inhibitor+mould material combination will be chosen, and employed lately in a prototype casting. In both essays serials a stepped geometry will be cast. These steps will offer surface samples with different temperature and cooling patterns, recorded with thermocouples. The chemical analysis of those surface films will provide the information needed to understand the role that the different inhibitors and materials play in the formation of surface films, whether these films are protective or not.

In this chapter, parameters and procedures followed to accomplish these objectives are presented. Tested materials and chemicals were chosen among commercial options currently existent in the market, to ensure that a near future implementation of the improvements found through this thesis are possible.

3.2 Casting of the inhibitor essays and alternative mould material essays

3.2.1 Component geometry

Figure 3.1.a shows the casting mould employed in both serials. The component has a stepped geometry with general dimensions of 80mmx60mm, being the steps 2, 4 and 8mm thick.
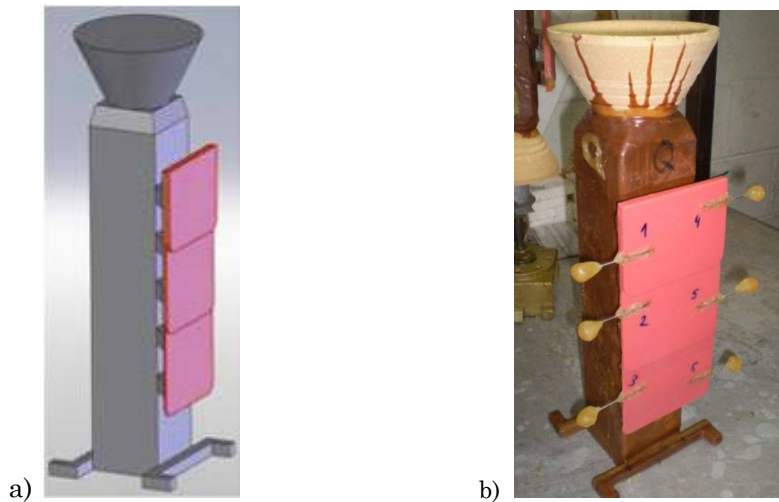
Figure 3.1: a) Surface characterization samples are extracted from the different steps of the part, in red colour b) Mould wax model, where 2 thermocouples are placed in each step

The 3 steps of the geometry provide flat surfaces that facilitate the extraction and analysis of samples. Each step is fed by a casting gate, 16 mm thick. Accordingly, each step possesses 2 different interface conditions, thus different reactions can be expected for them. The thinnest step, for example, possesses the one corresponding to the 2 mm thick areas and the one corresponding to the 18 mm wide areas. This last area is the result of placing the 16 mm thick gate in the 2 mm thick step. In summary, 6 thermocouples were placed in each mould, recording the 6 different interface temperature-time curves (T-t) available. Figure 3.1.b shows a wax model, were thermocouple sheaths have already been placed on the part surface.
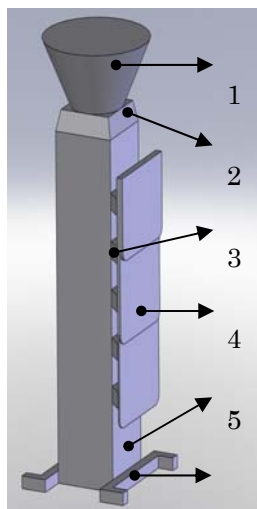
1: Commercial sprue crown
2: Foseco STEELEX filter, 10ppi
3: Trapezoidal gating system,
4: Casting part; steps 2, 4 and 8mm thick
5: Sprue tube
6: Stand

Figure 3.2: The designed and hand-made mould is composed of six components

All the investment moulds were constructed in MICROFUSIÓN ALFA, S.L. The selected geometry is directly injected in the company. The elements of the mould and gating system are mostly hand made and hand assembled, which implies long construction times for each mould. Minimizing the number of mould components to six, the effort employed in the construction and assembly of the components was significantly reduced (Figure 3.2).

3.2.2 Casting methodology

The melting procedure for the inhibitors essays and the mould material essays was identical. A M.F. FIM 60/120 induction furnace was used for the melting of Mg alloys, which was placed inside a steel crucible with 8l capacity. The crucible was preheated till dull red heat before being charged with ingots. When the melt reached 720-740ºC, the grain-refiner powder Nucleant 5000 (FOSECO) was introduced, wrapped inside aluminium foil. Due to the flammability of the grain-refiner, care must be taken in this process.

Nucleant 5000 is based on SiC particles. Carbon addition methods have become the major industrial grain refinement technique. His melt refining technique offers some important practical advantages such as lower operating temperature, large melt volumes and less fading with long holding time, comparing to other conventional refining techniques. Moreover, the addition of the carbon as SiC particles to AZ91 melt gives significant grain size reduction. SiC particles, found within the primary Mg grains, suggest that the refining effect may be due to a possible heterogeneous nucleation mechanism, or to a reduction of the growth rate of the primary phase [Lee00]. After grain refinement the melt was cleaned from oxides and casting temperature was fixed. Finally, all the oxides which were placed on the surface were removed. A preheated and inhibited investment-cast mould was taken out from a furnace and the casting was completed.

3.2.3 Melt protection

SF_6 is one of the most effective melt protectors, as seen previously in the literature review (Section 2.4.4). However, SF_6 could not be used as melt protector in the inhibitor experiments, as one of the inhibitors to be tested in the inhibitor essays is SF_6 itself. Subsequently, to avoid SF_6 contamination with during the testing of other inhibitors, these experiments were performed using flux Magrex 60 from FOSECO® as melt protector. Accordingly, in the alternative material essays, melting of the AZ91E alloy was completed under the protection of the SF_6 mixture. Further details of the selected inhibitors, and the mould inhibition technique, are given in Section 3.2.5 of this chapter.

3.2.4 Casting temperatures

Based on previous knowledge, two Mg casting temperatures were defined [Her12, Her10, Her09]. Magnesium melting maximum temperature was set around 750-760ºC. Severity of the mould-metal reactions increases sustainably with temperature and mould-metal reaction free surfaces are very difficult to obtain at higher casting temperatures. Magnesium minimum casting temperature was defined as 725ºC. Although Mg alloys melt around 600ºC, to fill thin walls in Mg gravity casting processes temperatures around 700ºC are needed, due to the low heat capacity of magnesium. Mould preheating temperatures were set to 520ºC and 550ºC. These two temperatures, combined with the

Mg melt temperature, should be high enough to ensure the filling of all the steps, including the 2mm thinnest one. Higher mould temperatures were discarded, due to the increase in the reactions rates as mentioned before. As a result, two different experimental conditions were defined: high and low temperature essays, summarized in Table3.1:

Table3.1: Temperature conditions for the magnesium melt and the mould, prior to the casting

Essay Conditions	Mg melt temperature (ºC)	Mould preheating temperature (ºC)
High temperatures	745	550
Low temperatures	725	520

3.2.5 Selection of the Mg alloy, inhibitors and alternative mould materials

- *Selection of a commercial magnesium alloy*

AZ91E magnesium alloy was chosen to perform the experiments. As stated in the literature review (Section 2.2), AZ91E is specially employed in casting due to its excellent castability high specific strength and relative low price. Actually, by using AZ91 alloy, thin walled castings with thicknesses minor than 1mm can be easily obtained in pressure assisted casting processes, like high pressure die casting [Yan08, Bla04]. The overall composition and main mechanical properties of this alloy is shown in Table 3.2 and Table 3.3, respectively:

Table 3.2: Composition (%wt) of AZ91E alloy [Ave99]

Alloy	Standard		% Al	% Mn	% Zn	% Si	% Fe max	% Ni max	% Cu max	Other Elements
	ASTM	UNS								
AZ91E	B93	M11918	8.3-9.2	0.17-0.50	0.45-0.9	0.20	0.005	0.0010	0.015	0.01 OE 0.30 OT

Table 3.3: AZ91E Mechanical properties after T6 [Ave99]

Alloy	R_m MPa	$Rp_{0.2}$ MPa	A % (a)	τ MPa	Hardness HR (b)
AZ91E-T6	275	145	6	145	66

a) 50mm extensometer, b) 500 kg, 10mm ball

3.2.6 Selection of alternative inhibitors

As a result of the literature review performed on melt protectors (Sections 2.4 and 2.5) and magnesium investment casting inhibitors (Section 2.8.3) $NaBF_4$, KBF_4 and FK liquid inhibitors and gaseous SF_6 were chosen to reduce mould-metal reactions in Mg investment casting. KBF_4 and FK have not been tested yet in magnesium investment casting experiments.

KBF_4 and $NaBF_4$ are similar chemicals in their properties, but one noticeable difference is the solubility of these salts in water. KBF_4 is only slightly soluble in water (4.4g/l at 20ºC) whereas

$NaBF_4$ is highly soluble in water: 973g/l at 20ºC. Due to this difference, Cingi only tested $NaBF_4$ in liquid state, after preparing aqueous solutions by dissolving 36.5 g powder per litre of H_2O [Cin06]. This powder-water relation was defined by the author as optimum. However, the solubility of KBF_4 increases exponentially with temperature, reaching to 62.5 g powder per litre of H_2O at 100ºC. In order to employ KBF_4, and compare effectively both inhibitors, solutions were made adding 38 g of powder per litre of warm water at 65ºC. This relation is the solubility limit of KBF_4 at that temperature [Zan04], and moreover it is similar to the quantity employed by Cingi.

FK has also been chosen for its employment in liquid state. Fluoroketones, unlike SF_6, are low temperature boiling liquids that can be evaporated into a carrier gas stream like the 3M™ Novec™ 612 Magnesium Protection Fluid. Experiments carried on Mg melt protection with Novec™ 612 have already given good results [Mil03], but gaseous FK is under patent of 3M®. As it is not soluble in water, moulds were dipped directly in the solution, prior to mould preheating.

As SF_6 is the most widely employed melt protector, this inhibitor will also be tested for comparison with the new inhibitors. The analysis of the reaction compounds may also provide more information about the reaction mechanisms, still under study. Some research works were analyzed to determine the concentration and flow of the SF_6 to be employed in the essays. Table 3.4 summarizes the experimental conditions employed in the works developed by Idris and Clegg, Zhang *et al* and Arruebarrena *et al* [Arr07, Zha04, Idr96].

Table 3.4: Experimental conditions employed in Mg investment castings protected with SF_6

Reference	Carrier gas	% SF_6	Time (sec)	Gas flow (l/min)	Chamber Yes	Chamber No	Reactions avoided Yes	Reactions avoided No
[Idr96]	CO_2		30	40		X		X
					X		X	
				25	X		X	
				10	X		X (dull)	
				5	X		X (dull)	
[Zha04]	CO_2	1%	40	0,19	X		X (ZrO_2)	
								X (SiO_2)
		>1%	40	0,19	X		X (ZrO_2)	
							X (SiO_2)	
[Arr07]	Ar	1%			X			X
		3%			X			X
		6%			X			X
		9%			X			X
	CO_2	1%			X			X
		3%			X			X
		6%			X			X
		9%			X		X	

The method of placing the ceramic mould inside an enclosure or chamber, and flushing the whole system (both the mould cavity and the enclosure) was firstly employed by Idris and Clegg. This method was applied to ensure that, during the pouring, the gas remains in the mould. The authors considered that, although SF_6 is heavier than air, it might be pushed out of the mould due to turbulences during the pouring of the metal. However, this method has not been utilized in this work, as the aim of the experiments is to reproduce the real casting conditions of the foundries. Higher concentrations of SF_6 than the ones employed in chambers should be expected, then, to achieve clean metallic surfaces. This effect can clearly be seen in Idri's work. All the flows employed gave clean surfaces, dull or metallic, achieving better results as long as the SF_6 content was increased [Idr96]. However, the essay without chamber produced reactions on the magnesium surface, although the highest flow rate was employed.

The experiments by Arruebarrena *et al.* were performed without any chamber. Different concentrations were tested and clear surfaces were achieved when 9% SF_6 in CO_2 was employed. However the SF_6 percentage employed by the authors is quite high due to the employment of conventional aluminosilicate moulds [Arr07]. As non-conventional moulds are going to be tested in this thesis, lower SF_6 concentrations could be expected in the SF_6 castings.

As a result of the information provided in Table 3.4, 4% SF_6 in CO_2 gaseous inhibitor was selected. Melt protection is effectively achieved with this inhibitor percentage, and CO_2 has proved to be very effective as a carrier gas. It will be flushed for 30 second, at a rate of 5l/min with the aim of employing the lowest volume of gas.

3.2.7 Selection of the alternative mould materials

- *Refractory flour*

Diagram of Figure 2.33 was employed by Cingi to analyze stability of binary oxides values at room temperature, denoted as ΔG_{298}^0. Figure 1 plots ΔG_{298}^0 vs. $10^4 / T_m$, where T_m is the melting point in Kelvin degrees [Cin06]. The dashed line in the middle separates acceptable refractory compounds (above the line) from unacceptable ones (below the dashed line). Unacceptable compounds are disqualified by the combined criteria of both melting point and chemical stability. For magnesium casting, high melting point is not very critical due to relatively low casting temperatures, but chemical stability is of importance [Cin06]. Figure 2.33 shows that MgO is one of the most stable compounds. Refractories with a free energy of formation similar to magnesia were analyzed (inside green circle): La_2O_3, SrO, CaO, UO_2; Y_2O_3, CeO_2; ZrO_2, HfO_2, $MgAl_2O_4$, BaO and Al_2O_3. However, even though these oxides are very stable some of them also have other properties which make them difficult to use in any application [Cin06]:

o BeO$_2$: Human Carcinogen

o UO$_2$, ThO$_2$: Radioactivity

o BaO, SrO, CaO: Slaking susceptibility

o La$_2$O$_3$, SrO, Y$_2$O$_3$, CeO$_2$, HfO$_2$, UO$_2$, BaO,: Expensive

o MgO: Short life investment casting slurries.
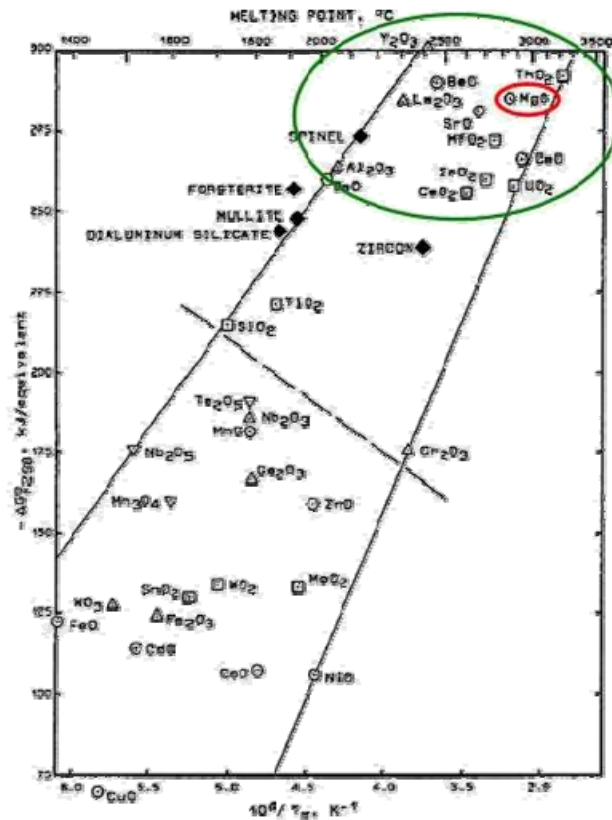
Figure 3.3: ΔG^0_{298} of binary oxides and some common tertiary oxides [Cin06]

Only three compounds remain after the elimination process: zirconia (ZrO$_2$), alumina (Al$_2$O$_3$) and spinel (MgAl$_2$O$_4$). Experimental castings performed with Al$_2$O$_3$ in magnesium investment casting have positioned alumina as an adequate material for avoiding mould-metal reactions[Cin06, Kim01, Kim00]. MgAl$_2$O$_4$ has never been employed in Mg investment casting. Zirconia has proved to give worse results than alumina [Cin06]. Due to this, Al$_2$O$_3$ and MgAl$_2$O$_4$ were chosen as the alternative refractory materials to be tested in this thesis.

- *Refractory binder*

As commented before, investment casting moulds comprise layers of refractory materials, being these layers made up of flour and colloidal binder. Non conventional binders have already been tested in different works [Ros04, Kim01, Kim00]. All the authors conclude that the employment of silica free binders reduces the mould-metal reactions. However, due to the small quantity of silica present in

the binder, it is possible to obtain reaction-free surfaces thanks to the use of inhibitors. Diagram of Figure 2.33 was employed again to select an appropriate non-conventional binder, and commercial ZrO_2 and Al_2O_3 were found. So, due to its better behaviour, an Al_2O_3 commercial binder was chosen. Conventional SiO_2 binder has also selected, as it is cheaper than the non-conventional ones and it can also provide reaction free surfaces.

3.2.8 Mould preparation

Summarizing, in the previous section alumina (Al_2O_3) and spinel ($MgAl_2O_4$) were chosen as alternative flours and alumina (Al_2O_3) and silica (SiO_2) as binders, to be experimented in the second serial of experiments: alternative mould essays. Conventional silica moulds have also been included to quantify the effectiveness of the alternative materials. However, to perform firstly the inhibitor essays, it was decided to employ only one type of mould to reduce the number of variables that influence in the inhibitor's effectiveness. Due to the high essay temperatures selected in Section 3.2.2, the use of conventional flour would probably lead to mould destruction. $MgAl_2O_4$ has never been experimented in investment casting so its behaviour is still unknown. Al_2O_3 has already been tested with positive results as alternative flour and alternative binder, so alumina moulds will be constructed for the inhibitor essays.

- *Aging of Al₂O₃ flour-Al₂O₃ binder slurry*

Preparation of the Al_2O_3 flour-Al_2O_3 binder mould gave several problems. The slurry was firstly prepared in a semi-industrial size tank, following the conventional procedure employed in ALFA foundry. Five hours later, the first pH measurement could not be performed, because the slurry had already jellified. The pH value is a critical value to be controlled during the slurry preparation, and must be kept between 3.4 and 4.3. Later trials were performed in laboratory conditions. After the initial flour-binder mixture, several steps were followed to obtain slurries as stable as the industrial ones, which have months' life. Table 3.5 shows the procedure followed in the last trial performed in the laboratory:

Table 3.5: Procedure followed to obtain stable Al_2O_3 flour-Al_2O_3 binder slurry

Time	pH	Additions Flour (g)	HCl 37% (ml)	Binder (ml)	rpm
0	4.35		2 drops	-	195
+5 min.	4.21	-	4 drops	-	
+10 min.	4.20	-	1.7	-	
+12 min.	3.12	180	-	-	
+16 min.	3.28	180	-	-	
+20 min.	-	180	-	-	
+23 min.	3.63	180	-	-	
+26 min.	3.78	180	-	-	
+29 min.	3.91	180	-	-	
+33 min.	3.88	180	-	-	
+39 min.	3.90	180	-	-	
+44 min.	3.99	90	-	-	
+49 min.	4.08	-	0.4ml	-	
+54 min.	3.86	-	-	20	
+58 min.	3.91	-	-	20	
+1:03 min.	4.02	-	0.4ml	-	
+1:09 min.	3.61	20	-	30	
+1:13 min.	4.00	-	-	-	
+1:23 min.	3.89	-	-	-	
+1:29 min.	4.01	-	-	-	
+1:35 min.	4.08	-	-	-	
+1:42 min.	4.13	-	3 drops	-	
+1:48 min.	3.97	-	2 drops	-	
+1:56 min.	4.00	-	0.3ml	-	
+1:59 min.	-	-	-	40	100
+2:03 min.	3.90	-	-	42	193
+2:05 min.	-	-	-	-	100
+2:15 min.	3.95	-	-	-	
+2:23 min.	3.90	-	-	-	
+2:34 min.	4.00	-	0.3ml	21	
+2:48 min.	3.90	-	0.2ml	40	126
+3:01 min.	3.83	-	-	-	
+3:07 min.	3.85	-	-	-	
+3:20 min.	-	-	-	40	
+4:06 min.	4.03	-	3 drops	-	
+4:27 min.	3.90	-	3 drops	30	
+5:05 min.	4.01	-	-	-	
+5:25 min.	4.01	-	-	-	
+5:35 min.	-	-	3 drops	40	230
+5:47 min.	4.01	-	-	-	
+5:53 min.	4.01	-	-	-	
+7:05 min.	END	-	-	-	

After all the additions, the slurry was stable just for one hour. After the last Al_2O_3 flour addition, the slurry was maintained by means of HCl additions that lowered its pH value. However, as time went on the viscosity of the slurry continued increasing so more Al_2O_3 binder was added in the mixture. The revolutions of the laboratory tank were also increased to avoid jellification, although industrial tanks normally work at around 100 rpm. Nevertheless, Al_2O_3 binders were finally discarded due to the difficulty to stabilise the slurry. The trials performed at industrial and laboratory scale indicate that further studies are needed to obtain stable Al_2O_3 binder slurries. Trade marks that commercialize alternative binders also agree that those binders need further research before reaching their industrial use. This rejection has reduced the number of moulds to be prepared.

As a result, 10 moulds were constructed for the inhibitor essays, to select the most suitable inhibitor. The best inhibitor was then employed in the alternative mould essays, for which 12 more moulds were constructed in MICROFUSIÓN ALFA S.L under an industrial environment. Table 3.6 and Table 3.7 include the experimental conditions applied to the two serials of experiments.

Table 3.6: Inhibitor essays. Experimental conditions

Nº	Refractory Flour	Binder	Casting T (Mg-mould) (ºC)	Inhibitor
1				-
2				$NaBF_4$
3			745-550	KBF_4
4				FK
5	Al_2O_3	SiO_2		SF_6
6				-
7				$NaBF_4$
8			725-520	KBF_4
9				FK
10				SF_6

Table 3.7: Alternative mould essays. Experimental conditions

Nº Essay	Binder	Flour	Casting T (Mg-mould) (ºC)	Inhibitor
1			745-550	-
2				KBF_4
3		Al_2O_3	725-520	-
4				Selected*
5			745-550	-
6	SiO_2	$MgAl_2O_4$		Selected*
7			725-520	-
8				Selected*
9			745-550	-
10		SiO_2		Selected*
11			725-20	-
12				Selected*

obtained from the Inhibitor Experiments, Table 3.6

3.3   Analysis of the result obtained in the inhibitor and alternative mould essays: the employed techniques

Diagram of Figure 3.4 details the structure followed in the analysis of the castings:
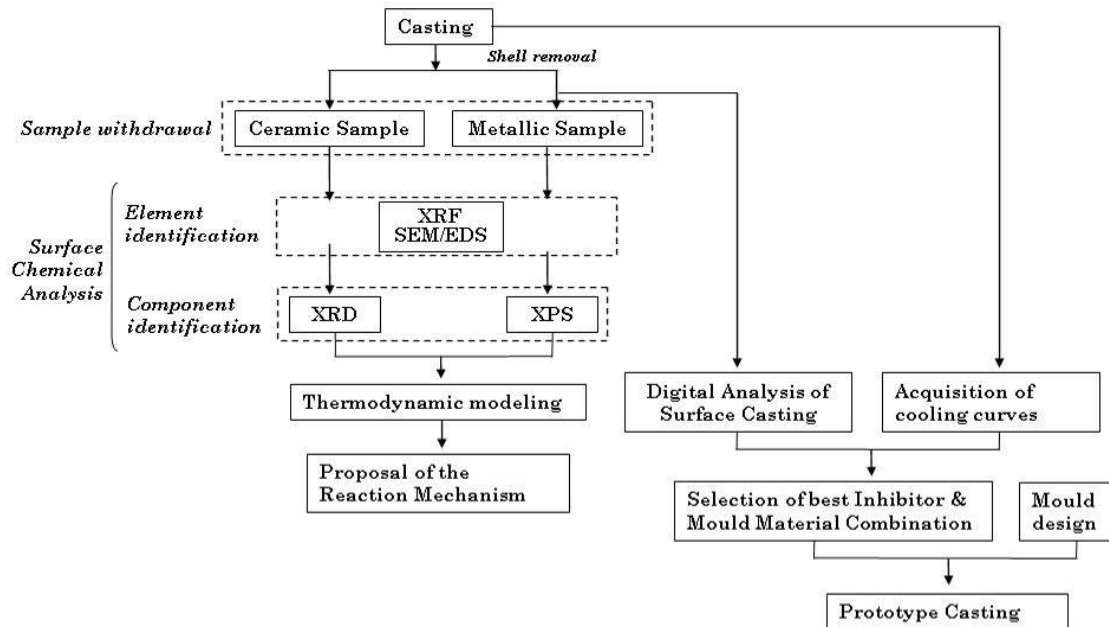
Figure 3.4: Diagram of the techniques employed for the analysis of each casting

Some practical features about the steps described in the diagram of Figure 3.4 are detailed below, as they are essential to understand the election and limits of the analysis techniques.

3.3.1 Digital analysis of the surface castings

Most previous investigators have assessed mould-metal reactions qualitatively only by visual comparisons of digital photographs. However, in this work image analysis of the casting was performed, taking into consideration the original method developed by Cingi [Cin06].

After the casting, all refractory material on the cast test piece was carefully removed and digital pictures of the casting surfaces were taken. For the removal of the refractory, high-pressure water blast was used. Next, image processing software was employed to convert the colour image to greyscale. Brightness and contrast were adjusted until only the reacted areas (black) and unreacted areas (white) were revealed. Afterwards, an image analyzer was used to measure the cumulative amounts of white areas and black areas. This method is based on the count of black and white pixels, and as result a value is given by the image analyzer. Maximum possible value for this number is 255 (all white, all unreacted). Minimum value is zero (all black, all reacted). This number is called arbitrarily as "quality index". Later on, this number can be expressed in terms of percentages.

The most important sources of errors in the quality index measurements can be originated from an incomplete cleaning of the refractory and the unclear boundaries between reacted and unreacted areas. Cingi estimated that an error margin of about ±10% can be given at the medium values of quality index [Cin06].

3.3.2 Sample withdrawal

Measurement of the cooling curves with thermocouples was performed as explained in Section 3.2.2, Casting Methodology. To correlate the metallic samples with the cooling curves, samples were extracted from the area next to the thermocouple edge. Its analogous ceramic sample from the shell was also extracted, in the cases where it could also be obtained. The size of the samples was 25mmx25mm. However, protected surfaces were not always located in the areas nearby the thermocouples. Therefore, sometimes the protected samples came from other areas of the casting.

The shell was carefully removed and preserved. The cast part was high-pressure water blasted to remove the remaining refractory material form the surface, as it is usual in investment casting.

The reacted layer is situated in the interface between the metallic casting and the ceramic mould. But, in some cases, after the shell removal the reacted layer may be divided in two. This effect is dependent on the severity of the mould-metal reactions. It was observed that, when the severity is quite high, all the interface and part of the mould gets stuck to the casting. Unfortunately, after the high-pressure water blast all the refractories are removed. In these cases, only the metallic sample can be obtained. Moreover, essential information about the beginning reaction mechanism may be lost, as the first reaction compounds are the ones nearer to the ceramic part and are water-blasted. On the contrary, when clean metallic surfaces are obtained, the shell can be easily removed and, apparently, the ceramic surface is non-reacted. Metallic and ceramic samples can be obtained and studied to determine the composition of the protective layer. Intermediate situation are the ones that divide the reacted layer into two surfaces, part of the layer stuck to the ceramic shell and the other part to the metallic part. In these cases, both the ceramic and the metallic samples can be obtained and the information of the reaction beginnings remains in the ceramic sample. By the analysis of both samples all the compounds that take part in the reactions can be identified.

Figure 3.5.a corresponds to one of the steps obtained in the inhibitor essays. The magnesium cast part is on the right of the picture, and the removed shell on the left. The surface of the magnesium part shows reacted areas (grey and dull) and non-reacted areas (metal shiny). Due to the metallic appearance of the protected samples, through this document these samples are often referred as non-reacted or clean surface samples, although it is known that a protective surface layer has grown on the casting surface.

The different areas can be even more easily identified looking to the ceramic shell: Reacted metallic surfaces correspond to grey areas of the shell. The more reacted the surface is, the darker the area becomes. In contrast, when protected magnesium surfaces are obtained, the shell continues maintaining its original white appearance. Figure 3.5.b and c show this effect with more detail, where a couple of magnesium and ceramic samples corresponding to a thermocouple recording area are marked.
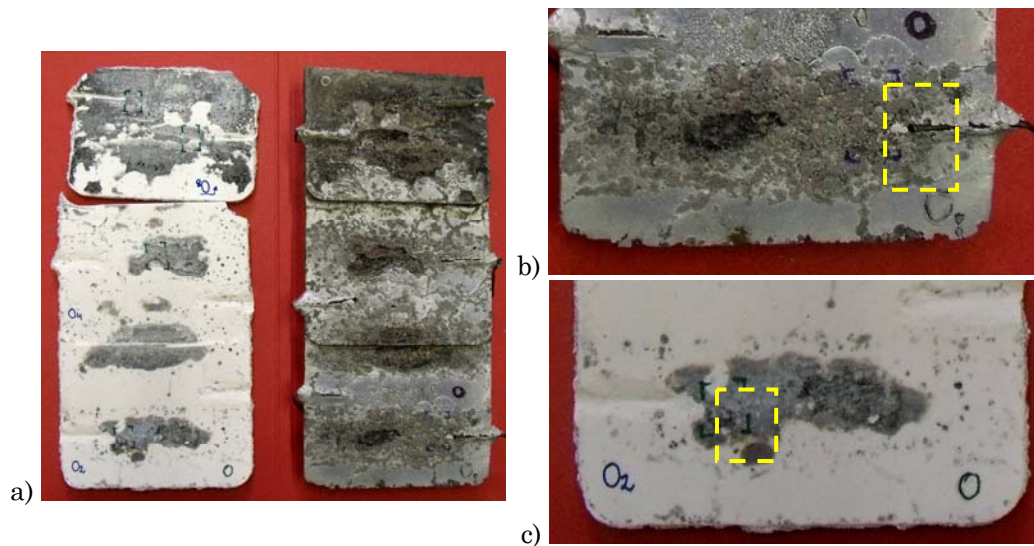
Figure 3.5: a) Ceramic (left) and metallic (right) components obtained in an experiment b) and c): a couple of samples from the same area

3.3.3 Analysis of the cooling curves of the different interfaces

Cooling curves were measured placing K-type thermocouples (chromel-alumel) at the mould-metal interface. Different locations and temperatures were recorded from the casting till the solidus temperature of the alloy. Data-acquisition software was used for registering the data, using time-steps of 0.05 s. Thermocouples were placed in different position of the casting surface, as indicated in Figure 2.19. Different positions mean different cooling curves, and it is more pronounced in components like the selected test part due to its differences in thicknesses. The different T-t curves recorded by the thermocouples lead to different interface conditions and, thus, different reaction levels in the surface of the casting. This information was used for setting correlations between solidification conditions and reaction rates, and for proposing the reaction mechanisms.

3.3.4 Surface chemical analysis

The objective of this analysis is to identify the compounds that are formed in the surface layer, whether this layer is protective or is covered with mould-metal reactions. However, due to the

industrial nature of the experiments, the estimation of these compounds by XRD appeared to be very complex, and the reliability of these first results was quite doubtful. Due to this, chemical analysis of the surface was performed in two stages. A prior step with XRF and SEM element identification techniques was introduced. The information extracted has helped sustainably to determine the compounds of the reaction layer successfully.

It can be seen in the diagram of Figure 3.4 that the techniques applied in the ceramic and metallic samples are different. Ceramic samples were analyzed by means of XRF and XRD. Metallic samples were analyzed successfully with SEM/EDS and XRF, but the analysis of the metallic samples by XRD technique was unsuccessful. The background signal from the AZ91E alloy is so high in the metallic samples that the interpretation of the spectrum was found to be impossible. This conclusion agrees with the work published by K. Aarstad in his thesis, who also attempted to analyze the protective films formed on magnesium [Aar04]. Aarstad concluded that the samples were not adequate for this kind of analysis, because they were too thin and uneven. A similar conclusion was also held by Pettersen *et al*, who analyzed the surface films formed on molten magnesium in different protective atmospheres. The authors recorded XRD-spectra from metallic samples exposed to SF_6 and SO_2 atmospheres. They found that the high intensity peaks from the bulk magnesium were the dominant feature in all the spectra, due to the thin surface film. The authors determined that the method cannot be expected to detect minor phases in the surface film [Pet02].

Due to this, it was decided to analyze the metallic samples with XPS, as this technique also allows the identification of surface compounds. The penetration depth of this technique is quite lower than in XRD, so the minor phases of the films can be detected. Table 3.8 summarizes the performance of the surface analysis techniques employed:

Table 3.8: Summary of the surface chemical analysis technique employed

Technique	X-ray Photoelectron Spectroscopy	Energy Dispersive Spectroscopy	Wavelength Dispersive X-ray Fluorescence	X-ray Diffraction
Abbreviation	XPS	EDS	XRF	XRD
Primary Excitation	X-ray	Electron	X-ray	X-ray
Detected Secondary	Photoelectron	X-ray	X-ray	X-ray
Elemental Range	3-92	6-92	4-92	Crystalline Materials
Detected Depth	3nm	1µm	50µm	10-100µm
Detection Limit	1%	0.1%	ppb	1%
Accuracy	30%	10%	10%	10%
Chemicals State ID?	Yes	No	No	Yes

- *XRF*

A Philips PW 2400 automatic sequential wavelength dispersive X-ray fluorescence spectrometer (WD-RF) of the department of Metallurgy and Materials Engineering of the Catholic University of Leuven (MTM–KULeuven) was employed for the qualitative analysis of the samples, to identify the elements present in the sample.

Figure 3.6: Philips PW 2400 automatic sequential wavelength dispersive X-ray fluorescence spectrometer (WD-XRF) at MTM-KULeuven

- *SEM/EDS*

Scanning electron microscope EOL JSM-5600LV, sited in Mondragon University and equipped with an energy dispersive X-ray spectrometer (EDS) was employed in the characterization. Profiles of both the ceramic and metallic samples were analysed by SEM/EDX, to observe the preferential location of different elements in the surface layers.

- *XRD*

XRD analysis of the samples was performed at the department of Metallurgy and Materials Engineering of the Catholic University of Leuven. For that purpose, a Seifert 3003 TT X-ray diffractometer was used to measure the X-ray diffraction. The Seifert 3003 TT goniometer is of the θ-θ type (source and detector move, the sample is fixed). The goniometer is equipped with a Cu tube. A parabolic multilayer X-ray mirror renders the initially divergent X-ray beam parallel, making the results more independent to sample surface irregularities, including vertical displacements of the sample due to thermal expansion. To coop with fluorescent radiation originating from the interaction of Cu-Ka radiation with Fe or Co containing samples, a flat graphite crystal monochromator is installed in front of the scintillation detector. A 12-position sample changer was used, rotating each specimen. Due to rotation, a larger number of crystallites are probed by the X-rays, which leads to a better reproducibility of the intensities.
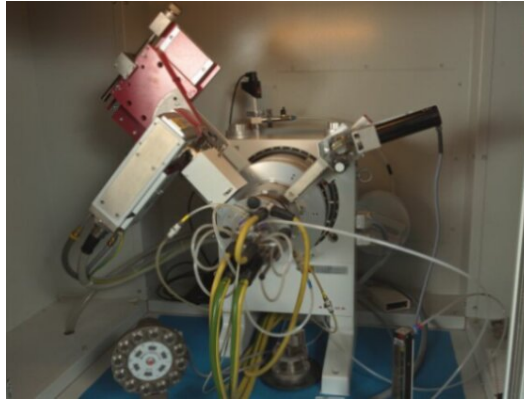
Figure 3.7: Seifert 3003 TT X-ray diffractometer, MTM-KULeuven

- *XPS*

XPS analyses were performed only for the best inhibitor-mould material combination, as the analysis of the samples with this technique was found to be long time consuming. MT 500 VG Microtech spectrometer from the Centro Nacional de Investigaciones Metalúrgicas (CENIM-CSIC), in Madrid was employed. The spectrometer is equipped with a dual (Mg/Al) X-ray source, three-chaneltron detector and Argon ion beam EX05 (Figure 3.8).
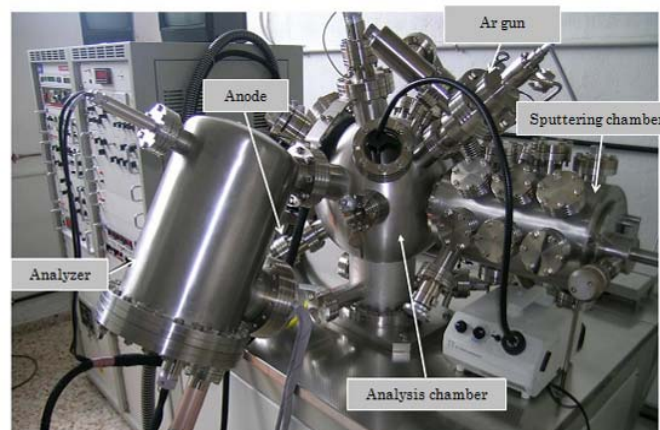
Figure 3.8: 500 VG Microtech spectrometer, located at CENIM-CSIC

3.3.5 Modelling of mould-metal reaction

Mould-metal reactions were modelled with FatSage®, considering the compounds encountered during the surface chemical analysis. Equilibrium module of this software performs complex equilibrium calculations for multicomponent systems, through Gibbs energy minimization. The stability of the components at a certain temperature and pressure is only considered, and the formation rates of the compounds are ignored. However, as stated in Chapter 2, Literature review, solidification times of the investment casting interfaces are high enough to consider that thermodynamic equilibrium prevails at the interface.

3.4 Conclusions

With the aim of developing a mould-metal reaction free process for the investment casting industry, in next chapters two serials of investment casting experiments will be performed. As a result, best inhibitor+ mould material combination for Mg investment casting will be chosen. Table 3.9 and Table 3.10 summarise the experimental conditions applied to the two serials:

Table 3.9: Inhibitor essays. Experimental conditions

Nº Essay	Refractory Flour	Binder	Inhibitor	Casting Temperature (Mg-mould) (ºC)	Designation
1			-	745-550	A-AH
2				725-520	A-AL
3			KBF_4	745-550	A-KH
4				725-520	A-KL
5	Al_2O_3	SiO_2	$NaBF_4$	745-550	A-NaH
6				725-520	A-NaL
7			FK	745-550	A-FH
8				725-520	A-FL
9			SF_6	745-550	A-SH
10				725-520	A-SL

Table 3.10: Alternative mould essays. Experimental conditions

Nº Essay	Binder	Refractory Flour	Casting Temperature (Mg-mould) (ºC)	Inhibitor	Designation
1			745-550	-	A-AH
2		Al_2O_3		KBF_4	A-AL
3			725-520	-	A-KH
4				Selected*	A-KL
5			745-550	-	Mg-AH
6		$MgAl_2O_4$		Selected*	Mg-AL
7	SiO_2		725-520	-	Mg-KH
8				Selected*	Mg-KL
9			745-550	-	Si-AH
10		SiO_2		Selected*	Si-AL
11			725-20	-	Si-KH
12				Selected*	Si-KL

* Best inhibitor from the Inhibitor Experiments (Table 3.6) will be employed in this serial

Mould designation was performed as follows: they were first identified by the refractory flour employed in the shell (Al_2O_3: A, $MgAl_2O_4$: Mg, SiO_2: Si), followed by the inhibitor (Nothing: A, KBF_4: K, $NaBF_4$: Na, FK: F, SF_6: S) and last by the casting temperature (high temperature essays: H, low

temperature essay: L) For example: mould A-KH corresponds to an alumina mould, protected with KBF$_4$ and casted at high temperature conditions.

AZ91E magnesium alloy was chosen to perform the experiments. A stepped geometry was employed in the castings. Each mould provided 6 different interface conditions, thus different reactions were expected from them.

Two different experimental conditions were defined for each mould: high and low temperature essays. These high temperatures, combined with the high solidification times expected from the interfaces, were severe enough to promote the appearance of mould-metal reactions. As it was commented in Chapter 2, Literature review, severe experimental conditions are often employed in investment casting industry to enhance the filling of complex components, which have thin and thick parts at the same time. The surfaces obtained after these experiments, thus, are representative of the process and helpful for the investment casting industry.

Analysis of the results obtained after the two serials was performed according to the diagram of Figure 3.9. At the end, a prototype was cast, and proposals for the mechanisms that lead both reacted and protected surfaces were presented.
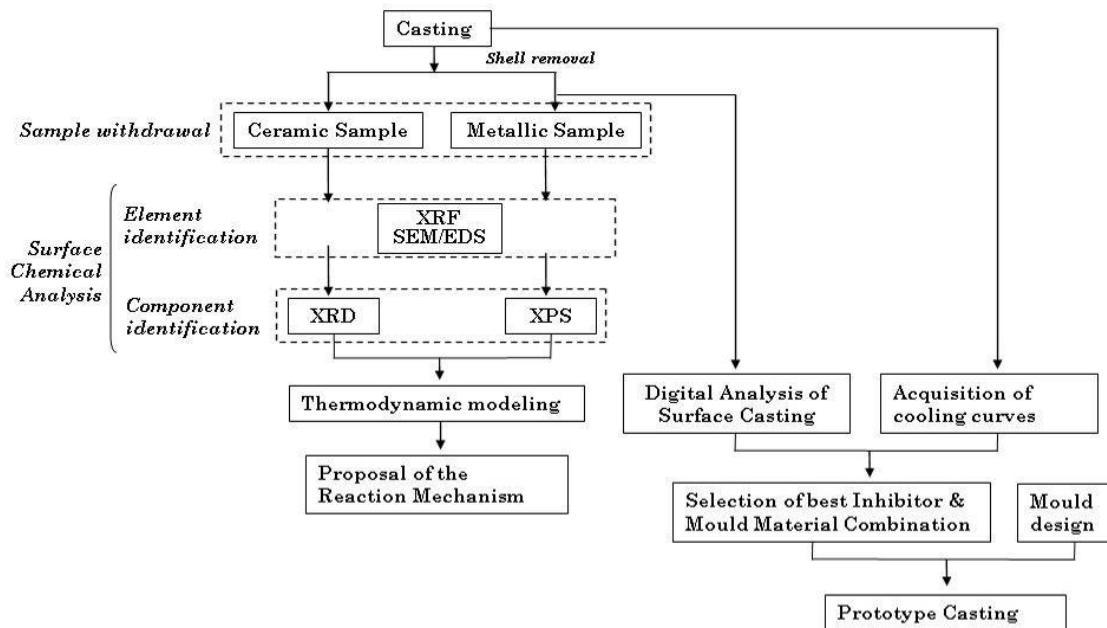
Figure 3.9: Diagram of the techniques employed for the analysis of each casting

CHAPTER IV
INHIBITOR EXPERIMENTS

4.1   Introduction

In the Inhibitor Experiments, $Al_2O_3 + SiO_2$ moulds were cast under five different atmospheres (open air, $NaBF_4$, KBF_4, SF_6 and FK) to analyse the protective behaviour of each inhibitor. The experimental conditions applied in the castings are resumed in Table 4.1:

Table 4.1: Inhibitor essays. Experimental conditions

Nº Essay	Refractory Flour	Binder	Inhibitor	Casting Temperature (Mg-mould) (ºC)	Designation
1				745-550	A-AH
2			-	725-520	A-AL
3				745-550	A-KH
4			KBF_4	725-520	A-KL
5				745-550	A-NaH
6	Al_2O_3	SiO_2	$NaBF_4$	725-520	A-NaL
7				745-550	A-FH
8			FK	725-520	A-FL
9				745-550	A-SH
10			SF_6	725-520	A-SH

In this chapter, the most effective inhibitor for Mg investment casting is selected. Surfaces obtained with the different inhibitors were analysed by means of XRF, SEM/EDS and XRD. The schematic diagram of Figure 4.1 shows in black the tasks performed in this chapter, according to the analysis methodology presented in Chapter 3.
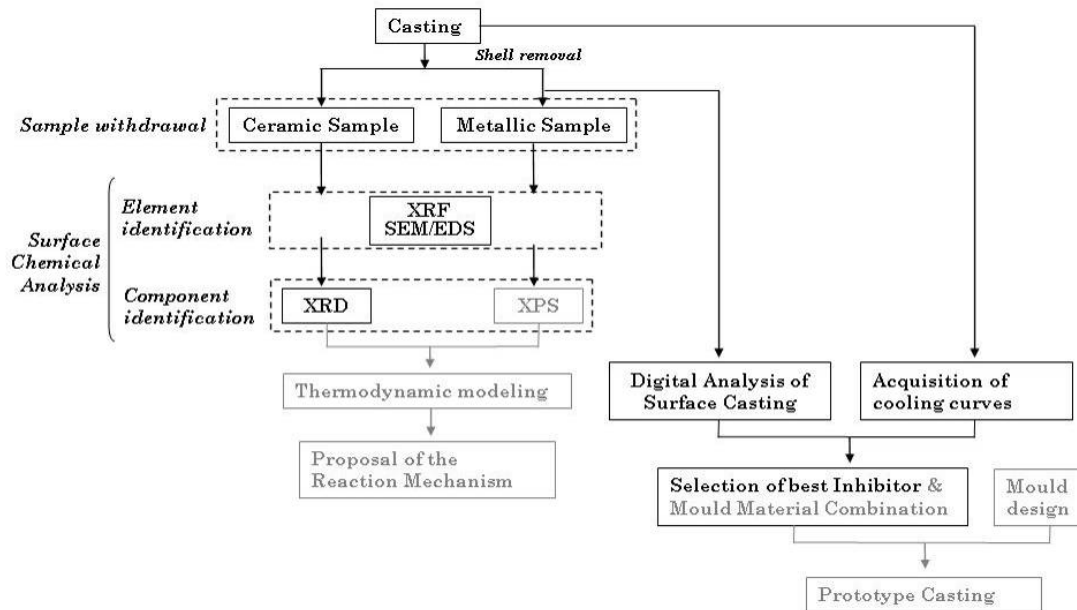
Figure 4.1: Results analysed in Chapter 4 (in black). Tasks in grey are detailed in next chapters

4.2   Casting and digital analysis of the surfaces

Table 4.2 reveals the pictures of the castings obtained in the Inhibitor experiments. The inhibitor effectiveness was evaluated by digital analysis, as explained in Chapter 3 (General methodology): digital pictures were processed until the reacted areas (black) and non-reacted areas (white) are shown, indicating the reacted percentage of each casting.

Open atmosphere essays (A moulds) produced severely reacted surfaces, as expected. The reactions deeply penetrated in the mould and high-pressure water blast had to be used to remove the stuck ceramic from the casting surface. Both high and low temperature essays (A-AH and A-AL) provided very similar results. Due to that, only essay A-AH was analysed. SF_6 did not provide better results compared to A-A moulds, as both casting surfaces (A-SH and A-SH) were almost completely reacted. It is believed that, due to turbulences generated during the alloy pouring, SF_6 escaped from the mould and the casting solidified without protective atmosphere. Even though, some small volumes of the inhibiting gas were trapped in the mould cavity and protected the Mg melt. As both essays (A-SH and A-SH) showed almost identical behaviour, only A-SH is shown in Table 4.2. Moulds inhibited with fluoroketones were destroyed during the casting. During mould preheating, products formed due to the thermal decomposition of the inhibitor (HF, for instance) could have caused this destruction.

Table 4.2: Quantitative analysis of the effectiveness of the tested atmospheres

Air	NaBF$_4$		KBF$_4$		SF$_6$
A-AH	A-NaH	A-NaL	A-KH	A-KL	A-SH
99%	84,5%	82%	93%	78%	96%

In contrast, the employment of KBF$_4$ and NaBF$_4$ provided large non-reacted areas on the castings (moulds K and Na). Both inhibitors showed, as expected, a decrease in the number of reactions in the essays at lower temperatures. For these two inhibitors, reactions were not so severe, so surfaces without stuck ceramic were found after shell removal. KBF$_4$ clearly proved to be the most effective inhibitor: essay A-KL was the less reacted, with 78% of its surface covered with mould-metal reactions. However, essay A-KH, performed at 745-550ºC, gave worse results than those performed with NaBF$_4$. Explanation for that can be found in the analysis of the cooling curves recorded by the thermocouples of each mould, Figure 4.2.

Temperatures recorded in essay A-KH were higher than the ones recorded in both NaBF$_4$ essays. The reaction time (until the alloy reaches solidus temperature) was also higher: around 1100-1200 sec for A-KH mould, against 1000-1100s in A-NaL and 1000s in A-NaH. Maximum temperatures at the interface are also higher in the A-KH experiment, where 750ºC was achieved. Conversely, on A-NaH and A-NaL castings maximum temperatures of 700ºC were not even reached. Because of that, severity of the reactions in essay A-KH increased and the 93% of the surface was covered with mould-metal reactions. In fact, interface conditions of essay A-KL, KBF$_4$ at low T, were even more severe

than the ones recorded in essay A-NaH. Although temperature values were similar for both, solidus time in essay 6 was longer: around 1100-1200 sec, which reaffirms KBF_4 as the best inhibitor.
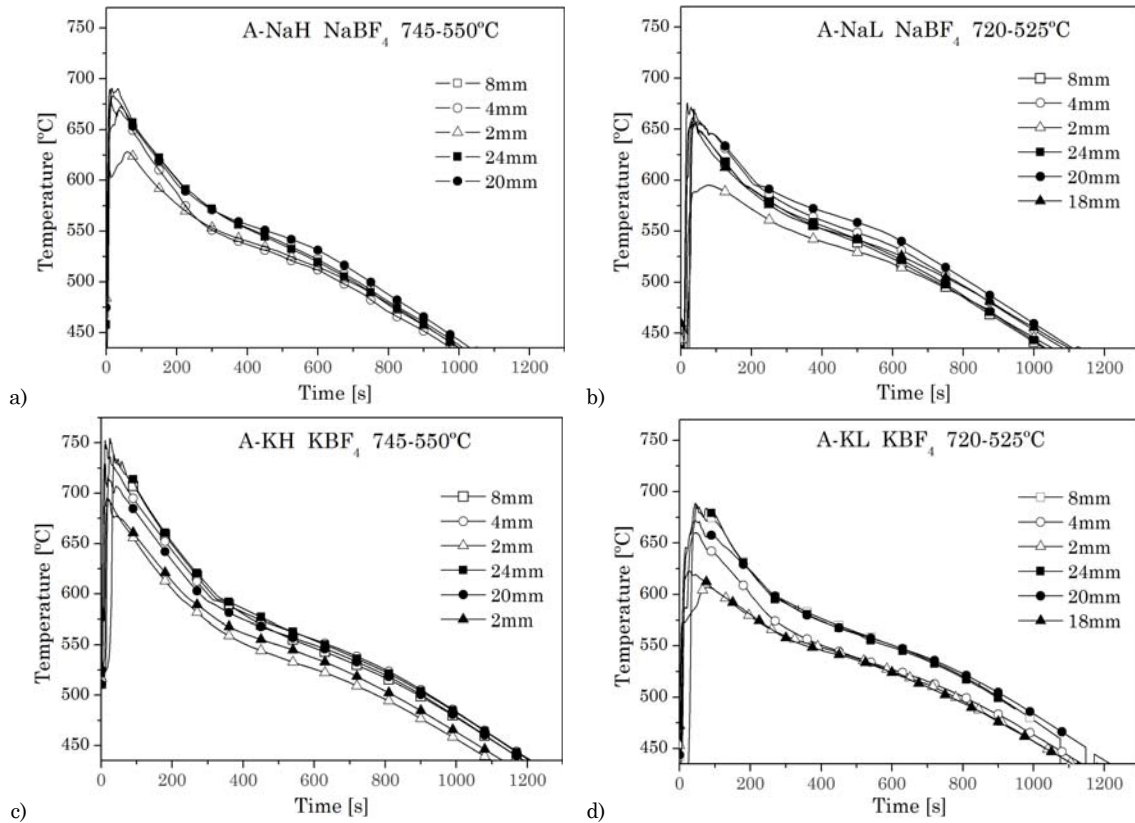
Figure 4.2: Time-temperature curves for $NaBF_4$ and KBF_4 experiments. Temperature values above the AZ91E solidus point are shown

More information was expected to be extracted from the cooling curves. The initial idea was to obtain, for each atmosphere, cooling curves placed on non reacted surfaces. The inhibitor would then be considered effective for those castings with surface cooling conditions equal or less severe than the corresponding to those thermocouples. Unfortunately, the analysis of the cooling curves leads to uncertain results. Figure 4.3, for example, shows again the curves recorded for the A-KL mould. In this casting, clean surfaces were obtained only for the thermocouples positioned in steps that are 2 and 4mm thick. The thermocouple on the 18mm thick step recorded a curve whose maximum temperature lied down in between of the 2 and 4mm temperature values. The solidification time of the 18mm thermocouple was almost the same when compared to the other two, despite of the higher thickness. Accordingly, the 18mm thermocouple was expected to be placed in a clean surface but, conversely, it was placed on a reacted area of the casting. The basis for the inconsistent cooling curves may be found in the methodology employed for recording the interface temperatures. Thermocouples are manually positioned on the wax model, so they may have slightly penetrated in the casting, recording temperatures that do not correspond to those in the interface.
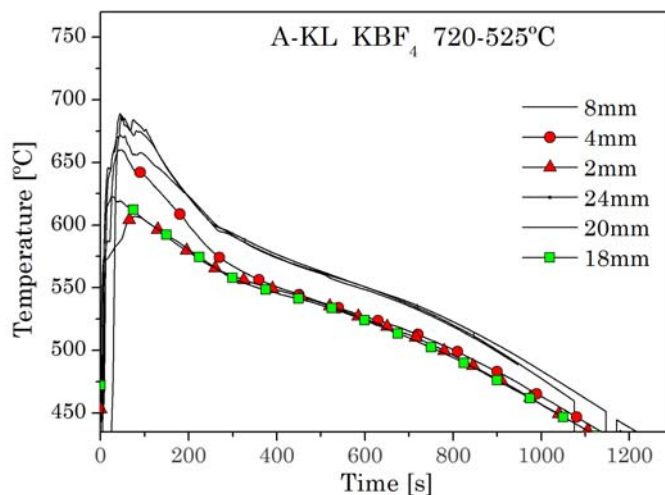
Figure 4.3: Analysis of the A-KL time-temperature curves, where the ones corresponding to 2mm and 4mm thick steps are marked in red, and the one corresponding to 18mm in green

4.3 Surface chemical analysis

Chemical analysis was performed in two stages, as detailed in Chapter 3: General methodology. The objective of these analyses was to determine which are the compounds that form the surface layer of the castings, whether this layer was protective or not. Due to the industrial nature of the experiments, the estimation of the compounds by XRD was very complex so firstly XRF and SEM element identification techniques were employed.

Samples were labelled as follows: first, designed with the mould name (Table 4.2) and then, followed with a number that corresponds to the sample thickness. Last letter differentiates between the metallic (m) and ceramic samples (c). For example: sample A-KL-18m* corresponds to a metallic sample, extracted from the 18mm thick area of A-KL casting. * indicates that the sample was not covered with mould-metal reactions.

4.3.1 Al$_2$O$_3$ mould and melt protector

- *XRF*

The aim of the XRF measurements is to detect the main elements present in the samples, and thus facilitate the identification of the compounds formed in the mould-metal reactions. Due to the industrial nature of the experiments and the materials involved in them, several impurities may be found in the samples. Consequently, to identify the origin of those impurities, the shell and the melt protector employed in the experiments have firstly been analysed (Table 4.3). The refractory shell employed in the inhibitor experiments was composed of silicon, aluminium, sodium and calcium.

Table 4.3 XRF measurements performed to the shell and melt protector employed. The relative weight % is qualitative

Al$_2$O$_3$+SiO$_2$ shell			Melt protector (MAGREX60®)		
Compound	Rel. Weigh	Std. Error	Compound	Rel. Weigh	Std. Error
Si	59.5	0.3	Cl	65	0.25
Al	38	0.25	K	17.5	0.4
Na	0.5	0.1	Mg	13	0.2
Ca	0.5	0.1	Na	4	0.2
			Br	0.1	0.005
			Zr	0.005	0.002

The refractory shell employed was composed of silicon, aluminium, sodium, and calcium. Calcium is known as one of the most common impurities in many metals, and accordingly it is also one of the main trace elements present in commercial Al$_2$O$_3$ powders, unless strict measures are taken to avoid it. Since the solubility of calcium in alumina is very low, it tends to segregate as calcium oxide (CaO) in the grain boundaries of Al$_2$O$_3$ ([Zha98, Lit99, Hir03]), and as calcium aluminate phase in the boundaries of ß-Al$_2$O$_3$ [Lu10]. CaO is also added to commercial Al$_2$O$_3$, as sintering of ceramic materials to theoretical densities often requires the addition of small amounts of sintering aids [Kim92].

Results of the Magrex® reveal that chlorine, potassium, magnesium and sodium were the main elements present in the flux. Small quantities of bromine and zirconium were also found.

- *XRD*

Non-casted Al$_2$/O$_3$+SiO$_2$ shell has also been analysed by XRD. Results are shown in the XRD spectrum of Figure 4.4, where it can be seen that Al$_2$O$_3$, SiO$_2$ and Na-β-Al$_2$O$_3$ are the main phases present in the investment shell. Some unknown peaks appear also in the spectrum, which could be related to impurities or to unmatched minor phases. According to the XRF results, these peaks correspond to calcium based compounds.
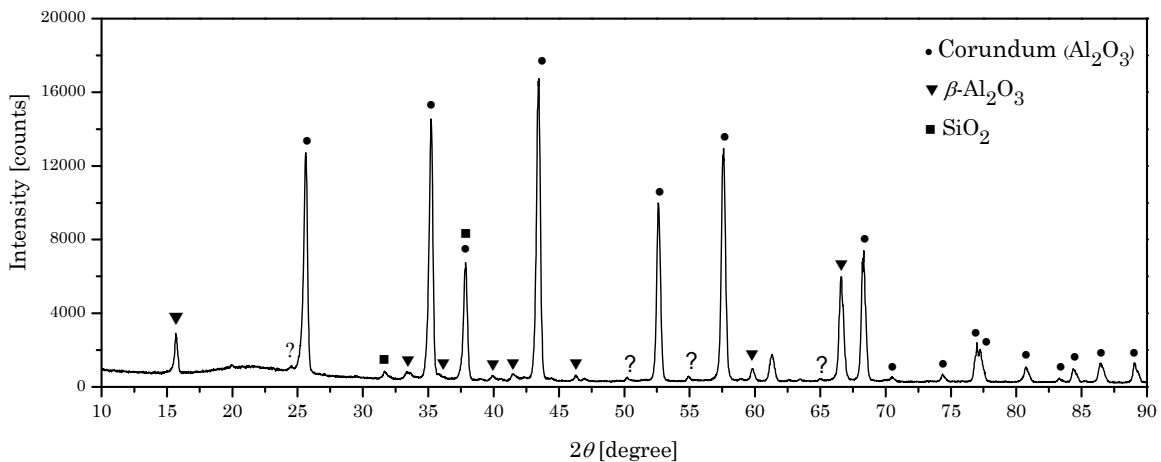
Figure 4.4: XRD spectrum of the Al$_2$O$_3$+SiO$_2$ shell employed in the experiments

Sodium alumina is known to be a non-stoichiometric oxide, assigned the formula $Na_2O.xAl_2O_3$ (5≤x≤11). The conventional method of synthesizing these materials begins with mechanical mixing of the precursor components of ß-alumina (containing Al, Na, Mg, and/or Li), followed by a solid-state reaction at temperatures of 1200ºC-1700ªC to decompose the reactants and form the ß- alumina phase [Mal11]. The unexpected presence of minor β-Al_2O_3 phase in not new and has already been reported: the Na trace impurities present in Al_2O_3 led to the formation of β-alumina in the work of Mitchell *et al*, after the firing at 1250ºC for 60 min of α-Al_2O_3 [Mit02]. The Na-β-Al_2O_3 present in the mould has probably been formed during the production of the fused commercial alumina powders, as Na impurities are typically found in the aluminium oxide powders production [Wen01]. Likewise, during the firing stage of the investment mould, sodium from the SiO_2 binder may have reacted with the commercial Al_2O_3 to form β-Al_2O_3.

4.3.2 Air: A-AH mould

- *Samples extracted from the A-AH mould*

When it comes to mould-metal chemical analysis, it is preferable to select an area where both the metallic and its analogous ceramic sample can be extracted, as explained before in Section 1.2 of Chapter 3, General methodology. Accordingly, from A-AH essay (Table 4.1) two pair of samples were selected: the metallic and ceramic samples corresponding to the 8mm and 24mm thick steps (A-AH-8c and A-AH-8m, A-AH-24c and A-AH-24m). Visual inspection of Figure 4.5 is enough to realize that both the casting and the shell are covered with mould-metal reactions.
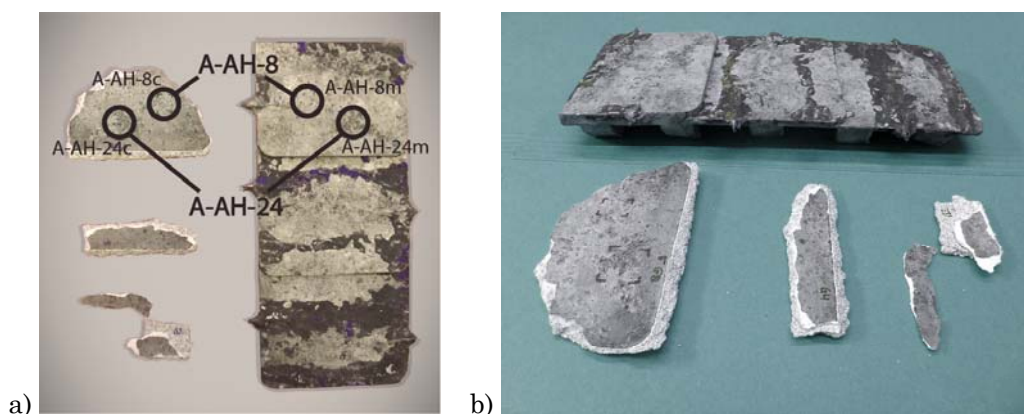
Figure 4.5: a) Part obtained in A-AH casting is shown in the right of picture, and the shell in the left. Samples were extracted from both b) Another perspective of the step and its shell

- *XRF*

XRF measurements performed on the four samples of the A-AH mould are shown in Table 4.4. Elements from both the casting and the shell are detected in all the samples, which confirm that the interface layer was divided in two during the shell removal stage. Zr, also found in the samples, is

possibly an oxidized impurity present in the mould. Fe is almost certainly coming from the iron-based crucible employed during the castings. The high Ca content present in both metallic samples indicates that calcium is also an impurity present in the AZ91E alloy.

Table 4.4: XRF measurements performed in samples A-AH-24 and A-AH-8. The relative weight % is qualitative. Elements from AZ91E alloy are marked in blue (Mg, Al, Zn, Mn, Ca); from the refractory shell in black (Al, Si, Ca, Na). Iron and zirconium are marked in red

A-AH-24						A-AH-8					
A-AH-24c			A-AH-24m			A-AH-8c			A-AH-8m		
El.	Rel. Weight	Std Error	El.	Rel. Weight	Std Error	El.	Rel. Weight	Std Error	El.	Rel. Weight	Std Error
Mg	2.5	0.4	Mg	72	0.4	Mg	69.5	0.4	Mg	68	0.4
Al	21.5	0.3	Al	21	0.4	Al	19	0.3	Al	23	0.4
Ca	7	0.3	Si	4	0.1	Ca	4	0.2	Si	5	0.12
Si	3	0.1	Zn	0.6	0.1	Si	3	0.1	Zn	0.9	0.09
Zn	2.5	0.1	Cl	0.3	0.07	Zn	1.5	0.1	Ca	0.7	0.09
Mn	1	0.1	Na	0.2	0.06	Mn	1	0.1	Mn	0.2	0.06
Na	0.5	0.09	Mn	0.2	0.07	Na	0.5	0.06			
Fe	0.15	0.06	Zr	0.06	0.03						

- *SEM/EDS*

Figure 4.6 and Figure 4.7 show SEM images taken from A-AH-8c and A-AH-8m samples, respectively. Thickness of the interface layer was measured in both samples, but these values can only be understood as qualitative. Thickness values are given as an indication of the reaction degree of samples, as no attempts to determine the average thicknesses were made.
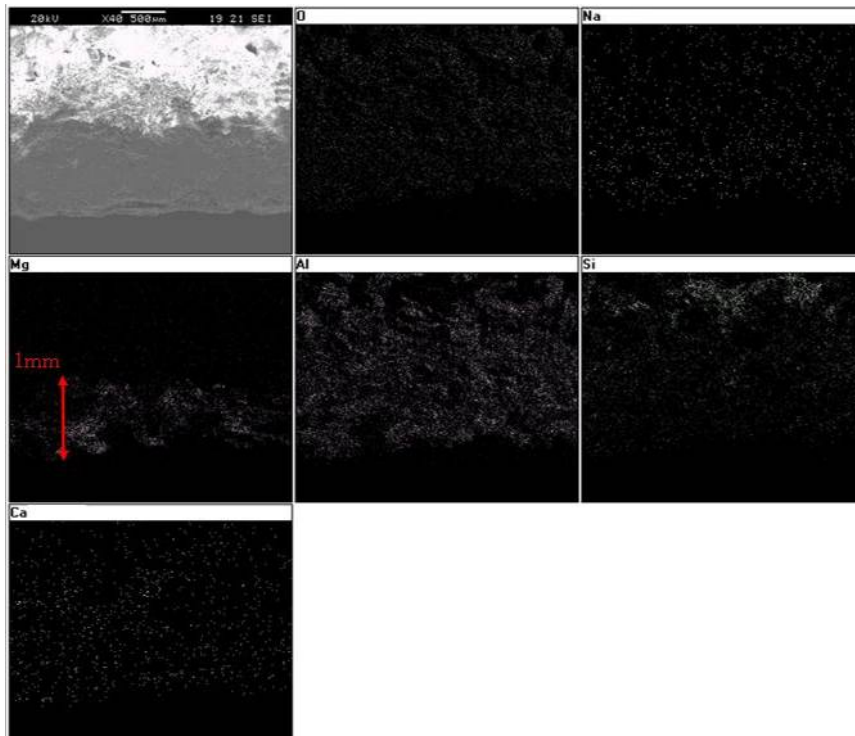
Figure 4.6: SEM/EDS results of A-AH-8c ceramic sample. Surface layer is about 1mm thick

The 1mm thickness of the interface layer on the ceramic sample was determined according to the elemental Mg mapping, as all the magnesium present in the sample comes from mould-metal reactions compounds. Conversely, the interface layer formed on the metallic sample is so thin that it could not be measured by EDS. Even though, the surface of A-AH-8m appears to be uneven, with bumps 70 -109µm high (Figure 4.7).
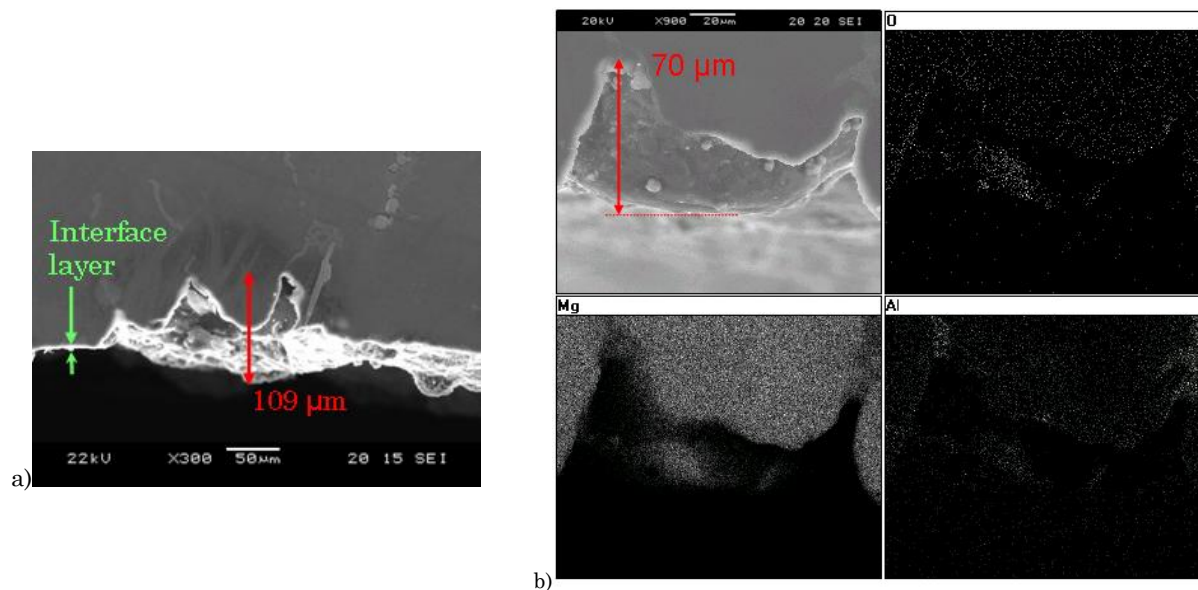
Figure 4.7: SEM/EDS results of sample A-AH-8m. Thickness of the surface layer cannot be determined by EDS

For A-AH mould, it is clear that most of the interface layer remained attached to the ceramic sample. Information of the interface layer along the depth was also obtained with this technique. Elemental mapping performed on sample A-AH-8c cross section reveals that the interface layer is composed mostly of aluminium and magnesium based compounds. Both elements seem to be evenly distributed along the surface layer depth (Figure 4.6 and Figure 4.7.b).

- *XRD*

XRD analysis of samples A-AH-24c and A-AH-8c reveals that the surface of the interface layer stuck to both ceramic samples is composed of Mg, MgO, Mg_2Si and $Mg_{12}Al_{17}$ (Figure 4.8).
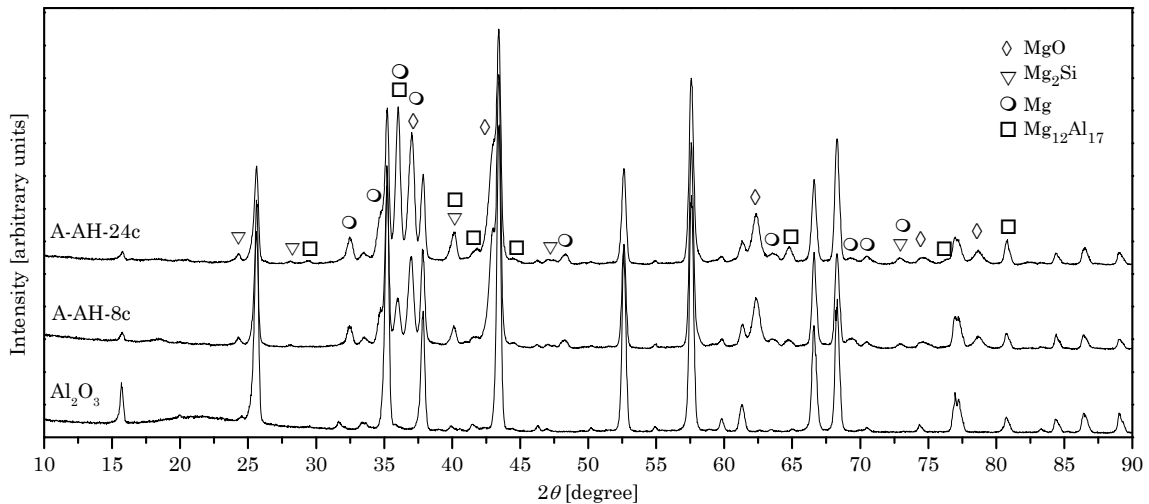
Figure 4.8: XRD spectrum of A-AH-24c and A-AH-8c, compared to Al_2O_3 shell material. Only the additional phases are shown

Due to reactions between Mg and mould materials (SiO_2 and Al_2O_3) MgO and Mg_2Si were formed, and the Mg melt was enriched in aluminium in such concentrations that $Al_{12}Mg_{17}$ end crystallising. Literature also shows the XRD presence of these three compounds in Mg MMCs reinforced with Al_2O_3 and SiC particles, for example, where a direct reaction between the magnesium melt and the refractories of the reinforcement happens [Kaw07, Xiu07, Boc00, Li00]. Further details about the reaction mechanisms are given in Chapters 6 and 7.

Concerning to the Mg phase, two different causes (or the combination of both) explain its presence in the ceramic sample. First, during the shell removal, not only mould-metal reaction compounds but also casting AZ91 alloy was attached to the ceramic sample. This would also explain the presence of Zn and Mn in the XRF analysis of the previous section. Secondly, during the casting Mg vapour diffused trough the ceramic mould, filling its holes and solidifying lately there as α-Mg. This last statement is in agreement with the XPS analysis reported by Sin *et al*, who found Mg inside of plaster moulds [Sin06].

4.3.3 NaBF$_4$ moulds: A-NaH & A-NaL

- *Samples extracted from NaBF$_4$ moulds:*

Regarding to A-NaH mould, two pair of samples corresponding to A-NaH-8 (A-NaH-8c and A-NaH-8m) and A-NaH-18 (A-NaH-18c and A-NaH-18m) were selected. From A-NaL essay, samples corresponding to A-NaL-20 (A-NaL-20c and A-NaL-20m), A-NaL-18 (A-NaL-18c and A-NaL-18m) and NaL-2* (NaL-2*c and NaL-2*m) were chosen. This last sample, unlike the others, corresponds to a sample without mould-metal reactions where the inhibitor protected effectively the surface.
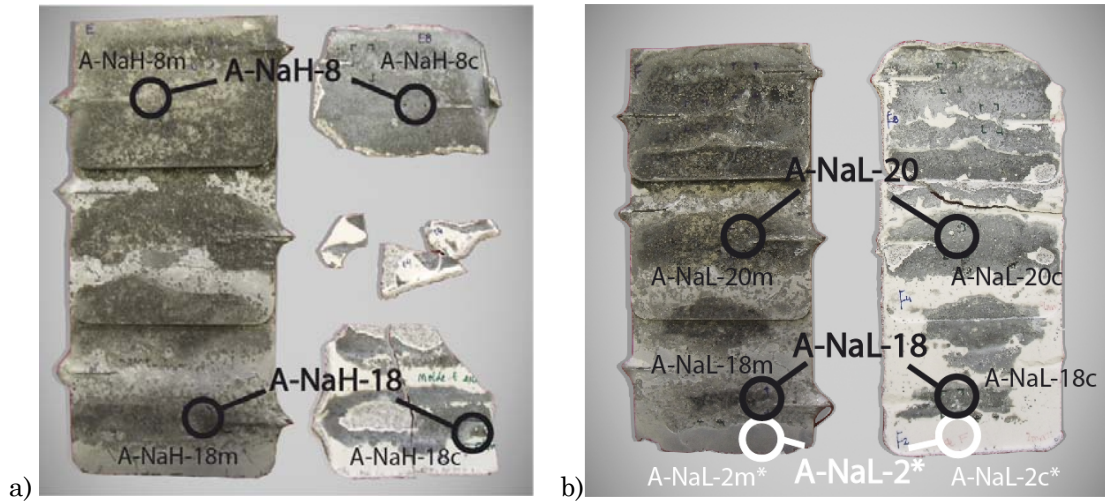
Figure 4.9: Samples selected for the chemical analysis of: a) step and shell obtained in the A-NaH casting b) step and shell obtained in the A-NaL casting

- *XRF*

Both moulds showed almost identical results after the XRF analysis. Due to that, in the table below (Table 4.5) only e results corresponding to the A-NaL mould samples are shown. XRF results obtained from A-NaH mould can be found in the Appendix A: XRF Analysis, Table A.1. Five of the six samples extracted from the A-NaL mould were analysed by XRF. A-NaL-2c* was not analysed, as no reaction was visible on the shell (Figure 4.9.b).

Table 4.5: XRF measurements performed in A-NaL mould samples. The relative weight % is qualitative and fluorine is marked in blue

A-NaL-20						A-NaL-18						A-NaL-2m*		
A-NaL-20c			A-NaL-20m			A-NaL-18c			A-NaL-18m					
El.	W %	Std. Error	El.	W %	Std. Error	El.	W %	Std. Error	El.	W %	Std. Error	El.	W %	Std. Error
Mg	66	0.6	Mg	70.5	0.4	Mg	48.5	0.6	Mg	66.5	0.6	Mg	73.	0.6
Al	22	0.4	Al	19	0.4	Al	34.5	0.5	Al	23.4	0.4	Al	15	0.2
Si	9	0.2	Zn	4.5	0.2	Si	10	0.2	Zn	5.5	0.2	F	10	0.7
Ca	1	0.1	Ca	2.5	0.1	F	5.5	1	Ca	2.2	0.2	Zn	0.6	0.04
F	1	0.7	Si	1	0.08	Ca	0.4	0.06	Si	1.6	0.09	Si	0.6	0.03
Zn	0.4	0.05	Mn	0.4	0.08	Na	0.3	0.7	F	0.8	0.7	Mn	0.1	0.03
						Zn	0.2	0.04	Mn	0.2	0.07			
						Mn	0.09	0.04						

A-NaL-2m* sample, which exhibited a clean surface, had also a high F content. This indicates that the protective effect is achieved due to the formation of fluorine based compounds. However, the presence of silicon may also indicate that, despite of the clean appearance of the surface, some reaction between magnesium and SiO_2 of the mould happened (Table 4.5).

Visual inspection of Figure 4.9.b is enough to realise that the rest of the samples are covered with mould-metal reactions. Accordingly, the XRF results obtained in samples A-NaL-20m and A-NaL-20c (Table 4.5) were similar to the ones obtained with the A-AH mould (Table 4.4): the use of $NaBF_4$ had no influence on the 20mm thick step, but in the 18mm thick step fluorine was detected. This may indicate that, although fluorine compounds are present on the layer, its behaviour is not protective.

- *SEM/EDS*

The SEM image of Figure 4.10 confirmed that sample A-NaL-2c* had no presence of mould-metal compounds, except for a few particles of a magnesium and fluorine from A-NaL-2m*. Therefore, when a protective surface layer is achieved the single analysis of the metallic sample is enough, as this layer is not split up during the shell removal.
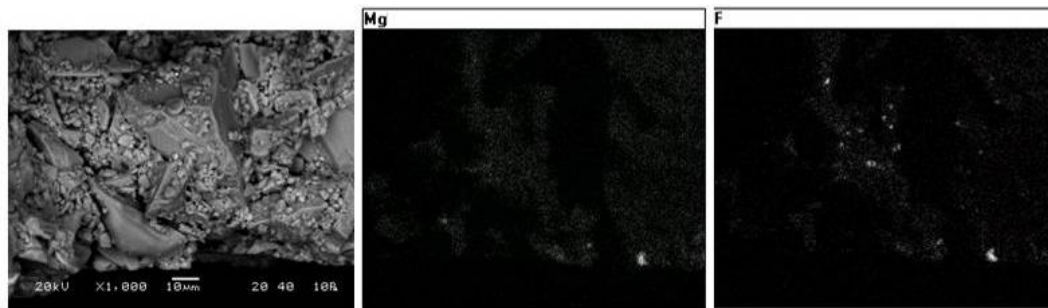
Figure 4.10: SEM/ EDS results of sample A-NaL-2c*. Elemental Mg and F mappings show the presence of few particles on the sample surface

Consequently, SEM/EDS analysis of sample A-NaL-2m* is shown in Figure 4.11. Protective effect is achieved through the formation of a dense, coherent layer composed of magnesium, aluminium, oxygen and, essentially, fluorine. The thickness of this layer is about 2.3µm.
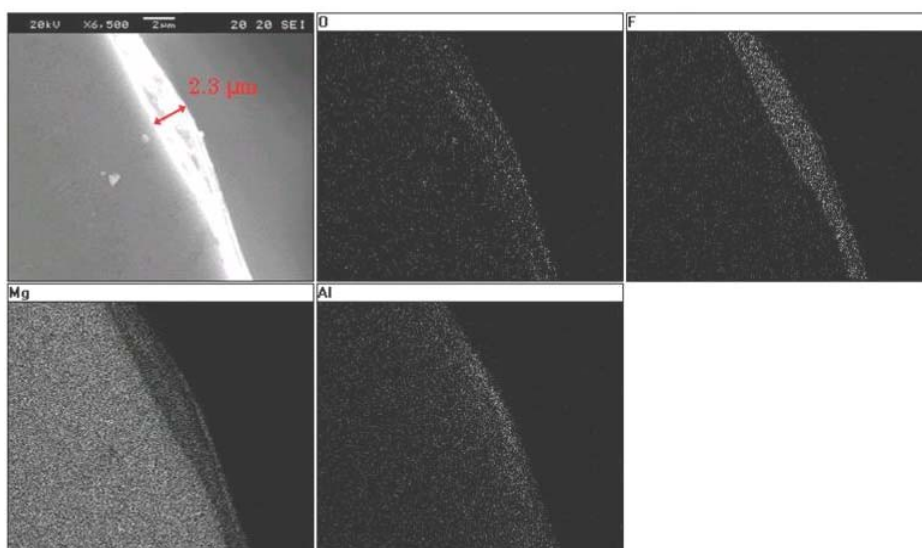
Figure 4.11: SEM /EDS results obtained on the A-NaL-2m* sample. The protective effect is achieved due to the formation of a fluorine containing dense layer

Explanation for the non-protective behaviour of sample A-NaL-18c is revealed in Figure 4.12. The EDS results show the presence of fluorine, in accordance with the XRF analysis. However, the fluorine mapping of this sample reveals that the fluorine compounds were not able to form the continuous and dense film observed in sample A-NaL-2m* and therefore the mould-metal reactions were not avoided. According to the magnesium mapping of Figure 4.12, Mg seems to come not only from the reaction products but also from the AZ91E alloy itself, stacked to the ceramic sample after shell removal. However, from the EDS mapping it is difficult to distinguish clearly between both situations and determine the thickness of the reaction layer.
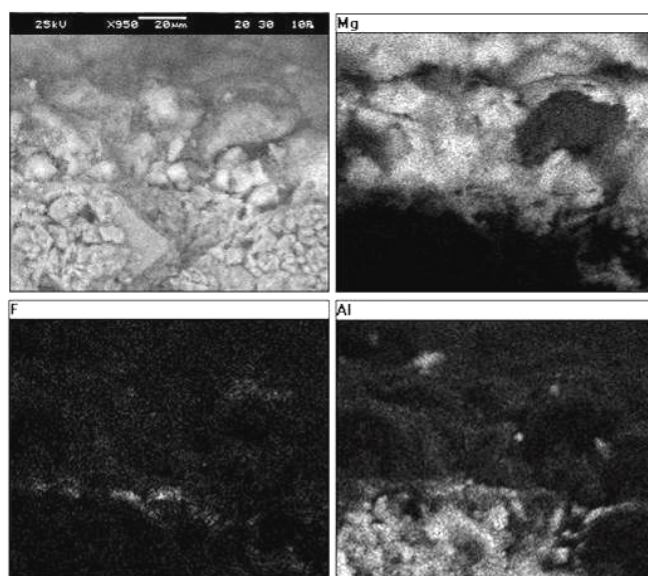
Figure 4.12: SEM/EDS results of sample A-NaL-18c. The fluorine film formed in this sample is discontinuous

- *XRD*

In Figure 4.13.a and Figure 4.13.b the XRD spectrums corresponding to A-NaL essay are shown. The results are similar to the ones obtained with the A-AH mould. The compounds of the reaction layer are mainly MgO, Mg_2Si, Mg and $Mg_{12}Al_{17}$ for the two ceramic samples, although the high of those peaks is smaller when compared to A-AH-24c spectrum (Figure 4.13.b). Thus, presence of reaction products is smaller in samples A-NaL-20c and A-NaL-18c than in A-AH-24c, as the intensity of the peaks depends on the phase concentration. This is due to the raise in the casting temperature and in the sample thickness of A-AH-24 step, which increase the severity of the reactions.

MgF_2 is also present in the fluorine-containing sample A-NaL-18c. Even though, as XRD technique is not able to determine the presence of minor phases the coexistence of other fluorine compounds cannot be discarded. Nevertheless, from these results what can be stated is that MgF_2 is the main fluorine compound responsible for the protective effect of $NaBF_4$.
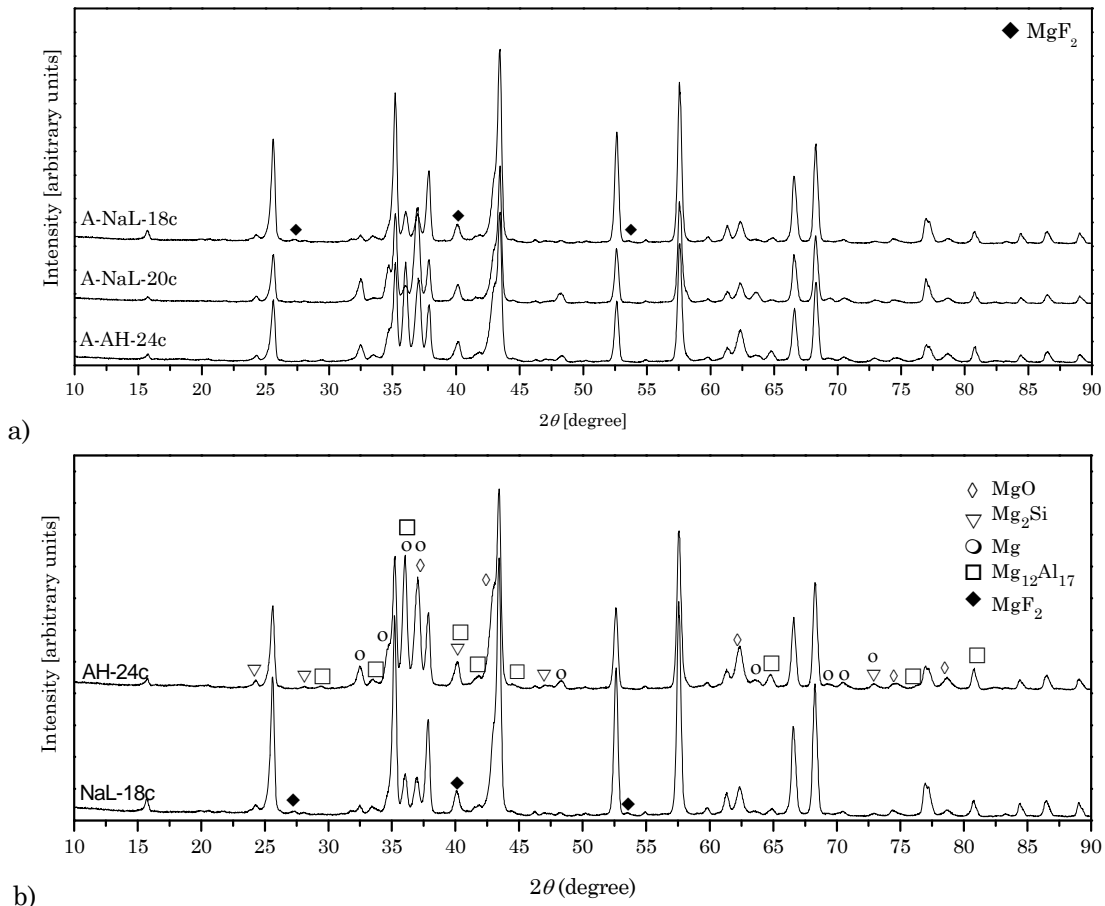
Figure 4.13: Comparison between the spectrums of sample A-AH-24c and: a) A-NaL-20c and A-NaL-18c b) A-NaL-18c. Only the additional phases are shown

Figure 4.14 shows the A-NaH essay spectrums, compared to the shell. MgO, Mg_2Si, Mg and $Mg_{12}Al_{17}$ are present in the samples, as in A-AH-24m. Due to the XRF results, the presence of MgF_2 was also expected in sample A-NaH-18c (as in A-NaL-18c). The quantity of fluorine detected in both samples by XRF is quite different: 2% in A-NaH-18c and 5.5% in A-NaL-18c. So in sample A-NaH-18c, due to its lower fluorine content, the XRD technique has not been able to detect the presence of MgF_2.
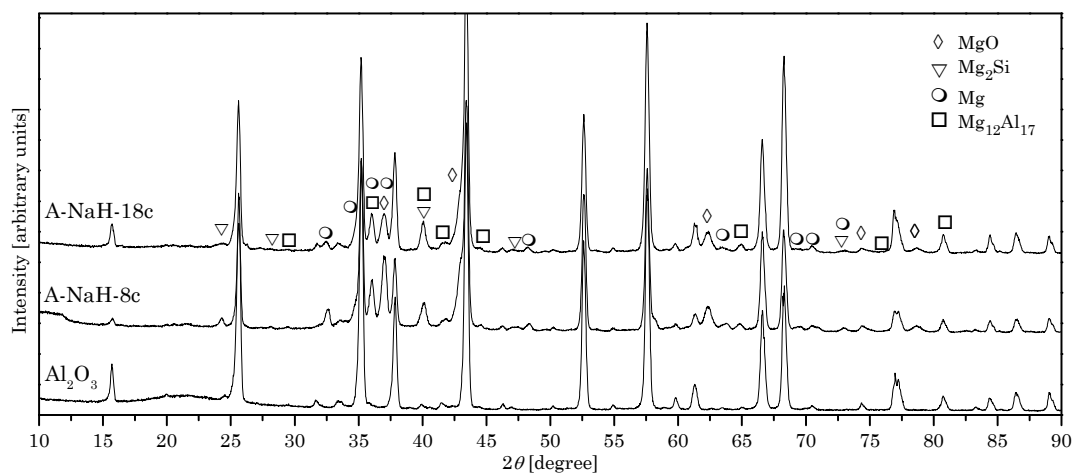
Figure 4.14: XRD spectrum of A-NaH-18c and A-NaH-8c and shell. Additional phases are shown

4.3.4 KBF₄ moulds: A-KH & A-KL

- *Samples extracted from KBF₄ moulds:*

From A-KH mould, three pairs of samples corresponding to A-KH-24 (A-KH-24c and A-KH-24m), A-KH-18 (A-KH-18c and A-KH-18m) and A-KH-2 (A-KH-2c and A-KH-2m) were selected. From A-KL essay, samples corresponding to A-KL-20 (A-KL-20c and A-KL-20m), A-KL-18 (A-KL-18c and A-KL-18m) and A-KL-2* (A-KL-2*c and A-KL-2*m) were chosen. A-KL-2* corresponds to a reaction-free sample, where KBF₄ protected effectively the surface. The localization of these samples is equal to the ones of A-NaL mould, which facilitates the comparison between NaBF₄ and KBF₄ inhibitors.
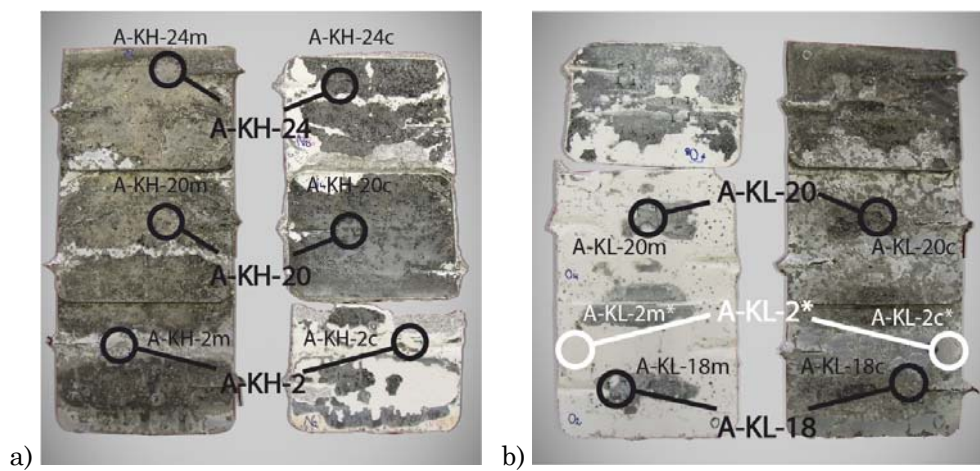
Figure 4.15: Samples selected for the chemical analysis of: a) A-KH essay b) A-KL essay

- *XRF*

Table 4.6 shows the XRF results corresponding to A-KL mould samples. Results obtained from A-KH samples are similar to the A-KL ones, and can be found in Appendix A (Table A.2).

Table 4.6: XRF measurements performed in A-KL mould samples. The weight % of each element is qualitative. Fluorine is marked in blue

A-KL-20						A-KL-18						A-KL-2m*		
A-KL-20c			A-KL-20m			A-KL-18c			A-18L-20m					
El.	W %	Std. Error	El.	W %	Std. Error	El.	W %	Std. Error	El.	W %	Std. Error	El.	W %	Std. Error
Mg	72.5	0.8	Mg	68	0.4	Mg	56.5	0.8	Mg	66.5	0.8	Mg	67	0.6
Al	14.5	0.3	Al	23.5	0.4	Al	23	0.4	Al	23.4	0.4	Al	17.5	0.3
Si	6	0.2	Zn	3.5	0.2	Si	10	0.2	Zn	5.5	0.2	**F**	**11**	**0.8**
F	**4**	**1**	Si	2	0.1	**F**	**7.5**	**1**	Ca	2.1	0.2	Si	2.5	0.08
K	1	0.1	Ca	2	0.1	K	1	0.1	Si	1.5	0.1	Zn	1.	0.06
Ca	0.3	0.05	Mn	0.5	0.1	Ca	0.6	0.08	**F**	**0.2**	**1**	Mn	0.2	0.04
Zn	0.2	0.03	Fe	0.3	0.07	Na	0.2	0.06	Mn	0.3	0.09			
Na	0.1	0.06				Zn	0.06	0.02	Fe	0.1	0.06			

Comparing the fluorine present in samples of A-NaL and A-KL moulds, it can be seen that the % present in A-KL mould is higher (Table 4.7) although the temperatures employed in A-KL casting were higher than in the A-NaL mould (reported in Section 4.1). Thus, it can be stated again that KBF_4 is more effective than $NaBF_4$ because its ability to form protective fluorine compounds is higher, even in tougher conditions.

Table 4.7: Fluorine % in the A-NaL and A-KL castings. Samples were extracted from steps of the same thickness

| | *20mm thick sample* | | | | *18mm thick sample* | | | | *2m* sample* | |
	NaL-m	*NaL-c*	*KL-m*	*KL-c*	*NaL-m*	*NaL-c*	*KL-m*	*KL-c*	*NaL*	*KL*
%F	-	1		4	0.8	2	7.5	0.2	5.5	11

- *SEM/EDS*

Figure 4.16.a shows a SEM image of sample A-KL-2m*. The protective film is a few nanometres thick, so the measurement of its thickness and the distribution of the elements in the layer cannot be analysed by EDS. Although the protective layer is quite even, protuberances like the one of Figure 4.16.b, which is 17µm high, were found. Wax pattern defects are likely to be the cause of those surface irregularities.

a)   b)
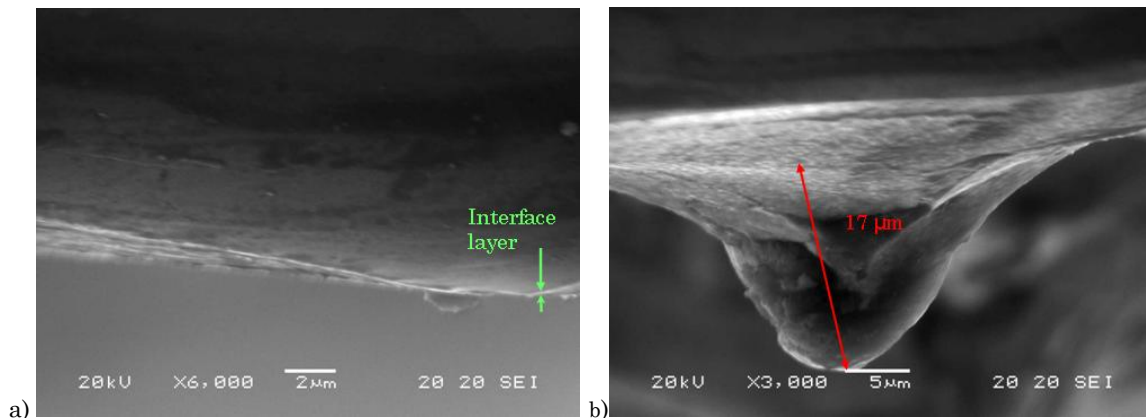
Figure 4.16: a) Protective film formed on the A-KL-2m* sample b) Protuberance found in the film

Figure 4.17 shows the EDS results of sample A-KL-18c. Analogously with the A-NaL-18c, the fluorine present in the film was not able to form a dense and coherent protective layer. In this case, however, the magnesium mapping shows two well distinguished zones: the one corresponding to the mould-metal reaction products, about 100µm thick, and the one corresponding to AZ91E alloy attached to the sample surface, around 30µm thick. Silicon is also present along the reaction film.
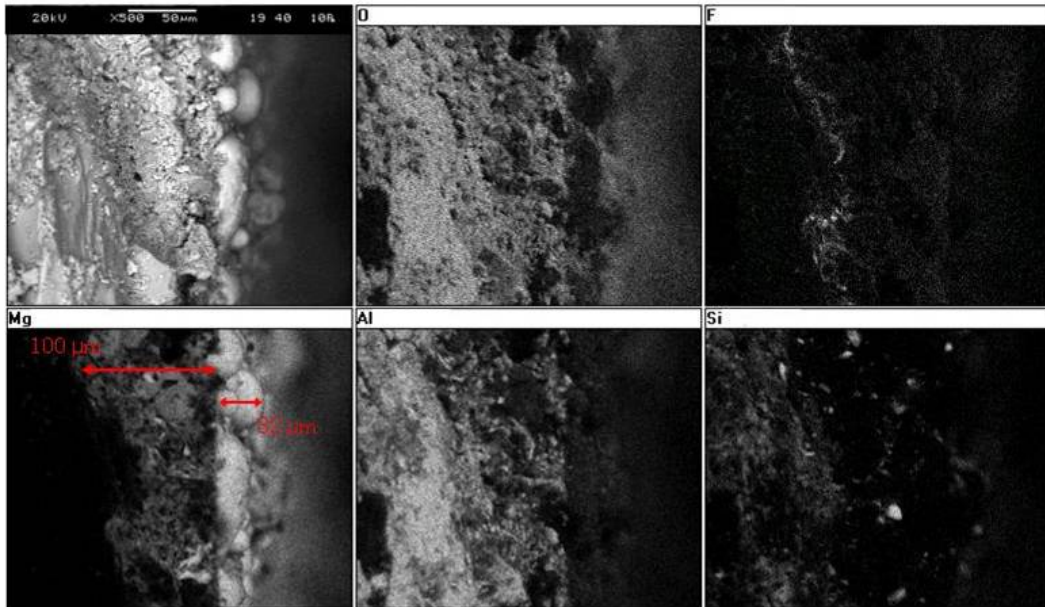
Figure 4.17: SEM/EDS results of sample A-KL-18c. The interface layer is about 100µm

Figure 4.17.b shows the EDS analysis of sample A-KL-20m, the only one without fluorine in its surface. The results reveal the presence of an oxide layer in the sample, about 13µm thick, which goes underneath the sample surface and can cause the detachment of AZ91E particles.
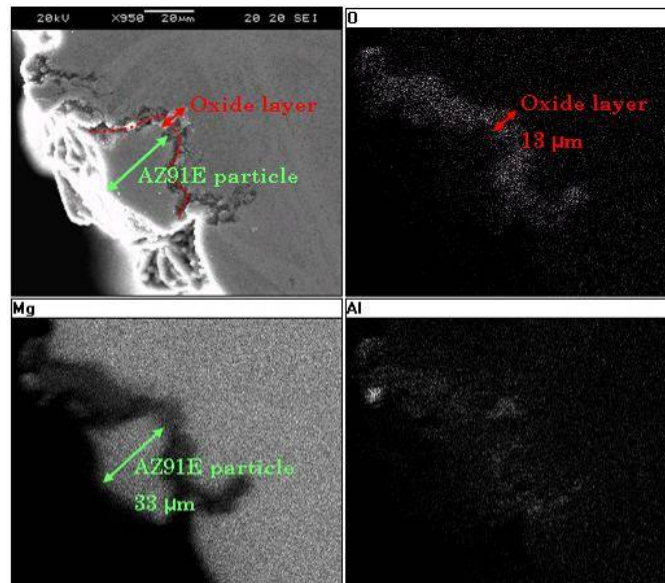
Figure 4.18: SEM/EDS results of sample A-KL-20m. The oxide layer is about 13µm and is placed between bulk AZ91E and a AZ91E particle, 33µm high

- *XRD*

The spectrums obtained from the two essays performed under KBF_4 atmospheres are almost identical to the ones obtained under $NaBF_4$ atmospheres. For those cases when the sample contains little fluorine (sample A-KH-20c), the spectrum is identical to the ones obtained in the A-AH mould, casted without inhibitor. The phases present are Mg, MgO, Mg_2Si and $Mg_{12}Al_{17}$. On the other hand, when

the interface layer contains enough fluorine, MgF_2 phase appears (A-KH-2c, A-KL-20c and A-KL-18c). In the case of sample A-KH-24c, however, the fluorine content of the sample (2 %) is so low that the phase identification is impossible.

Ceramic samples of the A-KH mould (A-KH-2c, A-KH-20c and A-KH-24c) were analysed by XRD, and three spectrums are shown in Appendix B: XRD Analysis, Figure B.1. Figure 4.20 shows again the spectrum of sample A-KH-2c, and compares it to the spectrum of the shell.
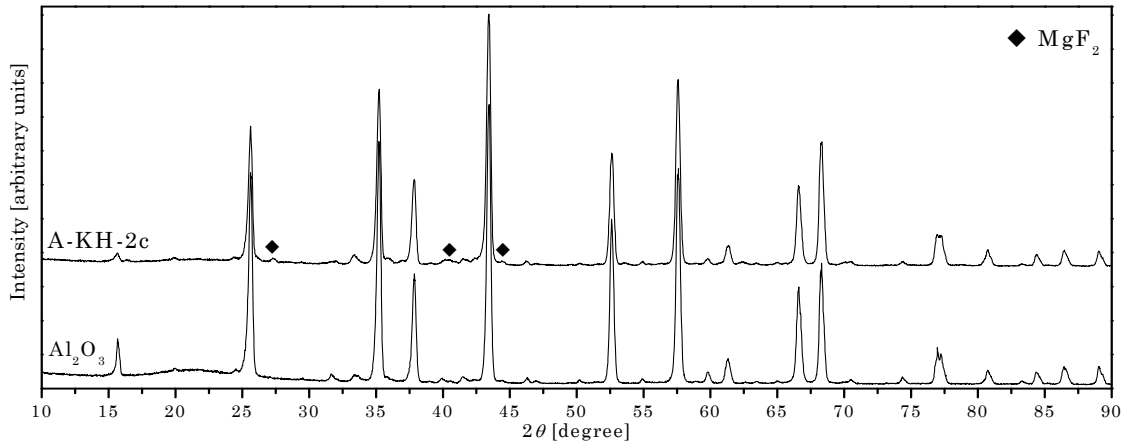
Figure 4.19: XRD spectrum of A-KH-2c, compared to shell material. Additional phases are shown

A-KH-2c, as it is shown in Figure 4.15, corresponds to a ceramic sample partially covered with mould-metal reactions. Due to that, the signal from the shell material is quite high. The main component of the reacted layer is MgF_2, and the intensity of the other reaction products (Mg, MgO, Mg_2Si and $Mg_{12}Al_{17}$) is so low that the peaks cannot be distinguished from the background of the signal.

Spectrums corresponding to samples A-KL-20c and A-KL-18c indicate the presence of reaction compounds and MgF_2. Concerning to A-KL-18c, the reaction products present in the spectrum are Mg, MgO, Mg_2Si and $Mg_{12}Al_{17}$ (Figure 4.20). The concentration of these phases is lower when compared to sample A-AH-24c.
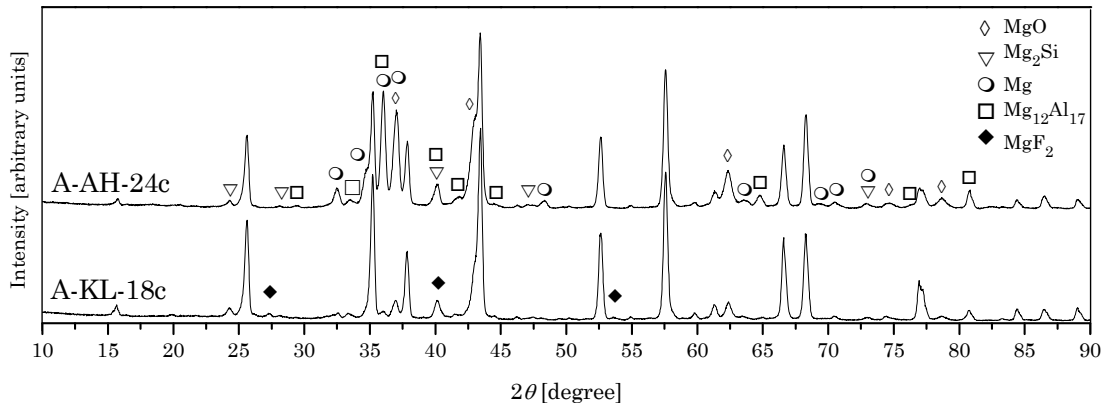
Figure 4.20: XRD spectrum of A-AH-24c and A-AH-8c, compared to A-AH-24c. Additional phases shown

Reaction products present in sample A-KL-20c are Mg, MgO and Mg_2Si. As illustrated by Figure 4.21, no $Mg_{12}Al_{17}$ is present in the surface layer:
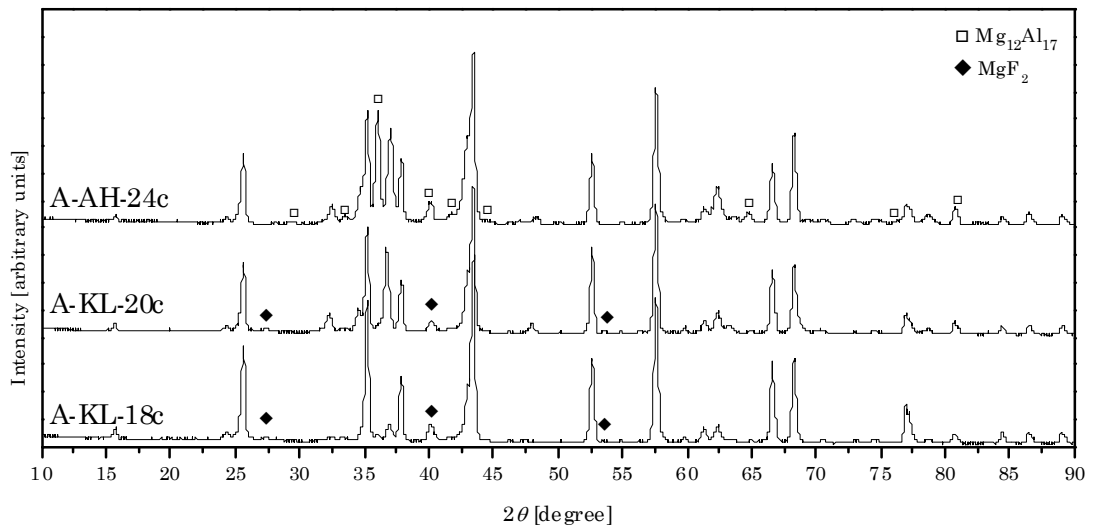
Figure 4.21: XRD spectrum of A-AH-24c and A-AH-8c, compared to shell. Additional phases are shown

A detailed view of the A-KL-20c spectrum (compared to the A-AH-24c one) reveals that the position of the peaks corresponding to the Mg phase is deviated, which in this case is probably due to the presence of substitutional aluminium in the magnesium alpha phase (Figure 4.22).
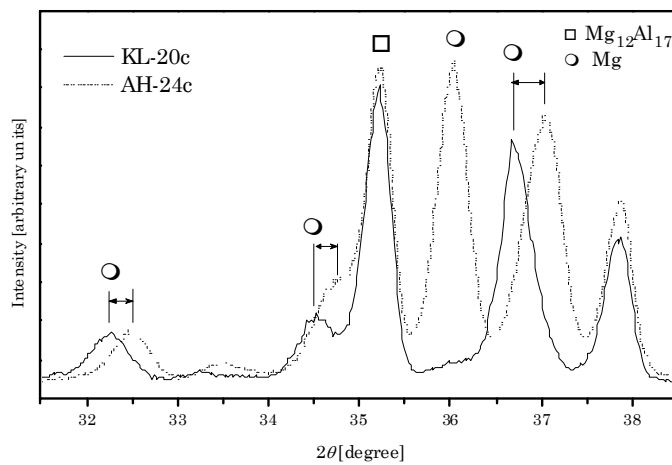
Figure 4.22: Detail of the XRD spectrum of A-KL-20c sample, compared to A-AH-24c

To understand this, it has to be considered that the formation of $Mg_{12}Al_{17}$ is the consequence of the thermal degradation of Al_2O_3. After the pouring, the Mg melt reacts with the Al_2O_3 present in the ceramic shell, MgO is formed and the melt is enriched in aluminium. When the aluminium concentration reaches a certain concentration, $Mg_{12}Al_{17}$ appears during the solidification. The A-KL essay corresponds to a casting were the mould-metal reactions were significantly reduced by the use of the inhibitor, so probably the quantity of Al_2O_3 decomposed has not been high enough to reach to the minimum % of decomposed Al necessary for $Mg_{12}Al_{17}$ to crystallise.

4.3.5 SF$_6$ mould: A-SH

- *Samples extracted from the A-SH mould*

Since SF$_6$ was displaced from the mould cavity during the pouring, the essay conditions of the casting were very severe so almost all the shell got stuck to the part. After the high-pressure water blast a big part of the refractories were removed and essential information was lost. Fortunately, the shell corresponding to the 2mm thick step was not destroyed during the mould removal, so samples A-SH-2m and A-SH-2c were selected to perform the chemical analysis of the interface layer (Figure 4.23).

Figure 4.23: Steps obtained in the A-SH casting. Most of the shell was destroyed during its removal

- *XRF*

XRF results do not show the presence of any sulphur or fluorine from the SF$_6$, which supports the previous statement about the SF$_6$ essays: during the pouring, SF$_6$ was displaced from the mould due to the incoming Mg melt, and the essays were performed without protective atmosphere. Both samples show the presence of iron impurities. In the case of the metallic one, chlorine coming from the melt protector has also been found.

Table 4.8: XRF measurements performed in A-KL mould samples. The weight % of each element is qualitative. Chlorine and iron are marked in blue and red, respectively

	A-SH-2					
	A-SH-2c			A-SH-2m		
Element	Rel. Weight	Std Error		Element	Rel. Weight	Std Error
Al	49.5	0.4		Mg	43	0.3
Mg	35	0.3		Al	41	0.4
Si	5.5	0.1		Si	7	0.2
Zn	5	0.2		Cl	6	0.3
Ca	2.5	0.2		Zn	1	0.09
Fe	0.3	0.07		Mn	0.5	0.09
Mn	0.2	0.06		Ca	0.3	0.05
				Fe	0.1	0.05

- *SEM/EDS*

Figure 4.24.b shows the EDS elemental mapping performed on sample A-SH-2c. Although no fluorine was detected by XRF, EDS reveals the presence of some particles but the dense and coherent morphology of the protective layer is not achieved.

The thickness of the surface layer is about 240µm, as it can be deduced from the Mg mapping (Figure 4.24.b). Nevertheless, the measurement of the layer depth is complicated, due to the high concentration of AZ91E alloy on the sample surface. Big particles of α-Mg are stuck to the surface sample, and consequently the metallic sample presents an irregular morphology of where cavities of even 615µm are seen, Figure 4.24.a. Iron particles are also visible in the sample, in accordance with XRF (Table 4.8).
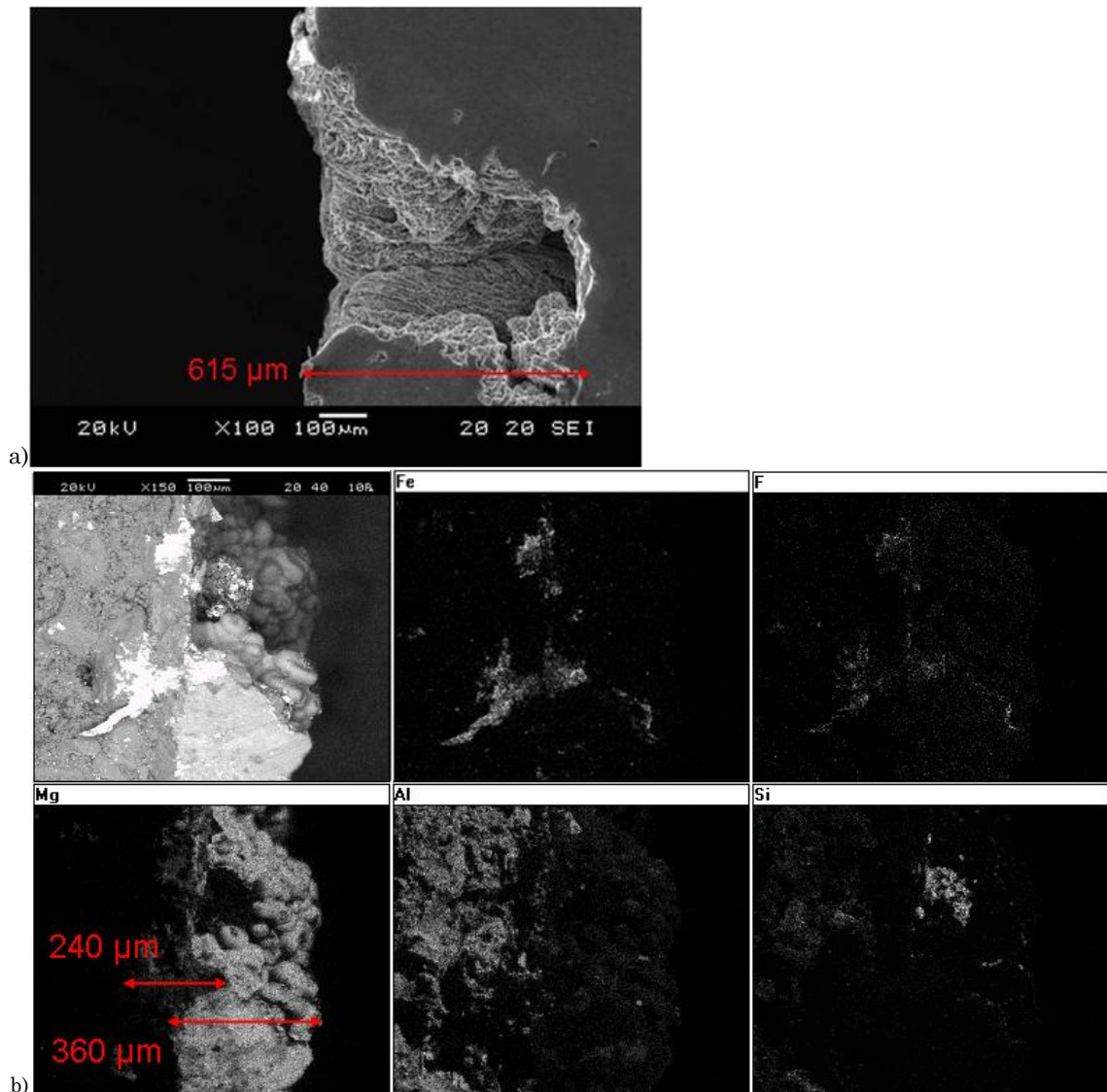
Figure 4.24: a) SEM image of sample A-SH-2m b) The EDS Mg mapping reveals high AZ91E concentration on sample A-SH-2c surface

- *XRD*

Figure 4.25 shows the A-SL-2c XRD spectrum, compared to the A-AH-8c one. Both samples present the same phases, although the Mg content in sample A-SH-2c is considerably bigger. Actually, peaks corresponding to minor phases of the shell itself, or to minor reaction products as Mg_2Si, are not discernable in the A-SH-2c spectrum due to the high intensity signal received from α-Mg.
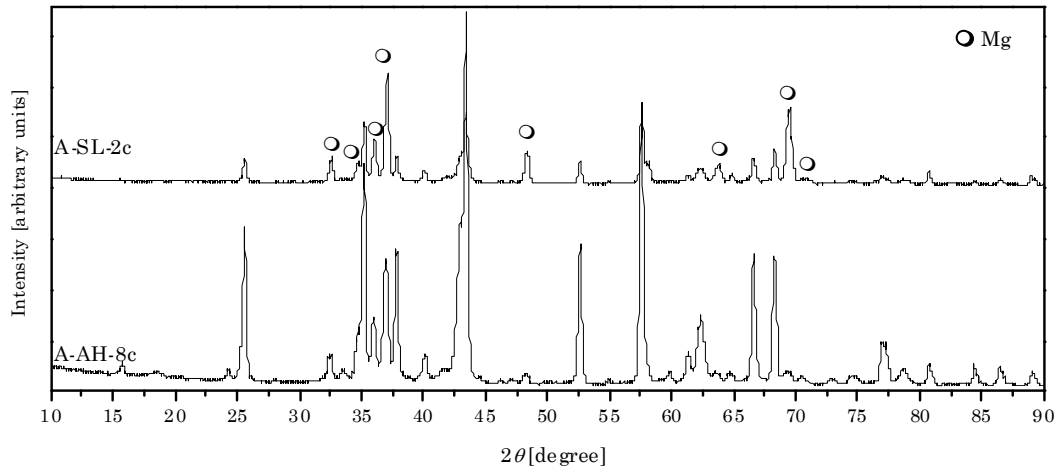
Figure 4.25: XRD spectrum of A-SH-2c, compared to sample A-AH-8c

4.4   Conclusions

As a result of the digital analysis of the castings, inhibitor effectiveness has been ranked in the order of surface reaction degree: Air→SF_6→$NaBF_4$→KBF_4, corresponding to KBF_4 the less reacted surface. Castings without inhibitor have lead to surface castings completely covered with mould-metal reactions, due to the severe experimental conditions applied (high casting temperatures and thick sections). SF_6 and Air atmosphere moulds have shown similar behaviors, as SF_6 was displaced from the mould during the pouring. Employment of KBF_4 and $NaBF_4$ has provided large non-reacted areas on the castings, but KBF_4 has proved to be the most effective one in Mg investment casting. FK moulds have been destroyed during the casting due to the thermal decomposition products of the gas.

Surfaces obtained with the different inhibitors have been analysed by means of XRF, SEM/EDX and XRD. The main conclusions obtained from these analyses are:

- For Al_2O_3 experiments, mould-metal reaction layers are composed of Mg, MgO, Mg_2Si and $Mg_{12}Al_{17}$ After the pouring, magnesium reacts with the mould materials, Al_2O_3 and SiO_2. MgO and Mg_2Si are formed, and the melt is enriched in aluminium until $Mg_{12}Al_{17}$ crystallises. The alpha Mg present in the surface layer comes from AZ91E particles, attached to the mould after the shell withdrawal. According to SEM/EDS, those compounds are evenly distributed along the surface layer depth. Summary of the compounds and elements detected on A-AH mould is presented in Table 4.9:

Table 4.9: Summary of the chemical analysis performed on A-AH mould

	A-AH-4		A-AH-8	
	A-AH-24c	AH-24m	A-AH-8c	A-AH-8m
SEM (thickness)	N.A.	N.M.	1mm	N.M.
EDX (element)	N.A.	N.M.	Mg, Al, Si, Na, Ca, O	N.M.
XRD (compound)	Mg ,MgO, Mg_2Si, $Mg_{12}Al_{17}$	N.M.	Mg, MgO, Mg_2Si, $Mg_{12}Al_{17}$	N.M.

N.M: No Measurable, N.A: Not Analysed.

- Due to the employment of the inhibitors, fluorine compounds are formed in the interface layers. For both $NaBF_4$ and KBF_4 atmospheres, SEM/EDS results reveal that the protective effect is achieved when a dense and coherent fluorine-based surface layer is formed. KBF_4 inhibitor, which is more effective, produces considerably thinner protective layers.

- Mould-metal reactions appear on the surface if the fluorine layer is incoherent. Compounds in the mould-metal reaction layer have been identified as Mg, MgO, Mg_2Si, $Mg_{12}Al_{17}$ and MgF_2 by XRD.

- Sample A-KL-20c did not contain $Mg_{12}Al_{17}$. Mould-metal reactions were significantly reduced by the use of the inhibitor, and the quantity of Al_2O_3 decomposed has not been high enough to reach to the minimum % of Al necessary for $Mg_{12}Al_{17}$ to crystallise.

- MgF_2 is the only fluorine compound identified by XRD.

Summary of the compounds and elements detected on $NaBF_4$ and KBF_4 low temperature essays are presented in Table 4.10 and Table 4.11:

Table 4.10: Summary of the chemical analysis performed on A-NaL mould

	A-NaL-20		A-NaL-18		A-NaL-2*	
	A-NaL-20c	A-NaL-20m	A-NaL-18c	A-NaL-18m	A-NaL-2c*	A-NaL-2m*
SEM (thickness)	N.A.	N.A	N.M.	N.A.	-	2.3 µm
EDX (element)	N.A.	N.A.	Mg, Al, F, O, Si	N.A.	Mg, F	Mg, Al, O, F
XRD (compound)	Mg, $Mg_{12}Al_{17}$, MgO, Mg_2Si	N.A.	Mg_2Si, Mg, $Mg_{12}Al_{17}$, MgO, MgF_2	N.A.	-	N.M.

N.M: No Measurable, N.A: Not Analysed.

Table 4.11: Summary of the chemical analysis performed on A-KL mould

	A-KL-20		A-KL-18		A-KL-2*	
	A-KL-20c	A-KL-20m	A-KL-18c	A-KL-18m	A-KL-2c*	A-KL-2m*
SEM (thickness)	N.A.	13 µm	100 µm	N.A.	-	N.M.
EDX (element)	N.A.	Mg, Al, Si, O.	Mg, Al, F, O, Si	N.A.	-	N.M.
XRD (compound)	Mg, MgO, Mg_2Si, MgF_2	N.A.	Mg_2Si, Mg, $Mg_{12}Al_{17}$, MgO, MgF_2	N.A.	-	N.M.

N.M: No Measurable, N.A: Not Analysed.

ALTERNATIVE MOULD EXPERIMENTS

5.1   Introduction

In the Alternative Mould Experiments, three different mould materials (SiO_2, Al_2O_3 and $MgAl_2O_4$) were cast in conjunction with KBF_4. The experimental conditions of the experiments, as detailed in Chapter 3: General methodology, are resumed in Table 5.1.

Table 5.1: Alternative mould essays. Experimental conditions detailed in Chapter 3

Nº Essay	Binder	Refractory Flour	Casting Temperature (Mg-mould) (ºC)	Inhibitor	Designation
1			745-550	-	A-AH
2				KBF_4	A-AL
3		Al_2O_3	725-520	-	A-KH
4				KBF_4	A-KL
5			745-550	-	Mg-AH
6				KBF_4	Mg-AL
7	SiO_2	$MgAl_2O_4$	725-520	-	Mg-KH
8				KBF_4	Mg-KL
9			745-550	-	Si-AH
10				KBF_4	Si-AL
11		SiO_2	725-20	-	Si-KH
12				KBF_4	Si-KL

In this chapter, the most effective mould material-inhibitor combination for Mg investment casting was selected. In the same way as in the Inhibitor Experiments, the results obtained in the High temperature castings do not reveal more information than the Low temperature ones. Due to that, only the results obtained in the Low temperature Castings are shown. Surfaces obtained with the SiO_2 and $MgAl_2O_4$ moulds have been analysed by means of XRF, SEM/EDS and XRD. Results obtained with Al_2O_3 have already been detailed in Chapter 4. The schematic diagram of Figure 5.1:

Results analysed in Chapter 5 are marked in black. Task in green have been performed previously, and the ones in grey will be detailed in next chapters shows in black the tasks performed, according to the analysis methodology presented in Chapter 3.
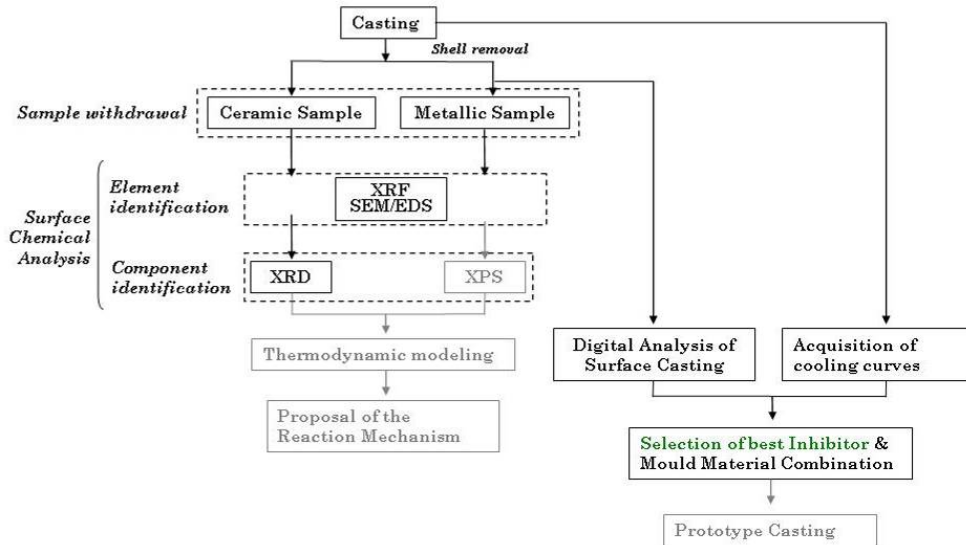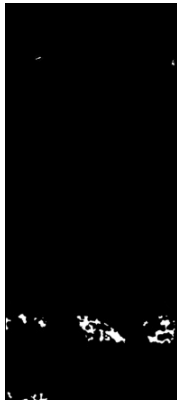
Figure 5.1: Results analysed in Chapter 5 are marked in black. Task in green have been performed previously, and the ones in grey will be detailed in next chapters

5.2 Casting and digital analysis of the surfaces

Table 5.2 reveals the pictures of the low temperature castings obtained for the three different shells, under the protective atmosphere of KBF_4.

Table 5.2: Qualitative analysis of the tested mould materials' effectiveness

Al_2O_3 + KBF_4 (A-KL)	$MgAl_2O_4$ + KBF_4 (Mg-KL)	SiO_2 + KBF_4 (Si-KL)
78%	89%	99%

The effectiveness of each mould was evaluated by digital analysis, as explained in Chapter 3 (General methodology) and performed previously in Chapter 4 (Inhibitor experiments). Al_2O_3 has clearly proved to be the most effective mould material: essay A-KL was the less reacted, with 78% of its

surface reacted. Surfaces obtained with $MgAl_2O_4$ and SiO_2 are mostly covered with mould-metal reactions, despite of the use of KBF_4. Due to this, castings without inhibitor have not been performed, since the alumina/air casting has already been analysed in Chapter 4. The ultimate round of castings performed is thus resumed in Table 5.3:

Table 5.3: Definitive experimental conditions for the alternative mould essays

Nº Essay	Inhibitor	Binder	Flour	Casting temperature ºC (Mg-mould)	Mould designation
1			Al_2O_3	745-550	A-KH
2				725-520	A-KL
3	KBF_4	SiO_2	$MgAl_2O_4$	745-550	Mg-KH
4				725-520	Mg-KL
5			SiO_2	745-550	Si-KH
6				725-520	Si-KL

Mould material effectiveness was ranked in the order of surface reaction decrease as follows: $SiO_2 \rightarrow MgAl_2O_4 \rightarrow Al_2O_3$. This grading does not correspond to the free energy data of formation of the oxides, as $MgAl_2O_4$ is more stable than Al_2O_3. To understand the poor behaviour of $MgAl_2O_4$, mould solidification and the nature of the protective gas have to be taken into consideration. Moulds are firstly dipped in a H_2O/KBF_4 solution and later, during mould preheating, BF_3 is released from the mould itself. The protective gas fills not only the mould cavity, but also the ceramic structure as the shell is porous. Due to that, a protective atmosphere is created during the pouring and also during the solidification stage; the final casting is surrounded by the inhibitor atmosphere.

During the casting cooling, $MgAl_2O_4$ moulds cracked, and atmospheric O_2 entered in the cavity. Steps that were not already covered with mould-metal reactions, where clean surfaces could have been obtained, oxidised and their surface covered with thermal oxidation products. Figure 5.2 shows an image of the middle step of the part, where zones covered with mould-metal reactions and with thermal oxidation are differentiated. These last ones are easily recognizable, as they grow up from non-reacted surfaces.

Figure 5.2: Image of the Mg-KL-4mm step, where mould–metal reactions and thermal oxidation zones are clearly distinguished

During the digital analysis of the surfaces thermal oxidation and mould-metal reaction zones are not differentiated, so the % of reacted $MgAl_2O_4$ surface of Table 5.2 underestimates this material's behaviour. Nonetheless, comparison of the upper step of the $MgAl_2O_4$ and Al_2O_3 castings reveals that, while the surface of the first one is entirely covered with mould-metal reactions, in the second one reaction-free surfaces are achieved. Owing to this fact, thermal oxidation is not enough to justify the unexpectedly poor performance of $MgAl_2O_4$.

5.3   Surface chemical analysis

Surface chemical analysis was performed in two stages, as detailed in Chapter 3. The objective of these analyses is to determine compounds that are form the surface layer of the castings, whether this layer is protective or not. Due to the industrial nature of the experiments, the estimation of the compounds is very complex so, before XRD, XRF and SEM element identification techniques are employed.

Sample designation is analogous to the one in Chapter 4. Samples are first designed with the mould name (Table 5.3) and followed with a number that corresponds to the step thickness. Last letter differentiates between the metallic (m) and ceramic samples (c). For example: sample A-KL-2m* corresponds to a metallic sample, extracted from the 2mm step of A-KL casting. * indicates that the sample is not covered with mould- metal reactions.

5.3.1 Refractory flours: $MgAl_2O_4$ and conventional SiO_2-based flour

- *XRF*

Table 4.3 shows the composition of the $MgAl_2O_4$ and conventional SiO_2-based refractory flours. The aluminium and silicon content on the spinel material reveals that the commercial flour is not only composed of $MgAl_2O_4$ phase. The surprising silicon presence in the flour is probably the other reason which justifies the poor behaviour exhibited by $MgAl_2O_4$ moulds. Conventional refractory flour is composed of Si, Zr, Al and a small quantity of magnesium.

Table 5.4 XRF measurements performed on the $MgAl_2O_4$ and SiO_2-based flour. The relative weight % is qualitative

$MgAl_2O_4$ flour			SiO_2-based flour		
Element	Rel. Weight	Std. Error	Element	Rel. Weight	Std. Error
Al	53	0.4	Si	58	0.5
Si	36	0.4	Zr	33	0.5
Mg	9	0.2	Al	9	0.2
Fe	0.70	0.1	Mg	0.2	0.05
Ca	0.7	0.1			

5.3.2 Spinel mould: Mg-KL

- *Samples extracted from the Mg-KL mould*

Regarding to Mg-KL mould, two pair of samples corresponding to Mg-KL-4 (Mg-KL-4 c and Mg-KL-4 m) and Mg-KL-2* (Mg-KL-2*c and Mg-KL-2*m) were selected. This last pair corresponds to a metallic sample without mould-metal reactions, where the inhibitor protected effectively the surface. Sample Mg-KL-4c is only partially covered with mould-metal reactions.
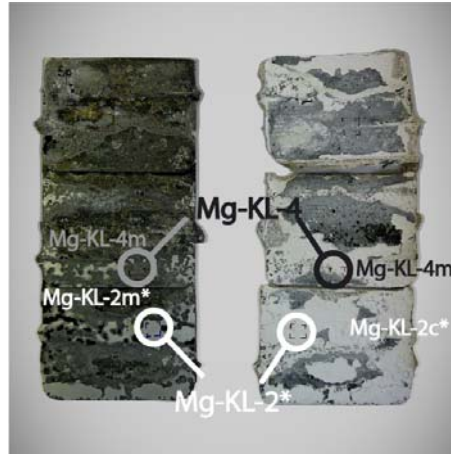
Figure 5.3: Step obtained in Mg-KL casting in shown in the left,
and the shell in the right. Samples were extracted from both

XRF measurements performed on the four Mg-KL samples are shown in Table 4.4. Fluorine was found in the two steps analysed, and only sample Mg-KL-4m does not contain fluorine. Potassium from KBF_4 is also present in the two ceramic samples.

Table 5.5 XRF measurements performed in samples Mg-KL-4 and Mg-KL-2. The relative weight values are qualitative. Fluorine and potassium are marked in blue and red, respectively

Mg-KL-4						Mg-KL-2*					
Mg-KL-4c			Mg-KL-4m			Mg-KL-2c*			Mg-KL-2m*		
El.	Rel. Weight	Std Error	El.	Rel. Weight	Std Error	El.	Rel. Weight	Std Error	El.	Rel. Weight	Std Error
Al	43	0.5	Mg	56.5	0.4	Al	39	0.70	Mg	45	0.6
Mg	35.5	0.5	Al	36.5	0.4	Si	25	0.5	Al	39.5	0.6
Si	12.5	0.2	Zn	5	0.2	Mg	17.5	0.4	F	12.5	1
F	5.5	1	Si	1	0.1	F	14	1.40	Si	0.9	0.05
K	3	0.2	Ca	0.5	0.07	K	2	0.2	Mn	0.8	0.08
Fe	0.4	0.06				Ca	0.5	0.075	Zn	0.6	0.05
Ca	0.2	0.04				Fe	0.3	0.07	Ca	0.6	0.06

- *SEM/EDS*

EDS results obtained on Mg-KL samples are analogous with the ones acquired on A-KL ones. Likewise in A-KL-2m*, the protective surface formed on the Mg-KL-2m* is so thin that its thickness cannot be deduced by EDS. In this case, however, the cross section of Figure 4.6 reveals that the layer is formed with oxygen, fluorine, magnesium and aluminium compounds.
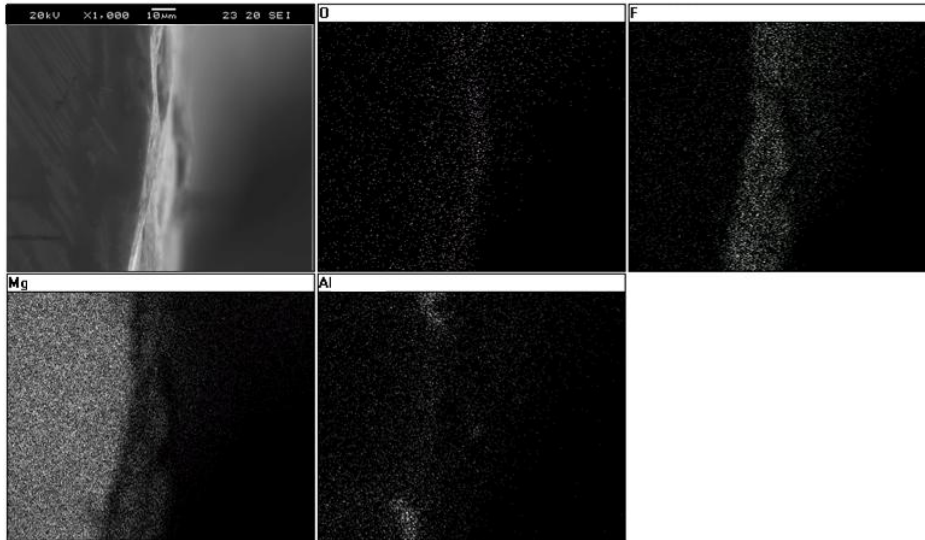
Figure 5.4: SEM/EDS results of the protective layer formed on sample Mg-KL-2m*

EDS analysis performed on sample Mg-KL-4c shows a surface film, 63µm thick, in which the fluorine distribution is loose and scattered. The mould-metal reaction layer is mostly composed of magnesium, aluminium, oxygen, fluorine and silicon compounds. Due to the employment of KBF_4, potassium particles are also present in the shell. Surface layer formed on sample Mg-KL-4m is too thin to be analysed by EDS, which indicates that most of the interface layer is attached to ceramic Mg-KL-4c sample.
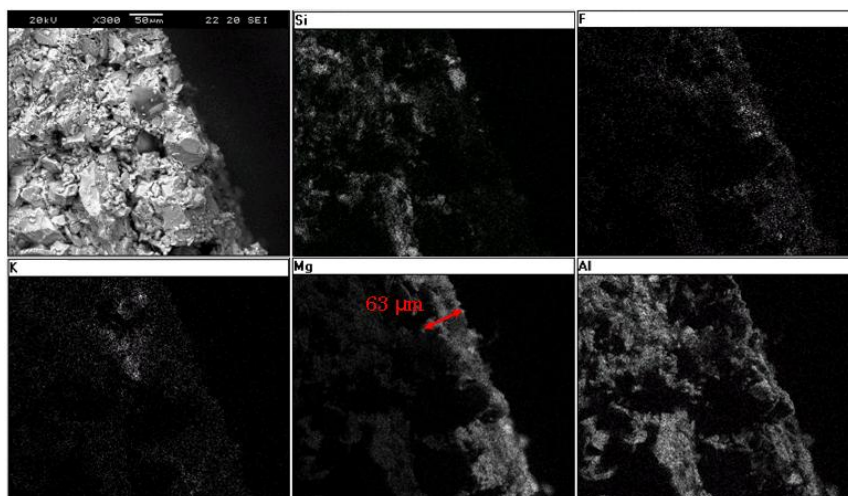
Figure 5.5: SEM/EDS results of sample Mg-KL-4c. Elemental mapping shows that t interface is layer is about 63 µm, formed with Mg, Al, O_2, Si and F compounds

- *XRD*

$MgAl_2O_4$ flour has also been analysed by XRD. Results are shown in the XRD spectra of Figure 5.6, where it can be seen that Al_2O_3, SiO_2, MgO and $MgAl_2O_4$ are present in the refractory powders. Although there are different factors that influence the height of the XRD spectra peaks, the big difference between the relative phases present in Figure 5.6 indicates that, in spite of the presence of other compounds, spinel is the main phase in the flour. Some unknown peaks, which are related to unmatched minor phases, appear also in the spectra.
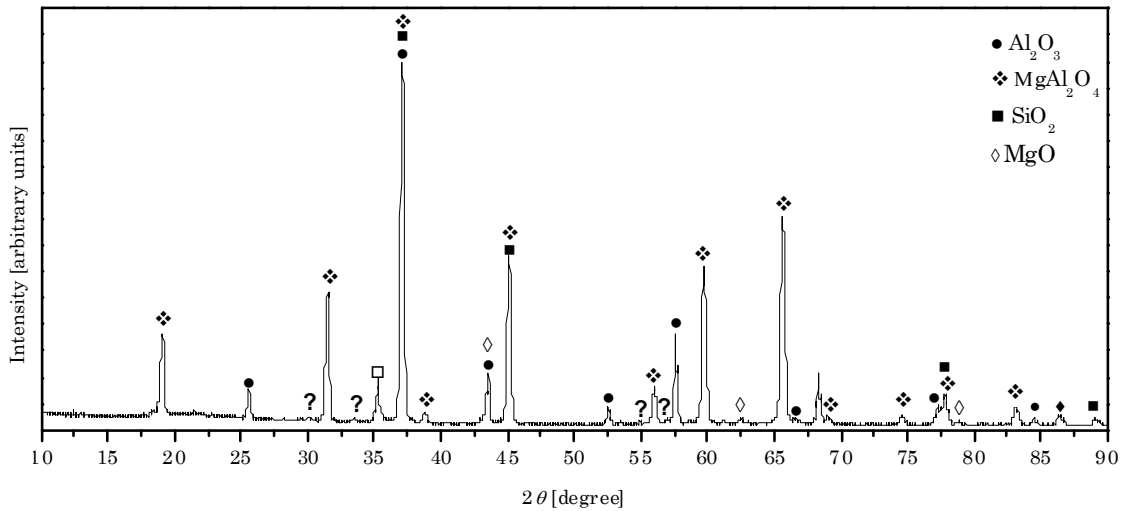
Figure 5.6: XRD spectra of the ($MgAl_2O_4$ flour+SiO_2 binder) shell

Figure 5.7 displays the XRD spectra obtained with Mg-KL-2c* and Mg-KL-4c samples:
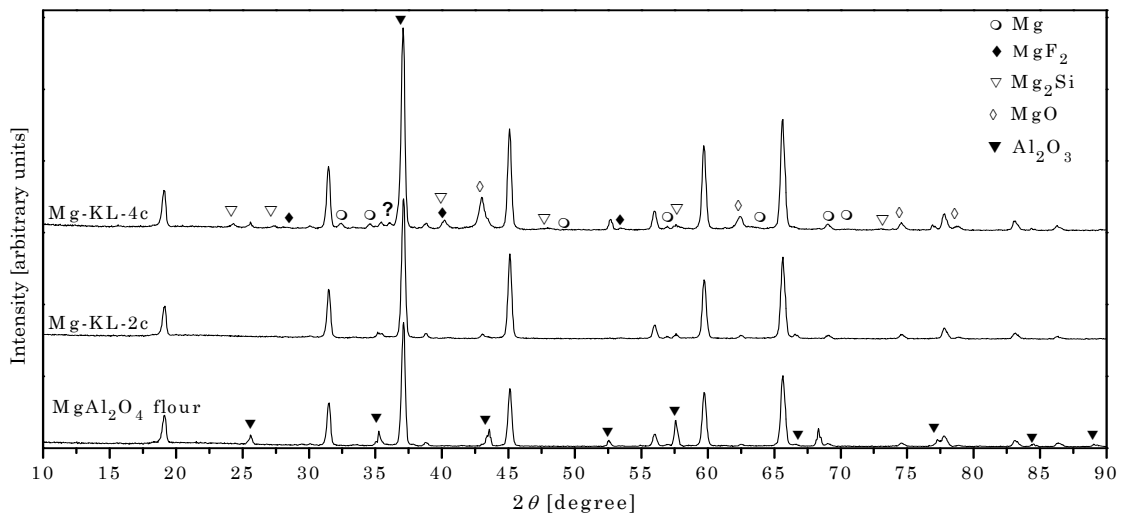
Figure 5.7: XRD spectra of Mg-KL-4c and Mg-KL-2c, compared to spinel-based mould material

As shown in Figure 4.5, Mg-KL-2m* metallic sample exhibits a clean and well-protected metallic surface. Accordingly, no mould-metal reaction products appear in the XRD spectra recorded on the Mg-KL-2c* ceramic sample. Comparing the Mg-KL-2c* shell with the $MgAl_2O_4$ refractory powders,

some slight differences appear. Al_2O_3, for example, is one of the minor phases present in the flour spectra but its presence is unrecognizable in Mg-KL-2c*.

According to Mg-KL-4c XRD spectra, reactions between Mg and $MgAl_2O_4$ mould generate a layer composed of Mg, MgO, Mg_2Si and Al_2O_3. Along with the A-KL results, the presence of Mg is due to Mg vapour diffusion and/or to alloy attachment onto the sample, after shell withdrawal. Existence of MgO and Mg_2Si is due to reactions between Mg and the SiO_2 present in the flour and binder, and the employment of KBF_4 promotes the appearance of MgF_2. Al_2O_3 content is significantly lower in $MgAl_2O_4$-based shells than in Al_2O_3 moulds, so the dissolved aluminium quantity has not been enough to promote $Mg_{12}Al_{17}$. Since the Al_2O_3 signal is unnoticeable in the Mg-KL-2c* spectra, the presence of this phase in the Mg-KL-4c spectra is due to reactions between the Mg melt and $MgAl_2O_4$.

5.3.3 Conventional flour mould: Si-KL mould

- *Samples extracted from Si-KL essay:*

Due to the employment of a conventional SiO_2-based mould material, the essay conditions of the casting were very severe and almost all the shell got stuck to the casting. Fortunately, a small part of the shell corresponding to the 2mm thick step was not destroyed during mould removal and samples Si-KL-2m and Si-KL-2c were able to be extracted (Table 5.2). These two samples are partially covered with a protective layer so metallic A-SH-2m sample, which is completely reacted, has also been analysed.

Figure 5.8: Samples selected from the Si-KL casting

- *XRF*

Fluorine was found in the XRF results of the three samples, even in the completely reacted metallic sample (Si-KL-2m) although the content in this last one is very low (0.4%). Calcium and Iron impurities are also found in all the samples.

Table 5.6 XRF measurements performed in Si-KL mould samples. The weight % of each element is qualitative. Fluorine is marked in blue. Iron and Calcium are marked in red

| | Si-KL-2* | | | | | Si-KL-2m | | |
| | Si-KL-2c* | | | Si-KL-2m* | | | | | |
El.	Rel. Weight	Std. Error	El.	Rel. Weight	Std. Error	El.	Rel. Weight	Std. Error
Si	67	0.80	Mg	58	0.6	Si	46.5	0.3
Al	12	0.2	Si	17	0.2	Al	40	0.3
Zr	10	0.3	Al	14	0.2	Mg	6.9	0.2
F	**3.5**	**1**	**F**	**8**	**0.8**	Zr	3.2	0.1
Mg	3	0.1	Zn	1	0.07	Zn	1	0.09
Fe	**0.3**	**0.75**	**Ca**	**0.7**	**0.07**	**F**	**0.4**	**0.7**
Ca	**0.15**	**0.05**	Mn	0.4	0.06	**Ca**	**0.2**	**0.05**
			Zr	0.3	0.03	**Fe**	**0.2**	**0.05**
			Fe	**0.06**	**0.03**	Mn	0.15	0.05

- *SEM/EDS*

Figure 5.9 shows SEM/EDS results obtained with sample Si-KL-2m. The ceramic layer (about 337µm thick and composed of oxygen, silicon and aluminium) found on the sample reaffirms how, when the mould is destroyed during its removal, the interface film and the shell are attached to the metallic sample. Fluorine detected with XRF was not discernable in this analysis, due to its low concentration.
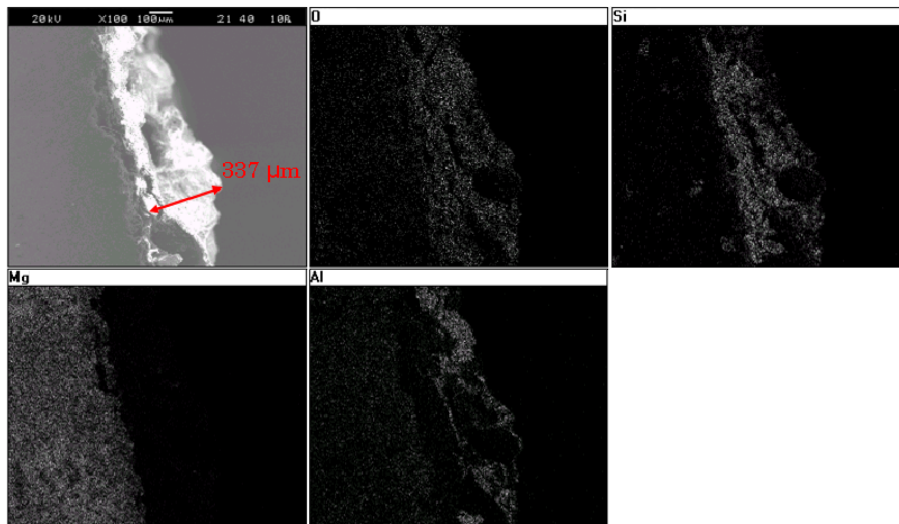
Figure 5.9: SEM/EDS results of sample Si-KL-2m. Interface layer and part of the ceramic shell are attached to the metallic sample

As explained before, sample Si-KL is not only covered with mould-metal reactions but also with a protective layer. These two situations are illustrated in Figure 5.9.a and Figure 5.9.b:
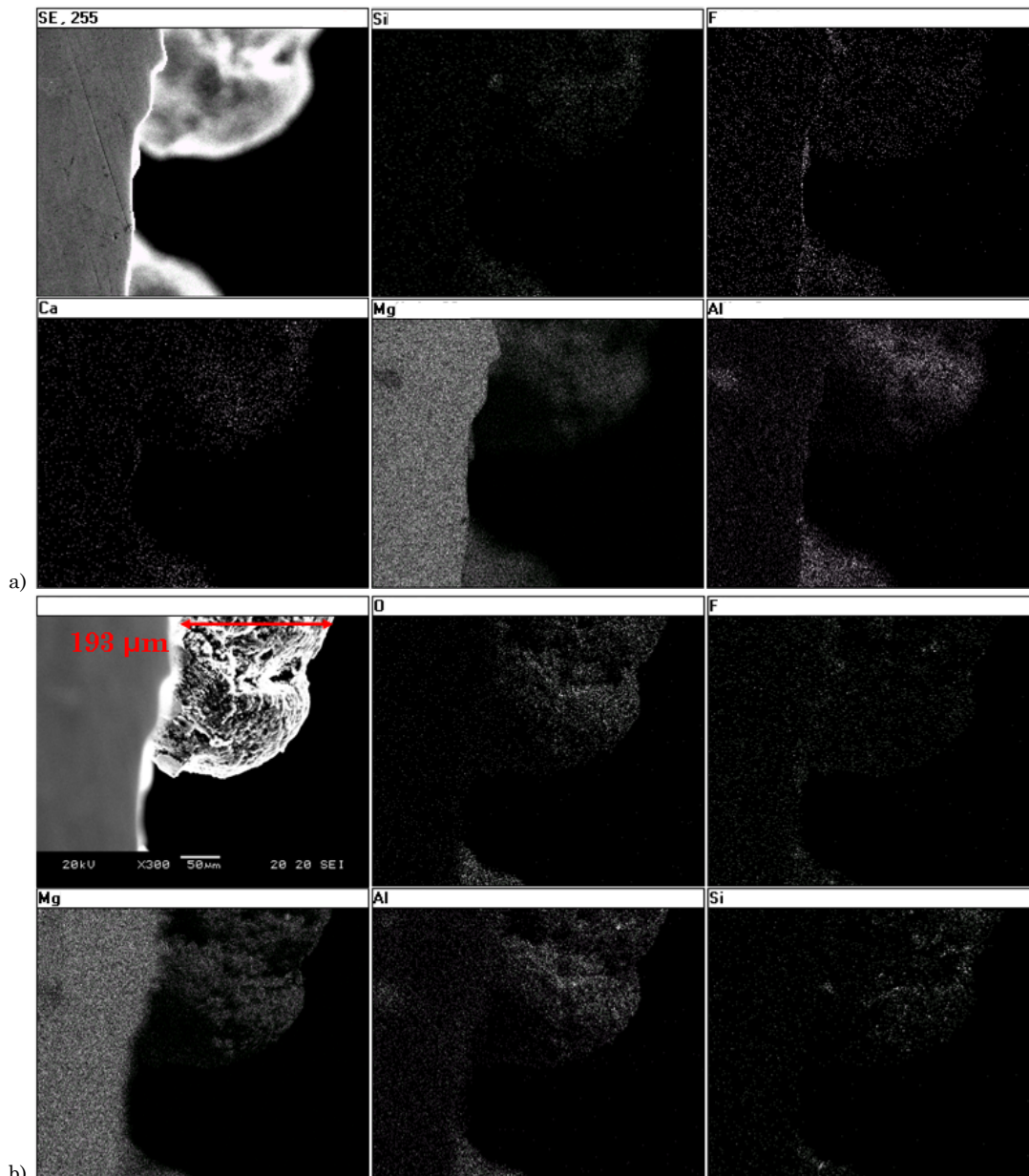
Figure 5.10: a) and b) SEM/EDS results of sample Si-KL-2m*, where the reacted and the protected area are clearly distinguished

According to the EDS mappings of Figure 5.9.a and Figure 5.9.b, the reacted layer is 193µm and comprises Mg, Al, Si, Ca, O, F and Zr (not shown). Composition of the protective layer has also been analysed through the detailed view of Figure 5.11. EDS results reveal that film thickness ranges between 3-13µm, and is composed of Mg, Al, O and F. Calcium may also be present in it, according to the Ca mapping of Figure 5.9.b. Thickness of the film seems to be related to aluminium: its concentration is higher in the thinnest parts, whereas the rest of the elements seem to be evenly distributed along the film.
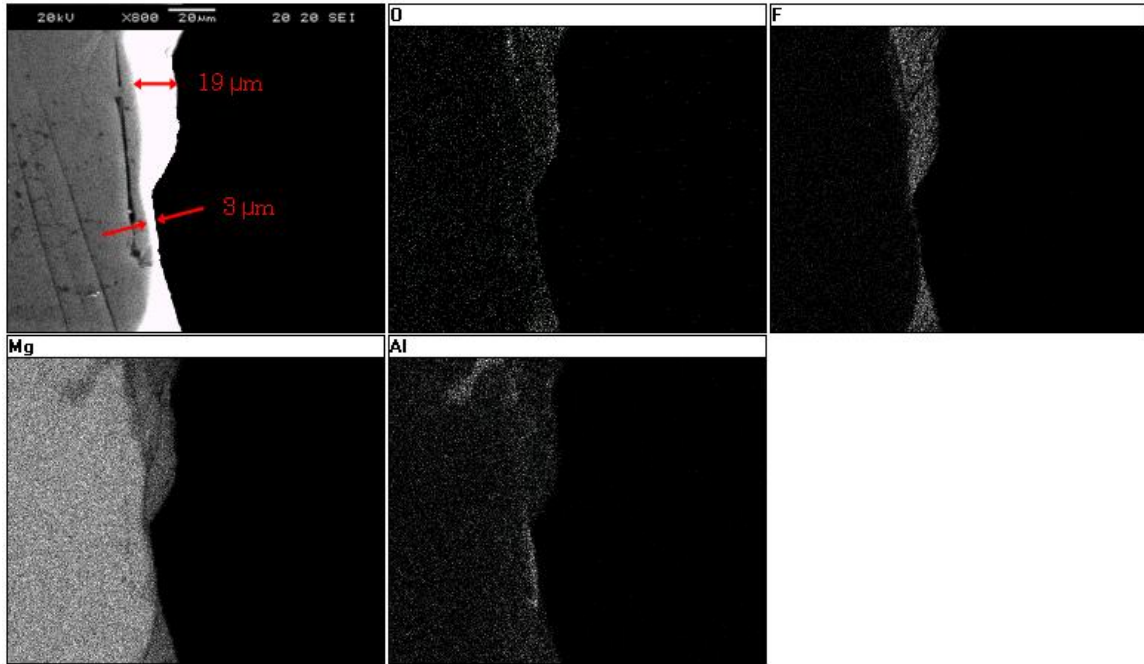
Figure 5.11: SEM/EDS results of the protective layer formed on sample Si-KL-2m*

- *XRD*

Figure 4.13 shows the XRD spectra obtained in the ceramic sample, which is only partially covered with mould-metal reactions (Figure 4.9). Analogously with the A-KH-2c XRD results, the signal from the shell material compounds is so high (Al_2O_3, $ZrSiO_4$ and SiO_2) that only MgF_2 is perceptible. Intensity of the other reaction products is so low that the peaks cannot be distinguished from the background of the signal.
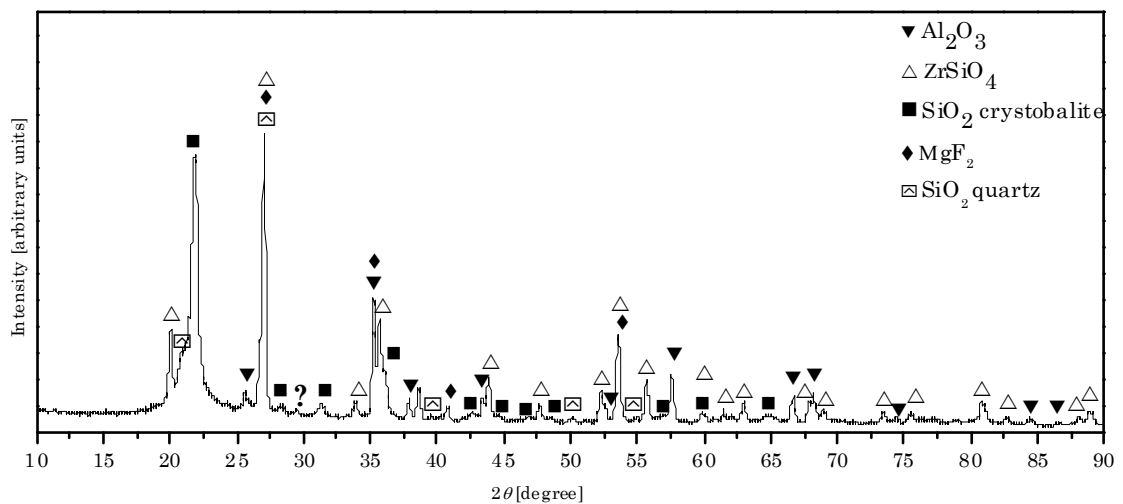
Figure 5.12: XRD spectra of sample Si-KL-2c

5.4 Conclusions

As a result of the digital analysis of the castings, the material plus inhibitor effectiveness is ranked in order of reaction degree as follows (more to less reacted): $SiO_2 \rightarrow MgAl_2O_4 \rightarrow Al_2O_3$. This grading does not correspond to the free energy data of formation of the oxides, as $MgAl_2O_4$ is more stable than Al_2O_3. The cracking of the mould during the cooling of the casting and the presence of SiO_2 on the flour may be the reason for the unexpected behaviour of the $MgAl_2O_4$-based moulds. Employment of Al_2O_3 mould + KBF_4 has proved to be the most effective one in magnesium investment casting. $MgAl_2O_4$ and SiO_2 surfaces have been analysed by XRF, SEM/EDX and XRD. Main conclusions obtained from these analyses are:

- For $MgAl_2O_4$ experiments, mould-metal reaction layers are composed of Mg, MgO, Mg_2Si and Al_2O_3. Mg_2Si is formed due to reactions between Mg and SiO_2, and Al_2O_3 is formed due to the reaction between MgO and $MgAl_2O_4$. Results obtained through this chapter on the surface layer formed on $MgAl_2O_4$ samples by SEM/EDS and XRD are resumed in Table 5.7:

Table 5.7: Resume of the chemical analysis performed on the $MgAl_2O_4$ mould

	Mg-KL-4		Mg-KL-2*	
	Mg-KL-4c	Mg-KL-4m	Mg-KL-2c*	Mg-KL-2m*
SEM: (thickness)	63µm	N.M.	--------	N.M.
EDS: (element)	Mg, Al, F, O, Si, K	N.M.	--------	Mg, Al, F, O
XRD: (compound)	Mg, MgO, Mg_2Si, Al_2O_3, MgF_2	N.M.	Shell compounds	N.M.

N.M: No Measurable, N.A: Not Analysed

- Mould-metal reaction layer formed on Si-KL moulds comprises Mg, Al, Si, Ca, O and, in some cases, F. Unfortunately, the XRD spectra reveals only the presence of MgF_2. Results obtained after chemical analysis of the surface layers of SiO_2 samples is resumed in Table 5.8

Table 5.8: Resume of the chemical analysis performed on the SiO_2 mould

	Si-KL-2*			Si-KL-2
	Si-KL-2c*	Si-KL-2m*		Si-KL-2m
		Reacted	Protected	
SEM : (thickness)	N.A.	193µm	3-19µm	337µm (surface layer + shell)
EDS: (element)	N.A	Mg, Al, Si, Ca, F, O	Mg, Al, Ca, O, F	
XRD: (compound)	MgF_2	N.A.	N.M.	N.A.

N.M: No Measurable, N.A: Not Analysed

- Along with the results obtained in the Al_2O_3 moulds, the protective character of the films analysed in this chapter resides in the formation of fluorine compounds. In this sense, MgF_2 was again the only fluorine phase identified with XRD. Differences between the films formed in the different moulds are related to their thickness. Likewise in Al_2O_3, the protective surface formed in the $MgAl_2O_4$ experiment is so thin that its thickness cannot be deduced by EDS although its composition is discernible: the film is formed with oxygen, fluorine, magnesium and aluminium compounds. The protective surface formed in the SiO_2 essays, the less effective one, is considerably thicker than the other two. SiO_2 film thickness ranges between 3 and 19μm, and is composed of Mg, Al, Ca, O and F. Thickness of the film seems to be related to aluminium, as higher concentration of aluminium appears when the protective film is thinner.

XPS ANALYSES FOR AL₂O₃ MOULDS.

6.1 Introduction

Best results in Mg investment casting are obtained when Al_2O_3 moulds are cast with KBF_4 inhibitor. Success of the mould material and inhibitor depends on the severity of the conditions employed, as surfaces covered with mould-metal reactions or surfaces effectively protected can be achieved. With the aim of understanding better both situations, in this chapter A-AH-24m and A-KL-2m* metallic samples have been analysed by XPS. Both samples were cast in Al_2O_3 moulds. Sample A-KL-2m* was obtained under the protective effect of KBF_4 and exhibits a clean, well protected surface; whereas sample A-AH-24m, obtained in air atmosphere, is covered with mould-metal reaction products. Chemical equilibrium calculations of the mould-metal reactions have been performed with FactSage®.

Previous analysis of the metallic samples by XRD technique was unsuccessful. The surface layers are so thin that the background signal from the AZ91E alloy is too high for a correct interpretation of the spectrum. Accordingly, through Chapter 4 information about the elements present in the surface layer was obtained, but the identification of the compounds is still unresolved. In view of that, in this chapter the metallic samples are analysed with XPS, as this technique also allows the identification of the surface compounds. However, the penetration depth of this technique is smaller than in XRD: information obtained by XPS is related to the very surface of the sample (less than 1nm).

To study the behaviour of the different refractory mould materials on Mg investment casting thermodynamic equilibrium calculations have been performed. These calculations have been p using the FactSage® Equilib module, which minimizes the total Gibbs free energy of a system. It calculates the concentrations of chemical species when specified elements or compounds react to reach a state of chemical equilibrium. As stated in Chapter 2, Literature review, consideration of Gibb's free energy of formation as the main criterion to determine the creation of compounds seems feasible in investment casting, due to the high temperature and slow cooling rate of the mould-metal interface. Solidification

time for the experiments performed in this work is up to 1000-1100 seconds.

According to the analysis methodology presented in Chapter 3, the diagram of Figure 4.1 shows in green the tasks performed in the previous chapter, in black the ones that are performed in through this chapter and in grey the ones that will be detailed in next chapters.
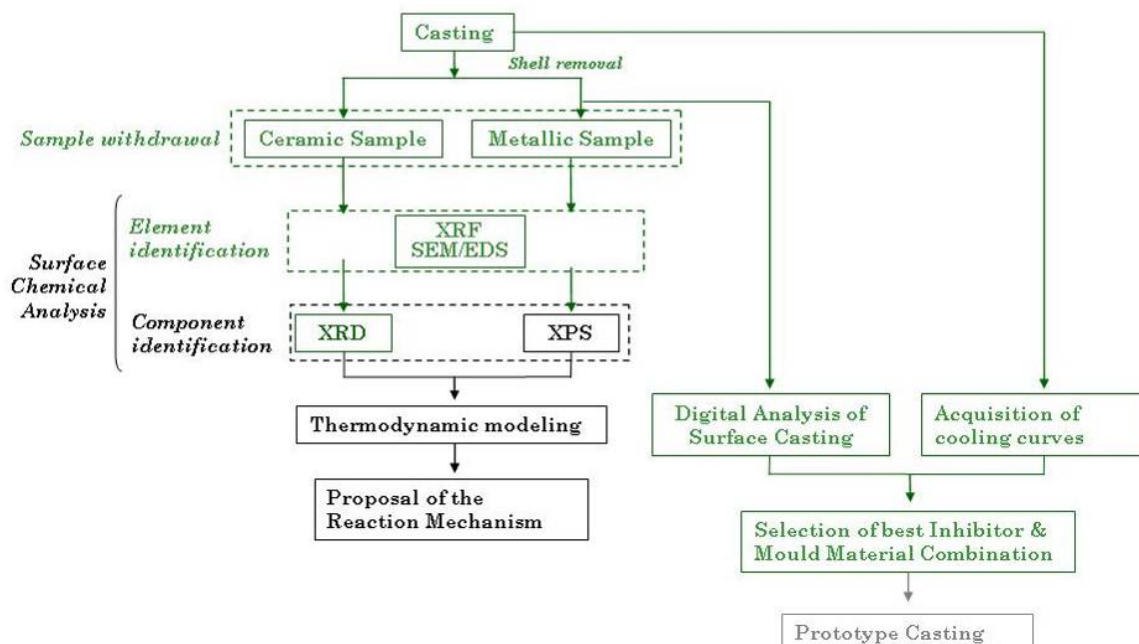
Figure 6.1: Results analysed in Chapter 6 are marked in black. Tasks in green have already been performed previously, and the ones in grey will be detailed in next chapter

6.2   XPS analysis of samples obtained under air and KBF$_4$ atmospheres

6.2.1   XPS general spectrum of the analysed samples

Figure 6.2 shows the full-range XPS scan survey of the samples A-AH-24m and A-KL-2m*. The survey spectrum alloys the identification of all the elements present on the sample surface. According to these results, surface layers formed on both samples are composed of C, O, Al, Mg, Si, Ca and Na compounds and F is also detected for sample A-KL-2m. To determine the chemical state of those elements C1s, O1s, Al2p, Mg2p, Si2p, Ca2p Na1s and F1s core level multiple spectrums will be analysed in the next sections. Figure 6.2.a and b shows the peaks used for the identification of the compounds. Several other peaks are observed in the spectrum, representing photoelectrons from another orbitals, x-Ray satellites, X-Ray ghosts and shake-up lines. These peaks do not identify alternative elements, but substantiate the existence of the surface species already indicated by the marked photoelectron peaks [Cas99].
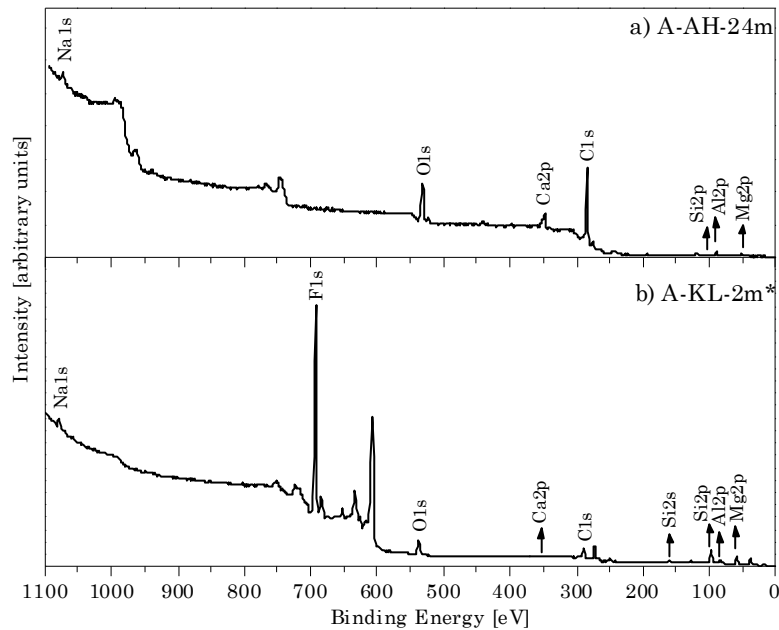
Figure 6.2: XPS survey spectra of samples: a) A-AH-24m b) Kl-2m*

Presence of a sharp F 1s core level in Figure 6.2.b indicates that the use of KBF_4 induces a fluorinated surface, as expected. The decrease in Ca 2p may also indicate that, due to the formation of the protective layer, the reactions between magnesium melt and the calcium phases of the mould were reduced.

6.2.2 Sample A-AH-24m: XPS high resolution spectrums

Na 1s spectrum of sample A-AH-24m reveals the presence of a single sodium compound at 1073eV (Figure 6.3.a), identified as $NaAlO_2$ [Pra98, Bar91]. According to Figure 6.3.b, the Ca 2p XPS spectrum is the combination of a low binding energy peak at 347.68 eV, and a high binding energy peak, centred at 349.25 eV. The LBE Peak corresponds to the presence of CaO on the surface [Nag12, Anz12], and/or formation of $Ca(OH)_2$ compound, as a result of the reaction of CaO with surrounding water vapour [Not11]. The presence of calcium oxide in the surface is probably due to the calcium content as an impurity in the bulk alloy: this effect has already been reported by Feliu *et al.* after the analysis of native air-formed oxide films in Mg-Al commercial alloys [Fel10]. Literature also mentions the formation of external CaO layers during the annealing of the MgO crystals that contain Ca as an impurity [Ota96, Mcc83, Sou97]. The HBE peak has been identified as $CaAl_2O_4$, in reference to the work published by Popoolaa *et al.* [Pop92].
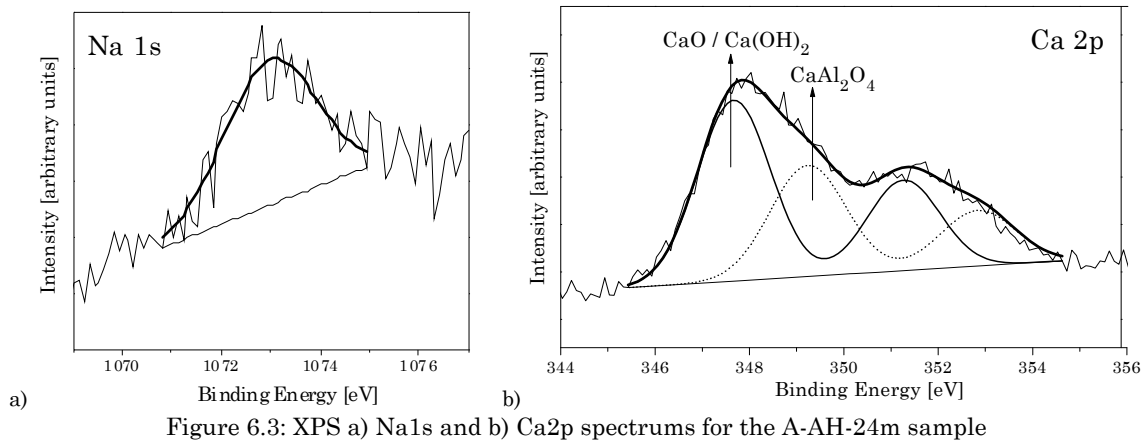
Figure 6.3: XPS a) Na1s and b) Ca2p spectrums for the A-AH-24m sample

The Si2p spectrum (Figure 6.4.a) is composed of three peaks, located at 100.4, 102.4 and 104.23eV. The low binding energy one can be attributed to SiC [Swa06, Che05] as the nucleant employed during the castings is the SiC-based Foseco's Nucleant5000; or to substoichiometric SiO_x [Sat03]. Actually, according to a recent work published by Boryakov et $al.$, it appears to be impossible to differentiate Si-C bonds from the $SiOx$ ones [Bor12]. The peak centred at 102.4 eV was identified as magnesium silicate, $MgSiO_3$, in accordance with the results published by Mato et $al.$, Brennan et al and Ge et $al.$ [Ge11, Bre08, Mat03]. The shoulder at higher BE (104.23) was attributed to SiO_2, in agreement with other previous works [Zep10, Swa07].

The XPS spectrum of Figure 6.4.b shows the presence of five different Al compounds. Low BE value corresponds to $NaAlO_2$, according to the value of 72.9eV reported by Barr et al [Bar91]. The 74.22 and 75.49 eV peaks are assigned to $MgAl_2O_4$ [Kam00] and the thermally formed Al_2O_3 [Cri04], respectively. This last peak may also have the contribution of $CaAl_2O_4$ compound, located at 75.9 eV as published by Popoolaa et $al.$ [Pop92]. HBE peak located at 76.7 eV corresponds to AlO(OH), in correspondence to known experimental data [1348, 1347].
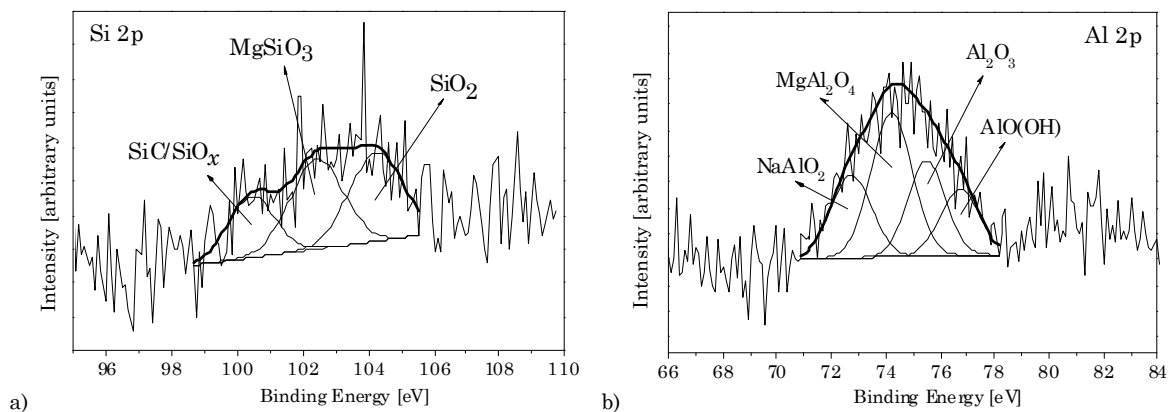
Figure 6.4: XPS a) Si2p and b) Al2p spectrums for the A-AH-24m sample

XPS Mg 2p spectrum is composed of three different Mg compounds, positioned at 50.75, 51.63 and 53 eV respectively (Figure 6.5). The broad LBE peak at 50.73 eV was identified as the combination of

MgAl$_2$O$_4$ and MgSiO$_3$ [Van10, Jeu08, Mat03]. The magnesium compound at BE=51.63 eV is indicative of fully oxidised MgO [Cas10, Jeu08].
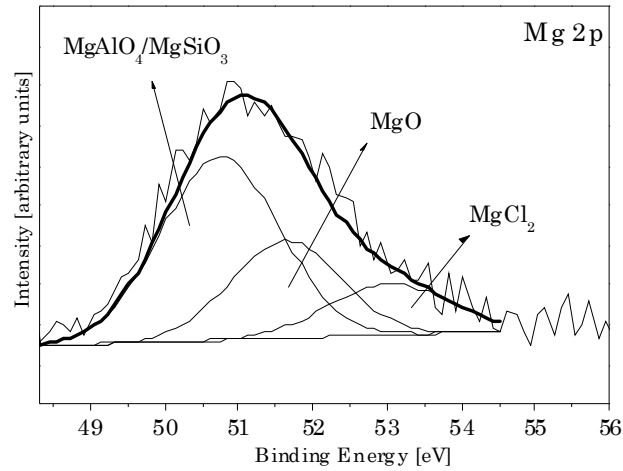
Figure 6.5: XPS Mg 2p spectrum, sample A-AH-24m

The Mg highest BE peak at 53 eV has been assigned to anhydrous MgCl$_2$ [Sio03b, Sio03a], although the general XPS spectrum of the sample does not reveal the presence of chlorine compounds. Fortunately, the XRF analysis performed on this sample exposes the presence of chlorine in the sample, as it can be seen in Table 6.1:

Table 6.1: XRF measurements performed in sample A-AH-24m. Chlorine is marked in blue

A-AH-24m		
Element	Rel. Weight	Std Error
Mg	72	0.4
Al	21	0.4
Si	4	0.1
Zn	0.6	0.1
Cl	0.3	0.07
Na	0.2	0.06
Mn	0.2	0.07
Zr	0.06	0.03

- *Sample A-AH-24m: Summary of the chemical analysis performed on A-AH-mould*

Summary of the chemical information obtained from the samples corresponding to the A-AH mould, Al$_2$O$_3$ + Air, through Chapters 4 and 6 is presented in Table 5.7.

Table 6.2: Summary of the chemical analysis performed on the Al_2O_3 + Air A-AH mould

	A-AH-4		A-AH-8	
	A-AH-24c	A-AH-24m	A-AH-8c	A-AH-8m
SEM: thickness	N.A.	N.M.	1mm	N.M.
EDS: element	N.A.	N.M.	Mg, Al, Si, Na, Ca, O	N.M.
XRD: compound	Mg, MgO, Mg_2Si, $Mg_{12}Al_{17}$	N.M.	Mg, MgO, Mg_2Si, $Mg_{12}Al_{17}$	N.M.
XPS: compound	N.A.	Na: $NaAlO_2$	N.A	N.A
		Ca: $CaO/Ca(OH)_2$; $CaAl_2O_4$		
		Si: SiC/SiO_x; $MgSiO_3$; SiO_2		
		Al: $NaAlO_2$, $MgAl_2O_4$, Al_2O_3, $CaAl_2O_4$, $AlO(OH)$	N.A	N.A
		Mg: $MgAl_2O_4$, $MgSiO_3$, MgO, $MgCl_2$		

N.M: No Measurable, N.A: Not Analysed. Duplicated compounds are marked in grey.

6.2.3 Sample A-KL-2m*: XPS high resolution spectrums

High-resolution Na 1s and Si 2s spectrums are shown in Figure 6.6.a and b, respectively. The Si 2s peak centred at 154.4 eV was identified as SiO_2, in accordance with the data published in the literature [Sur10, Gla00]. The high binding energy shoulder at 155.7 eV was associated to SiO_x [Arc07].

Regarding Na 1s core level, the spectra of Figure 6.6.a exhibits two wide subpeaks, located at 1073.4 and 1075.17 eV. The low BE peak was assigned to Na_2O [Bro07, Yos92]. The location of the high BE peak is quite unusual, as this value is close to the elemental value of sodium (1078 eV). Due to that, the few works that mention the presence of Na compounds at such high binding energies report that it cannot be assigned to any common sodium containing species. It is suggested that these species of sodium possess an intermediate oxidation level, between 0 and +1 [Ara08, Luk97].
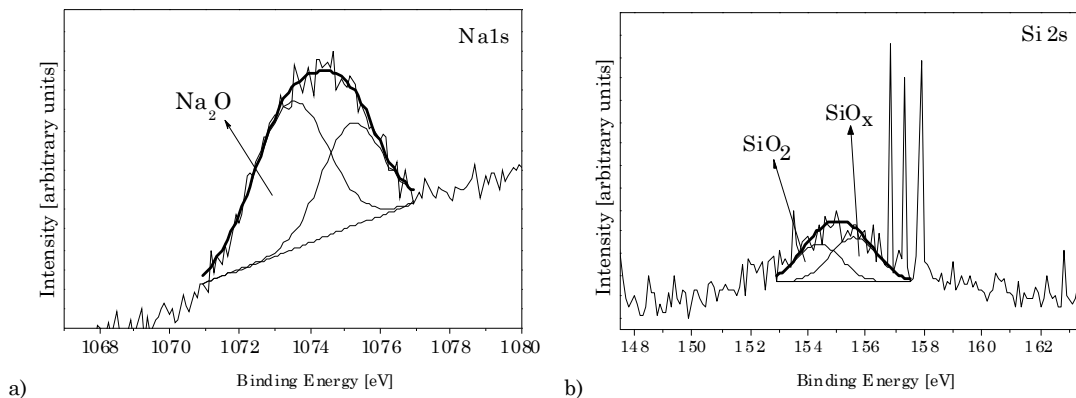
Figure 6.6: XPS spectrums for sample A-KL-2m*: a) Si2p b) Na1s

The Ca 2p spectrum of Figure 6.7.a contains a single calcium doublet with a binding energy of 347.8 eV. As in the Na 1s high resolution spectra of sample A-AH-24m, the peak was assigned to CaO and/or $Ca(OH)_2$; which are due to the surface oxidation of the calcium contained as an impurity in the bulk alloy.

The fitted high resolution Al2p XPS spectrum is given in Figure 6.7.b. The Al2p peak is in fact comprised by three components: lowest peak placed at BE, 75.5 eV, corresponds to thermally formed Al_2O_3 [Cri04] and/or to aluminium oxyfluoride, as stated by Kim *et al* [Kim04]. In these authors' work, aluminium oxyfluoride is formed after the diffusion of fluorine through the oxygen vacancies present in a non-uniform AlO_x oxide film. The other two components present in the Al 2p core level are attributed to Al−F bondings. The second component centred at 77.2eV corresponds to AlF_3 [Kön10, Bös97a]. The highest peak placed at 78.9eV is consistent with an aluminium-magnesium oxyfluoride compound ($AlMg_xO_yF_z$). Such an assignment is proposed with respect to a previous work by Böse *et al.* [Tre09].
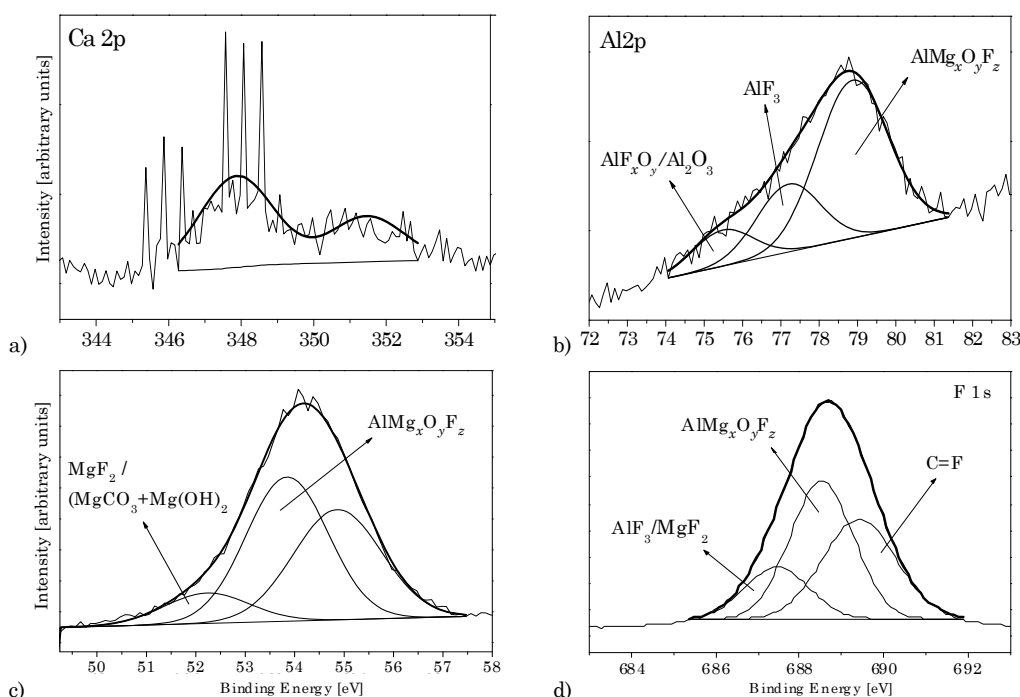
Figure 6.7: XPS spectra for A-KL-2m* sample: a) Ca2p b) Al2p c) Mg2p d) F1s

Böse *et al.* investigated the influence of the successive substitution of Al by Mg in AlF_3, and analysed the chemical state of the obtained doped products, which were partially X-ray amorphous. The XPS binding energies of Al, Mg and F measured in the work are resumed in Table 6.4. The stoichiometry of the products, estimated from the XPS analysis, is shown in Table 6.4. The surface stoichiometries of cations are close to the concentration ratio in the solution used for the co-precipitation.

Table 6.3: XPS data of different AlF$_3$ with Al substituted by Mg, as reported by Böse *et al.* [Bös97b]

	AlF$_3$	AlF$_3$	AlF$_3$	AlF$_3$	AlF$_3$	MgF$_2$
% Mg	5	11	24	48	57	99.999
Al 2p	78.07	78.19	78.47	78.48	78.57	-
Mg 2p	53.31	53.35	53.35	53.50	53.85	52.54
F 1s	688.37	688.51	688.69	688.65	688.71	687.32

Table 6.4: Stoichiometry of the compounds reported by Böse *et al.* [Bös97b]

%Mg	Surface stoichiometry)
3	$Al_{0.95}Mg_{0.05}F_{2.25}O_{0.14}$
10	$Al_{0.89}Mg_{0.11}F_{2.18}O_{0.22}$
20	$Al_{0.76}Mg_{0.24}F_{2.08}O_{0.18}$
35	$Al_{0.52}Mg_{0.48}F_{2.03}O_{0.18}$
50	$Al_{0.43}Mg_{0.57}F_{1.89}O_{0.19}$

The chemical shift of the Al 2p peak, 75.9eV from the reference values of Table 6.3 can be understood in terms of compound stoichiometry. The Al 2p values of the compounds synthesised by Böse *et al.* increase with the Mg content. So, the peak placed at 75.9eV would correspond to a Mg-Al oxyfluoride compound, with a higher Mg content than the ones reported in Table 6.3. In any case, the 75.9eV peak could also be assigned to $Al_{0.43}Mg_{0.57}F_{1.89}O_{0.19}$, as the F1s peak at 688.5eV (Figure 6.7.d) and the Mg 2p at 53.84eV (Figure 6.7.c) are in full accordance with the ones published for that compound in Table 6.3.

In addition to $AlMg_xF_yO_z$, the fitted Mg 2p spectrum of Figure 6.7.c reveals the presence of two additional components. In principle, the low BE peak, at 52.2, is assigned to MgF$_2$ in agreement with the values depicted in literature and gathered in Table 6.4 [Hsu08, Bös97b], although the contribution of magnesium hydroxides and carbonates cannot be fully discarded [Taj11, Yao01]. The highest BE peak at 54.9eV, is not possible to identify: at such high binding energies no chemical bond involving Mg is reported in literature.

Thus, the fitting of the F 1s spectra Figure 6.7.d corresponds to the sum of a low BE energy peak at 687.4eV, belonging to MgF$_2$ and AlF$_3$ [Kön10, Bös97b, Bös97a], the peak at 688.5eV, identified as $AlMg_xF_yO_z$, and a third peak, located at 684.4eV. The high BE peak correspond to oxyfluoride and/or carbon fluoride compounds [Goc09], being this last also detected in the C 1s high resolution spectra.

- *Sample A-KL-2m*: Summary of the chemical analysis performed on the KBF$_4$ protective surface layer*

The summary of the chemical information from sample A-KL-2m* is presented in Table 5.7:

Table 6.5: Summary of the chemical analysis performed on samples A-KL-2m* and A-KL-2c*

	A-KL-2m*
SEM: thickness	N.M.
EDS: element	N.M.
XRD: compound	N.M.
XPS: compound	Na: Na_2O, Na_xO $(0<x<1)$
	Ca: $CaO/Ca(OH)_2$
	Si: SiO_x; SiO_2
	Al: Al_2O_3, AlF_xO_y, AlF_3, $AlMg_xO_yF_z$
	Mg: $AlMg_xO_yF_z$, MgF_2, $Mg(OH)_2$, $MgCO_3$

N.M: No Measurable, N.A: Not Analysed

6.2.4 Comparison between protected and reacted surfaces

As commented before, the scan survey of Figure 6.2.b reveals a sharp F 1s core level in the protected surface of sample A-KL-2m*, indicating that the use of KBF_4 induces a fluorinated surface, as expected (Figure 6.8). Calcium, aluminium and magnesium are alloying elements of AZ91E alloy. Oxides (or its water corrosion products) of the three elements are present in the oxide film: $CaO/Ca(OH)_2$; Al_2O_3 and $Mg(OH)_2/MgCO_3$.
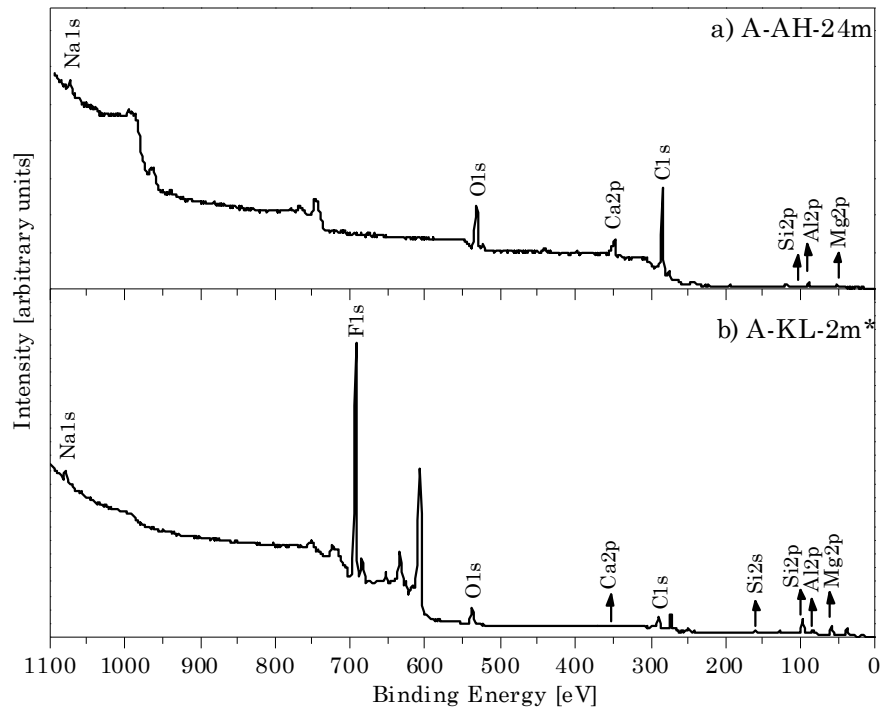
Figure 6.8: XPS survey spectra of samples: a) A-AH-24m b) Kl-2m*

Surface of the A-AH24m sample appears to be covered mostly with oxides, which are formed after mould-metal reactions. Surface of sample A-KL-2m* is covered with oxides but also with aluminium and magnesium fluorine compounds, being these lasts predominant in the film. The change in

composition from oxides to fluorides can be clearly seen after the comparison of the Al 2p and Mg 2p XPS spectra of both samples, Figure 6.9.
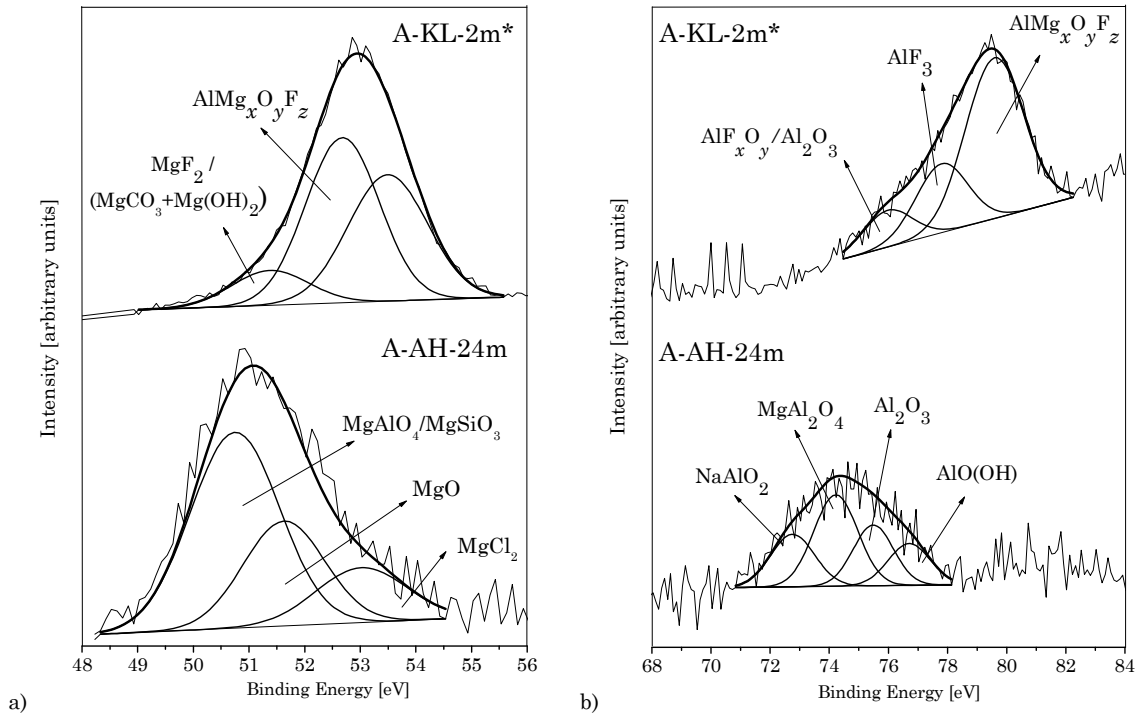
Figure 6.9: a) Mg 2p and b) Al 2p XPS spectra of the two samples, with peak fitting results

The protective layer is thus composed of oxides, hydroxides, fluorides and oxyfluorides. These finding supports the theories developed for SF_6 proposed by Pettersen *et al.* and Aarstad, mentioned in Chapter 2, which state that the protective effect is achieved due to the fluorine saturation of an initially formed oxide film [Aar04, Pet02]. This proposal supports also the theory held by Kim *et al.* [Kim04]. According to these authors, aluminium oxyfluoride is formed after the diffusion of fluorine through the oxygen vacancies present in a non-uniform AlO_x oxide film. Along with this theory, $AlMg_xO_yF_z$, would be formed after the fluorine diffusion through $MgAl_2O_4$, and MgF_2 after the one of MgO film.

The origin of this previous oxide film is uncertain. The oxide film can be formed due to mould-metal reactions, or to the thermal oxidation of the alloy. Thermal oxidation of AZ91E produces $MgAl_2O_4$, MgO, Al_2O_3 and its hydroxides, as stated in Chapter 2: Literature review. On the other hand, presence of sodium and silicon compounds on the survey spectra of sample A-KL-2m* (Figure 6.8) evidences that, even when a protective film is formed on the sample surface, reactions between the mould and the metal may exist to some extend, while the fluorine compounds are being formed.

6.3   Modelling of mould-metal reactions with Factsage®

To study the behaviour of the Al_2O_3-based refractory mould materials on Mg investment casting, thermodynamic equilibrium calculations have been performed. These calculations have been carried out using the FactSage® Equilib module. For that purpose, the different compounds encountered during the chemical analysis of the surface of sample A-AH-24m have been considered (Table 6.2). Chemical equilibrium simulations of the protective layer formed under KBF_3 atmospheres have not been performed, as the complex compounds found on sample A-KL-2m by XPS (Table 6.5) are not available in the Factsage® databases.

Main objective of the calculations performed in this chapter is to understand which are the chemical reactions that take place when magnesium reacts with the Al_2O_3 mould. After the literature review of Chapter 2, it is clear that the mechanisms that lead to the mould-metal reactions are not fully understood. According to the different authors, the following three situations may take place in magnesium investment casting when no inhibitor is used:

1. Molten metal reacts with gas in the mould and the reaction product (MgO) reacts with the mould [Cin06].

2. Molten metal reacts directly with the mould material [Jaf11, Arr07, Sin06, Idr96].

3. Metal vapours penetrate in the mould and react with the mould material [Jaf11, Sin06, Zha04].

Therefore, a major concern in magnesium casting is to determine if mould-metal reactions occur in the presence of oxygen, due to the formation of MgO; or they happen due to a direct reaction between Mg and the mould materials (whether Mg is in liquid or gaseous state). The FactSage® calculations performed through this section pretend to clarify this issue.

The three refractory phases found by XRD (Al_2O_3, SiO_2, β-Al_2O_3) have been taken into account in the FactSage® calculation. For each mould material, two different reactions have been performed: the reaction between the mould and Mg, and the reaction between the mould and MgO. Unfortunately, the Ca-based compound was not discernable in the XRD spectrum (Figure 4.4) so reactions between Mg/MgO and this material couldn't be simulated. Calculations have been performed at atmospheric pressure and 700^oC. According to Chapter 2, Literature review, mould-metal reactions occur while the alloy is in molten state, until it reaches its solidus temperature (437^oC for AZ91E). In the performed calculations, it has been seen that a decrease of the reaction temperature only changes the relative amount of the reaction products, so simulation with one temperature is enough to determine the trend of the reaction.

Only calculations performed with liquid magnesium are shown in this chapter. FactSage® results are identical when the magnesium phase is in liquid or gas state, which makes impossible to differentiate between previous situations 2 and 3. Due to this, after obtaining the reaction equations with the Equilib module, Reaction was used. This last module calculates changes in extensive thermochemical properties for a chemical reaction. To compare the different values obtained through this chapter, change in Gibbs energy ΔG^o was calculated for one mol of reactant Mg (liquid or gas). These calculations will allow to determinate the most probable reactions.

After defining the reactant species (Al_2O_3, SiO_2, β/β''-Al_2O_3, Mg, MgO), pressure (atmospheric) and isothermal temperature (700^oC) last step before performing the equilibrium calculation is to determine the amount of the reactants. The resultant product species depend on the amount of the elements added to the reaction. However, due to the nature of the experiments it is impossible to know the quantity of material that is involved in each reaction. Owing to this fact, each calculation was performed by inputting a variable alpha amount of reactant, identified as <A>. Simulation results show the amount of product phases present (y-axis) plotted as a function of alpha (x-axis).

Nevertheless, there are certain limitations in the use of thermodynamic equilibrium analyses. Reaction compounds are limited to the ones existing in the software databases. Composition and temperature gradients are also not considered in the calculations and physical processes, such as particle nucleation, agglomeration and adsorption are not taken into consideration. Despite of all the limitations, though, thermodynamic equilibrium analysis is a useful tool to study the chemistry of processes involving multiphases such as alloys, molten salts, oxides, aqueous solutions, and gases. It calculates the concentrations of chemical species and its thermodynamic properties when specified elements or compounds react or partially react to reach a state of chemical equilibrium.

Following FactSage® databases have been employed to perform the calculations:

o SGSL pure substances database

o GTLM light alloys database

o SGSL intermetallics database

o FToxid oxide compound database

- *Reactions between Mg, MgO and SiO$_2$ mould material*

Compounds present in chemical analysis of the A-AH mould are MgO, SiC/SiO_x; $MgSiO_3$; SiO_2 and Mg_2Si (Table 5.7). Results of the two calculations performed with SiO_2 are given in Figure 6.10.a and b. As the two figures show, quite different results are obtained by varying the amount of reaction phases. Formation of Mg_2Si is due to a direct reaction between the Mg melt and SiO_2 which can be modelled by adopting an alpha value of A=0.8 (Equations 6.1 and 6.2). Calculations performed with

Reaction module reveals that Mg₂Si is more stable when reactant magnesium is in gas state, rather than liquid.

$$(A=0.8) \quad Mg(l) + \tfrac{1}{4} SiO_2(s) \to \tfrac{1}{4} Mg_2Si(s) + \tfrac{1}{2} MgO(s) \qquad \Delta G^0 = -79.24 KJ \qquad 6.1$$

$$Mg(g) + \tfrac{1}{4} SiO_2(s) \to \tfrac{1}{4} Mg_2Si(s) + \tfrac{1}{2} MgO(s) \qquad \Delta G^0 = -116.98 KJ \qquad 6.2$$
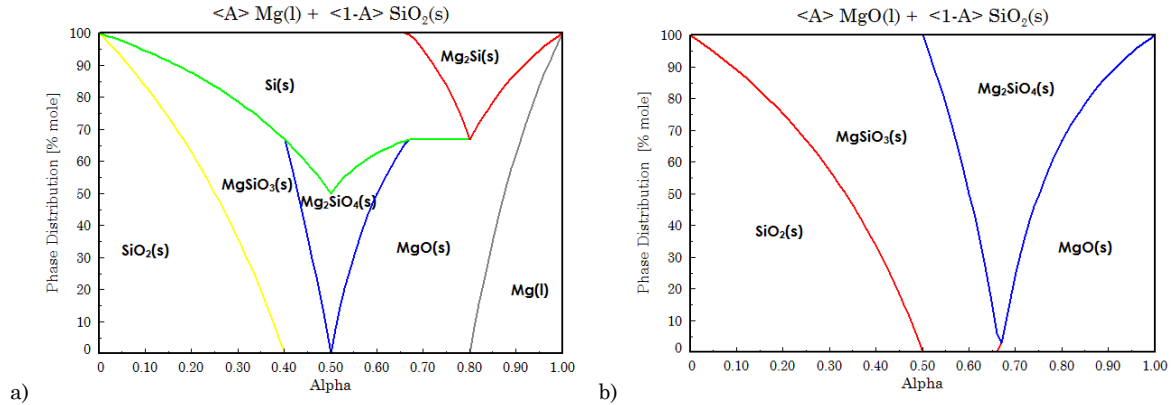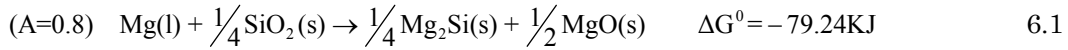
Figure 6.10: a) Direct reaction between the Mg melt and SiO₂ b) Reaction between MgO and SiO₂

MgSiO₃ is present in Figure 6.10.a and b, which leads to a wide variety of options. If it is considered that MgSiO₃ is formed due to a direct reaction, the reaction detailed in Equation 6.3 might take place:

$$(A=0.4) \quad Mg(x) + \tfrac{3}{2} SiO_2(s) \to \tfrac{1}{2} Si(s) + MgSiO_3(s) \qquad \begin{aligned} \Delta G^0_{x=l} &= -163.518 KJ \\ \Delta G^0_{x=g} &= -201.55 KJ \end{aligned} \qquad 6.3$$
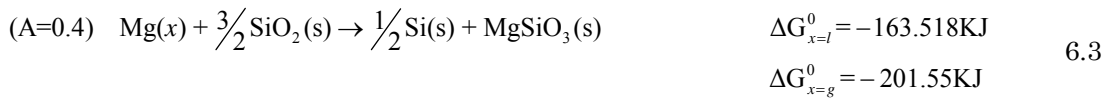
If it is considered that MgSiO₃ is formed due to a reaction between MgO and mould material, then reaction in Equation 6.4 may be happening:

$$\left. \begin{aligned} Mg(l) + \tfrac{1}{2} O_2(g) &\to MgO(s) \qquad \Delta G^0 = -496.53 KJ \\ (A=0.5) \quad MgO(s) + SiO_2(s) &\to MgSiO_3(s) \qquad \Delta G^0 = -34.05 KJ \end{aligned} \right\} \Delta G^0_{MgSiO_3} = -530.58 KJ \qquad 6.4$$
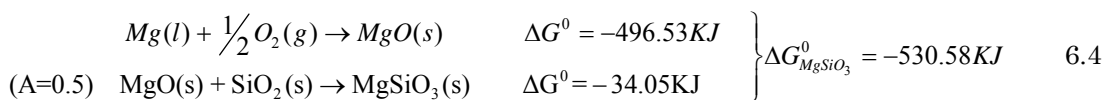
The calculated ΔG_0 values indicate that the reaction of Equation 6.4 is more likely to occur, as MgSiO₃ is more stable. Due to this, it is feasible to conclude that MgSiO₃ is formed due to a MgO-SiO₂ reaction. This MgO may be formed due to a mould-metal reaction (Equation 6.1), or it may be due to the air oxidation of the melt in the cavity. It is a well-known fact that molten magnesium oxidizes very rapidly when it is exposed to air. Even with infinitesimal amounts of oxygen in the atmosphere, molten magnesium will oxidize and form MgO. The calculations performed with FactSage® by Aarstad show that at 700°C only a O₂ partial pressure of $5 \cdot 10^{-54}$ bar is needed for magnesium oxidation to occur [Aar04]. Thus, thermodynamically, it is almost impossible to prevent magnesium oxidation in the presence of oxygen.

SiO$_2$ and SiO$_x$ compounds have also been found in the XPS analysis of sample A-AH-24m (Table 5.7). Determining the origin of these products is quite difficult. They may be related to shell compounds, or they may be formed due to the oxidation of solid silicon, obtained in Mg-SiO$_2$ direct reaction (Figure 6.10). Its presence can also be due to a latter reaction between the sample and the environment. In the presence of water, Mg$_2$Si tends to form oxides like SiO$_2$ and MgO [Esc10, Yas07].

- *Reactions between Mg, MgO and Al₂O₃ mould material*

According to the experimental chemical analysis of Table 5.7, MgO, Mg$_{12}$Al$_{17}$, MgAl$_2$O$_4$ and thermally formed Al$_2$O$_3$ are the compounds that may be formed after Al$_2$O$_3$-metal interaction. Before analysing the Factsage® results, however, it has also to be taken into account that the thermal oxidation of Mg-Al alloys produces oxide films which are a mixture of MgO, Al$_2$O$_3$ and MgAl$_2$O$_4$, as detailed in Chapter 2: Literature review.

Figure 6.11.a and b show the results obtained with the Factsage® chemical equilibrium calculations performed with this material. As justified in Chapter 4, Mg$_{12}$Al$_{17}$ is formed due to an aluminium enrichment of the Mg melt. According to Figure 6.11.a, due to direct reaction between liquid Mg and Al$_2$O$_3$, aluminium dissolves in liquid magnesium and crystallizes during the solidification. This reaction mechanism corresponds in Figure 6.11.a to an alpha value of A=0.45-1, as both MgAl$_2$O$_4$ and MgO are also present in the XPS analysis. Calculus of ΔGo of these reactions cannot be performed, due to the presence of a solid solution: Stoichiometry of the solution element in the equation cannot be solved.
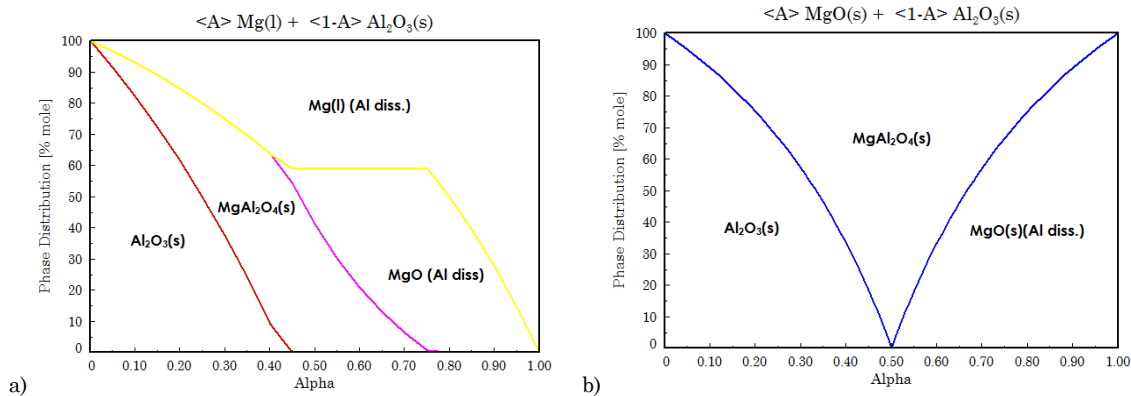
Figure 6.11: a) Direct reaction between Mg and Al$_2$O$_3$ b) Reaction between MgO and Al$_2$O$_3$

MgAl$_2$O$_4$ is also present in the reaction between MgO and Al$_2$O$_3$. According to Figure 6.11.b, not only spinel but also Al-dissolved MgO are formed with any alpha value between 0.5-1. Gibbs energy ΔGo can only be calculated in the case of A=0.5. This reaction is described as follows:

$$Mg(l) + \tfrac{1}{2}O_2(g) \rightarrow MgO(s) \qquad \Delta G^0 = -496.53\text{KJ}$$
$$(\text{A=0.5}) \quad MgO(s) + Al_2O_3(s) \rightarrow MgAl_2O_4(s) \quad \Delta G^0 = -46.31\text{KJ}$$

$$\Delta G^0_{\text{MgAl}_2\text{O}_4} = -542.84 KJ \qquad 6.5$$
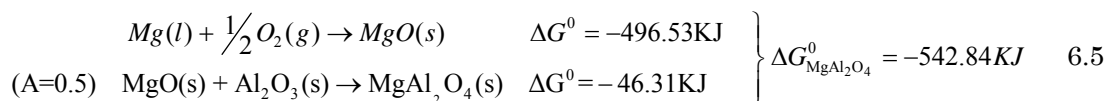
Presence of Al_2O_3 in the film can be due to non-reacted shell compounds, or to the oxidation of excess aluminium, or it may be also due to oxidation of AZ91E alloy.

- *Reactions between Mg, MgO and β-Al_2O_3 mould material (NaAl₉O₁₄)*

Sodium alumina is a non-stoichiometric oxide, assigned the formula $Na_2O.xAl_2O_3$. ($5 \leq x \leq 11$) and identified in the FactSage® database as $NaAl_9O_{14}$. According to Table 5.7 MgO, $Mg_{12}Al_{17}$, $MgAl_2O_4$, Al_2O_3 and $NaAlO_2$ are the compounds that may be formed after a (ß-Al_2O_3)-metal interaction. Logically, with exception of the sodium $NaAlO_2$ compound, the rest of the products are the ones detailed in the previous Al_2O_3-metal reactions. Figure 6.12.a and b show the results obtained after the Factsage® chemical equilibrium calculations.
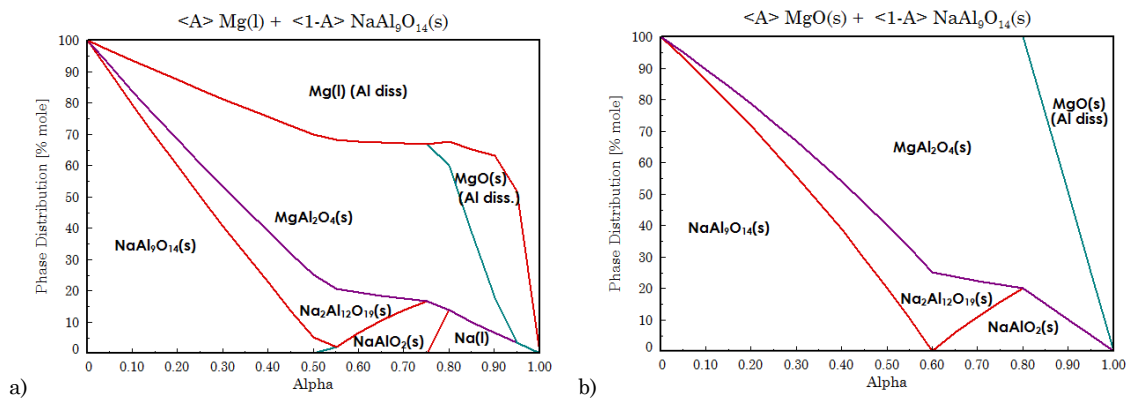
Figure 6.12: Reactions between $NaAl_9O_{14}$ and a) liquid Mg b) MgO

$NaAlO_2$ compound can be formed due to the two reaction mechanisms proposed in Figure 6.12.a and b. If $MgSiO_3$ is formed due to a reaction between MgO and β-Al_2O_3, the following reactions should be considered:

$$\left.\begin{array}{ll} Mg(l) + \frac{1}{2}O_2(g) \rightarrow MgO(s) & \Delta G^0 = -496.53 KJ \\ (A=0.8)\ MgO(s) + NaAl_9O14(s) \rightarrow MgAl_2O_4(s) + NaAlO_2(s)\ \Delta G^0 = -37.96 KJ \end{array}\right\} \Delta G_T^0 = -534.49 KJ \quad 6.6$$
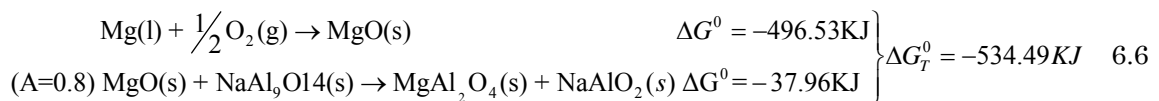
$MgSiO_3$ can also be formed after the direct reaction of Figure 6.12.a. A reaction mechanism with an alpha value of A=0.75 would imply the formation of $NaAlO_2$, $MgAl_2O_4$ and Al-dissolved liquid Mg, which is also possible. Again, the presence of dissolved aluminium may be the promoter of $Mg_{12}Al_{17}$.

6.4   Conclusions

After the XPS analysis performed on sample A-AH-24c, the summary of all the compounds and elements detected on the A-AH mould samples is presented in Table 6.6:

Table 6.6: Summary of the chemical analysis performed on the Al$_2$O$_3$ + Air A-AH mould

	A-AH-4		A-AH-8	
	A-AH-24c	A-AH-24m	A-AH-8c	A-AH-8m
SEM: thickness	N.A.	N.M.	1mm	N.M.
EDS: element	N.A.	N.M.	Mg, Al, Si, Na, Ca, O	N.M.
XRD: compound	Mg, MgO, Mg$_2$Si, Mg$_{12}$Al$_{17}$	N.M.	Mg, MgO, Mg$_2$Si, Mg$_{12}$Al$_{17}$	N.M.
XPS: compound		Na: NaAlO$_2$	N.A	N.A
		Ca: CaO/Ca(OH)$_2$; CaAl$_2$O$_4$		
	N.A.	Si: SiC/SiO$_x$; MgSiO$_3$; SiO$_2$		
		Al: NaAlO$_2$, MgAl$_2$O$_4$, Al$_2$O$_3$, CaAl$_2$O$_4$, AlO(OH)		
		Mg: MgAl$_2$O$_4$, MgSiO$_3$, MgO, MgCl$_2$	N.A	N.A

N.M: No Measurable, N.A: Not Analysed. Duplicate compounds are marked in grey.

To understand which are the chemical reactions that take place on these samples, Factsage chemical equilibrium calculations were performed. The three mould materials identified by XRD in Chapter 4 (Al$_2$O$_3$; SiO$_2$, β-Al$_2$O$_3$) were simulated to determine if the mould-metal reactions occur in the presence of oxygen, due to the formation of MgO; or if they happen due to a direct reaction between Mg and mould materials (whether Mg is in liquid or gaseous state).

Results show that some compounds (Mg$_2$Si and Mg$_{12}$Al$_{17}$) can only be formed due to a direct reaction between Mg and mould materials. Rest of the compounds encountered through the XPS analysis can be formed due to either Mg-Mould or MgO-Mould reaction mechanisms, if the appropriate amount of reactant is chosen. Due to this, determining the origin of most of the compounds is rather difficult. However, it is feasible to think that reactions between MgO and shell compounds also happen, as the compounds formed are more stable than the ones formed due to a direct reaction.

Table 6.7 summarises the information obtained from the XPS analysis of the protective layer:

Table 6.7: Summary of the chemical analysis performed on samples A-KL-2m*

	A-KL-2m*
SEM: thickness	N.M.
EDS: element	N.M.
XRD: compound	N.M.
XPS: compound	Na: Na$_2$O, Na$_x$O (0<x<1)
	Ca: CaO/Ca(OH)$_2$
	Si: SiO$_x$; SiO$_2$
	Al: Al$_2$O$_3$, AlF$_x$O$_y$, AlF$_3$, AlMg$_x$O$_y$F$_z$
	Mg: AlMg$_x$O$_y$F$_z$, MgF$_2$, Mg(OH)$_2$, MgCO$_3$

N.M: No Measurable, N.A: Not Analysed

The use of KBF_4 inhibitor induces a fluorinated surface film on the AZ91E casting. Surface films changes from a film composed mostly of oxides/hydroxides (formed after mould-metal reactions) to a surface covered with oxides, hydroxides, fluorides and oxyfluorides, being the last two predominant in the film. The protective layer is thus composed of oxides, hydroxides, fluorides and oxyfluorides. These finding supports previous theories which state the protective effect is achieved due to the fluorine diffusion through an initially formed oxide film [Aar04, Pet02]. Along with this theory, $AlMg_xO_yF_z$, would be formed after the fluorine diffusion through $MgAl_2O_4$, AlF_xO_y after diffusion through Al_2O_3 and MgF_2 after the one of MgO film.

The origin of this previous oxide film is uncertain. The oxide film can be formed due to mould-metal reactions, or to the thermal oxidation of the alloy. Thermal oxidation of AZ91E produces $MgAl_2O_4$, MgO, Al_2O_3 and its hydroxides, as stated in Chapter 2: Literature review. On the other hand, Presence of sodium and silicon compounds on the survey spectra of sample A-KL-2m* (Figure 6.8) evidences that, even when a protective film is formed on the sample surface, reactions between the mould and the metal may exist to some extend, while the fluorine compounds are being formed.

DISCUSSION ON REACTION & PROTECTION MECHANISMS

7.1 Introduction

As a result of the results obtained in this work, in this chapter the two mechanisms that lead to both reacted and protected surfaces have been proposed. The different surfaces encountered during the inhibitor and mould material experiments have also been analysed.

According to the analysis methodology presented in Chapter 3, the diagram of Figure 4.1 shows in green the tasks performed in previous chapters, in black the ones that are performed through this chapter and in grey the ones that will be detailed in next chapters.
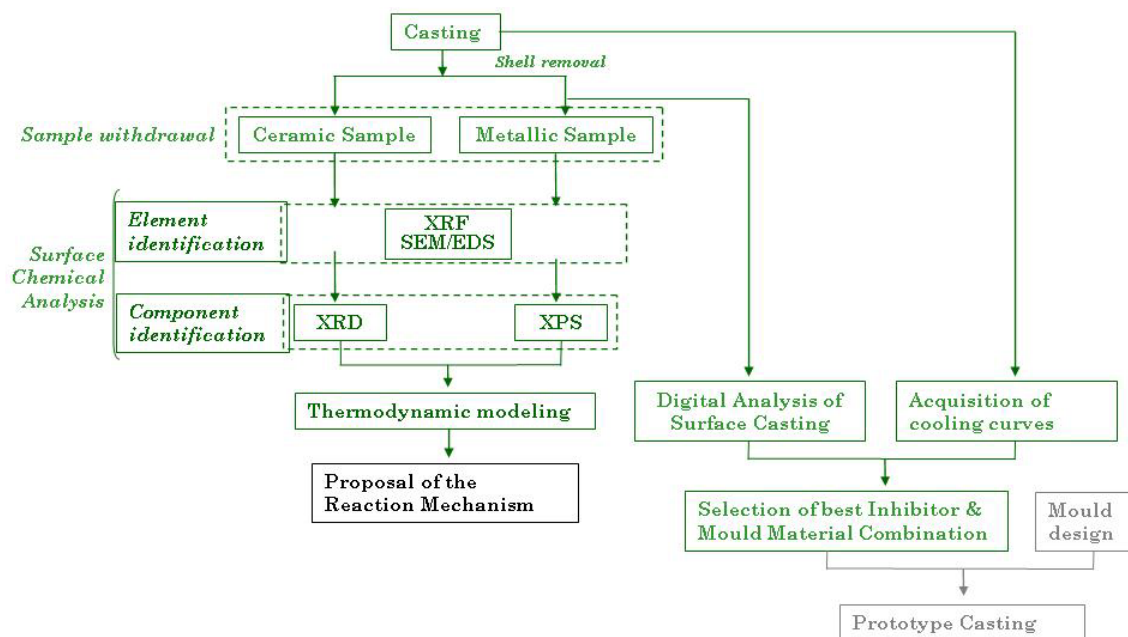
Figure 7.1: Results analysed in Chapter 7 are marked in black. Tasks in green have already been performed previously, and the ones in grey will be detailed in next chapter

7.2   Mould-Metal reactions...

As it has been reviewed in Chapter 2, four are the different reactions that may take place in Mg investment casting. According to the results obtained in Chapter 6, and the conclusions extracted after the literature review (Section 2.9), not only one but more than one may be happening at the same time: all seem likely to occur:

o Molten metal reacts with the atmosphere of the mould, and MgO is formed . Presence of MgO has been detected in all the reacted ceramic samples analysed by XRD, and the two metallic ones analysed by XPS. Although it is impossible to discern between oxidised MgO and "reacted" MgO (product of a mould-metal reaction), it is feasible to think that magnesium oxidation always occurs in investment casting. Even with infinitesimal amounts of oxygen in the atmosphere, molten magnesium will oxidize and form MgO. The calculations performed with FactSage® by Aarstad, indeed, show that at 700°C, only a O_2 partial pressure of $5 \cdot 10^{-54}$ bar is needed for magnesium oxidation to occur [Aar04]. Thus, thermodynamically, it is almost impossible to prevent magnesium oxidation. Melt can oxidise either during the filling of the mould due to the oxygen present in the mould cavity or during the solidification of the part due to the porous nature of the refractory shells, as stated by Cingi [Cin06].

o Molten metal reacts with the gas in the mould, and the reaction product reacts with the mould [Cin06]. As stated in Chapter 6, most of compounds encountered through the XPS analysis can be formed due to either Mg-mould or MgO-mould reaction mechanisms, if the appropriate amount of reactant is chosen. As seen above, MgO will always be formed in magnesium investment casting. Thus, it is feasible to think that reactions between MgO and shell compounds happen: Fatsage® has revealed that, when the compound is formed after a MgO-mould reaction, the energy jump is higher than if the reaction is simply a Mg-mould one. Fluorine-based inhibitors, as seen in Chapter 6, promote the formation of fluorine compounds in the surface of the casting, being MgF_2 one of them. MgF_2 is very stable, and does not react with the mould refractories as can be deduced form the calculations performed with FactSage® at 650ºC (Equations 7.1 and 7.2). Unfortunately, the rest of the F compounds are not available in the FactSage® database.
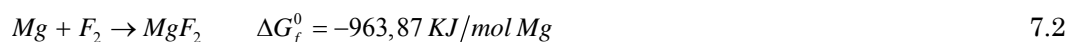
$$Mg + \frac{1}{2}O_2 \rightarrow MgO \qquad \Delta G_f^0 = -502,3\, KJ/mol\, Mg \qquad\qquad 7.1$$

$$Mg + F_2 \rightarrow MgF_2 \qquad \Delta G_f^0 = -963,87\, KJ/mol\, Mg \qquad\qquad 7.2$$

o Molten metal reacts with the mould [Jaf11, Arr07, Sin06, Idr96]. XPS analysis and the thermodynamic modelling of the A-AH mould reactions show that some compounds (Mg_2Si and $Mg_{12}Al_{17}$) can only be formed due to a direct reaction between magnesium (liquid and/or vapour) and mould materials.

o Magnesium penetrates in the mould and reacts there with it [Jaf11, Sin06, Zha04]. According to FactSage® calculations, the energy jump after the compound formation is higher when Mg vapour is the reactant, rather than liquid Mg. The literature review performed on the oxidation of magnesium and its alloys supports this theory. Liquid Mg alloys are associated with a high magnesium vapour pressure which activates the nodular growth of the oxides. Reactions can even occur at a considerable distance from the surface [Cze04, Cze02].

7.2.1 ...and experimental factors affecting them

Interface temperature and casting section thickness are the main factors that affect to the severity of mould-metal reactions. Increasing the casting thickness has proved to adversely affect to mould-metal reactions. For instance, essay A-KL, which has given the most satisfactory results, exhibits a clean surface in those sections that are 2, 4 and 8mm thick but is covered with mould-metal reactions in the 18, 20 and 24mm thick ones. The influence of the interface temperature, dependant of Mg casting temperature and mould preheating temperature, was demonstrated in the experiments performed through this work: essays at high temperatures have shown a higher % of reacted surface than their low temperature counterparts. These findings are in agreement with the results published by Idris *et al*, Yan *et al* and Sin *et al*, who also stated that suppression of the oxidation reaction in the mould is influenced by experimental temperatures and casting thickness [Yan07, Sin06, Idr96]

7.3   The protective layer...

In Chapters 4 and 6 the protective layer formed in the $Al_2O_3+KBF_4$ was analysed. According to the results obtained, the protective layer is thus composed of oxides, hydroxides, fluorides and oxyfluorides, being the last two predominant in the film. These findings supports previous theories which state the protective effect is achieved due to the fluorine diffusion through an initially formed oxide film [Aar04, Pet02, Kim00]. According to the Mg melt protection study performed by Aarstad, SF_6 must first dissociate to form small and reactive species to enter in the MgO film [Aar04]. In this work, the speed of dissociation of BF_3 would be the upper limit to the formation of the fluorine compounds. While BF_3 decomposes to form the more reactive species (such as F or F_2) magnesium reacts primarily to form the oxide layer.

Origin of the initial oxide may be due to thermal oxidation of the alloy itself, or to the presence of mould-metal reactions. Results obtained by XPS indicate that, even when a protective film is formed on the sample surface, reactions between the metal and low stability mould materials appear, which produces MgO. Same XPS results reveal the presence of CaO/Ca(OH), Al_2O_3 and $Mg(OH)_2/MgCO_3$.

Calcium, aluminium and magnesium are alloying elements of AZ91E alloy, and the thermal oxidation of the alloy produces a surface layer which contains those elements, as seen in the literature review.

7.3.1 ...when different mould materials are employed

Three refractory flours have been tested in this work: Al_2O_3, $MgAl_2O_4$ and SiO_2. When combined with KBF_4, effectiveness of the three materials was ranked in order of reaction degree as follows, from more to less reacted surface: $SiO_2 \rightarrow MgAl_2O_4 \rightarrow Al_2O_3$, being the alumina mould the most effective one. Effectively protected surfaces were achieved for the different mould materials. Differences in the three protective films arise from their thickness, and it is related to the stability of each mould materials.

The protective layer formed in the SiO_2 essay is thicker than the other two so its elemental composition can be analysed by SEM/EDS. Results shown in Figure 4.16 reveal that the elements present in the surface film are evenly distributed. It is believed that, while the initial oxide film is forming, fluorine diffuses through the film and the new fluorine compounds that finally block the growth of the mould-metal reaction layer are formed.
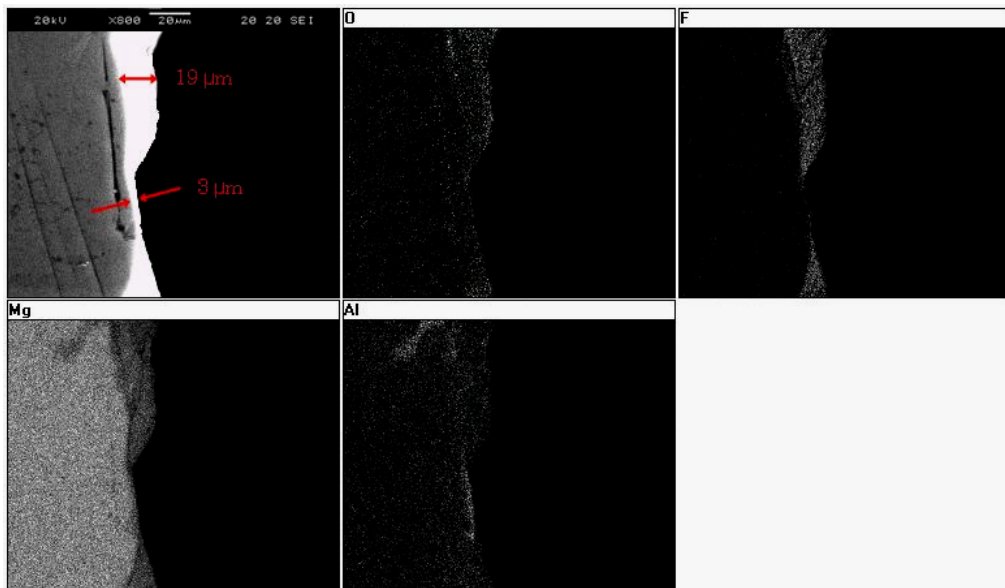
Figure 7.2: The protective film formed on the Si-KL-2m* sample

Severity of mould-metal reaction is higher for SiO_2 moulds than for Al_2O_3 or $MgAl_2O_4$, which means that the rate of the Mg/MgO-SiO_2 reactions is also higher. Thus, the initial oxide film grown in SiO_2 moulds is also faster, due to a higher presence of mould-metal reaction products. By the time that the new fluorine compounds have blocked the forthcoming reactions, the layer formed on the surface of the SiO_2 casting is thicker than the one formed on Al_2O_3 or $MgAl_2O_4$ moulds.

7.3.2 …when different inhibitors are employed

Alumina moulds with four different inhibitors were tested in this work. Mould-metal reaction free surfaces were achieved for two of them, $NaBF_4$ and KBF_4, but KBF_4 has proved to be more effective than $NaBF_4$. Both inhibitors are similar chemicals in their properties and owe their protector behaviour to the liberation of BF_3 gas. Moulds are firstly dipped in a $H_2O+KBF_4/NaBF_4$ solution and later, during the mould preheating, BF_3 is released from the mould itself. The protective gas fills not only the mould cavity, but also the ceramic structure as the shell is porous. Due to that, a protective atmosphere is created during the pouring and also during the solidification stage; the final casting is surrounded by the inhibitor atmosphere.

Difference in the protective behaviour of these two salts is due to the thermal decomposition temperature: while KBF_4 produces protective boron trifluoride at temperatures higher than 530^oC, $NaBF_4$ decomposes at 200^oC. Therefore, in the $NaBF_4$ experiments less fluorine is available at casting temperatures. As the protective effect is achieved after the formation of the fluorine compounds, this fluorine lack is the cause of the $NaBF_4$ reduced effectiveness.

7.3.3 …and reaction time

As explained before, severity of mould-metal reactions decreases when the interface temperature is down to 437^oC, the solidus temperature of the alloy. However, according to the results obtained with the $MgAl_2O_4$, below this temperature the mechanisms that produce the fluorine compounds are still active: during $MgAl_2O_4$ experiments moulds cracked when the interface had already solidified and atmospheric oxygen entered in the cavity. Three different situations took place on the casting surface:

o Part of the surface was already covered with mould-metal reactions.

o Part was already protected. The fluorides had already saturated the oxide film, achieving a protective layer.

o Part of the surface was covered with thermal oxidation products due to the presence of atmospheric oxygen.

Last option corresponds to casting areas where clean surfaces could be obtained. If the protective layer had been already formed, this film would have protected it from oxidation, in the same way that it protects the alloy from reactions with mould materials.

7.3.4 …and its absence: factors affecting its formation

The use of an inhibitor is not a clean-surface guarantee: sometimes the protective layer is not achieved. In those cases, surface is covered with mould metal reactions but fluorine is detected inside the surface layer either by XRF, SEM/EDS or XRD. SEM/EDS analysis of the cross section of the

surface layer reveals a random arrangement of the fluorine particles, instead of the dense and coherent fluorine structure observed for the protective films. Figure 4.24a. and b., for example, show the SEM/EDS fluorine analysis made on samples A-NaL-18c (inhibited with $NaBF_4$), A-KL-18c (inhibited with KBF_4) and A-SH-2c (inhibited with SF_6).
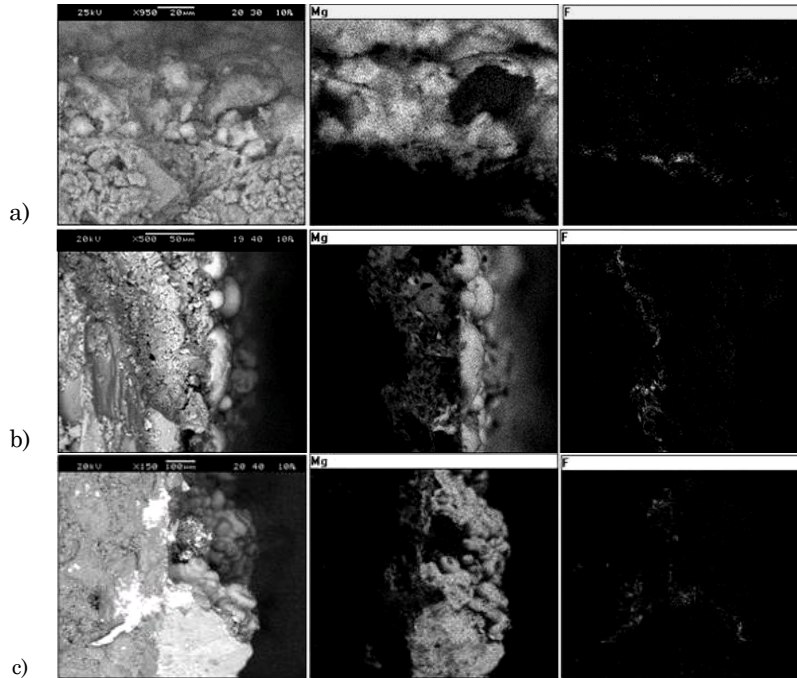
Figure 7.3: SEM/EDS fluorine mapping on sample a) A-NaL-18c b) A-KL-18c c) A-SH-2c

When a protective surface film is achieved, an initial oxide film in which fluorine diffuses is formed. Fluorine reacts with the oxides, creating the fluorine compounds that block the forthcoming mould-metal reactions. This initial oxide layer is so thin that the new fluorine compounds fill it completely. As a result, a dense and coherent protective film, composed of oxides and fluorides, is formed.

Those surfaces covered with mould-metal reactions have suffered more aggressive conditions than the protected ones. Likewise in mould-metal reactions, formation of the protective layer is influenced by interface temperature and casting section thickness. Increasing the casting temperature, for example, increases the rate of mould-metal reactions and forms a thicker initial oxide film. Although fluorine diffuses through this layer, the amount of new fluorine compounds is not able to fill the oxide film, as previously did. Instead of that, fluorine is distributed along the oxide film and the coherent structure that stops the mould-metal reactions is not formed. Increasing the casting thickness is also detrimental to the protective layer formation. According to literature, mould-metal reactions decrease considerably when the alloy reaches its solidus temperature (437ºC for AZ91E) [Cin06]. The thicker the casting section is, the more time it will take for the interface to reach solidus. This means that, for thick steps, the oxide film has more time to grow so initial thicker oxide layers can also be expected in this case.

7.4   Conclusions

As it has been reviewed in Chapter 2, four are the different reactions that may take place in Mg investment casting. According to the results obtained in Chapter 6, and the conclusions extracted after the literature review (Section 2.9), not only one but more than one may be happening at the same time: all seem likely to occur.

o Molten metal reacts with the atmosphere of the mould, as thermodynamically it is almost impossible to prevent magnesium oxidation. Melt can oxidise either during the filling of the mould due to the oxygen present in the mould cavity or during the solidification of the part due to the porous nature of the refractory shells, as stated by Cingi [Cin06].

o Molten metal reacts with the gas in the mould, and the reaction product reacts with the mould [Cin06]. As stated in Chapter 6, most of compounds encountered through the XPS analysis can be formed due to either Mg-mould or MgO-mould reaction mechanism, if the appropriate amount of reactant is chosen. Fluorine-based inhibitors promote the formation of fluorine compounds in the surface of the casting, being MgF_2 one of them. MgF_2 is very stable, and does not react with the mould refractories.

o Molten metal reacts with the mould [Jaf11, Sin06, Aar04, Idr96]. XPS analysis and the thermodynamic modelling of the A-AH mould reactions show that some compounds (Mg_2Si and $Mg_{12}Al_{17}$) can only be formed due to a direct reaction between magnesium (liquid and/or vapour) and mould materials.

The protective layer is composed of oxides, hydroxides, fluorides and oxyfluorides, being the last two predominant in the film. These finding supports previous theories which state the protective effect is achieved due to the fluorine diffusion through an initially formed oxide film [Aar04, Pet02]. The speed of dissociation of BF_3 would be the upper limit to the formation of the fluorine compounds. While BF_3 decomposes to form the more reactive species (such as F or F_2) magnesium reacts primarily to form the oxide layer. Origin of the initial oxide may be due to thermal oxidation of the alloy itself, or to the presence of mould-metal reactions.

This initial oxide layer is thin and the new fluorine compounds fill it completely, forming a dense and coherent protective film composed of oxides and fluorides. If the initial oxide film is too thick, the protective effect will not be achieved. The amount of new fluorine compounds is not able to cover the oxide film. Fluorides are distributed along the oxide film and the coherent structure that stops the mould-metal reactions is not formed.

Main factors that can thicken the initial oxide film are the interface temperature, section thickness, amount of fluorine released by the inhibitor and effectiveness of the refractory mould. Thus,

suppression of the mould-metal reactions is attached to those parameters. High melt and mould preheating temperatures are often employed in investment casting to enhance the filling of thin-walled elements, but those may be decreased after an efficient mould redesign, as will be seen in the next chapter. Modification of section thickness is also difficult.

Mould refractories than can be employed in Mg investment casting are less stable than MgO, so formation of an initial oxide film is always thermodynamically favourable. Depending on the experimental conditions the formation of the surface oxides may be avoided. For that, the cooling rate of the interface has to be higher that the formation rate of the mould-metal products. With severe conditions, an initial oxide film is formed. Due to this, inhibitors are used in conjunction with non-conventional moulds. An adequate combination of these two is the clue to avoid mould-metal reactions in magnesium investment casting. The protective layer is obtained after fluorine diffusion through an oxide film. The thinnest the oxide film, the faster that fluorine will diffuse through it creating the dense and coherent protective layer. Choosing an adequate mould material minimizes the thickness of this initial oxide film.

Effectiveness of the inhibitor is related to the thermal stability of the inhibitor and to the amount of fluorine available while the oxide film is forming. The inhibitor has to dissociate and release fluorine at an adequate rate, otherwise the oxide film may grow too much and the coherent morphology of the fluorine containing film can be lost. The casting has also to be surrounded by a protective atmosphere not only during the pouring but also during the solidification stage, as the the mechanisms that produce the fluorine compounds are still active.

CASTING OF A THIN-WALLED COMPLEX PROTOTYPE

8.1   Introduction

In this chapter, a real AZ91E aircraft housing has been cast. Cast housings for aircraft interiors are semi-structural applications ideally suited for the use of cast magnesium parts. Moreover, investment casting is a suitable process to obtain such complex, high quality components in single, small or medium series in a reduced time because of its repeatability, high dimensional accuracy and surface finishing. Components for these applications vary in size and wall thickness but are usually cast in aluminium investment casting, which is a well-known process.

Currently, magnesium industry is not able to reach the minimum thicknesses obtained with aluminium. Due to the low heat capacity of Mg, inertial forces combined with the high surface tension of the alloy make it very difficult to run through thin-walled cavities. High melt and temperatures are often employed in casting technologies to enhance the filling of thin-walled elements, which is detrimental for magnesium investment casting. Mg alloy temperature should not exceed 740-760ºC: further increases enhance the mould-metal reactions considerably. Therefore, a compromise between both handicaps is necessary to fulfil thin-walled cavities effectively. Use of filling and solidification simulation software to optimize the feeding systems of the mould is an adequate strategy to fill the mould thin cavities, in conjunction with adequate mould materials and inhibitors.

Before the AZ91E housing casting, mould design was solved by the use of Flow3D® and WinCast® simulation software. To avoid mould-metal reactions, non-conventional Al_2O_3 mould material and KBF_4 inhibitor were chosen based on results obtained in the previous chapters. According to the analysis methodology presented in Chapter 3, the schematic diagram of Figure 8.1 shows in green the tasks performed in the previous chapter and in black the ones performed through this chapter.
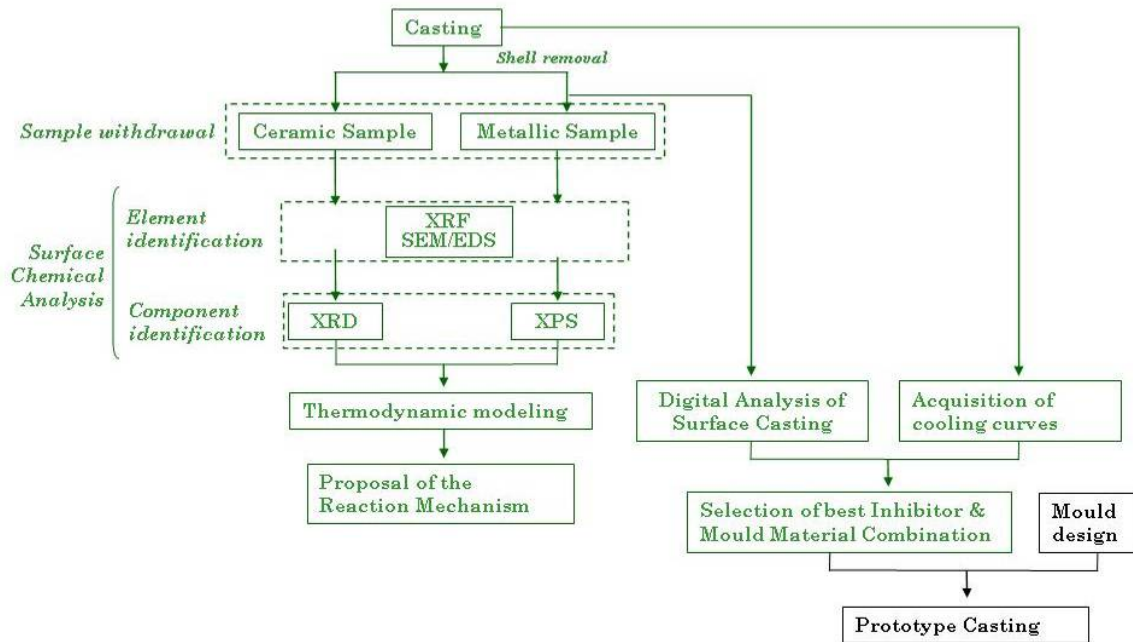
Figure 8.1: Tasks performed in Chapter 8 (black). Tasks in green have already been completed

8.2 Prototype mould design

8.2.1 Selected geometry: aeronautic housing

The geometry to be obtained is the housing of Figure 8.2. General dimensions of the part are 147x135x107mm^3. The average wall thickness of this thin-walled component varies from 12mm to 1.5mm, in the thinnest sections.
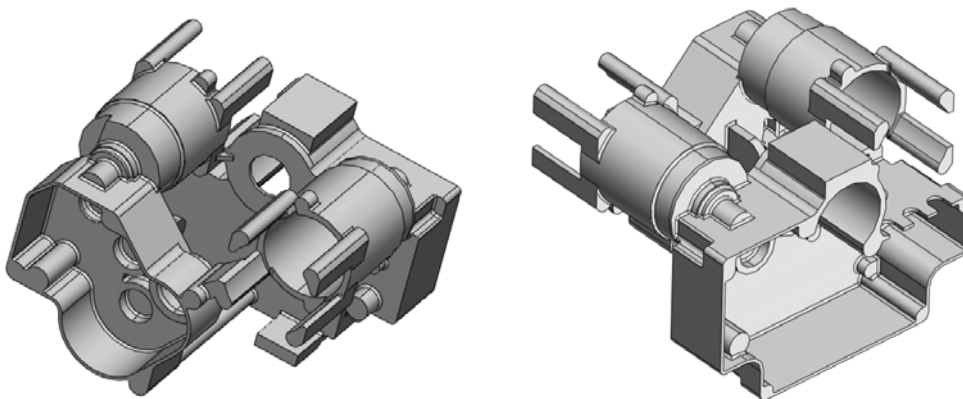
Figure 8.2: Different views of the prototype selected for the validation of the process

This housing is currently fabricated in investment casting of aluminium, where the wax patterns are coated with a first ceramic coat of commercial silica, zirconium silicate and colloidal silica binder system. Fused alumina is used as stucco and the mould and aluminium casting temperatures are 740ºC for the alloy and 630ºC for the preheated mould.

8.2.2 Prototype mould design

Due to the complexity of the prototype, the mould design was supported with Flow3D® and WinCast® simulation software. Taking the component as a starting point, WinCast® solidification software was used to determine the hot spots of the part. Feeder heads were included to the part to avoid shrinkage cavities, and the obtained results were employed to design the feeding system of the mould. Finally, Flow3D® software was used to validate the filling of the mould, as well as to identify the process parameters required for the casting of the thin-walled complex part.

- *Feeder head system*

First step for mould design was accomplished with the geometrical analysis of the housing. The objective of this analysis is to detect potential defect areas, where the hot spots of the part are located. During solidification, hot spots lead to shrinkage cavities. This kind of porosity is one of the most common defects in casting parts and it is caused only by the part's geometry. To avoid this problem, WinCast® commercial software has been employed. Through geometrical considerations, critical zones in the part have been identified (Figure 8.3.a, bright colours). In each zone, a feeder head has been included, to maintain the shrinkage cavities out of the part. Figure 8.3.b shows how the addition of feeders displaces the critical zones from the housing.

a)   b)
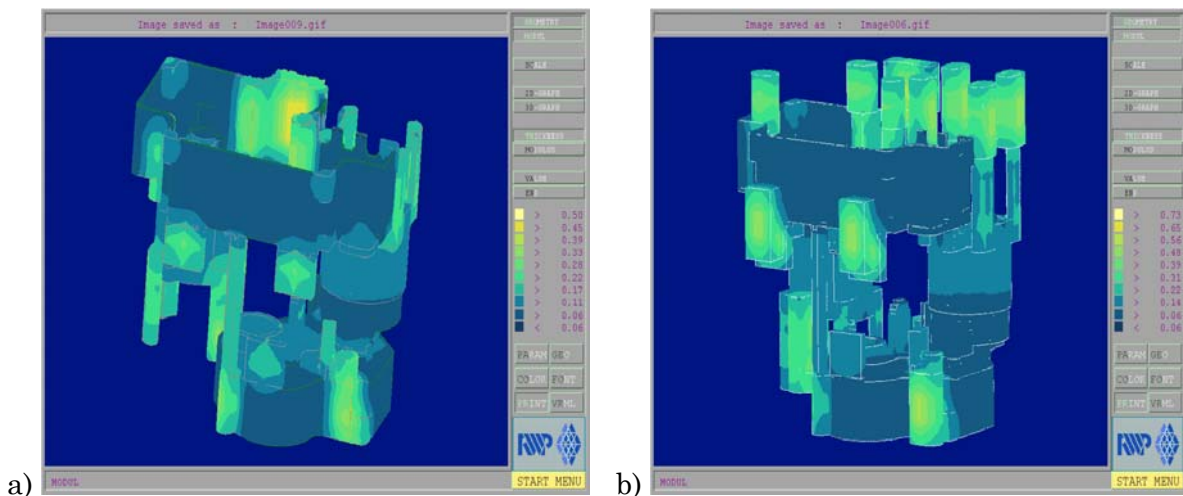
Figure 8.3: Hot spots location in: a) housing to be cast b) feeder heads included in the part

The obtained result was employed to design the gating and feeding systems of the mould, which was analyzed with the support of the commercial software Flow3D®.

- *Filling simulation*

Several gating and feeding systems were designed before reaching an appropriate mould design. The filling of thin walled elements with magnesium is quite challenging due to its low heat capacity. Pouring temperature of the metal should not exceed 750ºC-760ºC, as the severity of mould-metal reactions increases with temperature. Mould preheating temperature was set to 550ºC. To fill the mould, several gating systems were designed. Filling time was minimized to guarantee that the metal fills the whole mould before reaching the critical temperature of 534ºC, which limits the fluidity of molten magnesium.

In Figure 8.4 the filling sequence is presented in three pictures showing the temperatures in colour scale. Filling time in simulation is 1.5 seconds and corresponds to the last picture. Magnesium reaches the upper part of the mould with a temperature of 548ºC, ensuring the complete filling of the mould.
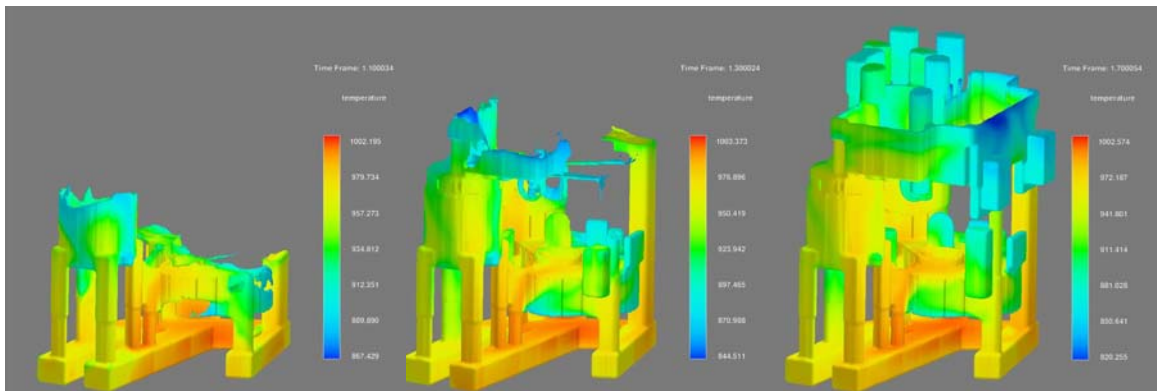
Figure 8.4: Pictures showing the filling of the prototype mould. Temperatures are shown in K

Turbulent flows of molten metal during the pouring can lead to porosity in the part. In the filling simulation of figure 3 it can be seen that the mould is filled with turbulent and non-uniform flows, perhaps due to a too fast filling. To avoid the presence of porosity, an extra upper part was included in the wax model of the part. This upper part acts as a venting tunnel for the entrapped gases, and gives rigidity to the wax model to support the successive ceramic coatings.

8.2.3 Process parameters

As a result of the numerical simulations and of the acquired experience in Mg investment casting, the parameters for the casting of the part were resumed in Table 8.1.

Table 8.1: Process parameters for the casting of the housing

Process Parameter	Value
Mould face coat material	Al_2O_3
Binder	Colloidal Silica
Stucco	Fused alumina
Mould temperature	550ºC
Mould inhibitor	KBF_4
Melt protector	$CO_2 + 4\% SF_6$
Mg alloy	AZ91E
Pouring temperature	750ºC

8.3 Prototype casting

This first attempt had a limited amount of success. Figure 8.5 shows results obtained after the housing casting, where dark areas correspond to zones covered with mould-metal reactions.

Figure 8.5: Different views of the prototype after its casting

Surfaces without mould-metal reactions have also been obtained. However, those are placed in the upper venting part rather than in the housing (Figure 8.6).

a)   b)
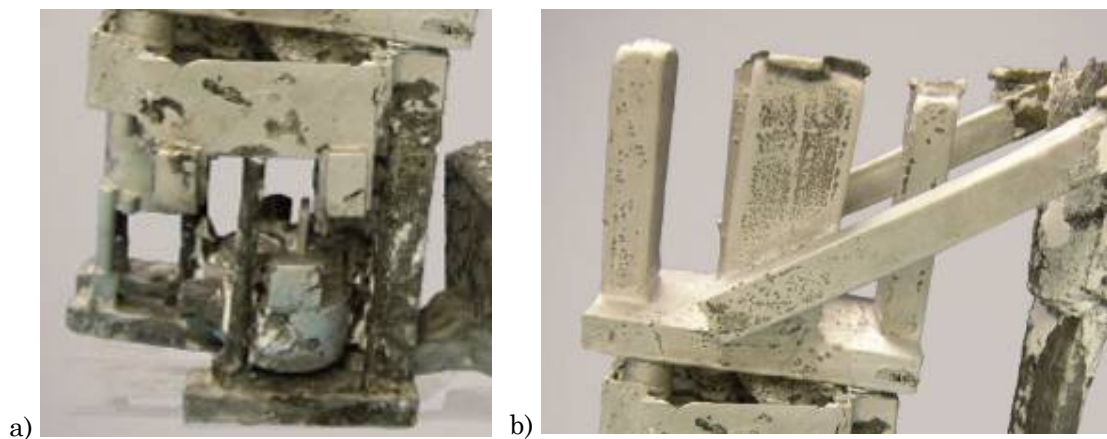
Figure 8.6: Detailed view of: a) the housing b) the upper part

Clean surfaces were obtained in the upper part, whose average thickness of 20–45mm is considerably higher than the one of the housing (1.5mm-12mm). In this case, mould-metal reactions are influenced by the interface temperature, and not by the section thickness. Molten metal starts cooling as it enters in the mould cavity. This decrease in the alloy temperature continues while the metal runs through the running system, fills the housing cavity and, finally, reaches the upper part of the mould. Meanwhile the mould itself, which was preheated before the pouring, is also cooling down. So the interface temperatures obtained in the housing cavity are higher than the ones obtained in the upper part. Although both interface temperature values must be quite similar, this difference is enough to promote mould-metal reactions in the housing. Nevertheless, to solve this reactivity problem a decrease in the alloy and mould casting temperature is not the only measure to be taken. This decrease would only enhance the filling problems of the thin walls. Although most of the mould was filled effectively, there are still small zones in the casting that present filling defects (Figure 8.7.a) and b). Therefore, mould gating and gating and feeding systems need to be redesigned.
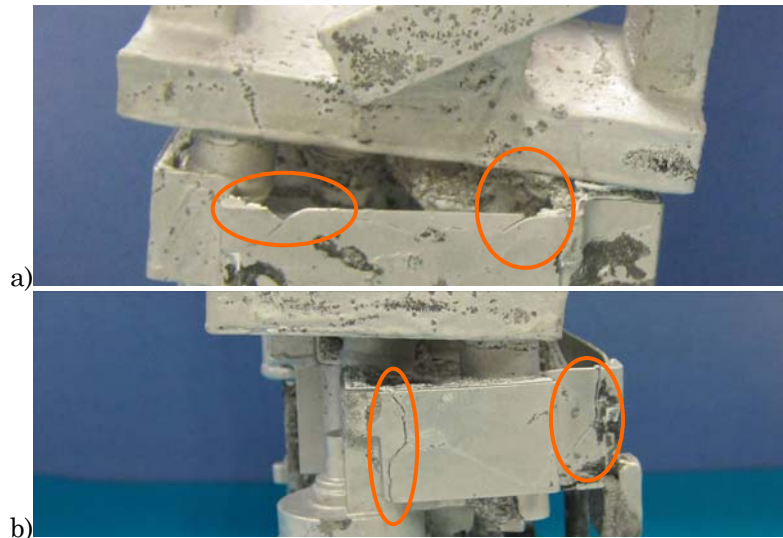
Figure 8.7: a) and b) detailed view of filling detects found on the casting

Accordingly, in a next essay the areas corresponding to the feeding gates where decreased, to achieve a faster filling of the mould while the alloy cools down. Casting temperatures were also decreased, to avoid the formation of mould-metal reactions. New process parameters for this trial are summarised in Table 8.2:

Table 8.2: New process parameters for the casting of the prototype

Process Parameter	Value
Mould preheating temperature	520ºC
AZ91E Pouring temperature	740ºC

Figure 8.8 shows results obtained after the second casting of the prototype. As it can be seen in the pictures, no mould-metal reaction products were formed on the casting. KBF$_4$ inhibitor protected

effectively the surface for the experimental conditions applied, demonstrating that the achievement of complex components by magnesium investment casting is possible.
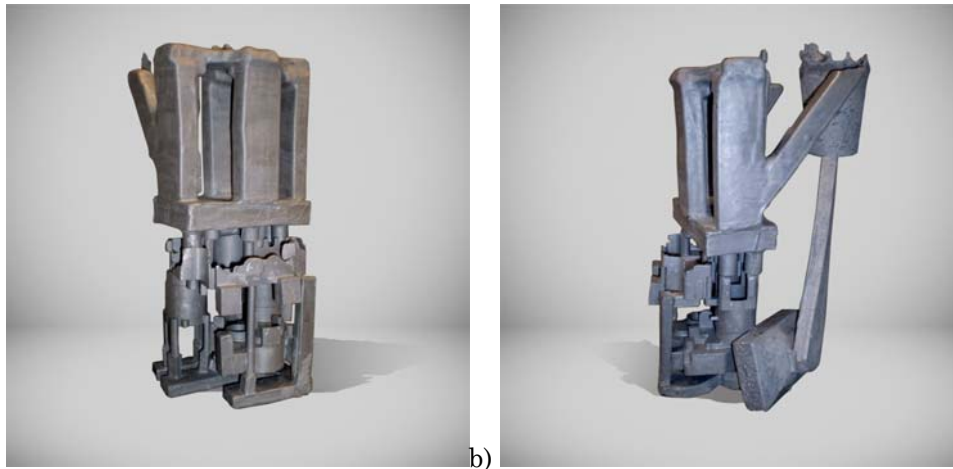
Figure 8.8: Different views of the second prototype casting, without mould-metal reactions

However, although the decrease in the interface temperature has avoided mould-metal reactions, filling of the thin walls has been worsen by this measure. Decreasing of the area of the feeding areas has not been enough to compensate the decrease in casting temperature, as it can be seen in Figure 8.9. Further developments in mould design should be performed, to ensure the production of the casting.
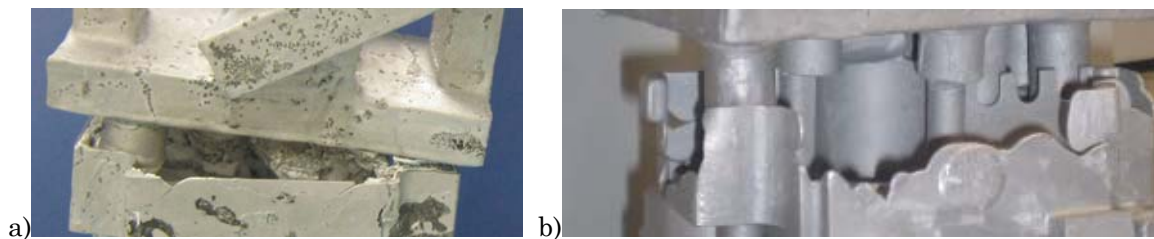
Figure 8.9: Filling detects found on a thin wall of the prototype: a) first trial b) second trial

8.4   Conclusions

Mould filling is enhanced with increases in melt temperature, mould temperature and section thickness. These factors also increase the severity of the mould-metal reactions. Thus, a compromise has to be found between filling ability, to produce thin-walled components, and mould-metal reactivity, which governs the quality of the cast surface. To overcome this problem, simulation tools are essential to design suitable feeding systems, determinate process parameters and predict defects associated to mould design.

In this chapter, several steps have been done to achieve an efficient design of magnesium investment moulds. Starting with the geometrical analysis of the casting part, best locations for feeder heads and

gating systems were determined. The preliminary mould design has been analyzed with Flow3D® filling software, to ensure a correct and defect-free part. Finally, process parameters for the investment casting of the part have been set and appropriate mould materials and inhibitors have been chosen. Based on the results obtained through the previous chapter, a Al_2O_3 based mould has been inhibited with KBF_4 before the alloy pouring.

Real AZ91E aircraft housing has been cast. Cast housings for the aircraft interior are semi-structural applications ideally suited for the use of cast magnesium, but are usually cast in aluminium investment casting. The first attempt to produce the magnesium housing had a relative success. Although the casting part is partially covered with mould-metal reactions, the upper part of the mould exhibits a clean surface even though it is composed of wide components. This means that, even if some factors need to be changed, the achievement of the housing by magnesium investment casting is possible. Accordingly, casting temperatures have been decreased and the area of the feeding system has been redesigned before a second casting of the housing. Results show a prototype without mould-metal reactions. Under the experimental conditions set in the second casting, KBF_4 inhibitor has protected the prototype effectively, even though the filling of some thin-walls has not been achieved. A redesign in the mould gating and feeding systems, should be enough to produce the casting.

CLOSURE

9.1   Concluding remarks

The main objective of the present dissertation is to minimize mould-metal reactions in magnesium investment casting. For that purpose, this thesis covers both theoretical and experimental work and it has been divided into 3 main sections.

The first section (Chapter 2) corresponds to the literature review performed. Main features necessary to understand the basis of mould-metal reactions in magnesium investment casting have been depicted, divided into four main subsections: oxidation of magnesium and its alloy, melt protection, general review of the reactions happening in Mg investment casting and, last, methods employed to avoid the formation of the mould-metal reactions (alternative mould materials and inhibitors).

The second section, corresponding to Chapters 3, 4, 5, and 8 consists in a serial of investment casting experiments performed to obtain mould-metal reaction free surfaces. It comprises, in turn, two main subsections: selection of an inhibitor (Chapter 4) and mould material (Chapter 5).

In Chapter 3, the parameters and procedures followed in the inhibitor and alternative mould material experiments have been presented. Tested materials and chemicals have been chosen among commercial options currently existent in the market, to ensure that a near future implementation of the improvements found through this thesis are possible. The analysis techniques employed to accomplish the general objectives have also been presented.

In Chapter 4, Al_2O_3+SiO_2 moulds were cast under five different atmospheres (open air, $NaBF_4$, KBF_4, SF_6 and FK) to analyse the protective behaviour of each inhibitor. As a result of the digital analysis of the castings, inhibitor effectiveness has been ranked in the order of surface reaction degree: Air→SF_6→$NaBF_4$→KBF_4, corresponding to KBF_4 the less reacted surface. Castings without inhibitor have led to surface castings completely covered with mould-metal reactions, due to the severe

experimental conditions applied (high casting temperatures and thick sections). SF_6 and Air atmosphere moulds have shown similar behaviors, as SF_6 was displaced from the mould during the pouring. Employment of KBF_4 and $NaBF_4$ has provided large non-reacted areas on the castings, but KBF_4 has proved to be the most effective one in magnesium investment casting. FK moulds have been destroyed during the casting due to the thermal decomposition products of the gas. Surfaces obtained with the different inhibitors have been analysed by means of XRF, SEM/EDX and XRD. The main conclusions obtained from these analyses are:

o For Al_2O_3 experiments, mould-metal reaction layers are composed of Mg, MgO, Mg_2Si and $Mg_{12}Al_{17}$. After the pouring, magnesium melt reacts with the mould materials, Al_2O_3 and SiO_2. MgO and Mg_2Si are formed, and the melt is enriched in aluminium until $Mg_{12}Al_{17}$ crystallises. The alpha magnesium present in the surface layer comes from AZ91E particles, attached to the mould after the shell withdrawal. According to the SEM/EDS results, those compounds are evenly distributed along the surface layer depth.

o Due to the employment of the inhibitors, fluorine compounds are formed in the interface layers. For both $NaBF_4$ and KBF_4 atmospheres, SEM/EDS results reveal that the protective effect is achieved when a dense and coherent fluorine-based surface layer is formed. KBF_4 inhibitor, which is more effective, produces considerably thinner protective layers.

o Mould-metal reactions appear on the sample surface if the fluorine layer is incoherent. Compounds in the mould-metal reaction layer have been identified as Mg, MgO, Mg_2Si, $Mg_{12}Al_{17}$ and MgF_2 by XRD.

o Sample A-KL-20c did not contain $Mg_{12}Al_{17}$. Mould-metal reactions were significantly reduced by the use of the inhibitor, and the quantity of Al_2O_3 decomposed has not been high enough to reach to the minimum % of Al necessary for $Mg_{12}Al_{17}$ to crystallise.

o MgF_2 is the only fluorine compound identified by XRD.

In Chapter 5, three different mould materials (SiO_2, Al_2O_3 and $MgAl_2O_4$) were cast in conjunction with KBF_4. As a result of the digital analysis of the castings, the material plus inhibitor effectiveness is ranked in order of reaction degree as follows (more to less reacted): $SiO_2 \rightarrow MgAl_2O_4 \rightarrow Al_2O_3$. This grading does not correspond to the free energy data of formation of the oxides, as $MgAl_2O_4$ is more stable than Al_2O_3. The cracking of the mould during the cooling of the casting and the presence of SiO_2 on the flour may be the reason for the unexpected behaviour of the $MgAl_2O_4$-based moulds. Employment of Al_2O_3 mould + KBF_4 has proved to be the most effective one in magnesium investment casting. $MgAl_2O_4$ and SiO_2 surfaces have been analysed by XRF, SEM/EDX and XRD. Main conclusions obtained from these analyses are:

o For $MgAl_2O_4$ experiments, mould-metal reaction layers are composed of Mg, MgO, Mg_2Si and Al_2O_3. Mg_2Si is formed due to reactions between Mg and SiO_2, and Al_2O_3 is formed due to the reaction between MgO and $MgAl_2O_4$.

o Mould-metal reaction layer formed on Si-KL moulds comprises the followings elements: Mg, Al, Si, Ca, O and, in some cases, F.

o Along with the results obtained in the Al_2O_3 moulds, the protective character of the films analysed in this chapter resides in the formation of fluorine compounds. In this sense, MgF_2 was again the only fluorine phase identified with XRD. Differences between the films formed in the different moulds are related to its thickness. Likewise in the Al_2O_3, the protective surface formed in the $MgAl_2O_4$ experiment is so thin that its thickness cannot be deduced by EDS although its composition is discernible: the film is formed with oxygen, fluorine, magnesium and aluminium compounds. The protective surface formed in the SiO_2 essay, the less effective one, is considerably thicker than the other two. SiO_2 film thickness ranges between 3 and 19µm, and is composed of Mg, Al, Ca, O and F. Thickness of the film seems to be related to aluminium, as higher concentration of aluminium appears when the protective film is thinner.

In the third section the mechanisms that lead to protected and reacted surfaces are presented (Chapters 6 and 7).

In Chapter 6, results obtained after the XPS analysis and the thermodynamic modelling of the mould-metal reactions happening in Al_2O_3-based mould in air or KBF_4 atmospheres have been presented. After the XPS analysis performed on sample A-AH-24c, the summary of all the compounds and elements detected on the A-AH mould samples is presented in Table 9.1.

Table 9.1: Summary of the chemical analysis performed on the Al_2O_3 + Air A-AH mould

	A-AH-4		A-AH-8	
	A-AH-24c	A-AH-24m	A-AH-8c	A-AH-8m
SEM: thickness	N.A.	N.M.	1mm	N.M.
EDS: element	N.A.	N.M.	Mg, Al, Si, Na, Ca, O	N.M.
XRD: compound	Mg, MgO, Mg_2Si, $Mg_{12}Al_{17}$	N.M.	Mg, MgO, Mg_2Si, $Mg_{12}Al_{17}$	N.M.
XPS: compound	N.A.	Na: $NaAlO_2$	N.A	N.A
		Ca: $CaO/Ca(OH)_2$; $CaAl_2O_4$		
		Si: SiC/SiO_x; $MgSiO_3$; SiO_2		
		Al: $NaAlO_2$, $MgAl_2O_4$, Al_2O_3, $CaAl_2O_4$, $AlO(OH)$		
		Mg: $MgAl_2O_4$, $MgSiO_3$, MgO, $MgCl_2$	N.A	N.A

N.M: No Measurable, N.A: Not Analysed. Duplicate compounds are marked in grey.

To understand which are the chemical reactions that take place on these samples, Factsage chemical equilibrium calculations were performed. The three mould materials identified by XRD in Chapter 3

(Al$_2$O$_3$; SiO$_2$, β-Al$_2$O$_3$) were simulated to determine if the mould-metal reactions occur in the presence of oxygen, due to the formation of MgO; or they happen due to a direct reaction between Mg and mould materials (whether Mg is in liquid or gaseous state). Results show that some compounds (Mg$_2$Si and Mg$_{12}$Al$_{17}$) can only be formed due to a direct reaction between magnesium and mould materials. Rest of the compounds encountered through XPS analysis can be formed due to either Mg-mould or MgO-mould reaction mechanism, if the appropriate amount of reactant is chosen. Due to this, determining the origin of most of the compounds is rather difficult. However, it is feasible to think that reactions between MgO and shell compounds also happen, as the compounds formed are more stable than the ones formed due to a direct reaction.

Table 9.2 summarises the information obtained from the XPS analysis of the protective layer:

Table 9.2: Summary of the chemical analysis performed on sample A-KL-2m*

	A-KL-2m*
XPS: compound	Na: Na$_2$O, Na$_x$O (0<x<1)
	Ca: CaO/Ca(OH)$_2$
	Si: SiO$_x$; SiO$_2$
	Al: Al$_2$O$_3$, AlF$_x$O$_y$, AlF$_3$, AlMg$_x$O$_y$F$_z$
	Mg: AlMg$_x$O$_y$F$_z$, MgF$_2$, Mg(OH)$_2$, MgCO$_3$

Use of KBF$_4$ inhibitor induces a fluorinated surface film on AZ91E casting. Surface films changes from a film composed mostly of oxides/hydroxides to a surface covered with oxides, hydroxides, fluorides and oxyfluorides, being the last two predominant in the film. The protective layer is thus composed of oxides, hydroxides, fluorides and oxyfluorides. These finding supports previous theories which state that the protective effect is achieved due to the fluorine diffusion through an initially formed oxide film [Aar04, Pet02]. Along with this theory, AlMg$_x$O$_y$F$_z$ would be formed after the fluorine diffusion through MgAl$_2$O$_4$, AlF$_x$O$_y$ after diffusion through Al$_2$O$_3$ and MgF$_2$ after the one through MgO film. The origin of this previous oxide film is uncertain. The oxide film can be formed due to mould-metal reactions, or to the thermal oxidation of the alloy. Thermal oxidation of AZ91E produces MgAl$_2$O$_4$, MgO, Al$_2$O$_3$ and its hydroxides, as stated in Chapter 2: Literature review. On the other hand, Presence of sodium and silicon compounds on the survey spectra of sample A-KL-2m* (Figure 6.8) evidences that, even when a protective film is formed on the sample surface, reactions between the mould and the metal exist to some extend, while the fluorine compounds are being formed.

As a result of the results obtained in this work, in Chapter 7 the two mechanisms that lead to both reacted and protected surfaces have been proposed. On this basis, through this chapter the different surfaces encountered during the experiments have been analysed.

As it has been reviewed in Chapter 2, four are the different reactions that may take place in Mg investment casting. According to the results obtained in Chapter 6, and the conclusions extracted

after the literature review (Section 2.9), not only one but more than one may be happening at the same time: all seem likely to occur.

o Molten metal reacts with the atmosphere of the mould, as thermodynamically it is almost impossible to prevent magnesium oxidation. Melt can oxidise either during the filling of the mould due to the oxygen present in the mould cavity or during the solidification of the part due to the porous nature of the refractory shells, as stated by Cingi [Cin06].

o Molten metal reacts with the gas in the mould, and the reaction product reacts with the mould [Cin06]. As stated in Chapter 6, most of compounds encountered through the XPS analysis can be formed due to either Mg-mould or MgO-mould reaction mechanism, if the appropriate amount of reactant is chosen. Fluorine-based inhibitors promote the formation of fluorine compounds in the surface of the casting, being MgF_2 one of them. MgF_2 is very stable, and does not react with the mould refractories.

o Molten metal reacts with the mould [Jaf11, Arr07, Sin06, Idr96]. XPS analysis and the thermodynamic modelling of the A-AH mould reactions show that some compounds (Mg_2Si and $Mg_{12}Al_{17}$) can only be formed due to a direct reaction between magnesium (liquid and/or vapour) and mould materials.

The protective layer is composed of oxides, hydroxides, fluorides and oxyfluorides, being the last two predominant in the film. These finding supports previous theories which state the protective effect is achieved due to the fluorine diffusion through an initially formed oxide film [Aar04, Pet02]. The speed of dissociation of BF_3 would be the upper limit to the formation of the fluorine compounds. While BF_3 decomposes to form the more reactive species (such as F or F_2), magnesium reacts primarily to form the oxide layer. Origin of the initial oxide may be due to thermal oxidation of the alloy itself, or to the presence of mould-metal reactions.

This initial oxide layer is thin and the new fluorine compounds fill it completely, forming a dense and coherent protective film composed of oxides and fluorides. If the initial oxide film is too thick, the protective effect will not be achieved. The amount of new fluorine compounds is not able to cover the oxide film. Fluorides are distributed along the oxide film and the coherent structure that stops the mould-metal reactions is not formed.

Main factors that can thicken the initial oxide film are the interface temperature, section thickness, amount of fluorine released by the inhibitor and effectiveness of the refractory mould. Thus, suppression of the mould-metal reactions is attached to those parameters. High melt and mould preheating temperatures are often employed in investment casting to enhance the filling of thin-

walled elements, but those may be decreased after an efficient mould redesign. Modification of section thickness is also difficult.

Mould refractories than can be employed in Mg investment casting are less stable than MgO, so formation of an initial oxide film is always thermodynamically favourable. Depending on the experimental conditions the formation of the surface oxides may be avoided. For that, the cooling rate of the interface has to be higher that the formation rate of the mould-metal products. With severe conditions, an initial oxide film is formed. Due to this, inhibitors are used in conjunction with non-conventional moulds. An adequate combination of these two is the clue to avoid mould-metal reactions in magnesium investment casting. The protective layer is obtained after fluorine diffusion through an oxide film. The thinnest the oxide film, the faster that fluorine will diffuse through it creating the dense and coherent protective layer. Choosing an adequate mould material minimizes the thickness of this initial oxide film.

Effectiveness of the inhibitor is related to the thermal stability of inhibitor and to the amount of fluorine available while the oxide film is forming. The inhibitor has to dissociate and release fluorine at an adequate rate, otherwise the oxide film may grow too much and the coherent morphology of the fluorine containing film can be lost. The casting has also to be surrounded by a protective atmosphere not only during the pouring but also during the solidification stage, as the mechanisms that produce the fluorine compounds are still active.

Last, in Chapter 8 a real AZ91E aircraft housing has been cast. Cast housings for the aircraft interior are semi-structural applications ideally suited for the use of cast magnesium, but are usually cast in aluminium investment casting. The first attempt to produce the magnesium housing had a relative success. Although the casting part is partially covered with mould-metal reactions, the upper part of the mould exhibits a clean surface even though it is composed of wide components. This means that, even if some factors need to be changed, the achievement of the housing by magnesium investment casting is possible. Accordingly, casting temperatures have been decreased and the area of the feeding system has been redesigned before a second casting of the housing. Results show a prototype without mould-metal reactions. Under the experimental conditions set in the second casting, KBF_4 inhibitor has protected the prototype effectively, even though the filling of some thin-walls has not been achieved. A redesign in the mould gating and feeding systems should be enough to produce the casting.

9.2   Future work

This dissertation has provided new insight on the mould-metal reactions in magnesium investment casting. However, further research work is left in order to completely understand some open questions outlined in this thesis.

Regarding investment casting experimental work, redesign of the casting mould should be considered to minimise turbulent flows during mould filling. Serials of experiments in which different Mg melt and mould preheating temperatures are applied should de performed to obtain different interface conditions. Further analysis of those interface cooling curves and its shape in relation with mould-metal reactions should then be performed. After the new experiments, separate influence of the Mg casting temperature and the mould preheating temperature should also be evaluated.

Regarding refractory mould materials, careful analysis of the commercial materials should be performed to avoid the presence of impurities. Development of new shells should also imply a previous mechanical testing to avoid shell cracking.

Regarding protective inhibitors, further experiments should be performed with new inhibitors. Magnesium melting industry is currently developing non-toxic and environmentally friendly melt protectors which could be useful for the investment casting industry. Casting with gaseous inhibitors should be performed inside a chamber, to ensure a protective atmosphere during the solidification stage. Since BF_3 is toxic, the toxicity level in the environment after KBF_4 castings should be measured. If the toxicity level is too high, casting experiments should be performed inside a chamber.

XPS analyses were performed only for Al_2O_3 mould material and KBF_4 inhibitor. Rest of the materials and inhibitors tested through this work should also be analysed. Employment of surface characterisation techniques, as Auger Electron Spectroscopy or Secondary Ion mass spectrometry, should be also considered to determine the thickness and composition profile of the surface films.

Last, regarding prototype casting, a redesign of the mould gating and feeding systems has to be done.

9.3   Published work

Within the present thesis different contributions in national and international conferences were presented:

o Herrero-Dorca, N.; Arruebarrena, G.; Sarriegi Etxeberria, h.; Rodriguez, P.P; Andres, U.; Bilbao, Y.; Hurtado, I.; "Análisis de materiales de molde alternativos para minimizar las reacciones en microfusión de magnesio" *Proceedings of the XII Congreso Nacional de Materiales*, Alicante (Spain), 2012.

o Herrero-Dorca, N.; Sarriegi Etxeberria, H.; Hurtado, I.; Andres, U.; Rodriguez, P.; Arruebarrena, G.; "Analysis of Different Inhibitors for Magnesium Investment Casting"; *IOP Conference Series: Materials Science and Engineering,* vol. 27, 2012.

o Sarriegi Etxeberria, H.; Arruebarrena, G.; Herrero-Dorca, N.; Azpilgain, Z.; Hurtado, I.;"Thermal Diffusivity measurements by Laser Flash Method of AZ Mg alloys in their whole melting range"; *Proceedings of the International Conference on processing & manufacturing of advanced materials*; Quebec (Canada), 2011.

o Herrero-Dorca, N.; Sarriegi Etxeberria, H.; Beristain, U.; Tercero, I.; Hurtado, I.; Andrés, U.; Bilbao, Y.; Rodríguez, P.P.; Arruebarrena, G.; "Microfusión de la aleación AZ91E para un componente aeronáutico de paredes delgadas "; *Proceedings of the XI Congreso Nacional de Materiales*; Zaragoza (Spain); 2010.

o Herrero-Dorca, N.; Arruebarrena, G.; Sarriegi Etxeberria, H.; Beristain, U.; Rodriguez, P.P; Andres, U.; Bilbao, Y.; Weiss,K.; Hurtado, I.; "Investment Casting of AZ91E Thin-Walled Complex Component"; *Proceedings of the 8th International Conference on Magnesium Alloys and their Applications*; Weimar; 2009; ed. K.U.Kainer (Wiley-VCH Verlag, Weinheim 2010); p.158-164; 2008. ISBN 978-3-527-32732-4.

o Arruebarrena, G.; Herrero-Dorca, N.; Sarriegi Etxeberria, H.; Lopez, K.; Rodriguez, P.P.; Hurtado, I.;"Thermal Conductivity of High-Pressure Die-Cast AM50 and AZ91D Alloys "; *Proceedings of the 8th International Conference on Magnesium Alloys and their Applications*; Weimar; 2009; ed. K.U.Kainer (Wiley-VCH Verlag, Weinheim 2010) ; p.96-102; 2008. ISBN 978-3-527-32732-4.

o Arruebarrena, G.; Hurtado, I.; Sarriegi, H.; Herrero-Dorca, N.; Gorosarri, A.; Weiss, K.; Rodríguez, P.P.; Oyarbide, M.; "Análisis de Microestructuras y Propiedades Mecánicas en Aleaciones de Mg Coladas a la Cera Perdida"; *Proceedings of the. X Congreso Nacional de Materiales*; Donostia-San Sebastian;Spain; June 2008; vol.1; p. 121-124; ISBN 978-84-608-0769-8.

o Herrero-Dorca, N.; Gorosarri, A.; Arruebarrena, G.; Rodriguez, P.P.; Oiarbide, M.; Hurtado, I.;"Simulación y Experimentación del Proceso de Microfusión para la Aleación de Magnesio AZ91E"; *Proceedings of* the X Congreso Nacional de Materiales; Donostia-San Sebastian; Spain; June 2004; p. 215-218; ISBN 978-84-608-0769-8.

REFERENCES

[Aar04]   Aarstad, K.: "Protective Films on molten magnesium", *PhD thesis, Norwegian University of Science and Technology,* 2004.

[Ale77]   Aleksandrova, Y. P.; Roshchina, I. N.: "Interaction of magnesium with gases", *Metal Science and Heat Treatment,* vol. 19, pp. 218-221, 1977.

[Anz12]   Anzai, A.; Fuchigami, M.; Yamanaka, S. *et al.:* "Preparation of calcium-doped boron nitride by pulsed laser deposition", *Materials Research Bulletin,* 2012.

[Ara08]   Aradhya, S. V.; Garimella, S. V. and Fisher, T. S.: "Electrothermal bonding of carbon nanotubes to glass", *Journal of The Electrochemical Society,* vol. 155, pp. 161-2008.

[Arc07]   Archanjo, B. S.; Carvalho, L. A. S.; Rassa, M. *et al.:* "Nanowires and nanoribbons formed by nethylphosphonic acid", *Journal of Nanoscience and Nanotechnology,* vol. 7, pp. 3071-3080, 2007.

[Arg03]   Argo, D.; Lefebvre, M.: "Melt protection for the AJ52 magnesium strontium alloy", *Magnesium Technology,* vol. 4, pp. 15-21, 2003.

[Arr08]   Arruebarrena, G.: "Mechanical behavior and prediction of properties of new magnesium alloys vs. commercial alloys for aeronautics applications", *PhD thesis, Mondragon Unibertsitatea,* 2008.

[Arr07]   Arruebarrena, G.; Hurtado, I.; Vainola, Jukka *et al.:* "Development of investment-casting process of Mg-alloys for aerospace applications", *Advanced Engineering Materials,* vol. 9, pp. 751-756, 2007.

[ASM88]   ASM Handbook: "ASM handbook volume 15: casting", *Ed. ASM International,* 1988.

[Ave99]   Avedesian, M. M.; Baker, H.: "Magnesium and magnesium alloys (ASM Specialty Handbook)", *Ed. ASM International,* 1999.

[Bac04]   Bach, F. W.; Karger, A.: "Environmental friendly protection system for molten magnesium", *Proceedings of the 6th International Conference Magnesium Alloys and Their Applications,* pp. 1001-1005, 2004.

[Bae08]   Bae, C. J.: "Integrally cored ceramic investment casting mold fabricated by ceramic stereolithography", *PhD thesis, The University of Michigan,* 2008.

[Bar91]   Barr, T. L.: "Recent advances in X-ray photoelectron spectroscopy studies of oxides", *Journal of Vacuum Science & Technology A: Vacuum, Surfaces, and Films,* vol. 9, pp. 1793-1805, 1991.

[Bla04]   Blawert, C.; Hort, N. and Kainer, K. U.: "Automotive applications of magnesium and its alloys", *Transactions of the Indian Institute of Metals,* vol. 57, pp. 397-408, 2004.

[Boc00]   Bochenek, A.; Braszczynska, K. N.: "Structural analysis of the $MgAl_5$ matrix cast composites

containing SiC particles", *Materials Science and Engineering: A,* vol. 290, pp. 122-127, 2000.

[Bor12]   Boryakov, A. V.; Nikolitchev, D. E.; Tetelbaum, D. I. *et al.:* "Chemical and phase compositions of silicon oxide films with nanocrystals prepared by carbon ion implantation", *Physics of the Solid State,* vol. 54, pp. 394-403, 2012.

[Bös97a]   Böse, O.; Kemnitz, E.; Lippitz, A. *et al.:* "C 1s and Au 4f7/2 referenced XPS binding energy data obtained with different aluminium oxides,hydroxides and-fluorides", *Fresenius' Journal of Analytical Chemistry,* vol. 358, pp. 175-179, 1997.

[Bös97b]   Böse, O.; Kemnitz, E.; Lippitz, A. *et al.:* "XPS analysis of b-AlF₃ phases with Al successively substituted by Mg to be used for heterogeneously catalyzed Cl/F exchange reactions", *Applied Surface Science,* vol. 120, pp. 181-190, 1997.

[Bre08]   Brennan, B.; McDonnell, S. and Hughes, G.: "Photoemission studies of the interface formation of ultrathin MgO dielectric layers on the oxidised Si (111) surface", *Journal of Physics: Conference Series,* vol. 518, pp. 1980-1984, 2008.

[Bro07]   Broder, T. L.; Silvester, D. S.; Aldous, L. *et al.:* "Electrochemical oxidation of nitrite and the oxidation and reduction of NO₂ in the room temperature ionic liquid [C2mim][NTf₂]; the latter behaves as a "melt" rather than an "organic solvent"", *The Journal of Physical Chemistry B,* vol. 111, pp. 7778-7785, 2007.

[Cas10]   Casey, P.: "Growth and characterisation studies of MgO and Mg silicate dielectric layers on Si and InP surfaces", *PhD thesis, Dublin City University,* 2010.

[Cas99]   Cashion, S.: "The use of sulphur hexafluoride (SF₆) for protecting molten magnesium", *PhD thesis, The University of Queensland,* 1999.

[Cas02]   Cashion, S. P.; Ricketts, N. J. and Hayes, P. C.: "The mechanism of protection of molten magnesium by cover gas mixtures containing sulphur hexafluoride", *Journal of Light Metals,* vol. 2, pp. 43-47, 2002.

[Cha75]   Chase, M. W.; Curnutt, J. L.; Prophet, H. *et al.:* "JANAF thermochemical tables, 1975 supplement", *Journal of Physical and Chemical Reference Data,* vol. 4, 1975.

[Che05]   Chen, C. W.; Huang, C. C.; Lin, Y. Y. *et al.:* "The affinity of Si-N and Si-C bonding in amorphous silicon carbon nitride (a-SiCN) thin film", *Diamond and Related Materials,* vol. 14, pp. 1126-1130, 2005.

[Che10]   Chen, H.: "Effect of melt temperature on the oxidation behavior of AZ91D magnesium alloy in 1,1,1,2-tetrafluoroethane/air atmospheres", *Materials Characterization,* vol. 61, pp. 894-898, 2010.

[Che06]   Chen, H.; Lui, J. and Huang, W.: "Oxidation behaviour of molten magnesium in air/HFC-134a atmospheres", *Journal of Materials Science,* vol. 41, pp. 8017-8024, 2006.

[Cho06]   Choi, B. H.; You, B. S. and Park, I. M.: "Characterization of protective oxide layers formed on molten AZ91 alloy containing Ca and Be", *Metals and Materials International,* vol. 12, pp. 63-67, 2006.

[Cho03]   Choi, B. H.; You, B. S.; Park, W. W. *et al.:* "Effect of Ca addition on the oxidation resistance of AZ91 magnesium alloys at elevated temperatures", *Metals and Materials International,* vol. 9, pp. 395-398, 2003.

[Cin06]   Cingi, C.: "Mold-metal reactions in magnesium investment castings", *PhD thesis, Helsinki University of Technology,* 2006.

[Cou79]   Couling, S. L.: "Use of Air/CO₂/SF₆ mixtures for improved protection of molten magnesium", *Proceedings of the 36th Annual World Conference on Magnesium*, pp. 54-57, 1979.

[Cri91]   Criss, G. H.: "Fused silica refractories for industrial applications", *Materials Science Forum*, vol. 34-36, pp. 689-694, 1991.

[Cri04] Crist, B. V.: "Handbooks of monochromatic XPS spectra", Ed. *Mountain View: XPS International LLC,* 2004.

[Cze04] Czerwinski, F: "The early stage oxidation and evaporation of Mg-9%Al-1% Zn alloy", *Corrosion Science,* vol. 46, pp. 377-386, 2004.

[Cze02] Czerwinski, F.: "The oxidation behaviour of an AZ91D magnesium alloy at high temperatures", *Acta Materialia,* vol. 50, pp. 2639-2654, 2002.

[Dah01] Dahle, A. K.; Lee, Y. C.; Nave, M. D. *et al.:* "Development of the as-cast microstructure in magnesium-aluminium alloys", *Journal of Light Metals,* vol. 1, pp. 61-72, 2001.

[Dit05] Dittrich, T.; Muffler, H. J.; Vogel, M. *et al.:* "Passivation of TiO_2 by ultra-thin Al-oxide", *Applied Surface Science,* vol. 240, pp. 236-243, 2005.

[Eli02] Eliezer, D.; Alves, H.: "Corrosion and oxidation of magnesium alloys", *Handbook of Materials Selection,* pp. 267-291, 2002.

[Eml66] Emley, E. F.: "Principles of magnesium technology", *Ed. Pergamon Press*, 1966.

[Esc10] Escalera-Lozano, R.; Pech-Canul, M. I.; Pech-Canul, M. A. *et al.:* "The role of Mg_2Si in the corrosion behavior of Al-Si-Mg alloys for pressureless infiltration", *The Open Corrosion Journal,* vol. 3, pp. 73-79, 2010.

[Fel10] Feliu Jr, S.; Galvín, J. C.; Pardo, A. *et al.:* "Native air-formed oxide film and its effects on magnesium alloys corrosion", *The Open Corrosion Journal,* vol. 3, pp. 80-91, 2010.

[Fot06] Fotea, C.; Callaway, J. and Alexander, M. R.: "Characterisation of the surface chemistry of magnesium exposed to the ambient atmosphere", *Surface and Interface Analysis,* vol. 38, pp. 1363-1371, 2006.

[Fou02] Fournier, V.; Marcus, P. and Olefjord, I.: "Oxidation of magnesium", *Surface and Interface Analysis,* vol. 34, pp. 494-497, 2002.

[Fri06] Friedrich, H. E.; Mordike, B. L.: "Magnesium technology,", *Ed.Springer-Verlag,* 2006.

[Fru69] Fruehling, J. W.; Hanawalt, J. D.: "Protective atmospheres for melting magnesium alloys", *Modern Casting,* vol. 56, pp. 159-164, 1969.

[Ge11] Ge, Y. F.; Jiang, B. L.; Yang, Z. Y. *et al.:* "Microstructure and Corrosion Resistance Behavior of Composite Micro-Arc Oxidation and SiO_2 Coatings on Magnesium Alloys", *Advanced Materials Research,* vol. 160, pp. 1834-1838, 2011.

[Gje96] Gjestland, H.; Westengen, H. and Plahte, S.: "Use of SF_6 in the magnesium industry: an environmental challenge", *Proceedings of the 3rd International Magnesium Conference*, pp. 33-41, 1996.

[Gla00] Glasauer, S. M.; Hug, P.; Weidler, P. G. *et al.:* "Inhibition of sintering by Si during the conversion of Si-rich ferrihydrite to hematite", *Clays and clay minerals,* vol. 48, pp. 51-56, 2000.

[Goc09] Gocheva, I. D.; Tanaka, I.; Doi, T. *et al.:* "A new iron oxyfluoride cathode active material for Li-ion battery, Fe_2OF_4", *Electrochemistry Communications,* vol. 11, pp. 1583-1585, 2009.

[Gou05] Gougousi, T.; Barua, D.; Young, E. D. *et al.:* "Metal oxide thin films deposited from metal organic precursors in supercritical CO_2 solutions", *Chemistry of materials,* vol. 17, pp. 5093-5100, 2005.

[Ha06a] Ha, W. K.; Youn, J. I. and Kim, Y. J.: "Environmentally conscious gas mixtures for magnesium melt protection", *Materials Science Forum,* vol. 510-511, pp. 806-809, 2006.

[Ha06b] Ha, W. K., Young J. I.: "Effects of cover gases on melt protection of Mg alloys", *Journal of Alloys and Compounds,* vol. 422, pp. 208-213, 2006.

[Her09]   Herrero-Dorca, N.; Arruebarrena, G.; Sarriegi Etxeberria, H. *et al.:* "Investment casting of AZ91E thin-walled complex component", *Proceedings of the 8th International Conference on Magnesium Alloys and their Applications,* pp. 158-164, 2009.

[Her12]   Herrero-Dorca, N.; Etxeberria, H. S.; Hurtado, I. *et al.:* "Analysis of different inhibitors for magnesium investment casting", *IOP Conference Series: Materials Science and Engineering,* vol. 27, 2012.

[Her10]   Herrero-Dorca, N.; Sarriegi Etxeberria, H.; Beristain, U. *et al.:* "Microfusión de la aleación AZ91E para un componente aeronáutico de paredes delgadas", *Proceedings of the XI Congreso Nacional de Materiales,* 2010.

[Hil02]   Hillis, J.: "The international program to identify alternatives to SF_6 in magnesium melt protection", *Proceedings of the 2nd International Conference on SF6 and the Environment,* pp. 21-22, 2002.

[Hir03]   Hirata, T.; Ota, S. and Morimoto, T.: "Influence of impurities in Al_2O_3 ceramics on hot corrosion resistance against molten salt", *Journal of the European Ceramic Society,* vol. 23, pp. 91-97, 2003.

[Hou94]   Houghton, J. T.; Meira Filho, L. G.; Bruce, J. *et al.:* "Climate change 1994.Radiative forcing of climate change and an evaluation of the IPCC IS92 emission scenarios", *Ed. Harris, N. and Maskell, K.,* 1994.

[Hsu08]   Hsu, J. C.; Wang, P. W. and Chen, H. L.: "MgF_2 film deposited by IAD with end-Hall ion source using SF_6 as working gas", *Key Engineering Materials,* vol. 364, pp. 762-767, 2008.

[Idr96]   Idris, M. H.; Clegg, A. J.: "Processing and evaluation of investment cast magnesium-base alloy", *Transactions of the American Foundrymen's Society,* pp. 237-1996.

[Iid88]   Iida, T.; Guthrie, R. I. L.: "The physical properties of liquid metals", *Ed. Oxford University Press,* 1988.

[Jaf11]   Jafari, H.; Idris, M. H. and Ourdjini, A.: "High temperature oxidation of AZ91D magnesium alloy granule during in-situ melting", *Corrosion Science,* vol. 53, pp. 655-663, 2011.

[Jeu08]   Jeurgens, L. P. H.; Vinodh, M. S. and Mittemeijer, E. J.: "Initial oxide-film growth on Mg-based MgAl alloys at room temperature", *Acta Materialia,* vol. 56, pp. 4621-4634, 2008.

[Jon95]   Jones, S.; Marquis, P. M.: "Role of silica binders in investment casting", *British Ceramic Transactions,* vol. 94, pp. 68-73, 1995.

[Jon03]   Jones, S.; Yuan, C.: "Advances in shell moulding for investment casting", *Journal of Materials Processing Technology,* vol. 135, pp. 258-265, 2003.

[Kam00]   Kameshima, Y.; Yasumori, A. and Okada, K.: "XPS and X-ray AES (XAES) study of various aluminate compounds", *Journal of the Surface Science Society of Japan,* vol. 21, pp. 481-487, 2000.

[Kaw07]   Kawamori, S.; Machida, T.: "Microstructure and mechanical properties of alumina-dispersed magnesium fabricated using mechanical alloying method", *Materials Transactions,* vol. 48, pp. 373-379, 2007.

[Kim07]   Kim, J.; Wong, K. C.; Wong, P. C. *et al.:* "Characterization of AZ91 magnesium alloy and organosilane adsorption on its surface", *Applied Surface Science,* vol. 253, pp. 4197-4207, 2007.

[Kim04]   Kim, D. S.; Yu, Y. Y. and Char, K.: "Characterization of aluminum oxyfluoride barrier in magnetic tunnel junctions", *Journal of Applied Physics,* vol. 96, pp. 2278-2285, 2004.

[Kim03]   Kim, M. H.; Park, W. W.; You, B. S. *et al.:* "Effects of protective gases on the oxidation behaviour of Mg-Ca base molten alloys", *Materials Science Forum,* vol. 419-422, pp. 575-580, 2003.

[Kim01]   Kim, S.; Hong, T. and Kim, Y.: "Evaluation of thermal stability of mold materials for magnesium investment casting", *Materials Transactions,* vol. 42, pp. 539-542, 2001.

[Kim00]   Kim, S.; Kim, M.; Hong, T. *et al.:* "Investment casting of AZ91HP magnesium alloy", *Metals and Materials International,* vol. 6, pp. 275-279, 2000.

[Kim92]   Kim, S. S.; Baik, S.: "Interfacial segregation of Mg and Ca and its effects on microstructural evolution during sintering of alumina", *Solid State Phenomena,* vol. 25, pp. 269-276, 1992.

[Kön10]   König, R.; Scholz, G.; Scheurell, K. *et al.:* "Spectroscopic characterization of crystalline AlF$_3$ phases", *Journal of Fluorine Chemistry,* vol. 131, pp. 91-97, 2010.

[Kor04]   Korpiola, K.: "High temperature oxidation of metal, alloy and cermet powders in HVOF spraying process", *PhD thesis, Helsinki University of Technology*, 2004.

[Lee08]   Lee, J. K.; Kim, S. K.: "Development of novel environment-friendly magnesium alloys", *Advanced Engineering Materials Research,* vol. 47-50, pp. 940-943, 2008.

[Lee00]   Lee, Y. C.; Dahle, A. K. and St John, D. H.: "The role of solute in grain refinement of magnesium", *Metallurgical and Materials Transactions A (Physical Metallurgy and Materials Science),* vol. 31A, pp. 2895-2905, 2000.

[Li00]   Li, L.; Lai, M. O.; Gupta, M. *et al.:* "Improvement of microstructure and mechanical properties of AZ91/SiC composite by mechanical alloying", *Journal of Materials Science,* vol. 35, pp. 5553-5561, 2000.

[Lit99]   Litton, D.; Garofalini, S. H.: "Atomistic structure of sodium and calcium silicate intergranular films in alumina", *Journal of Materials Research,* vol. 14, pp. 1418-1429, 1999.

[Liu09]   Liu, J. R.; Chen, H. K.; Zhao, L. *et al.:* "Oxidation behaviour of molten magnesium and AZ91D magnesium alloy in 1,1,1,2-tetrafluoroethane/air atmospheres", *Corrosion Science,* vol. 51, pp. 129-134, 2009.

[Lu10]   Lu, X.; Xia, G.; Lemmon, J. P. *et al.:* "Advanced materials for sodium-beta alumina batteries: Status, challenges and perspectives", *Journal of Power Sources,* vol. 195, pp. 2431-2442, 2010.

[Luk97]   Lukaszewicz, J. P.: "X-ray photoelectron spectroscopy studies of sodium modified carbon films suitable for use in humidity sensors", *Journal of Materials Science,* vol. 32, pp. 6063-6068, 1997.

[Mal11]   Mali, A.Petric, A.: "Synthesis of sodium ß"-alumina powder by sol-gel combustion", *Journal of the European Ceramic Society,* vol. 32, pp. 1229-1234, 2011.

[Mat03]   Mato, S.; Alcala, G.; Skeldon, P. *et al.:* "High resistivity magnesium-rich layers and current instability in anodizing a Mg/Ta alloy", *Corrosion Science,* vol. 45, pp. 1779-1792, 2003.

[Mcc83]   Mc Cune, R. C.; Wynblatt, P.: "Calcium segregation to a magnesium oxide (100) surface", *Journal of the American Ceramic Society,* vol. 66, pp. 111-117, 1983.

[Med09]   Medved, J.; Mrvar, P. and Voncina, M.: "Oxidation resistance of cast magnesium alloys", *Oxidation of Metals,* vol. 71, pp. 257-270, 2009.

[Meu00]   Meulenberg, W. A.; Telle, R.; Rothe, H. *et al.:* "Fabrication and investigation of ceramic shell moulds for investment casting", *Ceramic Forum International*, vol. 77, pp. 30-35, 2000.

[Mil03]   Milbrath, D. S.: "Development of 3M™ Novec™ 612 Magnesium protection fluid as a substitute for SF$_6$ over molten magnesium", *Proceedings of the International Conference on SF$_6$ and the Environment*, 2003.

[Mir10]   Mirak, A.; Davidson, C. J. and Taylor, J. A.: "Characterisation of fresh surface oxidation films formed on pure molten magnesium in different atmospheres", *Corrosion Science,* vol. 52, pp. 1992-2000, 2010.

[Mit02]   Mitchell, L. D.; Whitfield, P. S.; Margeson, J. *et al.:* "Sucrose synthesis of nanoparticulate alumina", *Journal of Materials Science Letters,* vol. 21, pp. 1773-1775, 2002.

[Nag12]   Nagpure, I. M.; Pitale, S. S.; Coetsee, E. *et al.:* "The cathodoluminescence degradation and surface characterization of beta-Ca$_3$(PO$_4$)$_2$: Tb phosphor", *Optical Materials,* vol. 34, pp. 1398-1405, 2012.

[Nor97]   Nordlien, J. H.; Ono, S.; Masuko, N. *et al.:* "A TEM investigation of naturally formed oxide films on pure magnesium", *Corrosion Science,* vol. 39, pp. 1397-1414, 1997.

[Not11]   Noto, L. L.; Pitale, S. S.; Terblans, J. J. *et al.:* "Surface chemical changes of CaTiO$_3$:Pr^{3+} upon electron beam irradiation", *Physica B: Condensed Matter,* vol. 407, pp. 1517-1520, 2011.

[Ota96]   Ota, H.; Sakai, K.; Aoki, R. *et al.:* "Superstructure observation on a MgO (100) surface", *Surface Science,* vol. 357, pp. 150-154, 1996.

[Pet02]   Pettersen, G.; Ovrelid, E.; Tranell, G. *et al.:* "Characterisation of the surface films formed on molten magnesium in different protective atmospheres", *Materials Science & Engineering A (Structural Materials: Properties, Microstructure and Processing),* vol. A332, pp. 285-294, 2002.

[Piw94]   Piwonka, T. S.: "Reactions at the mold/metal interface in investment castings", *42nd Annual Technical Meeting of the Investment Casting Institute,* 1994.

[Pop92]   Popoola, O. O.; Kriven, W. M.: "Interfacial structure and chemistry in a ceramic/polymer composite material", *Journal of Materials Research,* vol. 7, pp. 1545-1552, 1992.

[Pra98]   Pradier, C. M.; Hinnen, C.; Jansson, K. *et al.:* "Structural and surface characterization of perovskite-type oxides; influence of A and B substitutions upon oxygen binding energy", *Journal of Materials Science,* vol. 33, pp. 3187-3191, 1998.

[Put88]   Putz, H.; Schön, J. C. and Jansen, M.: "Investigation of the energy landscape of Mg$_2$OF$_2$", *Computational Materials Science,* vol. 11, pp. 309-322, 1998.

[Rei34]   Reimers, H. A.: "Method for inhibiting the oxidation", *U.S. Patent 1972317,* 1934.

[Rev00]   Revankar, V.; Baker, P.; Schultz, A. H. *et al.:* "A replacement for SF$_6$: The MagShield system", *Proceedings of the IMA 2000 Annual World Magnesium Conference,* 2000.

[Ric03]   Ricketts, N. J; Cashion, S. P. and Bailey, R.: "Industrial trials with the AMCover gas system for magnesium melt protection", *Proceedings of the Light Metals Technology Conference,* 2003.

[Ric01]   Ricketts, N. J; Cashion, S. P.: "Hydrofluorocarbons as a replacement for sulphur hexafluoride in magnesium processing", *Proceedings of the TMS Annual Meeting,* pp. 31-36, 2001.

[Ros04]   Rosefort, M.; Korte, S. and Bührig-Polaczek, A.: "Investment casting of magnesium", *Proceedings of the 6th International Conference Magnesium Alloys and Their Applications,* pp. 752-757, 2004.

[Sat03]   Sato, K.; Izumi, T.; Iwase, M. *et al.:* "Nucleation and growth of nanocrystalline silicon studied by TEM, XPS and ESR", *Applied Surface Science,* vol. 216, pp. 376-381, 2003.

[Sch40]   Schneider, A.Esch, U.: "Über die reaktion zwischen magnesium und schwefeldioxid", *Zeitschrift für Metallkunde,* vol. 32, pp. 173-177, 1940.

[Sha04]   Shamasundar, S.Manjunatha, T. M.: "Computer simulation and analysis of investment casting process", *Foundry,* pp. 29-44, 2004.

[Sha88]   Sharma, R. A.: "Phase Equilibria and Structural Species in MgF$_2$-MgO, MgF$_2$-CaO and MgF$_2$-Al$_2$O$_3$ Systems", *Journal of the American Ceramic Society,* vol. 71, pp. 272-276, 1988.

[Shi07]   Shih, T. S.; Liu, J. B. and Wei, P. S.: "Oxide films on magnesium and magnesium alloys", *Materials Chemistry and Physics,* vol. 104, pp. 497-504, 2007.

[Sid08]   Sidhu, B. S.; Kumar, P. and Mishra, B. K.: "Effect of Slurry Composition on Plate Weight in Ceramic Shell Investment Casting", *Journal of Materials Engineering and Performance,* vol. 17(4), pp. 489-498, 2008.

[Sin06]   Sin, S. L.; Dube, D. and Tremblay, R.: "Interfacial reaction between AZ91D magnesium alloy and plaster mould material during investment casting", *Materials Science and Technology,* vol. 22, pp. 1456-1463, 2006.

[Sio03b]   Siokou, A.; Kefalas, D. and Ntais, S.: "XPS study of hydrated $MgCl_2$ impregnated on flat SiO_2/Si (100) Mo and Au substrates", *Surface Science,* vol. 532, pp. 472-477, 2003.

[Sio03a]   Siokou, A.; Ntais, S.: "Towards the preparation of realistic model Ziegler-Natta catalysts: XPS study of the $MgCl_2TiCl_4$ interaction with flat SiO_2/Si (100)", *Surface Science,* vol. 540, pp. 379-388, 2003.

[Sou97]   Souda, R.; Hwang, Y.; Aizawa, T. *et al.:* "Ca segregation at the MgO (001) surface studied by ion scattering spectroscopy", *Surface Science,* vol. 387, pp. 136-141, 1997.

[Stj03]   StJohn, D. H.; Dahle, A. K.; Abbott, T. *et al.:* "Solidification of cast magnesium alloys", *TMS Annual Meeting,* pp. 95-100, 2003.

[Sur10]   Suri, R.: "Investigation of MOS Interfaces with Atomic-Layer-Deposited High-k Gate Dielectrics on III-V Semiconductors", *PhD Thesis, North Carolina State University,* 2010.

[Swa06]   Swain, B. P.; Dusane, R. O.: "Multiphase structure of hydrogen diluted a-SiC: H deposited by HWCVD", *Materials Chemistry and Physics,* vol. 99, pp. 240-246, 2006.

[Swa07]   Swaminathan, S.; Spiegel, M.: "Thermodynamic and kinetic aspects on the selective surface oxidation of binary, ternary and quarternary model alloys", *Applied Surface Science,* vol. 253, pp. 4607-4619, 2007.

[Syv07]   Syvertsen, M.; Aarstad, K.; Tranell, G. *et al.:* "The Role of Fluorine Solubility in the Protection of Molten Magnesium", *Proceedings of the 7th International Conference Magnesium Alloys and Their Applications,* pp. 207-214, 2007.

[Taj11]   Tajima, K.; Hotta, H.; Yamada, Y. *et al.:* "Electrochromic switchable mirror foil with tantalum oxide thin film prepared by reactive DC magnetron sputtering in hydrogen-containing gas", *Surface and Coatings Technology,* vol. 205, pp. 3956-3960, 2011.

[Tra04]   Tranell, G.; Syvertsen, M.; Bech, K. *et al.:* "Alternatives to SF_6/SO_2 for magnesium melt protection: final report of the IMA-SINTEF collaboration project", 2004.

[Tre09]   Tressaud, A.; Labrugère, C.; Durand, E. *et al.:* "Switchable hydrophobic-hydrophilic layer obtained onto porous alumina by plasma-enhanced fluorination", *Science in China Series E: Technological Sciences,* vol. 52, pp. 104-110, 2009.

[Van10]   Van Vegten, C. H.: "Aerosol Synthesis of Supported Metal and Metal Oxide Systems and their Catalytic Applications", *PhD thesis, Eidgenössische Technische Hochschule ETH Zürich,* 2010.

[Ven10]   Venkat, Y.; Singh, S. and Das, N.: "Improvement in refractoriness of ceramic shells for directional solidification casting of gas turbine components", *International Journal of Cast Metals Research,* vol. 23, pp. 130-135, 2010.

[Vin06]   Vinodh, M. S.: "On the initial oxidation of MgAl alloys", *PhD thesis, Universität Stuttgart,* 2006.

[Wan11]   Wang, X. F; Xiong, S.: "Protection behavior of SO_2-containing cover gases to molten magnesium alloy", *Transactions of Nonferrous Metals Society of China,* vol. 21, pp. 807-813, 2011.

[Wan08]   Wang, X. M.; Zeng, X. Q.; Zhou, Y. *et al.:* "Early oxidation behaviors of Mg-Y alloys at high temperatures", *Journal of Alloys and Compounds,* vol. 460, pp. 368-374, 2008.

[Wen01]   Wende, M. C.; Broekaert, J. A. C.: "Investigations on the use of chemical modifiers for the direct determination of trace impurities in Al_2O_3 ceramic powders by slurry electrothermal evaporation coupled with inductively-coupled plasma mass spectrometry (ETVG-ICPG-MS)", *Fresenius' Journal of Analytical Chemistry,* vol. 370, pp. 513-520, 2001.

[Wil11]   Wilson, P. J.; Blackburn, S.; Greenwood, R. W. *et al.:* "The role of zircon particle size distribution, surface area and contamination on the properties of silica-zircon ceramic materials", *Journal of the European Ceramic Society,* vol. 31, pp. 1849–1855, 2011.

[Xio07]   Xiong, S. M.; Liu, X. L.: "Microstructure, Composition, and Depth Analysis of Surface Films Formed on Molten AZ91D Alloy under Protection of SF_6 Mixtures", *Metallurgical and Materials Transactions A,* vol. 38, pp. 428-434, 2007.

[Xio10]   Xiong, S. M.; Wang, X. F.: "Protection behaviour of fluorine-containing cover gases on molten magnesium alloys", *Transactions of Nonferrous Metals Society of China (English Edition),* vol. 20, pp. 1228-1234, 2010.

[Xiu07]   Xiuqing, Z.; Haowei, W.; Lihua, L. *et al.:* "In situ synthesis method and damping characterization of magnesium matrix composites", *Composites Science and Technology,* vol. 67, pp. 720-727, 2007.

[Yan07]   Yang, G.; Jie, W.; Hao, Q. *et al.:* "Study on process of magnesium alloy investment casting", *Materials Science Forum,* vol. 561-565, pp. 1019-1022, 2007.

[Yan08]   Yang, Z.; Zhang, J.: "Review on research and development of magnesium alloys", *Acta Metallurgica Sinica (English Letters),* vol. 21, pp. 313-328, 2008.

[Yao01]   Yao, H. B.; Li, Y.; Wee, A. T. S. *et al.:* "The alloying effect of Ni on the corrosion behaviour of melt-spun Mg-Ni ribbons", *Electrochimica Acta,* vol. 46, pp. 2649-2657, 2001.

[Yas07]   Yasakau, K. A.; Zheludkevich, M. L.; Lamaka, S. V. *et al.:* "Role of intermetallic phases in localized corrosion of AA5083", *Electrochimica Acta,* vol. 52, pp. 7651-7659, 2007.

[Yas98]   Yasrebi, M.; Kemp, W. W. and Sturgis, D. H.: "Aging of aqueous investment casting slurries, causes and solutions", *46th Annual Technical Meeting and Exhibition of the Investment Casting Institute,* 1998.

[Yas02]   Yasrebi, M.; Taft III, K. M.; Sturgis, D. H. *et al.:* "Method for processing materials to increase slurry lifetime", *U.S.Patent 6390179,* 2002.

[Yos92]   Yoshitake, H.: "Reaction mechanism and environments of active sites of hydrogenation on metal catalysts", *PhD thesis, University of Tokio,* 1992.

[Yua02]   Yuan, C.; Jones, S.; Withey, P. A. *et al.:* "Development of alumina primary coat for single crystal investment casting ceramic mould", *British Ceramic Transactions,* vol. 101, pp. 59-64, 2002.

[Zan04]   Zanetti, M. C.; Fiore, S.; Ruffino, B. *et al.:* "Waste characterization and reuse in an aluminum and magnesium foundry", *Proceedings of the 1st International Conference on Advances in Mineral Resources Management and Environmental Geotechnology,* pp. 413-418, 2004.

[Zen01]   Zeng, X.; Wang, Q.; Lu, Y. *et al.:* "Behaviour of surface oxidation on molten Mg-9Al-0.5Zn-0.3Be alloy", *Materials Science and Engineering A,* vol. 301, pp. 154-161, 2001.

[Zep10]   Zeppilli, S.; Arnault, J. C.; Gesset, C. *et al.:* "Thermal stability and surface modifications of detonation diamond nanoparticles studied with X-ray photoelectron spectroscopy", *Diamond and Related Materials,* vol. 19, pp. 846-853, 2010.

[Zha98]   Zhang, L. P.; Li, M. and Diebold, U.: "Characterization of Ca impurity segregation on the TiO_2 (110) surface", *Surface Science,* vol. 412, pp. 242-251, 1998.

[Zha04]   Zhang, Z.; Morin, G.: "Effect of inhibitor gas on mould-magnesium reactions in investment casting", *Proceedings of the Magnesium Technology 2004 Symposium,* pp. 197-202, 2004.

[Zha09a]   Zhang, Y. Q.; Motegi, T.; Tanabe, F. *et al.:* "Effect of SF_6 cover gas humidity and concentration on efficient protection of molten magnesium", *Materials Science Forum*, vol. 610- 63, pp. 1003-1008, 2009.

[Zha09b]   Zhao, L.; Liu, J. R.; Chen, H. K. *et al.:* "The characterization of surface films formed on molten magnesium and AZ91D alloy in air/1,1,1,2-tetrafluoroethane atmospheres", *Journal of Alloys and Compounds,* vol. 480, pp. 711-716, 2009.

ACKNOWLEDGEMENTS

APPENDIX

XRF analyses

Table 12A.1: XRF measurements performed on A-NaH samples. The relative weight % is qualitative. Fluorine is marked in blue

A-NaH-18						A-NaH-8					
A-NaH-18c			A-NaH-18m			A-NaH-8c			A-NaH-8m		
El.	Rel. Weight	Std Error	El.	Rel. Weight	Std Error	El.	Rel. Weight	Std Error	El.t	Rel. Weight	Std Error
Mg	60.5	0.6	Mg	66.5	0.4	Mg	81	0.8	Mg	68	0.3
Al	33	0.4	Al	22.5	0.3	Al	10.5	0.3	Al	24	0.3
Si	3	0.11	Zn	4	0.2	Si	6.5	0.2	Ca	2.5	0.2
F	2	0.8	Ca	3	0.1	F	0.2	0.1	Zn	1.7	0.1
Zn	0.56	0.06	Si	1	0.1	Ca	0.1	0.05	Si	1.5	0.07
Ca	0.4	0.06	Mn	0.5	0.09	Zn	0.1	0.4	Mn	1	0.1
Mn	0.3	0.07	Fe	0.3	0.07						

Table A.2: XRF measurements performed on A-KH samples. The relative weight % is qualitative. Fluorine is marked in blue

| A-KH-24						A-KH-20						A-KH-2					
A-KH-24c			A-KH-24m			A-KH-20c			A-KH-20m			A-KH-2c			A-KH-2m		
El.	W %	Std Err.	El.	W %	Std Err.	El.	W %	Std Err.	El.	W %	Std Err.	El.	W %	Std Err.	El.	W %	Std Err.
Mg	52	0.6	Mg	73.7	0.3	Mg	66.7	0.4	Mg	73.5	0.3	Al	49	0.72	Mg	68	0.7
Al	37.5	0.5	Al	22.5	0.3	Al	26	0.4	Al	19.5	0.3	Mg	34.5	0.43	Al	15	0.3
Si	5.5	0.2	Si	1.3	0.06	Si	4.6	0.14	Ca	2.5	0.2	Si	10	0.37	F	12	0.9
F	2	0.9	Ca	1	0.1	Zn	0.5	0.06	Si	1.5	0.07	F	5.5	1.35	Si	2	0.07
Zn	1	0.09	Zn	0.8	0.06	K	0.5	0.1	Zn	1.5	0.09	K	0.4	0.16	Ca	1.5	0.1
Na	0.7	0.09	Mn	0.5	0.07	F	0.4	0.2	Mn	0.7	0.09	Ca	0.3	0.080	Zn	1	0.06
Zn	0.3	0.08				Ca	0.3	0.06	F	0.2	0.1	Na	0.2	0.081	Mn	0.5	0.06
Mn	0.1	0.07				Mn	0.3	0.07	Fe	0.1	0.04	Fe	0.09	0.043			

XRD analyses
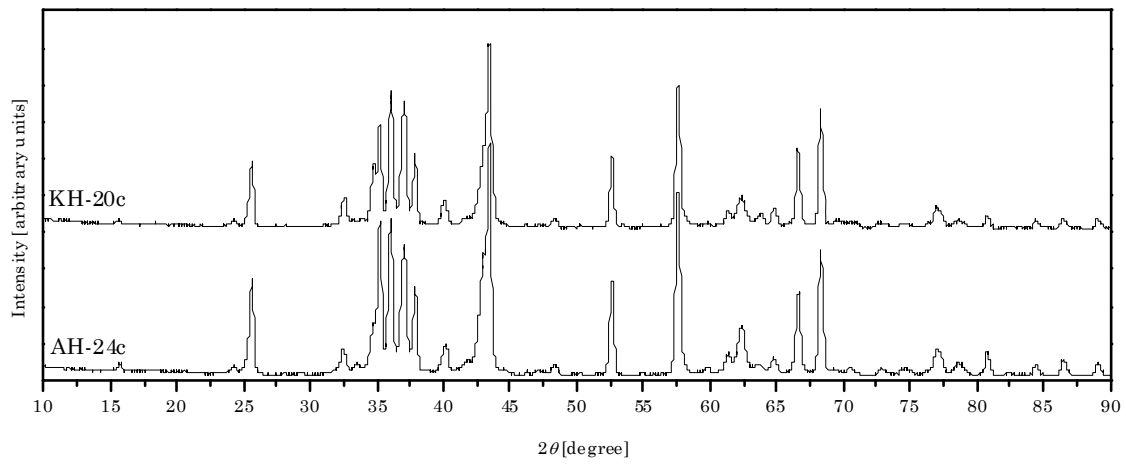
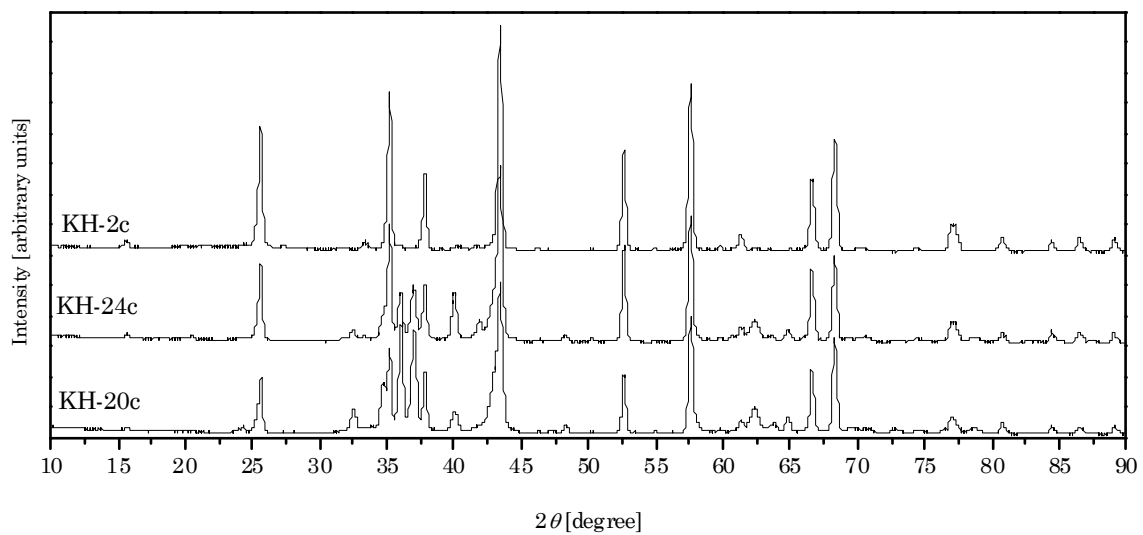Figure 12A.121: XRD spectrum of samples A-KH-20c and A-AH-24c

Figure A.2: XRD spectrum of the ceramic samples extracted form A-KH essay